Imperial College of Science, Technology and Medicine

University of London

INACCESSIBLE EQUIPMENT MONITORING VIA VIBRATORY SIGNATURE ANALYSIS UTILISING DATA COLLECTED BY REMOTE ACCELEROMETERS

by

Marcos Pellegrini Ribeiro

A thesis submitted to the University of London
for the degree of Doctor of Philosophy

Department of Mechanical Engineering
Imperial College of Science, Technology and Medicine
London SW7

April 1999

Iron rusts from disuse, stagnant water loses its purity,
and in cold weather becomes frozen:
even so does inaction sap the vigour of the mind.
(Leonardo da Vinci)

To my mother Anna
To Agustin Valido and Mônica (In memoriam)

Abstract

The research described in this thesis is focused on vibration monitoring in machinery whose location makes it difficult to gain direct access. In particular, interest is focused on electrical submersible pumps (ESPs) used in the petroleum industry, which are situated in deep petroleum wells.

In this study, a signal processing technique has been developed for the purpose of analysing vibration signals generated by ESPs and detected by remotely-located accelerometers. Analysis of vibration signals has been achieved by adapting the original Prony method to generate time-frequency representations that are able to handle signals containing stationary and non-stationary components with high levels of noise.

Analysis were made applying the extended Prony time-frequency representation (PTFR) to simulated signals, and compared with the analysis resulted from the application of four other signal processing techniques: the Fourier transform, the Morlet wavelet transform, the Wigner-Ville and the pseudo Wigner-Ville distributions. The new method was also applied to signals generated by a small-scale experimental model which replicated, as closely as possible, the type of signals normally found in full-size ESP installations.

The extended PTFR applied to simulated and experimental signals, has been shown to be capable of detecting variations in the amplitude levels of weak components

embedded in strong noise and non-stationary processes with an amplitude ratio of 1:100 (-40 dB).

Unexpectedly, the results also reveal that the extended PTFR can represent non-stationary processes, thus providing a new way to analyse signals with these components.

Although this project was stimulated specifically by a need to develop methods for monitoring the performance of ESPs, the resulting technique has relevance for other situations where it is difficult to install delicate sensors to measure vibrations, such as motors that drive large furnace doors, internal mechanical components (gears, shafts bearings) of mills, and mixers operating with strong corrosive compounds etc.

Acknowledgements

I would first like to thank my supervisors, Prof. D. J. Ewins and Mr. D. A. Robb, whose knowledge of the field of vibration and feedback on my work have been invaluable in helping me complete this study.

I am especially grateful to T.P.S. Kempner, who has helped me with the thesis writing. His suggestions made the work much clearer than it would otherwise have been.

I would like to express my gratitude to the Petróleo Brasileiro S.A. for the chance and financial support provided to realise this research.

Finally, I express my special gratitude to my mother to whom this thesis is dedicated. Without her love and assistance this thesis would not have been completed.

Nomenclature

$\boldsymbol{a}$ = frequency scaling factor

$\boldsymbol{A}$ = amplitude

$\boldsymbol{a(k)}$ = parameters

$\boldsymbol{a_b}$ = backward linear prediction coefficient vector

$\boldsymbol{a_f}$ = forward linear prediction coefficient vector

AIC = Akaike Information Criterion

AR = autoregressive process

ARMA = autoregressive moving average process

$\boldsymbol{c_k}$ = Prony series exponential damping

$\boldsymbol{c_v}$ = proportional viscous damping

$\boldsymbol{[C_v]}$ = damping matrix of the system

$\boldsymbol{d(t)}$ = deterministic function of time

$\boldsymbol{E}$ = Modulus of elasticity

ESP = electrical submersible pump

$\boldsymbol{e_b}$ = backward linear prediction error

$\boldsymbol{e_f}$ = forward linear prediction error

FT = Fourier transform

$\boldsymbol{f(t)}$ = temporal function

$\boldsymbol{f_s}$ = sample frequency

$\boldsymbol{f_0}$ = centre frequency of a Gaussian window

$\boldsymbol{g(t)}$ = weighting window applied in the time domain

h(n) = weighting window applied in the frequency domain

[H(w)] = receptance FRF matrix

I = Second moment of inertia

IFT = inverse Fourier transform

[K] = bending stiffness matrix

k_{yii} = Stiffness of each wire element

l = length of a wire element

LSQ = least-squares linear prediction estimation

m = mass

[M] = mass matrix

n = data sample number of a discrete time sequence

N = sequence length, number of data samples

p = polynomial order

$PTF[A_k]$ = Prony time-frequency distribution matrix

PWVD = Pseudo-Wigner-Ville Distribution

q = frequency line in the Prony time-frequency plane

R = vector outer product

r(t) = temporal function

RLS = recursive least-squares estimation

s(n) = discrete raw signal

s(t) = analog signal

$S[n_q]$ = Prony time-frequency plane projection on the frequency domain

SNR = signal-to-noise ratio

t = time

T_s = sampling interval

u = time shifted each incremental period ***dT***

$W_{j,k}$ = Malat wavelet

WM = Morlet wavelet

WVD = Wigner-Ville Distribution

$\hat{x}(n)$ = estimator

$x(n)$ = discrete data vector

$x(t)$ = signal

$x^*(t)$ = Hilbert transform or conjugate of a signal

$y(n)$ = discrete system response function

$y(t)$ = sample record of a stationary random process

z = roots of the characteristic polynomial

d= data lag

$e(n)$ = error over the N data samples

$L(d)$ = autocorrelation sequence

m_k = Malat wavelet coefficients

h = squared error

h_b = backward linear prediction squared error

h_f = forward linear prediction squared error

n = frequency (Hz)

q = phase

$\hat{r}_p$ = AR input white noise variance estimator

t = time delay

w = frequency (rad/s)

Table of Contents

Chapter 1
Introduction

1.1. Background and Context of the Research

The research described in this thesis is concerned with assessing the condition and performance of inaccessible machinery by using signal processing techniques in the analysis of vibration data gathered from remote transducers. The study will focus on the analysis of deep-well petroleum pumping equipment, and in particular on the electrical submersible pump (ESP). Interest in this area results from difficulties experienced by engineers of the Brazilian Petroleum Industry when analysing the performance of ESPs installed downhole in petroleum wells which, due to their virtual inaccessibility, has proved to be a costly and time-consuming exercise. However, although the focus is on pumping equipment used in the petroleum industry, the work is equally relevant to any situation where it is difficult to install delicate measuring instruments, such as artificial lift equipment located in deep wells, large furnace door motors and internal mechanical components (gears, shafts, bearings) of mills and mixers operating with corrosive compounds. It should be noted that there is a scarcity of research into vibration analysis where the transducers used to gather data are

placed at some considerable distance from the equipment. This is somewhat surprising given the many situations, apart from petroleum wells, where it is necessary to monitor and detect failures in equipment in locations that are difficult to access, and where it is difficult to install sensors nearby.

Given the high investments in industrial machinery nowadays, it is extremely costly if a plant has to be shut down for any length of time. Consequently, a tremendous amount of effort and innovation is being devoted to the maintenance process. For example, early detection and replacing of a faulty bearing could alleviate the temporary shut-down of a paper mill. In certain cases, machines can be destroyed completely if the fault is not detected at an early stage, such as when a rotor blade breaks in a turbine. When this event occurs it can lead to a sudden change in the vibration of the shaft, which, given an appropriate measuring device and methodology, can be detected sufficiently early to avoid a major catastrophe, and thereby save on high repair and other costs. At the present time, however, we do not possess an adequate methodology for analysing vibration data from machinery located in such a remote and hostile environment as an off-shore oil well. It will therefore be the main objective of this study to develop a suitable method of analysing vibration data gathered by means of transducers located at some distance from the equipment. In which circumstance the signal components of interest may be masked by other spurious components.

In order to gain a clearer insight into what our task entails, we will now provide a brief description of a typical oil well, the electrical submersible pumps which we intend to monitor, and the connections between the pump and the surface.

1.2. Electrical Submersible Pump (ESP)

Electrical submersible pumps (ESPs) have been traditionally used for over half a century for moving large volumes of fluids where other means of artificial lifts have not been feasible. It is not uncommon for these pumps to handle more than 500 m^3 of fluid per day. A typical pump assembly is composed of hundreds of centrifugal sections with a small diameter (commonly around 4" to 5" of diameter) serially mounted. The pump is coupled to a motor which has a seal assembly and is filled with an insulation fluid that is heavier than water. In the Brazilian installations this motor is generally between 100 and 200 HP and is a two-pole, three-phase machine. It runs at a relatively constant speed of 3500 rpm (approximately 58 Hz) on 60 Hz frequency supply. The electrical supply is provided through a long electrical cable attached to the tubing that supports the assembly. The motor housing is cooled by the well fluids moving past the exterior surface of the motor.

Figures 1.1 and 1.2 show the internal section (stage) of a pump and its petroleum well installation respectively.

In Figure 1.3 a diagram is shown which represents a typical petroleum well electric submersible pump installation unit, and in Figure 1.4 the pump section is shown in detail.

Fig. 1.1 - Pump section

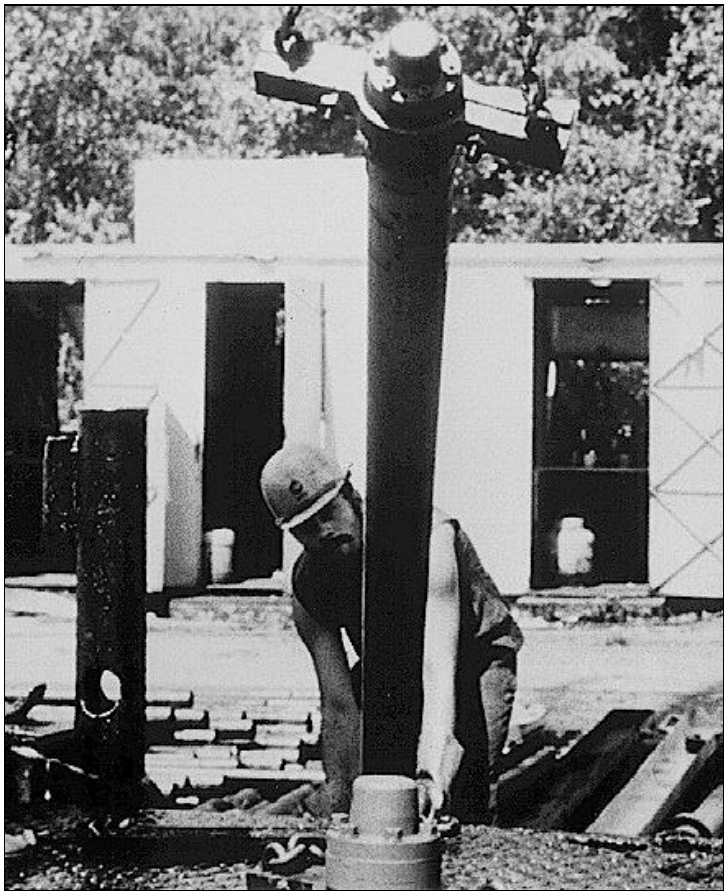

Fig. 1.2 - Pump being installed in a petroleum well

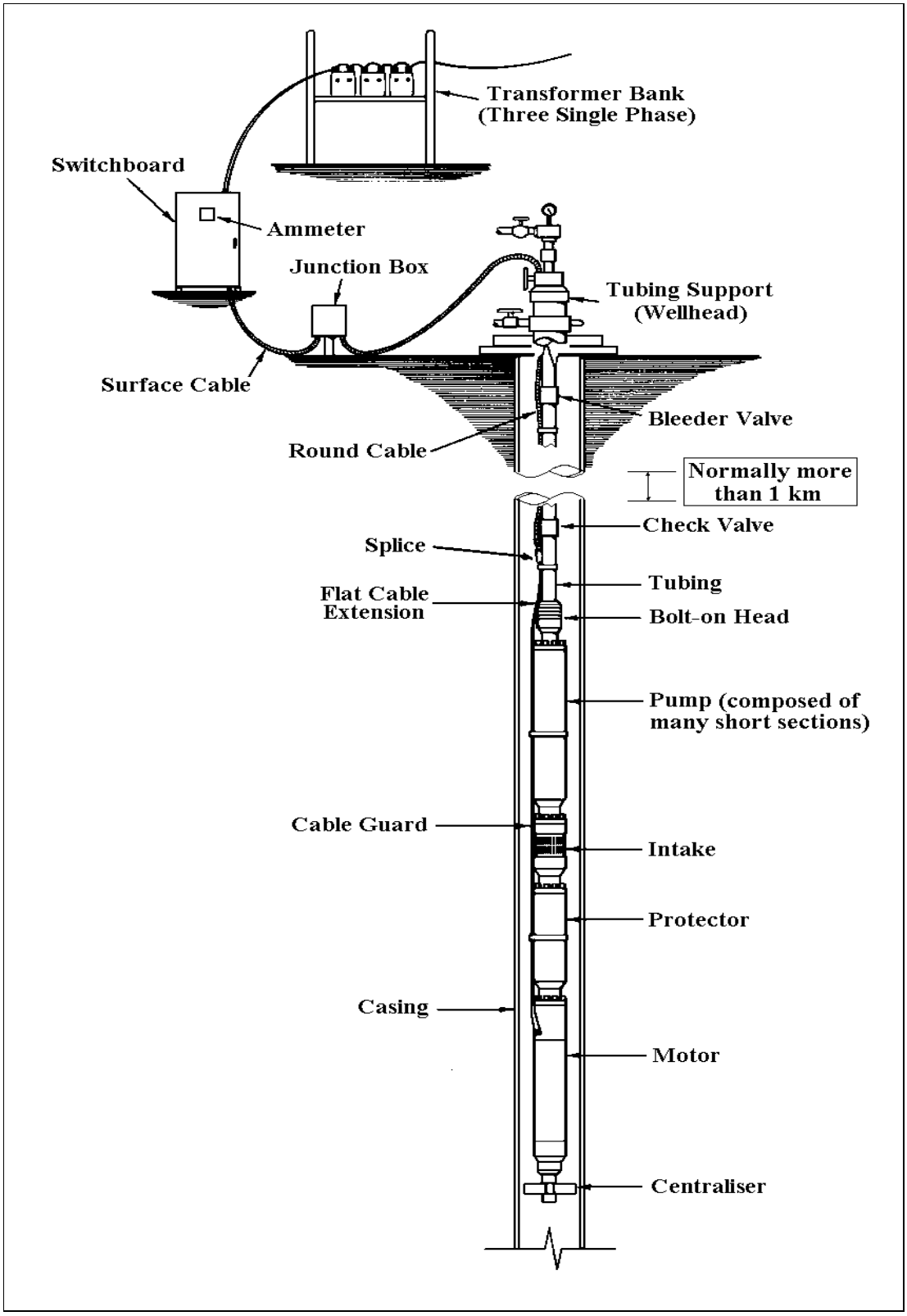

Fig. 1.3 - Typical ESP installation

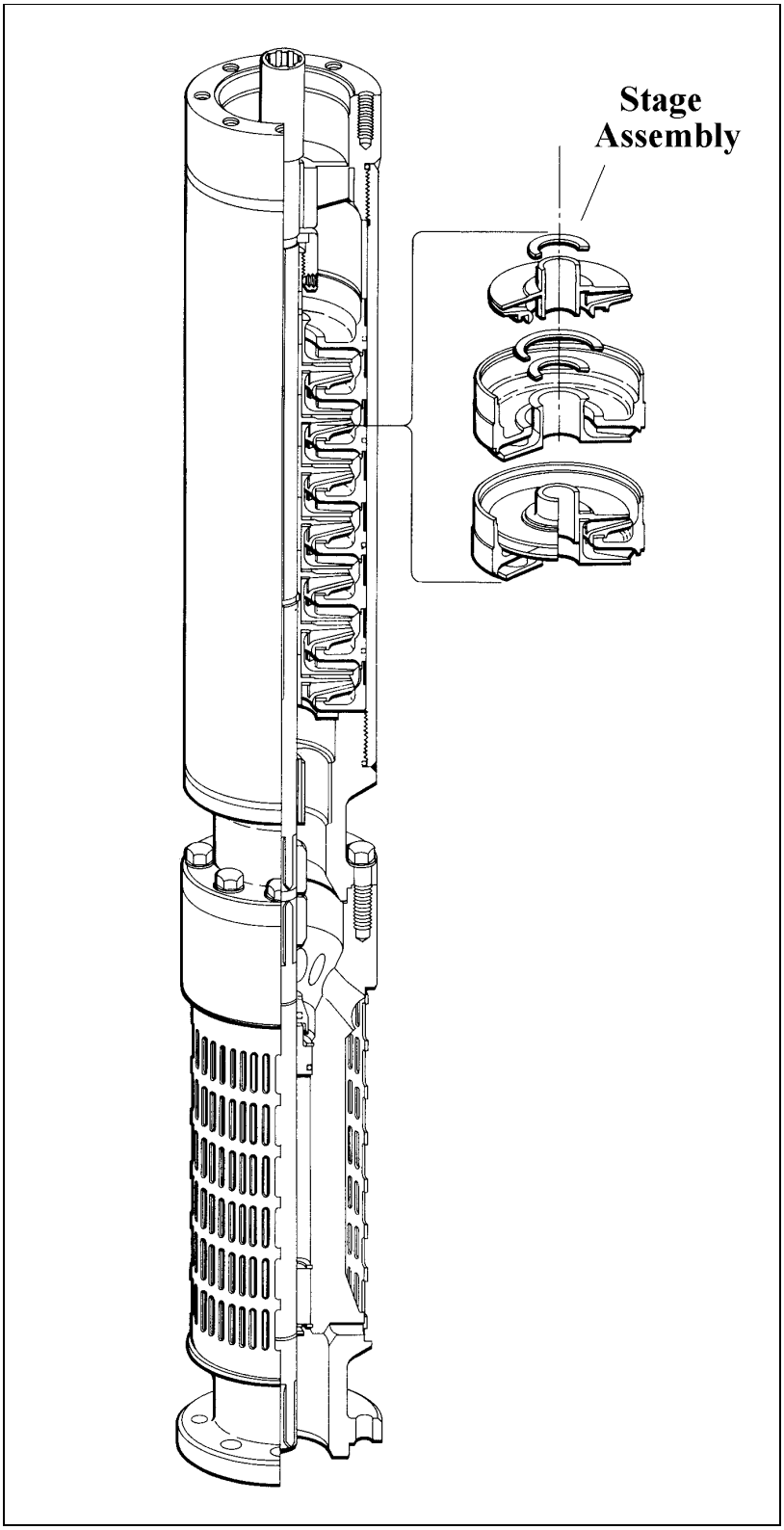

Fig. 1.4 - Detail of the pump section and stage assembly

1.3. Existing Monitoring Techniques

Until recently, the only means of performance analysis available for ESPs, in the hostile environment of the petroleum well, with its high temperature and pressures, has been through monitoring from the surface the electrical current of the motor that drives the equipment. Haynes et al [1989/1990] and Krytes and Haynes [1989], are examples of works which show how motor-driven machinery is monitored by analysing the electrical motor current. However, work undergone in the Brazilian oil wells has shown this method to be extremely unreliable due to the tendency for errors to be made in the diagnosis. For example, when using this type of analysis it is difficult to distinguish between variations in the electrical current from when a shaft in the pump breaks, compared to when a pump fills with gas, as both situations present low current peaks. However, in each of these scenarios different actions are required, in the former, the ESP has to be pulled out of the well as the pump is cooled by a fluid that is pumped through its casing, and an inoperative pump will lead to a burnt out motor due to an increase in temperature of the internal motor. In the case of the latter problem, if a pump fills with gas, the operator has to turn the motor on and off several times until the pump is fully filled again with fluid [Ribeiro et al, 1991]. Figure l.5 shows an electrical current graph where an incorrect interpretation resulted in a burnt out motor.

Although further attempts have been made to develop the technique for processing the signal of the electrical current, they have not yet been proved to be effective. For example, Jeon and Li [1995] developed a non-linear model-based fault detection for a single compressor by measuring the motor current and angular velocity. This fault detection scheme sought to detect faults without prior experience of them. It employs an algorithm with non-linear difference equations that model the dynamics of the compressor. However, they conclude in their work that this method is limited when applied to analyse equipment under large mechanical friction conditions. The authors state that in these cases, the results will present a large variance and this may lead to erroneous interpretations of faults with the equipment. ESP equipment normally generates a large amount of friction

between the impellers and the case. For, despite the existence of small clearances in the pump, the long shaft, in which the impellers are fixed, will exhibit large whirling, and contact between the impellers and the case is inevitable. Furthermore, as the pump cannot be lubricated, due its operational conditions, a large friction noise will be made, even in new equipment. Consequently, the method developed by Jeon and Li [1995] is not appropriate for analysing faults in ESPs.

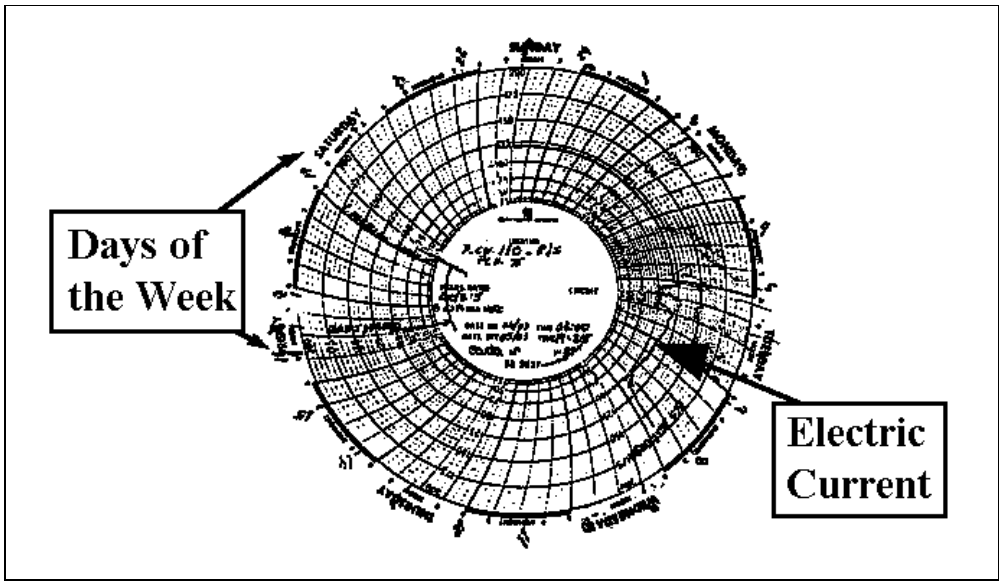

Fig. 1.5 - Electrical current graph of an ESP taken from a Brazilian wellhead.

In another work that analyses equipment by processing the signal of the electrical current of the motor, Burnett and Watson [1996] state that the majority of the techniques applied to analyse the electrical current signal are not efficient if the data are collected from equipment not operating in steady-state conditions. To overcome this limitation, the authors applied techniques used in non-stationary analysis for processing the electrical current of a motor subjected to transient conditions. The techniques used include: the spectrogram, the Wigner-Ville distribution, and the Morlet wavelet transform. Burnett and Watson [1996] found that the best method to detect the broken bars of a rotor in the signal of the electrical current of a typical induction motor is the Morlet wavelet transform. However, although the graphs show a difference between the motor, with and without broken rotor bars, this difference is so small that it would be eliminated in the vibration

signal of an ESP, due to the large impedance that exists in the transmission of the current signal through the long electrical cable (often more than 2 kilometres long).

In Burnett and Watson's work [1996], the proposed techniques were only tested to detect faults in electrical motors, in which the analysis of the electrical current is more appropriate. The simulated fault analysed in the work generates strong electrical components that are easily detected in the current signal (broken motor rotor bar). No simulation was made in their work where mechanical faults are generated by external sources that do not generate such a clear electrical current perturbation, as for example in the case of a broken shaft of a pump.

1.4. Previous Research Attempts to Analyse ESP Vibration

Due to the unreliability of analysing the signal of the electrical current, research has moved on to focus on the analysis of the pump's vibrations. Vibration in complex machinery is related to different parameters of the excitation forces and its operating conditions. The vibration behaviour of the machinery is related to external and internal forces, which determine the significant frequency and amplitude behaviour. It is these particular vibrations from the machinery, which are related to a specific behaviour, that we intend to analyse for fault detection purposes. Analysis and information about the ESP vibration can be found in the works of Sparks and Wachel [1977], Brookbank [1992], Benedek [1995] and Makiola [1995].

Sparks and Wachel [1977] state that a pump or a compressor vibration is basically dependent on the head curve slope, operating point, system flow damping, and strong reactive resonances in the pipe network, particularly if they coincide with the vortex frequencies. Based on several case studies, they define several conditions for developing pipe network resonances due to centrifugal pulsations. In a study that sought to reduce industrial plant noise pollution, Makiola [1995] describes the noise characteristics of various pumps using three-dimensional charts considering the

impeller diameter, flow rates, inlet pressures, and pump speeds. He states that a major influence on the pump vibration is provided by variations in the rotation speed. In Benedek [1995], a one-phase and two-phase one-dimensional fluid vibration in complex pipe networks was investigated, and a transfer matrix is used to represent the flow in rigid pipe hydraulic sections. His findings suggest that the flow and the pressure ripple of a centrifugal pump do not influence the eigenfrequencies of a pipe loop. In Brookbank [1992] a study of a more specialised analysis into ESP vibration is presented. He analysed the ESP vibration on a test-bench and defined several sources, the most predominant being the vibration caused by the unbalance of rotating parts. Out-of-balance conditions may be due to casting defects in the pump impellers such as voids, inclusions or core shift (which allows the impellers vanes to be off centre). The second most predominant cause of ESP vibration is shaft straightness. Shafts may be up to 10 metres long and do require extensive hand straightening. Bent or crooked shafts produce vibrations in both radial and axial directions at the rotation frequency and at two times the rotation frequency. The third major cause of ESP vibration is rubbing in the sleeve bearing, impeller wear ring or between rotating and stationary parts. An intermittent rub that has a contact once every other revolution will generate a sub-harmonic vibration at one half of the rotation speed. Another cause of sub-harmonic vibration, with frequency varying from 0.42 to 0.48 times of the rotation speed, is due to the oil whirl phenomena, a condition in which several insulation fluid filled closed slots of the electrical motor act as lightly loaded hydrodynamic bearings.

As mentioned above, there is limited existing research in ESP vibration signal analysis, with most based on the application of the Fourier transform technique in the analysis of the data. One of the first attempts at analysing the vibrations of ESPs installed downhole in a petroleum well was made by Aliev [1982]. In a number of experiments at different locations and with different pumps, Aliev placed transducers to gather vibration data at various distances from the pumps. He noted that, as a result of noise interference, it was better to measure the amplitude and shape of the ESP's acoustic oscillations rather than to make a spectral investigation of its vibration. He also argued that the ESP's motor protector, a chamber filled with fluid to isolate the motor

against the environment, does not influence the spectra. However, he did not explain how and why he arrived to these conclusions. What the study did show was that it was possible to monitor an ESP by its vibrations transmitted through the long tubing that is supporting it.

In a later study by Maksutov and Aliev [1984], 1100 ESPs were analysed in a more systematic way. The authors describe a phenomenon of separation of magnetic harmonics from mechanical harmonics when the equipment voltage is reduced. The study showed that magnetic fields create a double frequency component due to the motor dipole, and that the mechanical oscillation is determined by the first rotation harmonic level.

Research conducted using an experimental test rig by Moore [1990], was the first major systematic empirical study into the analysis of ESP equipment operating under controlled conditions. This study was undertaken on two sites: on one site the ESP did not operate due to an electrical insulation failure; on the other, an Anglia water plant, where the pump was installed in a well 38 meters in depth, satisfactory results were obtained. In this study, accelerometers were placed on the pump and at the wellhead and several types of wear, such as to the bearings and the pump's coupling, were simulated and the obtained data processed through the Fourier transform. The findings showed that the wear in the pump journal bearing was characterised by an increase in the amplitude of the component at rotation frequency. Moore reports that four weeks before the ESP failed, data gathered from the transducer attached to the pump revealed an increase of between 30 to 60 times the rotation amplitude vibration. But the transducer installed at the wellhead only showed the same problem two and half weeks later. One possible explanation for this delay in identifying the problem could be the use of inadequate filtering techniques associated with the Fourier transform. What is encouraging about the results is that they show that vibrations can be measured by transducers located at some distance from the pump, although the distance of 38 meters used in the Moore's project means we cannot be sure if the

same results can be achieved when vibrations are measured in petroleum wells at distances in excess of a 1000 meters.

The findings of Moore's study are significant to the extent that he demonstrated, contrary to the findings of Aliev [1982], that it could be useful to monitor several parameters, including: riser-borne vibration; pump and motor vibration using sensors mounted on the upper motor bearing and on the pump suction casing; and motor cooling water conductivity. However, although Moore has provided much new information which will be utilised in this study, the work is limited for our purposes as it was carried out in a well of a water plant, where the conditions are not comparable to those found in petroleum wells. Firstly, it is not feasible to fix a transducer on the pump itself as it would not survive the harsh environment of the petroleum well; and secondly, delicate transducers are likely to be damaged during the installation process. Furthermore, the Fourier technique used in all three studies cited above, could be inadequate for our purposes. According to Bendat and Piersol [1986], the Fourier technique does not handle well signals containing noise and non-stationary conditions, normally found in petroleum installations.

The analysis of vibrations at the wellhead is extremely problematic because they are composed of a number of elements: (i) the vibration from the ESP itself; (ii) noise and spurious vibrations generated by several types of equipment located near the petroleum wellhead and transmitted through the pipe network; and (iii) the vibration generated by fluid slugs flowing through the petroleum pipes. The fluid slug is also found in water pipes in houses: when air enters into the water system and flows with the water, an intermittent vibration appears. In the case of the petroleum wellhead, gas is normally dissolved in the oil at high pressure inside the reservoir. When the oil comes to the surface the pressure decreases and the gas starts to dissociate from the oil, causing large bubbles and slugs. In a study by Leducq [1991], in which he sought to describe a new method of deriving multiphase flow patterns by applying a time-frequency analysis to fluctuating pressure and acceleration measure at the pipe-wall, he stated that the majority of these components, associated with turbulent fluid-induced

vibrations, have frequencies varying from 6 to 24 Hz. He also attempted to characterise transitions between two-phase flow regimes. Four experiments were carried out, one for gas-oil flow studies and three for air-water flow studies, and the data were analysed using the Morlet wavelet transform. The work showed that it is possible to get access to the void fraction of the two-phase flow by non-intrusive measurements analysed in this way. Leducq and Hervieu [1991] concluded that two wavelet components corresponding to two characteristic scales of flow configuration seemed sufficient to characterise the flow configuration, and this can lead to a simplified signal processing technique. As we will show below in the simulation carried out in Chapter 3, we expect that the spurious component amplitude level will be greater by as much as 50 times the level of the weak component amplitude (ESP vibration collected in the wellhead). As a consequence, the signal to be analysed will be assumed to be composed as the slugs described in the work of Leducq and Hervieu [1991], where several types of noise (white, random, pink, chirp) represent the platform environmental noise, and the 58 and 60 Hz weak vibrations, which is related to the rotation and motor magnetic field, with an amplitude level 50 times less than the spurious slugs and noise (SNR -34 dB).

Given the complexity of the vibrations to be analysed, it is necessary to look in more detail at the various signal processing techniques available for analysis of signals containing high-level noise and non-stationary processes.

1.5. Noise Filtering and Non-Stationary Analysis: A Review of the Literature

A suitable signal processing technique for using in the analysis of vibration data generated downhole in a petroleum well will have to be able to discriminate, within the vibration signal, a weak deterministic component embedded in high level noise and non-stationary processes. However, the advances of the last decade have been mainly restricted to the development of methods for handling non-stationary signals, with

very little improvement in the area where signals are embedded in high-level noise. A review of the literature made into noise filtering techniques and methods to process non-stationary components is described below.

1.5.1. Noise Filtering

The measurement of periodic components embedded in noise is a very common problem, which arises, for example, when analysing the complicated vibration produced by several machines working together. If the frequencies and amplitudes of any periodic components in the vibration can be measured, then this is the first step towards tracing their origins. Less problematic is the retrieval of a periodic signal from random noise when a reference waveform is available with which the signal is known to be synchronous. This arises in A.C. testing when an alternative voltage is applied to a system and a weak voltage induced elsewhere is to be measured in the presence of the noise. Another context is that of impulse testing, when a repeated delta function impulse is applied to a system, and the repeated response is to be measured. The problem is further simplified if the shape of the signal to be retrieved is known, and one merely wants to determine the phase lag relative to a reference signal. Such is the case in pulsed radar when the amplitude and delay of an echo or reflected signal are to be determined in the presence of noise [Bendat and Piersol, 1986].

Sometimes the shape of the signal to be extracted is known (at least approximately) but no synchronising signal exists. This is the case with the seismic measurements related to nuclear explosions and earthquakes. The signals associated with each physical condition have their known characteristics and the problem is to determine in the presence of noise whether such a signal has occurred and which type it is. The problem of deciding which of several known types of signal has arrived occurs in digital communications systems, and is often simplified when the arrival time is known. Morse code provides a simple binary example. During each of successive

equal periods there is either a uniform signal or no signal, and a device which will distinguish between the alternatives in the presence of noise is required [Cover, 1991]. The various situations are classified according to whether the signal is coherent or incoherent (i.e. whether a synchronising waveform is available or not) and according to whether the signal is structurally determinate or indeterminate (i.e. whether the shape of the signal is known in detail or whether only statistical information such as the power spectrum is known).

It is worth noting here that digitising per se presents quantization errors that may eliminate weak components in a signal. Due to the technical conditions, the time values of the signals are represented with finite precision, which corresponds directly to the data word length. The amplitude is separated in a number of intervals and this is called amplitude quantization. Physically, this process of amplitude quantization means that some values deviate from the real magnitudes. These maximum deviations amount to a half step of quantization and cause a superimposed disturbance signal with random amplitude distribution. This problem is called “noise of quantization”.

A further problem that may arise is that associated with the round-off error through calculation. In situations where the detection of weak components is required, it may be more appropriate to separate and classify all possible sought waveforms, before performing any kind of filtering or smoothing operation on the signal. If this is not carried out beforehand, the weak components of the signal that need to be identified may be eliminated, particularly when applying an average to a signal with very weak components, embedded in high-level noise. This would be likely to occur because the quantization and round-off errors, through the averaging process, may eliminate the little difference there is between those signals which have weak components and those which do not.

1.5.2. Basic Techniques for Noise Filtering

A basic technique used for noise filtering is based on a time-averaging procedure. It is important to point out that with this technique, if the correct phase synchronisation is not carried out, the specific component that is being sought will be eliminated. Furthermore, when one attempts to analyse the whole spectrum signature, it is necessary to perform a phase synchronisation for each component present in the signal, and this may be rather impractical [Bendat and Piersol, 1986]. According to Bendat and Piersol, this procedure is also problematic when applied to signals with non-stationary components present, as they can generate severely distorted results. This is the case of the petroleum wellhead vibration, which includes components caused by fluid slug vibration. In these situations, Bendat and Piersol argue that there may be a strong temptation in analysing non-stationary data to treat it as if the data were a sample record from a stationary random process. In certain special cases of non-stationary data parameters, time-averaging analysis procedures can produce meaningful results. For the case of probability density functions, however, time-averaging procedures will generally produce severely distorted results. In particular, the probability density function computed by time-averaging data with a non-stationary mean square value will tend to exaggerate the probability density of low and high amplitude values at the expense of intermediate values.

Another technique used for filtering noise is the autocorrelation method. However, a problem with the autocorrelation method is described in the work of To and Ewins [1990], where attention has been drawn to the effects of noise and leakage on estimators of Frequency Response Functions (FRF). The study shows that the leakage problem for auto and cross-spectra emerges during the processing of finite data records and, as a result, it is difficult to specify which FRF estimator will produce the best estimate of FRF. Furthermore, attempts to apply the autocorrelation method to filter signals containing strong noise have not produced satisfactory results because

this method tends to eliminate the weak components through its calculations [Ribeiro, 1991].

A further limitation with the autocorrelation computation is that the phase information is lost and a damping applied to the resulting data. However, as reported in the works of Cappellini et al [1978] and Dyne [1995], it is possible to use matched filters, which are defined as filters that have an impulse response equal to a time-reversed form of the transient that it aims to detect. The response of the filter to a noiseless copy of the transient is therefore the autocorrelation function of the transient. However, problems are expected with this technique, as it is necessary to know a priori some information about the component to be detected in signals containing high-levels of noise and non-stationary processes.

1.5.3. Recent Developments in Noise Filtering Techniques

Of the most recent works that focus on noise filtering, none address the problem of signals containing such strong spurious components as are to be dealt with in this study. Nevertheless, the most useful include those on the Kalman technique [Noriega and Pasupathy, 1992, Rousseax and Troquet, 1986, Pitarque et al, 1991, Gibson et al, 1975], time-frequency [Womack and Cruz, 1994], the maximum likelihood estimator [Cerrato and Eisenstein, 1977], non-linear [Servière and Baudois, 1995], and autoregressive [Hsu and Giordano, 1977] filtering techniques.

In one of the first relevant works about the Kalman filter, Gibson et al [1975] applied this technique for sequentially identifying predictor coefficients in digital speech analysis. They demonstrate that a Kalman filter-based computer routine is feasible and closely related to the autocorrelation and the covariance methods. The level of Gaussian noise applied to the signal to test the algorithm in a voiced/unvoiced

decision was very low (1/100 times of the component to be detected, SNR 40 dB) and was correlated to the level of the background noise. The results show that the speech filtering quality was degraded if the low-level noise is applied. One advantage of the algorithm based on the Kalman filter developed by Gibson et al [1975] is the capacity of this algorithm for multi-channel analysis; that is, it is appropriate to analyse data collected from several sources. In another work of Kalman filtering, Rousseax and Troquet [1986] applied deconvolution of the intracavitary ventricle's pressure through Kalman filtering to model the heart muscle. The main advantage of their method is the capacity of applying the deconvolution for both time-invariant and time-varying systems through the Kalman filter. The authors did not state the level of Gaussian white noise added to signals collected in the experiments. In the work of Pitarque et al [1991] is presented an algorithm based on the Kalman filter to retrieve sinusoidal frequencies from noisy data. An interesting feature of this algorithm is that it establishes a connection between a state-space formulation and the Pisarenko decomposition. The SNR of Gaussian noise applied in the Pitarque et al experiments was -12 dB (4 times the level of the components to be detected). The main conclusion of their work is that the Kalman filter can be applied directly to the raw data instead of applying to the autocorrelation sequence. In a more recent work about Kalman filtering, Noriega and Pasupathy [1992] propose an algorithm based on a fixed-lag Kalman filter approach for automatic pre-processing time data-sequence in real-time. This algorithm involves a model which uses a state vector that consists of the signal, its first three differences, and a special variable used to implement data editing functions. Two versions of the algorithm were developed, the first based on the conventional form of Kalman filter, and the second one using a sequential processing technique. In the simulations with real data, collected from an electromagnetic airborne survey flown over the Bourget area in Quebec, Canada, the authors added a white Gaussian noise with an amplitude 1/3 (SNR 9.5 dB) of the components to be detected and achieved satisfactory results in their signal filtering analysis.

In the study by Womack and Cruz [1994] on time-frequency noise filtering, the authors analyse seismic data using two techniques: the Gabor representation and the singular value decomposition (SVD). The results of the analysis of synthetic data indicate that the Gabor representation can outperform the SVD technique. The level of the Gaussian white noise used in the simulation was set to 1/4 (SNR 12 dB) of the component to be detected.

In an application of the maximum likelihood estimator, Cerrato and Eisenstein [1977] developed two algorithms for applying the deconvolution in a signal with components embedded in noise. However, only theoretical formulations are presented in their work and no signal is provided to test their algorithm.

Servière and Baudois [1995] propose to estimate frequency spectra of noisy signals through non-linear functions of the observations. The objective is to estimate the frequency spectra of two linear filters that combine signals collected from two different sources. No assumptions regarding the statistical distribution of the noise are made in their work. The non-linearity is represented as an exponential real function which can be separated into a product of functions. This allows the separation from, firstly, the terms containing the sources and, secondly, the terms containing the noisy signals. The results of the simulation show that the number of samples depends on the SNR. The authors argue that 2000 signal samples are necessary for analysing signals with 5 dB SNR (noise level 0.56 times the component amplitude level), and 3500 signal samples are necessary for analysing signal with 0 dB (noise level equal the component amplitude level). No information about the data sampling conditions are given.

There have been a number of studies that focus on underwater noise reduction and, of these, the majority of the signals are collected by means of a large number of sensors in an

array for the purpose of source detection (radar), where the noise is theoretically modelled. These include works by Finette et al.[1993], Collins et al [1994], and Quinquis and Rossignol [1996].

In Finette et al [1993], the focus is on source signature extraction in an ocean environment. The main technique used for source extraction is the deconvolution through Green's functions as matched filters. This technique involves a multi-dimensional data collection procedure through several sensors and is not viable to be applied in the case of data collecting from sensors installed in the one-dimensional petroleum wellhead data collection condition. The conclusion of this work is that source signatures were extracted in a noisy multi-path environment for low SNR sources. The SNR considered for signature source extraction is estimated to vary between 0-3 dB. A drawback of this technique is that it is necessary to know in advance of the source signature to be detected.

In another research on underwater signals, Collins et al [1994] present a variation of a noise-cancellation processor based on the Bartlett processor. A substitution of the noise model time series for covariances is proposed. To test this method, noisy data were collected from an array of 13 sensors (hydrophones) placed at a depth of 400 m in the sea. The aim was for the processing signal technique to detect a 25 Hz source located at an unknown ocean location. The processed signal contained a high-level noise (SNR -20 dB). The results of the experimental analysis of the data showed that the proposed noise-cancelling technique was able to filter the high-level noise present in the signal. However, as in the work of Finette et al [1993], this technique requires a number of sensors multi-dimensionally placed, as well as the necessity to know in advance the composition of the source signal to be detected, which is not possible in the case when analysing an ESP from vibrations transmitted through the production pipe and collected in the wellhead, and for this reason it will not be considered further in this study.

In a more recent work about underwater signals, Quinquis and Rossignol [1996] present an interesting filtering technique based on the Malat wavelet transform. The level of noise present in the analysis of experimental signal was very high (SNR -50 dB). However, this technique involves a prior knowledge of the noise data composition for transformation into a wavelet orthogonal domain. To accomplish the noise filtering, four correlated observations are necessary, one for the signal with noise, and three with pure noise. This is not possible in the case of ESP analysis because the noise generation condition in a petroleum platform is not stable. The problem of handling non-stationary noise was reported by the authors, who concluded that development is still necessary to improve this technique for these filtering conditions.

1.5.4. Singular Value Decomposition and Autoregressive Techniques for Filtering Noise

Developments in noise filtering autoregressive techniques have been made by Hsu and Giordano [1977]. In this study, the authors developed an autoregressive algorithm to identify components of signals with time-varying spectra in the presence of noise and signal interferences. Power spectral estimation is accomplished using several autoregressive spectral estimators (Yule-Walker, maximum entropy, and the gradient linear prediction methods) as well as by the conventional Fourier transform. The maximum amplitude of the noise added to the signals was equal to the amplitude of the components to be detected (SNR 0 dB). However, the authors do not specify the statistical assumptions of the noise utilised in the simulation.

In the work of Liu [1996], the state space method is applied through a singular value decomposition (SVD) for noise cancelling. At the heart of this technique is the eigendecomposition of the autocorrelation matrix in signal and noise subspaces. A criterion, which is correlated to the signal subspace, was developed to define the lowest matrix rank. This sets the order to be utilised in the method's calculations. In Liu's study, a

comparison is made between the state space method, through the singular value decomposition (SVD), and the original Prony technique. Liu considered the original Prony technique to be less effective than the SVD for noise filtering. However, it may be argued that in Liu's work, it was incorrect to use the same order to execute the Prony exponential evaluation as that defined in the SVD evaluation, as this results in a misleading comparison between the two methods. The separation of two subspaces in the SVD reduces the order of the method due the generation of ill-conditioned signal subspace matrices. As a consequence, a low order, associated with the signal subspace matrices, is set to perform the SVD method calculations. On the other hand, the original Prony technique "seeks" exponentials in one matrix containing both components and noise data. In this case, it is necessary to use higher orders to represent all components in the signal, including those associated with noise. As a consequence, it may be argued that the signal with white noise, used to compare both techniques (SNR 3 dB) in Liu's work, should be analysed through the original Prony technique with a much higher order than that set to perform the SVD method.

To conclude this section on noise filtering, it would appear that existing techniques are inadequate for filtering out weak components in signals where both noise and non-stationary processes are present. Firstly, to analyse vibrations signals in the presence of high-level noise requires a large quantity of data for statistical averaging in the filtering process, which could lead to the weak component being filtered out. Secondly, also present in the signal are strong non-stationary processes that corrupt the signal. However, if one applies existing techniques of non-stationary analysis for filtering purposes, short lengths of data are required for a better representation of the local variations in the signal, is not consistent with the use of large quantity of data points in the statistical averaging and Fourier transform techniques. An attempt to seek a technique that can filter out strong spurious components through non-stationary analysis is the subject of the next section.

1.5.5. Techniques for Non-Stationary Analysis

As mentioned above, the majority of signal analysis has been restricted to the measurement of stationary random data. The theoretical ideas, error formulas, and processing techniques do not generally apply when the data are non-stationary [Bendat and Piersol, 1986]. However, although much of the random data of interest in practice are non-stationary when viewed as a whole, it is nevertheless often possible to constraint data to be at least stationary for measurement and analytical purposes. Procedures to set non-stationary conditions to stationary ones are commonly used. One, for example, is to analyse part of the signal in which a specific set of conditions, such as standard variation and variance, are fixed, and then to change these conditions for the subsequent parts of the signal, until the entire signal has been represented in adequate detail by piecewise stationary segments. However, there are a number of situations where this approach to data collection and analysis does not make it feasible, and individual samples of data must be analysed as non-stationary data. A common situation is that in which the non-stationary phenomenon of interest is unique and cannot be repeated under some statistical restrictions. Examples include ocean waves, atmospheric turbulence, and economic time-series data. The basic factors producing such data are too complex to allow the performance of repeated experiments under similar conditions. The analysis of data in these cases must be accomplished by calculations on single sample records as they involve non-stationary components [Bendat and Piersol, 1986].

Non-stationary processes do not possess an ordinary spectral density because they have a time-dependent covariance structure. These covariance structures describe the evolution of the second-order properties of the process. In the very special case of weak stationary processes, the second-order properties can be successfully represented in the frequency domain by ordinary spectral densities. The definition

of a "time-varying spectrum" therefore can be considered as a natural generalisation of the idea of a spectrum, but additionally exhibiting the time-dependent changes of the second-order structure of the process. It should be noted that changes of this structure are not necessarily given alone by changes of the mean power of the process. In particular, if one deals with non-stationary processes possessing a slow evolution time of second order structure ("quasi-stationary"), the time-varying spectrum will exhibit different times of stationarity within different frequency bands [Martin and Flandrin, 1985].

The method most often adopted in the vibration analysis of equipment is based on frequency spectra. Analysis using this method has dramatically improved since the development of the fast Fourier transform algorithm (FFT) in 1965. Since then, the Fourier transform, with the associated concepts of convolution and correlation, have been used extensively in signal processing [Bendat and Piersol, 1986, Braun, 1986, Randall, 1980, Price, 1988, Bruel & Kjaer, Mechefske and Mathew, 1992a, 1992b, 1993 and 1995, Powell, 1992, Flashpohler, 1994, Lee and Joh, 1994, Delzingaro and Mathews, 1995]. Whereas the Fourier series allows a periodic function to be represented as an infinite sum of harmonic oscillations at definite frequencies equal to the multiples of the fundamental, the Fourier transform allows a non-periodic function to be expressed as an integral sum over a continuous range of frequencies [Champney, 1973]. However, care has to be taken when applying the Fourier transform to non-stationary processes, as this technique may lead to incorrect results through its calculation [Bendat and Piersol, 1986]. In these cases, the energy spectrum of the standard Fourier transform does not tell us when a non-stationary event occurred. There exist natural and man-made signals whose spectral content is changing so rapidly that finding an appropriate short-time window is problematic since there may not be any time interval for which the signal is more or less stationary [Cohen, 1989].

Normally, the non-stationary processes are depicted by what is known as “time-frequency representation” techniques. The basic feature behind these techniques is the “time-frequency plane”, which is the conjunction of the time and frequency domain signal representations. The graph of Figure 1.6 shows the different directions to “view” the time and frequency domain description of a signal and its respective “time-frequency feature” analysis. The graph shows a signal with four components: two stationary sine waves with frequencies 24 and 80 Hz, a transient (48 Hz) and a non-stationary (32 Hz) component. The signal shown in the graph 1.6 (a) is decomposed and two different views of its components are shown: the frequency domain view (1.6 (b)) and the time-frequency domain view (1.6 (c)), which will be the referred from now on as “time-frequency plane”. The time-frequency plane represents the “component energy distribution or intensity” of a signal, and what should be mainly noted in a time-frequency plot is the way in which the points are distributed in the plane to determine whether a component exists or not.

The non-stationary analysis motivation started with the necessity to analyse human speech. Classic works of Gabor [1946], Ville [1948] and Page [1952], have been developed as an alternative for the varying spectra. The basic idea is to devise a joint function of time and frequency, a distribution that will describe the energy density or intensity of a signal simultaneously in time and frequency. In an ideal case, such a joint distribution would be used and manipulated in the same manner as any density function of more than one variable. Many divergent attitudes towards the meaning, interpretation, and use of these distributions have arisen over the years, ranging from the attempt to describe a time-varying spectrum to merely using them as carrying the information of a signal in a convenient way [Cohen, 1989].

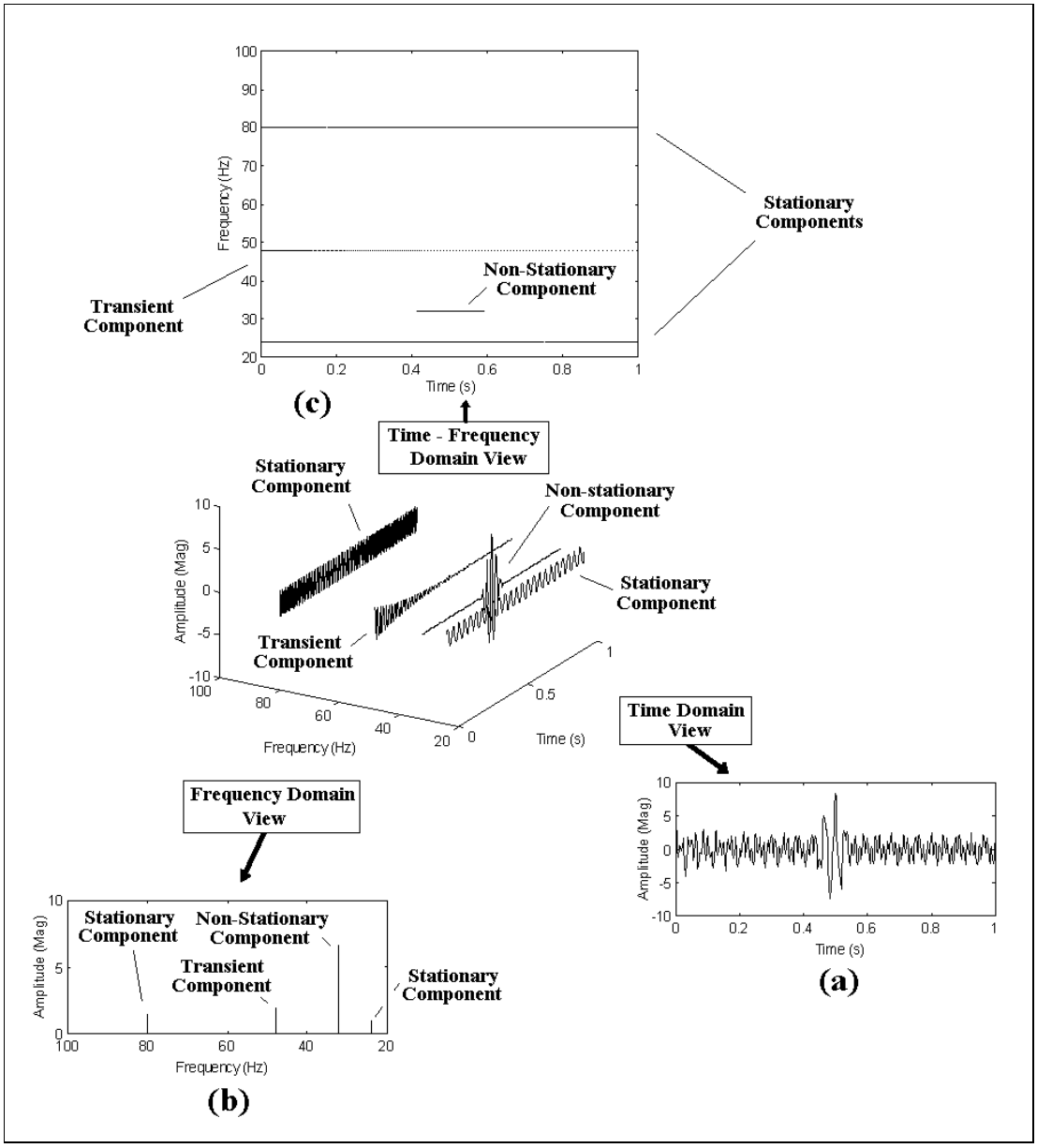

Fig. 1.6 - Different time frequency domain views

In a stationary process the ensemble averages are independent of the time ***t***. If, in addition, the process is ergodic, then any other sample function is completely representative of the process as a whole. For non-stationary analysis, a general assumption on which several signal processing methods are based, including for example the short-time Fourier transform (STFT), is the so-called locally-stationary process. In techniques which are based on this assumption, a short data window centred at time ***t*** and spectral coefficients are calculated for a short length of data.

However, there is a fundamental problem with this approach, in that high-resolution cannot be obtained simultaneously in both the time and the frequency domains [Newland, 1993]. Two additional techniques which have also been developed for non-stationary analysis, the Wigner-Ville distribution and the wavelet transform, are described in the next section.

1.5.6. Wigner-Ville Distribution and Wavelet Transform

The methods considered to be most suitable for the analysis of non-stationary processes include: the wavelet transform (Morlet and Malat techniques,); and the pseudo-Wigner-Ville distribution. New developments in non-stationary analysis using these techniques can be found in the works of Bonaldo [1993], Newland, [1993] Flandrin [1985, 1989], Moss and Hammond [1994]. For example, new algorithms to perform the wavelet transform, which improves the speed of the calculations, have been developed by Newland [1993] (Malat wavelet), and Bonaldo [1993] (Morlet wavelet). In Cohen [1989], Flandrin et al [1985], and Flandrin [1989], time-frequency windows are applied to the Wigner-Ville distribution calculations in order to reduce the appearance of cross-terms that normally appear in this distribution, which results in a "smoothed" version of this distribution called the pseudo-Wigner-Ville distribution. In a further development, Moss and Hammond [1994] applied Kondera's modification to reduce the spread in frequency caused by the lag time window and thereby to improve the resolution of this distribution. However, the authors point out that when applying this modification in multi-component analysis, a priori information is needed about the signal.

Spectral analysis of non-stationary processes has attracted much attention since the Wigner-Ville distribution has been applied for signal processing. It has been shown

that a wide class of random processes with second-order non-stationary properties, possess a Wigner-Ville spectrum [Cohen, 1989]. The Wigner-Ville method, which is based on a concept of instantaneous ensemble average correlation functions, is a straightforward option for analysing non-stationary processes. As with the STFT, the data window is also centred at a time ***t*** but it has been adapted to shift a sliding window through the data sample.

Although these recently-developed techniques are well suited for non-stationary analysis, it is argued here that they are not adequate to detect deterministic components embedded in signals with high-levels of noise. For instance, a major drawback of the Wigner-Ville distribution, reported by Cohen [1989], is that this distribution propagates noise. It has been shown that if there is noise present in a small section of the signal, it will appear again within the distribution. This effect is a general property of the Wigner-Ville distribution, and is related to the interference caused by cross-terms, which appear when the cross-correlation of the two signals is non-zero. In this case part of the data of one shift are repeated in the following one, causing redundant information. Another drawback of the Wigner-Ville distribution is the fact that negative amplitude values may be obtained in the results. To reduce these problems, windows can be applied in the time and frequency domains, and it is then renamed the “pseudo-Wigner-Ville” distribution. However, this window operation on the pseudo-Wigner-Ville distribution, also known as smoothing and which forces the distribution to generate positive values, causes a loss of phase information [Cohen, 1989].

In order to overcome the limitations of the Wigner-Ville and the pseudo-Wigner-Ville distributions, alternative families of orthogonal basis functions called wavelets have been attempted. The localised nature of wavelets makes them an effective tool in the analysis of vibration signals, but the use of wavelets for machinery monitoring is not as straightforward as Fourier analysis. Wavelets can be used to compare several

signals only if each signal starts at the same position in time or space, which is a difficult condition to fulfil in signal processing. Even when related to the same signal, different wavelets cannot be used for comparison because it is impossible to be sure whether any change in the wavelet domain is due to a shift in the location of the signal. Therefore, each data set must be re-positioned to the same point in time or space before it is transformed to the wavelet domain. This can be done through a simple pulse to identify a specific point in the machine cycle [O'Brien and MacIntyre, 1994], but the problem with this procedure is that it is not feasible for all types of equipment. In the case of petroleum submersible pumps, a pulse signal would have to be generated by the pump through a delicate electronic instrument that would have to be installed downhole in the petroleum well, which given the conditions of the installation and the environment, do not make this a realistic possibility.

A further important limitation associated with the wavelet technique is that the frequency is logarithmically scaled and, as a result, low resolution is obtained at higher frequencies [Barschdorf and Femmer, 1995]. In fact, there is a fundamental principle (Uncertainty Principle) for time-dependent spectra which makes it impossible for the wavelet transform, to achieve high-resolution in time and frequency simultaneously. For when high resolution is necessary to detect a weak component in the time-frequency plane, this method will usually present amplitude peak leakage through its computations, due to the use of the discrete Fourier transform, which is limited by the Uncertainty Principle [Newland, 1993]. Given the limitations of the Wigner-Ville distribution and wavelet transform methods for the purpose of this study, the autoregressive parametric spectral estimation method (AR) will be considered next.

1.5.7. Autoregressive Techniques

There is much written material about the autoregressive parametric spectral estimation method (AR) method, but less empirical experimentation. The main feature of this method is its capacity to obtain high spectral resolution with short data sets. Mechefske and Mathew [1992a, 1993] compared the Fourier transform with the autoregressive method in a study that sought to detect and diagnose faults in low-speed rolling element bearings. When they applied the Fourier transform method, they found that a lengthy data set was necessary. This was because standard velocity and accelerometer measurement transducers are generally insensitive at low frequencies, therefore, an adequate data sample is required to compensate for this insensitivity. However, the authors found that this is not the case with the AR method because it only needs short data lengths to analyse signals, which resulted in a successful fault diagnosis.

Mechefske and Mathew argue that between 30000 to 50000 data points are required, depending on the amount of noise present in the signal, and collecting this amount of data from rapidly rotating machinery is not a problem. A high sampling rate may be used to collect the data in a relatively short time. Longer sampling times are required for low-speed bearings in order to analyse the low frequency bandwidths of interest. One of the advantages of the model-based approach to spectral estimation of AR techniques is that a higher resolution is achievable with these techniques than with traditional Fourier transform based techniques, especially for short data sets. The extended sample times required to achieve acceptable frequency spectra has resulted in the Fourier transform method being deemed impractical for monitoring low-speed rolling element bearings. The study made by Mechefske and Mathew shows that only the AR spectral estimate revealed a clear difference between a defective bearing and a good bearing.

In a study by Mars et al [1992], based on previous work by Martin [1986], the AR method was extended to a time-frequency representation. In this study into non-

stationary signals, a time-frequency representation was generated through a time-shifting operation. The authors developed a hybrid technique combining a high-frequency resolution estimator (autoregressive method on a sliding window) with a power estimator (maximum likelihood method). This technique was successfully applied to simulated seismic signals, with AR order 6 and considering a SNR of 20 dB. However, the AR technique may give rise to problems as it is based on the assumption that the unavailable data outside the window are not zero [Marple, 1986], and this does not hold true in non-stationary analysis. Also, the SNR considered in Mars et al [1992] simulation was more favourable than the proposed in this study (SNR -34 dB).

1.5.8. The Original Prony Method

As we have seen above, the autoregressive technique is not suited for non-stationary analysis, primarily due the assumption that the unavailable data outside the window are not zero. It is therefore necessary to consider a method which is not limited by this assumption, and which is able to seek out transient components (short time duration components). Non-stationary processes will now be considered as a special type of transient, and the method arguably most suitable to analyse transient components is the original Prony technique. For example in Poggio and Blaricum's [1978] study, an evaluation of transient data was made by the use of the original Prony method. In that study the original Prony method was applied to analyse the impulse response of a double exponential excited circuit in a synthesised network. The results show that the original Prony method is useful to determine complex natural resonances and complex amplitudes associated with exponential representation of waveforms.

According to Marple [1982], if the process undergoing spectrum analysis consists of an unknown number of sinusoids embedded in additive noise, a better spectral performance can be obtained by methods that produce spectral line estimates in which

the original Prony method is included. The original Prony method is a technique for modelling sampled data as a linear combination of exponentials. This method has the capacity to seek out weak components in high level noise and to generate high resolution frequency scales [Marple, 1987, Ribeiro, 1991]. Another significant advantage is that the original Prony technique evaluates the exponential damping and the phase for each component sought, and this can be used for filtering purposes. Normally, a deterministic component presents no amplitude decay along the time axis, and this is shown by the very low exponential damping values obtained using the original Prony technique. Thus, deterministic component selection can be made due to the low exponential damping values calculated by the original Prony method, to the detriment of the transient ones (noise and non-stationary components) which present high exponential damping values. A further positive feature of the original Prony technique is that it brings together high-resolution analysis with limited signal data, and in doing so, a better "instantaneous" representation of the stationary and non-stationary components can be obtained. This is achieved by utilising short data lengths in its calculations, which facilitates the representation of short length duration phenomena in a signal. The signal can then be represented by several short length data samples in order to obtain a better description of non-stationarities, arguably an ideal condition for non-stationary analysis.

However, previous research has found the original Prony method to be unsatisfactory when applied to signals with noise. Bucker [1977] found in a comparative study using the original Prony method and the Fourier transform, applied for bearing estimation from narrow-band signals in a realistic ocean environment, that the Fourier transform worked better in the presence of noise. Also, according to Poggio and Blaricum's study [1978], the original Prony method was shown to have problems in the areas of rank deficiency, aliasing, and noise effects. But it should be pointed that in these cases, the original Prony method used was an old version. It did not include new developments to the method made around 1981 such as applying least-squares fitting and covariance incorporated in the first step of the technique's calculations. One

possible way to overcome the above problems is to apply a very efficient algorithm for the calculations in the original Prony method.

An attempt was made by Ribeiro [1991] to apply the original Prony method in an empirical study in a petroleum platform wellhead. In a comparative study of the original Prony method and the Fourier transform technique, the study sought to analyse vibrations generated from an ESP installed downhole in the well, and transmitted through the pipe from a depth of 1000 meters. Figure 1.7 shows vibration data being collected from a land petroleum wellhead and Figure 1.8 shows vibratory data being collected from a petroleum wellhead of a sea platform manifold. Figures 1.9 and 1.10 show schematic diagrams representing a land petroleum wellhead and petroleum wellhead of sea platform vibratory data collection respectively.

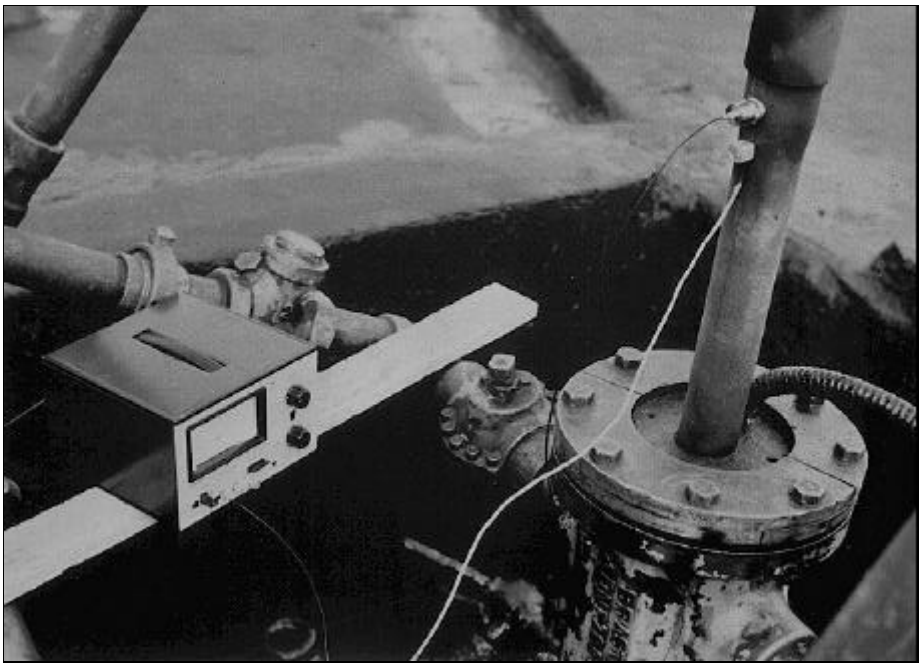

Fig. 1.7 - Vibratory data collection on a petroleum wellhead

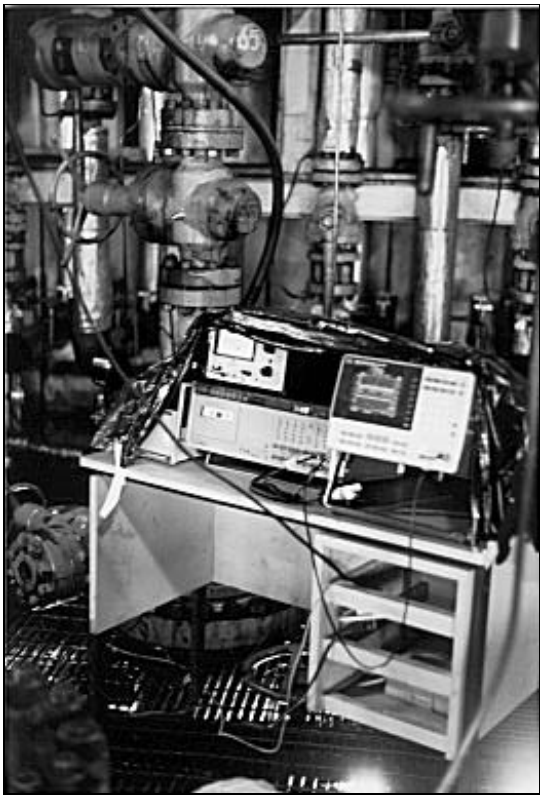

Fig. 1.8 - Vibratory data collection on a petroleum wellhead of a sea platform manifold

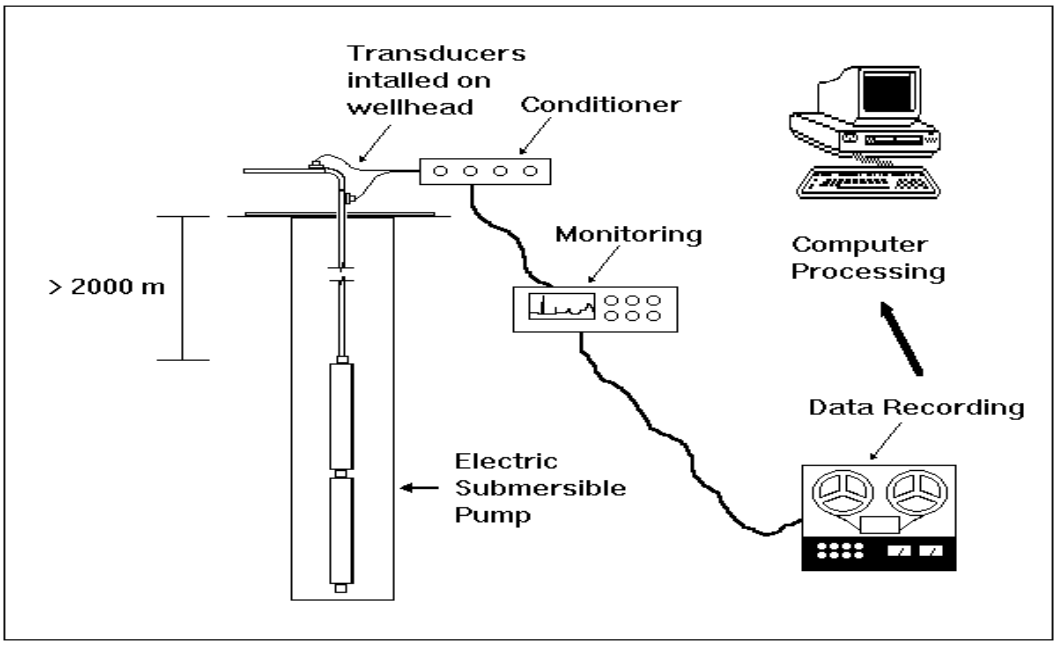

Fig. 1.9 - Schematic diagram of a land petroleum wellhead ESP vibration signal collecting and processing

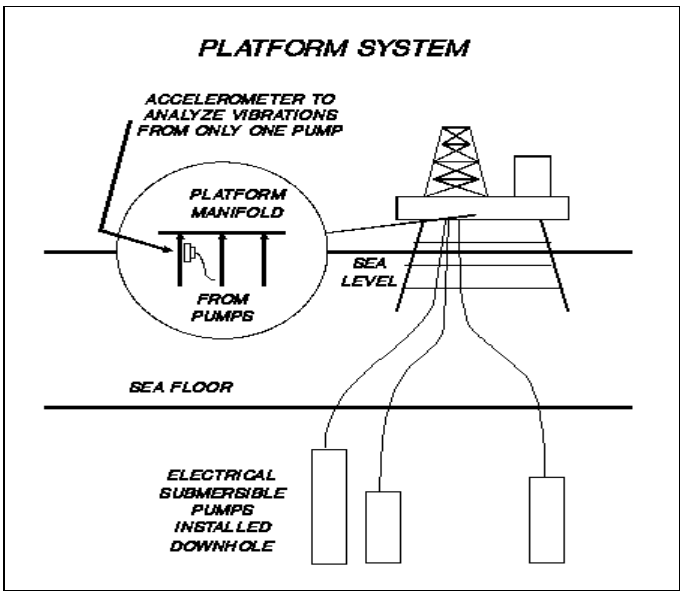

Fig. 1.10 - ESP vibration signal collecting in a petroleum wellhead of a sea platform

To gather the data in a petroleum wellhead on a sea platform, an accelerometer was fixed on the tubing, 1 meter below and perpendicular to the main pipe line, as shown in Figure 1.11.

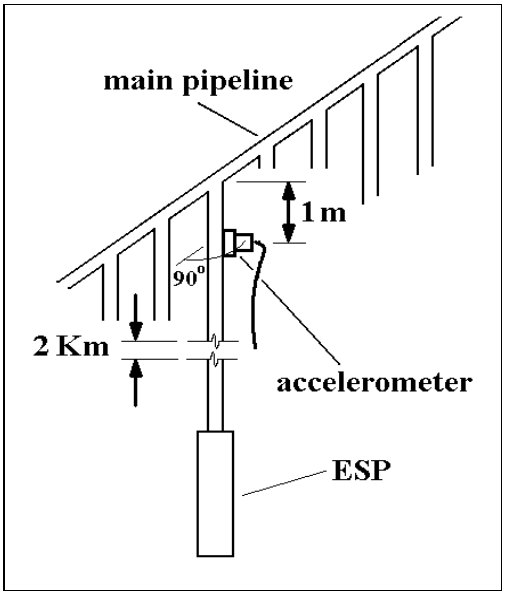

Fig. 1.11 - Location of an accelerometer in a petroleum wellhead on a sea platform for vibration data collection

The research findings revealed that the signal collected in the platform wellhead contained a lot of spurious components, whose amplitudes could reach 100 times the component to be measured and analysed. These include platform environmental noise, and fluid slugs. Figure 1.12 shows a typical signal that was collected on the wellhead number 65 of the Vermelho Platform in Campos Basin, Brazil. In the graph, strong modulations in the signal due to flow turbulence can be seen.

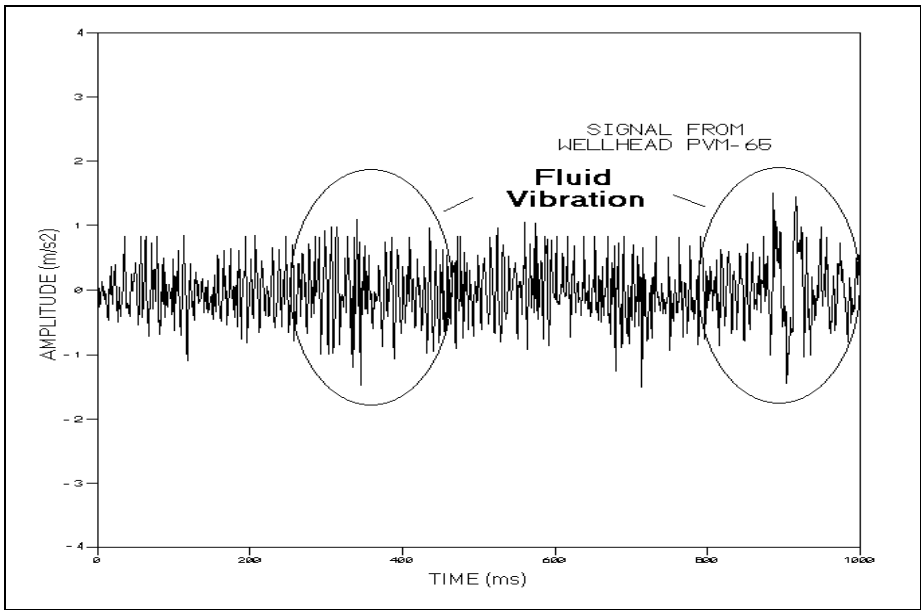

Fig. 1.12 - A real signal collected on a petroleum wellhead sea platform

The frequency range from 0 to 200 Hz was selected for analysis of the resulting signal with particular attention given to two components: (i) the pump rotational frequency (58 Hz) and (ii) the electrical supply frequency (60 Hz).

The results showed that when the Fourier transform method is applied to the signal, strong components will hide the weak signals generated by the ESP. In Figure 1.13 a graph is shown with the results of applying the Fourier transform to the signal.

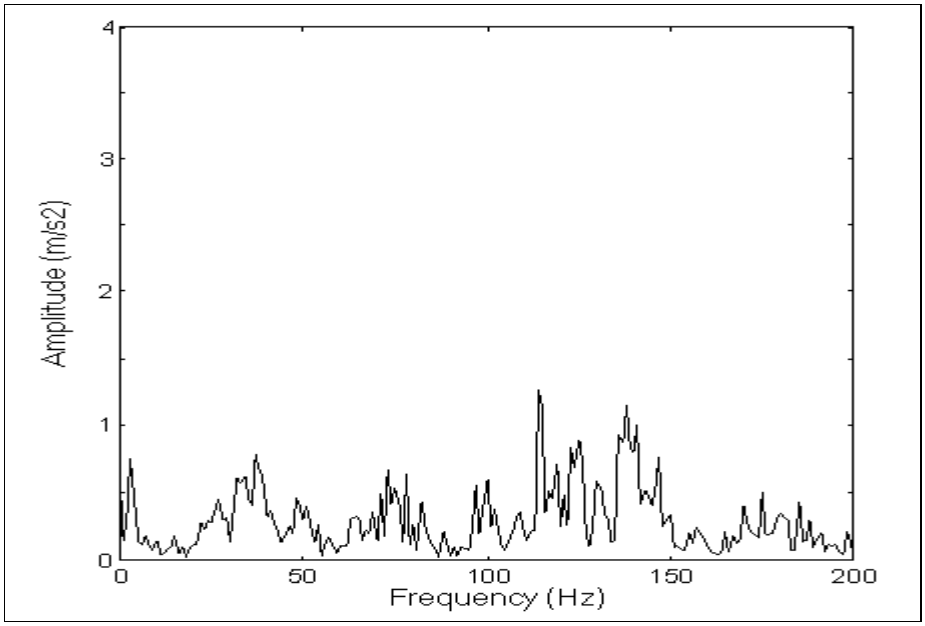

Fig. 1.13 - Fourier transform of the signal from platform of Vermelho

It can be seen that there is effectively no discrimination between the rotation (58 Hz) and electrical (60 Hz) frequencies. Another drawback associated with this method is the difficulty in handling the non-stationary components generated by fluid vibrations (fluid slugs). The Fourier transform and short Fourier transform methods do not detect clearly deterministic components in the presence of noise and non-stationary processes. A higher sampling rate, larger quantity of data, and longer time average may be required in order to improve the resolution and to detect the weak components in the high-level noise, but this is rather impractical in many situations. A further problem was encountered when performing data averaging, in that the results of the analysis were distorted, which may be due to the presence of non-stationary components. Also, the ESP rotation frequency desired to monitor may be varying due to the variable fluid load that the pump is subjected, which represents a further difficulty for analysing this component through the Fourier transform.

The components sought by the original Prony method in the signal are generally complex exponentials, which not only carry information of the frequency, but also of

its phase and exponential damping values that are useful for filtering purposes [Ribeiro, 1991]. The original Prony method was used in the analysis of the signal collected on the manifold of the Platform of Vermelho due to its capacity of obtaining high-resolution with few data samples, and its capacity of evaluating the component exponential damping for filtering purposes. The aim was to obtain a good discrimination of any exponential peak fitted by the method, including the weak ones that are hidden by the strong components, and to filter out the spurious ones through a "exponential damping selectivity".

The fact that some low exponential damping values, associated with specific non-transient components, were obtained by the original Prony method demonstrates that this technique is potentially useful for filtering purposes. See, for example, the exponential damping value obtained for the 57.15 Hz component (-0.004) compared with the one obtained for the 47.77 Hz component (-0.1) in the table reproduced in Appendix A. This means that the 47.77 Hz component is more "transient" than the 57.15 Hz, which may suggest that the latter presents a more deterministic behaviour than the 47.77 Hz. However, in spite of this result, it is not sufficient evidence to assume that this deterministic behaviour is associated with the ESP's vibration. The ESP rotation vibratory component, possibly associated with 57.15 Hz, seem to be still heavily damped and no estimate about the noise level is available.

The results of this attempt into ESP spectral analysis, show that the original Prony method may detect the rotation (58 Hz) and the electrical (60 Hz) frequencies of the ESP equipment. (See table in Appendix A, values of lines 12^{th} and 13^{th}). However, the findings also suggest that for our purposes, it is still necessary to develop the original Prony method further.

The results of the above study give rise to the following questions:

(i) is it possible to use the exponential damping values calculated by the original Prony technique to filter out the spurious components present in the signal?

(ii) to what extent do vibrations generated by other sources near the transducer (such as platform environmental noise and fluid slugs) conceal the pump's vibration signal, now weakened due to the damping loss effect caused in its transmission through the petroleum pipe?

In the above discussion, the difficulties involved in searching for an adequate signal processing technique to filter out noise and non-stationary processes present in the signal, and thereafter able to detect weak components for fault detection purposes, have been demonstrated. The basic problem areas which an adequate signal processing technique will have to overcome, given the particular nature of the signal we seek to analyse, have been outlined as have the limitations of the existing techniques. It is apparent, therefore, that after reviewing the available literature, an adequate signal processing method which is able to detect weak components embedded in both high level noise and non-stationary conditions is not available.

What has been shown is that, although the original Prony method is potentially more advantageous than the Fourier transform method, due to its capacity for filtering out noise, in its present form it is still inadequate for handling non-stationary conditions. An attempt will therefore be made to overcome this problem by considering non-stationary processes as special types of transients, to which, it is agreed, the original Prony technique is well suited [Marple, 1986]. However, for this to succeed the original Prony method has to be extended to generate a time-frequency representation. Any system not in a steady state can be said to be in a transient state, which includes damped stationary conditions and non-stationary conditions [Meirovitch, 1967]. What differentiates both conditions is the parameter variation degree of freedom. In the case of wide non-stationary conditions, all parameters that

govern the process may vary in time (mean, variance, standard deviation, kurtosis etc). In the transients considered for original Prony technique detection, only the amplitude of damped components is allowed to vary in time. As a consequence, some distortions may be expected in the original Prony method's calculations due to other parameter variation, as for example, the variation in the component frequency values.

It has been argued above that the Wigner-Ville distribution, which does generate time-frequency representations, is severely limited for the purposes of this study due to noise propagation and the amplitude peak leakages that appear when the Fourier transform is applied through its computations. It has also been argued, that the wavelet transform, which also generates time-frequency representations, presents difficulties when analysing signals that start at a different positions in time or space and that contains relevant high-frequency components. Therefore, at this stage the possibility of adapting the original Prony method will be examined, in order to seek a viable alternative to existing signal processing techniques for the analysis of the ESP signals.

1.6. Towards an Extension of an Existing Signal Processing Technique

It has been demonstrated above that most existing methods are unable to deal with signals containing high levels of noise and non-stationary components. Therefore, as the main objective of this research is to develop a signal processing technique that is able to filter out strong spurious components, whilst retaining the weak ones, an attempt will be made to filter out the non-stationary conditions and noise by considering them as transients. However, to achieve this it is necessary to adapt the original Prony method to generate time-frequency representations, in much the same way as they are generated in the Morlet wavelet transform and Wigner-Ville

distribution methods, in which "sliding" windows are applied to the signal in the time domain.

The main advantages in extending the original Prony method are as follows:

(a) It needs short lengths of data to perform its calculations, a feature which is necessary for better local non-stationarities detection.

(b) It generates high-resolution graphs with short data lengths, which is useful when it is not practical to collect large quantities of data.

(c) It represents transients which are useful for an approximate representation of non-stationary components.

(d) It provides the component exponential damping information which can be used for filtering purposes.

However, it is expected that problems will be encountered with the method to the extent that (i) it may present instabilities in its calculations due to the nature of polynomial and matrix evaluations; and (ii) it may need more computational effort for its calculations than the Wigner-Ville distribution and the wavelet transform techniques.

In the course of developing a new approach to analyse equipment through remote accelerometers, a number of research tasks need to be undertaken in the area of signal processing. These include:

(a) the extended Prony time-frequency representation will be tested in a comparative simulation study with the wavelet transform, the Wigner-Ville distribution and pseudo-Wigner-Ville distribution techniques. These methods will be compared

and contrasted in how they handle signals embedded in high-level noise with non-stationary components (see Chapters 2 and 3);

(b) test and empirical validation of the extended theoretical formulations. For this purpose, experimental data will be generated on a rig that is constructed to replicate, as far as possible given the restraints of this research programme, a petroleum well (see Chapter 4).

1.7. Scope and Structure of the Thesis

The remaining Chapters of this thesis have been organised in the following way: theoretical background; simulation, experimental analysis; discussion, conclusions and new research directions. The theoretical material (Chapter 2) provides the mathematical foundation for the simulation and experimental analysis (Chapters 3 and 4), which in turn provide the basis for the discussion and the conclusions in Chapters 5 and 6. Figure 1.15 shows a diagram of the structure of this thesis.

The methods for signal processing are presented in Chapter 2. Non-stationary signal processing analysis is fully explained, together with the way the original Prony technique is extended to analyse on a time-frequency plane basis, as in the pseudo-Wigner-Ville distribution or in the wavelet techniques.

In Chapter 3, several simulations using the methods developed for signal processing are presented, and some conclusions discussed.

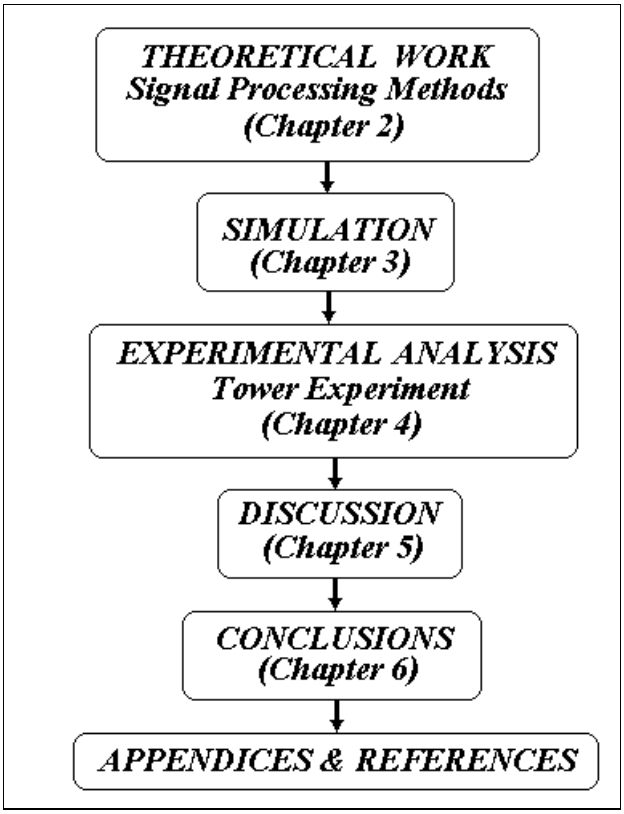

Fig. 1.15 - Thesis flow chart diagram

The experimental analysis involving an experimental apparatus is described in Chapter 4. A scale model that seeks to replicate a petroleum well has been constructed. The tubing of a petroleum well is represented by a 40 meters length wire stretched vertically from the top to the ground level of the Queen's Tower of the Imperial College. This experiment provides some insight into what to expect in terms of remote sensor measurements. All data collected in the experiment are specific, although the signals obtained may resemble other signals collected in a situation in which a remote transducer is used to collect vibration data.

In Chapter 5 is presented an analytical overview of this study which includes a discussion about the relationship between the simulation/experiment and a "live" situation.

The major achievements and contributions of the research are summarised in Chapter 6, which also includes general conclusions and suggestions for new areas of further research.

Appendix A presents a Table generated by the original Prony method applied on the real wellhead data analysis. In the Appendix B, the technical drawings of the experimental supports are presented. In the Appendix C, a theoretical assumption for SNR level is made. In the Appendix D, the Kaiser-Bessel windows applied in the simulation signals of Chapter 3 are defined.

Chapter 2
Theoretical Background

2.1. Introduction

In this Chapter the theoretical background of the signal processing methods employed in this study, together with the theoretical formulation of the extended Prony time-frequency representation, will be presented.

As non-stationary analysis will be addressed, signal processing techniques that are considered relevant for this purpose, the wavelet transform (both the Morlet and Malat techniques), the Wigner-Ville distribution, and the extended Prony time-frequency representation developed in this study, are explained. This will be followed by a brief explanation about the convolution bandwidth filtering technique applied in this research.

The signal analysis undertaken throughout this work involves developing and testing signal processing methods with the aim of determining: (i) how a particular technique can handle noise; (ii) how a particular technique can handle non-stationary components (iii) how a particular method can handle both non-stationary and noise components; and (iv) how to improve the detection of a weak deterministic component in a signal in which both components are present. The intention is to improve the detection of weak deterministic components in signals that contains strong non-

stationary processes and high-level noise. In view of the difficulties in handling non-stationary processes and high-level noise at the same time, a different filtering approach will be explored. A signal with deterministic components embedded in high-level noise has to be pre-processed in such a way as to emphasise the deterministic components to be filtered. If one wants to detect weak components buried in noise, the signal processing technique has to supply additional information about these components that the classic Fourier transform, the wavelet transform and the Wigner-Ville distribution are unable to yield. One technique that gives this additional information about the signal components is the original Prony method. That is, in addition to the component amplitudes and phases, the original Prony technique also evaluates exponential damping, which can be used for our filtering purposes. However, some modifications have to be made to the method to generate time-frequency representations, such as the ones generated by the wavelet transform and the Wigner-Ville distribution, to process non-stationary signals. These modifications will be discussed later in this Chapter.

To demonstrate the need for generating an extended time-frequency representation via the original Prony method, the wavelet transform and the Wigner-Ville distribution techniques will be compared and contrasted via the simulations of Chapter 3. This will be followed by an analysis of multi-component signals resembling the live signal collected at the wellhead (see Chapter 3 below). However, first a brief discussion about non-stationary signal analysis will be made to provide an insight into the matter.

2.2. The Problem of Non-Stationary Process Analysis

Bendat and Piersol [1986] state that an appropriate general methodology does not exist for analysing the properties of all types of non-stationary random data from individual sample records. This is due partly to the fact that a non-stationary conclusion is a negative statement specifying only a lack of stationary properties, rather than a positive statement defining the precise nature of the non-stationarity. It follows that special techniques must be developed for non-stationary data that apply only to limited classes of these data. The usual approach is to hypothesise a specific

model for each class of non-stationary random process. A non-stationary time-history record data, ***x(t)***, may be constructed in many ways. Three different models may be used [Bendat and Piersol, 1986]:

$$x(t) = d(t) + y(t)$$

$$x(t) = d(t) \cdot y(t)$$

$$x(t) = u.y(t^n)$$

where ***y(t)*** is a sample record of a stationary random process and ***d(t)*** is a deterministic function of time that is repeated exactly on each record. The first model represents a process whose mean value is varying in time. The second model represents a process whose mean square value is varying in time. The third model represents a process whose frequency is varying in time. Such elementary non-stationary models can be combined or extended to generate more complex models as required to fit various physical situations. A problem related to these complex models appears when the quantity of combinations which is necessary to represent a non-stationary process is large enough for their realisation. As Bendat and Piersol [1986] argue, the measurement of non-stationary spectral density functions can be a formidable task.

To introduce non-stationary analysis techniques with these comments in mind, an analysis of the signal processing methods mentioned above will be made.

2.3. Wavelet Transforms

Wavelet transforms were developed in France by J. Morlet in 1987, a geophysicist, to aid seismic analysis. They can be considered as the localised equivalent of Fourier transforms and work on the principle that all signals can be reconstructed from sets of

local signals of varying scale and amplitude, but constant shape [O'Brien and MacIntyre, 1994].

In the wavelet transform, the signal is decomposed into wavelet components in the same way that it is decomposed into harmonic components in the Fourier transform. Each wavelet component is called a level and when the separate wavelet levels are added together, the original signal is recovered. In the discrete Fourier transform, the sequence length N of the signal determines how many separate frequencies can be represented. In the wavelet transform when $N=2^n$ there are $n+1$ wavelet levels. A set of wavelet components consists of signals of a specified shape that can be scaled and translated. The components of a decomposed signal depend on the shape of the analysing wavelet. There are an infinite number of these, but only the ones which meet the conditions to give accurate decomposition, and are also orthogonal to each other, are utilised [Newland, 1993].

The overall effect of the transformation is to transfer the data from one domain to another; whereas the Fourier transform moves from a time domain to a frequency domain with sines and cosines as the basic functions, the wavelet transform moves data from a space domain to a scale domain, where the wavelets are the basic function (see Figures 2.1 and 2.2 represent two types of wavelets: Malat and Morlet respectively). The size of the data to be transformed must be an integer power of 2, i.e. of length 2^n, as it has to be for the FFT algorithm [O'Brien and MacIntyre, 1994].

To compare wavelet transforms of different signals, but collected from the same source, each signal must start at the same position in time or space, which is a difficult condition to fulfil in signal processing.

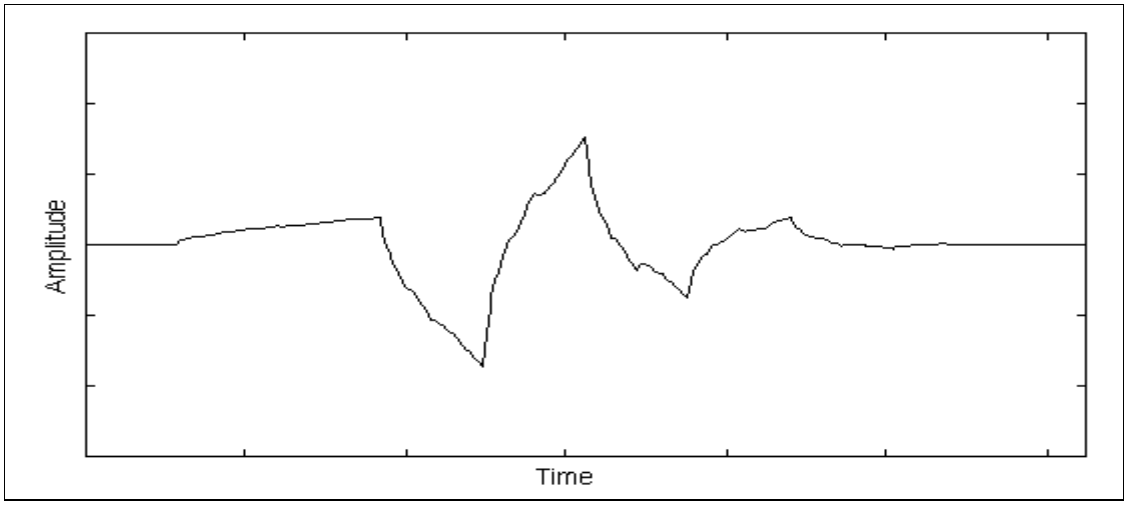

Fig. 2.1 - Shape of a Malat wavelet basic function
[Newland, 1993]

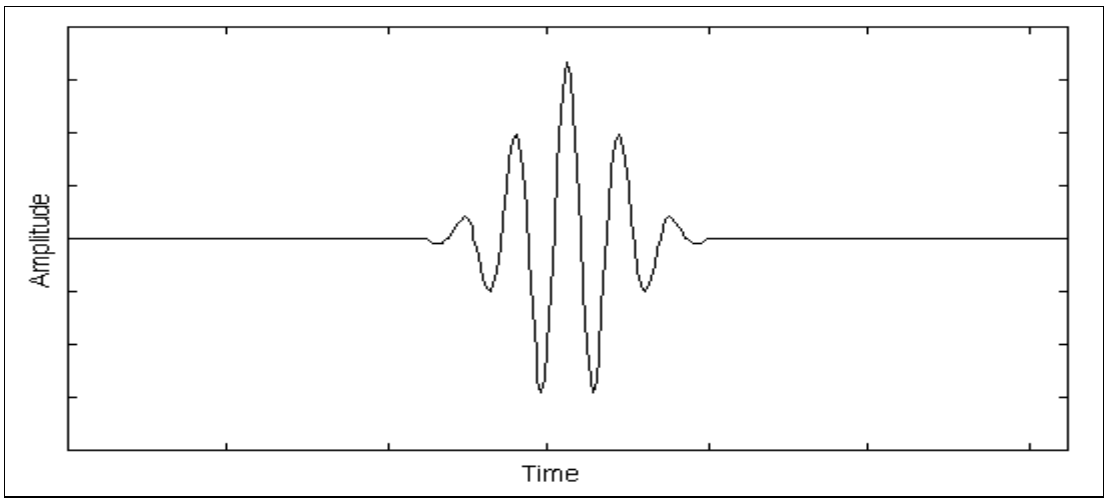

Fig. 2.2 - Shape of a Morlet wavelet basic function [Bonaldo, 1993]

Even related to the same signal, different wavelets cannot be used for comparison because it is impossible to be sure whether any change in the wavelet domain is due to a shift in the location of the signal [O'Brian and MacIntyre, 1994]. In order to represent what O'Brian and MacIntyre claim, a graph of two signals is presented below. Figure 2.3 shows the Morlet wavelet time-frequency description of 2 signals containing a Dirac delta function with amplitude 1, located at two different time axis positions. If we want to compare the signals with deltas on both graphs they must be located in the same position on the time axis. It should be noted that in the case of

these signals, the deltas are similar, but if a more complex signature is considered a Morlet graph is unable to compare two complex similar signals in a straightforward way. Therefore, as O'Brian and MacIntyre state, to compare data, such as in the case of condition monitoring, each data set must be matched in order to start at the same position in time or space before it is transformed to the wavelet domain.

Two forms of wavelet transforms will be discussed below: the first is based on the work of Malat [Newland, 1993], and the second on the work of Morlet [Bonaldo, 1993].

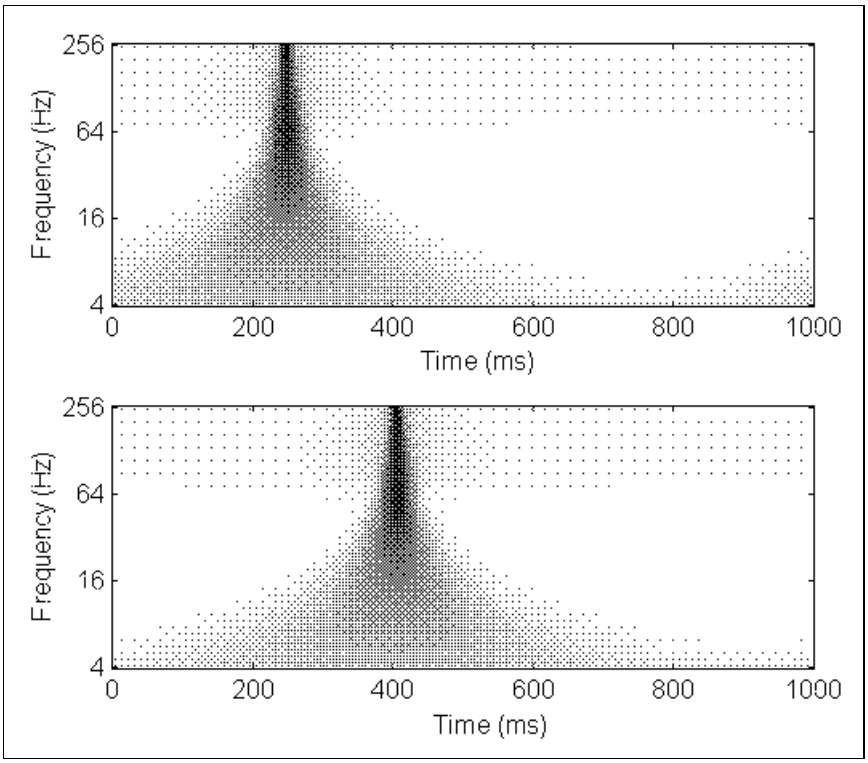

Fig. 2.3 - Morlet wavelet transform of two signals with a Dirac delta located in different time axis positions in a time-frequency plane plot

2.3.1. Malat Wavelet Transform

The wavelet set utilised in the Malat analysis is also known as the Daubechies wavelet. The fundamental basis of the Malat wavelet transform is that any random signal, x***(t)***, may be represented by [O'Brien and MacIntyre, 1994]:

$$\begin{aligned} x(t) &= m_0 + m_1 W_{0,0}(t) + m_2 W_{1,1}(2t) + m_3 W_{1,0}(2t-1) + \\ &\quad m_4 W_{2,0}(4t) + m_5 W_{2,1}(4t-1) + m_6 W_{2,2}(4t-2) + \\ &\quad m_7 W_{2,3}(4t-3) + m_8 W_{3,0}(8t) + \ldots \\ &= m_0 + \sum_{j=0}^{\infty} \sum_{k=0}^{2^j-1} m_{2^j+k} W_{j,k}(2^j t - k) \end{aligned} \tag{2.1}$$

where m_k are numerical constants called wavelet coefficients, t the time, and the $W_{j,k}$ is the wavelet scaling function defined as:

$$W_{j,k}(t) = W(2^j t - k) \quad for \quad j \geq 0 \quad and \quad 0 \leq k \leq 2^j - 1 \tag{2.2}$$

To implement this technique a table of coefficients m_k is given in Newland [1993]. As Newland [1993] points out, there are many different sets of coefficients, m_k, but in order to generate good wavelets these coefficients have to satisfy three different categories of conditions. The first is that the sum of the coefficients must always equal 2. This is called the conservation of area condition in which the scaling function $W_{j,k}$ area remains constant during iterations. The second category sets the accuracy, and basically implies that the Fourier transform of the scaling function $W_{j,k}$ must be periodically zero. If the function $W_{j,k}$ extends to infinity without zeroing, it will not represent a local signal variation precisely. The third category is required to ensure the orthogonality between the scaling function, $W_{j,k}$, and its corresponding generated wavelets.

2.3.2. Morlet Wavelet Transform

The Morlet wavelet transform technique was developed in the 1980s and has been applied with reasonable success in non-stationary analysis [Bonaldo, 1993]. In this technique, a temporal Gaussian window with variable width is used. The time window is reduced to detect any variation of high frequencies and is enlarged to detect any variation in low frequencies. Physically, Morlet's wavelet analysis is equivalent to passing the signal through a constant relative bandwidth filter bank. Each wavelet component can be seen as the output in time of a constant filter. A Gaussian function is utilised because the resulting function in the frequency domain remains Gaussian, only differing by a parameter multiplication. This has the advantage of simplifying the calculations performed by this method.

The Morlet wavelet is defined by the following formula:

$$WM(t,n) = \frac{1}{\sqrt{a}} \int_{-\infty}^{+\infty} s(t) \cdot g\left(\frac{t - t}{a}\right) \cdot dt \qquad (2.3)$$

where ***s(t)*** is the signal in which is applied the window function:

$$g\left(\frac{t - t}{a}\right) = e^{-\left(\frac{t-t}{a}\right)^2/2} \cdot e^{-i2\pi n\left(\frac{t-t}{a}\right)} \qquad (2.4)$$

which denotes a Gaussian multiplied by a complex harmonic function and where ***t*** is the time delay and ***a*** the scaling factor applied to the tested frequency ***n*** in the Morlet wavelet transform.

To perform the Morlet wavelet transform on a signal sample, an algorithm using the Fast Fourier Transform was developed by Bonaldo [1993]. The objective was to reduce dramatically the time of the calculations and to make the Morlet wavelet analysis suitable for processing by computer. This technique was then applied by

Bonaldo to analyse surge in compressors. Figure 2.4 shows a diagram of the Morlet wavelet transform calculations.

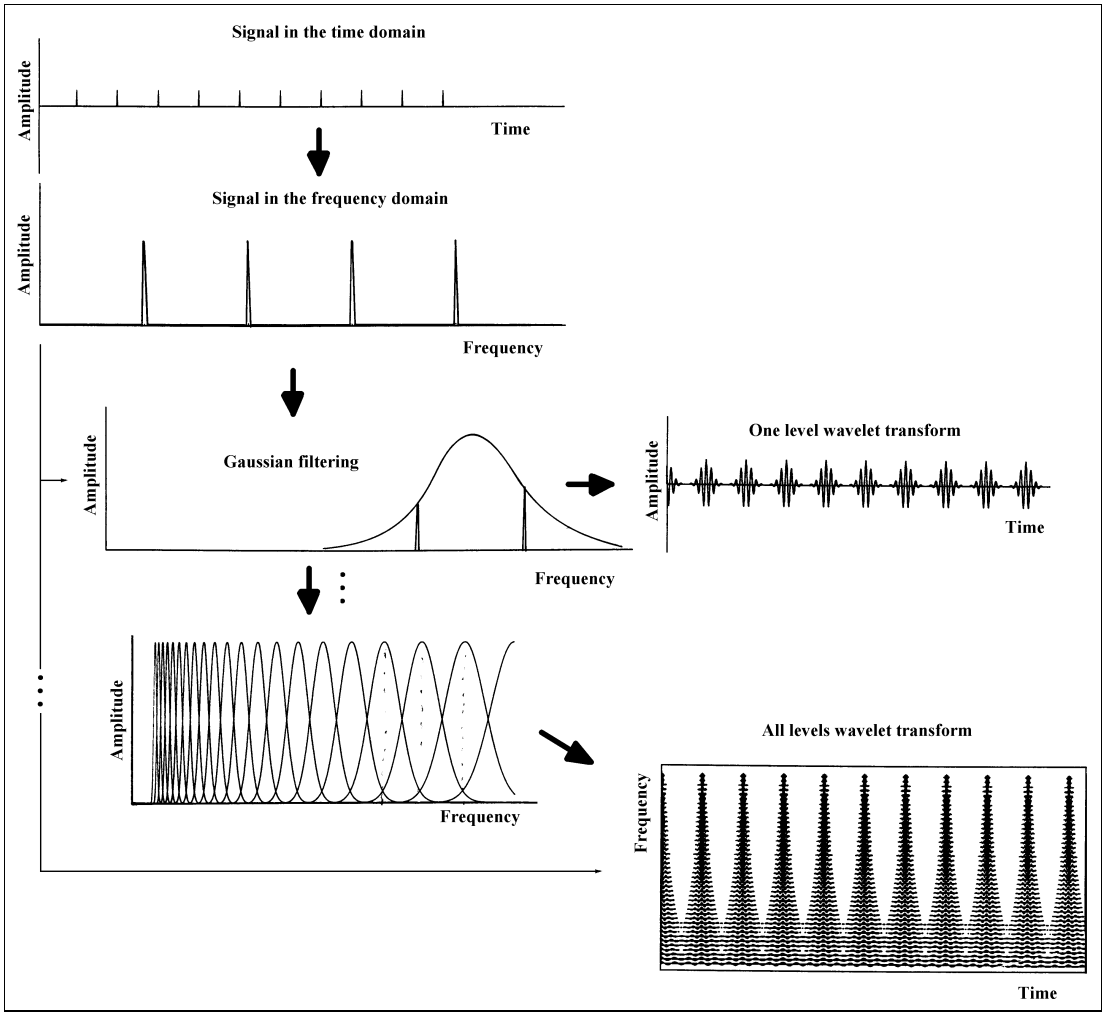

Fig. 2.4 - Morlet wavelet calculation diagram

Bonaldo began to develop the algorithm by considering the theorem of Parseval, which can be represented by the formula:

$$\int_{-\infty}^{+\infty} f(t)\ r(t)\ dt = \int_{-\infty}^{+\infty} FT(f(t))\ FT(r(t))\ dn \tag{2.5}$$

where ***FT*** is the Fourier transform which is applied to the temporal functions ***f(t)*** and ***r(t)***.

Inserting the defined wavelet transform, equation (2.3), into (2.5) will give:

$$\frac{1}{\sqrt{a}}\int_{-\infty}^{+\infty} s(t).g\left(\frac{t-t}{a}\right).dt = \frac{1}{\sqrt{a}}\int_{-\infty}^{+\infty} FT\left((s(t)\right).FT\left(g\left(\frac{t-t}{a}\right)\right).dn \qquad (2.6)$$

From this point, Bonaldo redefined the sliding Gaussian window on the time domain as:

$$g\left(\frac{t+t}{a}\right) = \frac{1}{\sqrt{2p}} e^{-\left(\frac{t+t}{a}\right)^2/2}.e^{+i2pn_0\left(\frac{t+t}{a}\right)} \qquad (2.7)$$

Equation (2.7) is a Gaussian function multiplied by a complex harmonic function with "anticlockwise" rotation (note the positive signs of the function arguments). Bonaldo next developed an expression which is the Fourier transform of (2.7):

$$FT\left(g\left(\frac{t+t}{a}\right)\right) = \frac{1}{\sqrt{2p}}\int_{-\infty}^{+\infty} e^{-\left(\frac{t+t}{a}\right)^2/2}.e^{+i2pn_0\left(\frac{t+t}{a}\right)}.e^{-i2pnt}.dt \qquad (2.8)$$

Making the following variable substitution and rearranging the integrand of equation (2.8):

$$t_1 = t + t \quad \Rightarrow \quad t = t_1 + t$$

$$e^{-\left(\frac{t_1}{a}\right)^2/2}.e^{+i2pn_0\left(\frac{t_1}{a}\right)}.e^{-i2pnt_1}.e^{+i2pnt}$$

$$e^{+i2pnt}.e^{-p\left(\frac{t_1^2}{2pa^2}+i2\frac{t_1}{a}(an-n_0)\right)}$$

Substituting the integrand of equation (2.8) gives:

$$FT\left(g\left(\frac{t_1+t}{a}\right)\right) = \frac{e^{+i2pnt}}{\sqrt{2p}}\int_{-\infty}^{+\infty} e^{-p\left(t_1^2/2pa^2+2i\frac{t_1}{a}(an-n_0)\right)}.dt_1 \qquad (2.9)$$

Rewriting the exponent of the integrand of equation (2.9):

$$-p\left(\frac{t_1^2}{2p\,a^2}+2i\frac{t_1}{a}(an-n_0)\right)=-p\left(\frac{t_1}{a\sqrt{2p}}+i\sqrt{2p}(an-n_0)\right)^2+2p(an-n_0)^2$$

and substituting the exponent of the integrand of equation (2.9) by the right hand term of the above expression results in:

$$FT\left[g\left(\frac{t_1+t}{a}\right)\right]=\frac{e^{+i2pnt}}{\sqrt{2p}}\cdot e^{-2p^2(an-n_0)^2}\cdot\int_{-\infty}^{+\infty}e^{-p\left(t_1/a\sqrt{2p}+i\sqrt{2p}(an-n_0)\right)^2}\cdot dt_1 \qquad (2.10)$$

Making another variable substitution, and differentiating the exponential function of the integrand of equation (2.10) gives:

$$t=t_1/a\sqrt{2p}+i\sqrt{2p}(an-n_0)$$

$$e^{-pt^2}=e^{-p\left(t_1/a\sqrt{2p}+i\sqrt{2p}(an-n_0)\right)^2}$$

$$-2pte^{-pt_1^2}dt=-2p\left(t_1/a\sqrt{2p}+i\sqrt{2p}(an-n_0)\right)e^{-p\left(t_1/a\sqrt{2p}+i\sqrt{2p}(an-n_0)\right)^2}dt_1$$

$$a\sqrt{2p}\,e^{-pt^2}dt=e^{-p\left(t_1/a\sqrt{2p}+i\sqrt{2p}(an-n_0)\right)^2}dt_1$$

Substituting the right hand exponential term of the above expression in (2.10) and rearranging:

$$FT\left[g\left(\frac{t+t}{a}\right)\right]=a\,e^{-2p^2(an-n_0)^2}\cdot e^{+i2pnt}\cdot\int_{-\infty}^{+\infty}e^{-pt^2}\cdot dt \qquad (2.11)$$

The right hand integral of the equation (2.11) equals to 1 and simplifying will give:

$$FT\left[g\left(\frac{t+t}{a}\right)\right]=a\cdot e^{-2p^2(an-n_0)^2}\cdot e^{+i2pnt} \qquad (2.12)$$

It is noted in equation (2.12) that the Fourier transform of the filter is a complex Gaussian function and its centre is located at the frequency, $\boldsymbol{n_0}$. Substituting (2.12) in (2.6) will lead to:

$$\frac{1}{\sqrt{a}}\int_{-\infty}^{+\infty} s(t).g\left(\frac{t-t}{a}\right)dt = \sqrt{a}\int_{-\infty}^{+\infty} FT\left(s(t)\right).e^{-2p^2(an-n_0)^2}.e^{+i2pnt}.dn \qquad (2.13)$$

The right hand integral of the equation (2.13) corresponds to an Inverse Fourier transform (***IFT***) operation applied to a Gaussian window centred at frequency $\boldsymbol{n_0}$ and rewriting the equation (2.13) will lead to the main equation of the algorithm:

$$WM(t,n_0) = \sqrt{a}\ IFT\left(FT\left(s(t)\right).e^{-2p^2(an-n_0)^2}\right) \qquad (2.14)$$

Redefining equation (2.14) to a discrete domain will give:

$$WM(t,f_0) = \sqrt{a}\ .IFT\left(\hat{S}(n.f_s).exp\left(-2p^2\left(\frac{a.n}{f_s}-f_0\right)^2\right)\right) \qquad (2.15)$$

where $\boldsymbol{f_s}$ is the sample frequency and $\boldsymbol{f_0}$ is the centre frequency of the Gaussian window.

After applying the wavelet transform it is possible to recover the original signal by summing all frequency lines related to the same time shift. This is due to the fact that the sum of the contributions of the Gaussian filters to generate one frequency line is equal to the related signal data point projected in the time axis of the time-frequency plane [Bonaldo, 1993]. In the graphical plot of the Morlet wavelet transform, the levels are called “octaves” due the characteristic of scaling frequency in factors of two. To improve the graph resolution, a sub-division of the octaves, fractions between $\boldsymbol{n}$ and $\boldsymbol{n+1}$ from $\boldsymbol{2^n}$ to $\boldsymbol{2^{n+1}}$ which we will call voices, are used.

The Morlet wavelet transform is a technique that has been widely used for non-stationary analysis and, as a consequence, will be compared and contrasted with other techniques in this study.

2.4. Wigner-Ville Distribution

The Wigner-Ville distribution was first defined for quantum mechanics by E. P. Wigner (1932) and, later, by J. Ville (1948) who derived a joint representation from a mathematical foundation to utilise it in signal representation. This distribution approximates a specified time-frequency description in the minimum mean-square error sense. This distribution presents a time-frequency representation of the non-stationary auto-covariance function of the process, and it is a time-frequency representation that preserves the time-frequency dualism of stationary processes, tolerates linear filtering and modulation, and gives the expected instantaneous frequency of the process as a first local moment of the representation. Thus, the Wigner-Ville distribution can be interpreted as a generalised time-varying spectrum.

Some care has to be taken with terminology, as many words such as “distribution” in the probability sense, are used for historical reasons. Distributions first arose in quantum mechanics where the words “probability density” or “distribution” are applied in the conventional meaning of the words. Therefore, distributions should be read as “intensities” or “densities”, or simply as how the energy is “distributed” in the time-frequency cells [Cohen, 1989].

Like the Morlet wavelet transform, the Wigner-Ville distribution is commonly used in the analysis of non-stationary processes [Flandrin and Escudié, 1985, Chiollaz and

Frave, 1993, Moss and Hammond, 1994]. The technique was developed to overcome a limitation of the short-time Fourier transform (STFT), where high-resolution cannot be obtained simultaneously in both the time and the frequency domains [Newland, 1993]. In the STFT, a short data window is applied, centred at time ***t,*** and spectral coefficients are calculated for this short length of data. The window is then moved to a new position and the calculation repeated. The Wigner-Ville distribution was developed to utilise the Fourier transform in a similar way. Due to this similarity the Wigner-Ville distribution has been interpreted by Flandrin and Escudié [1984] as a modified version of the STFT.

In the Wigner-Ville distribution, no reduction of the number of data points in the time-shifting operation is necessary. The starting point for this distribution is the Fourier transform of the ensemble-average instantaneous correlation [Chiollaz and Frave, 1993]:

$$FT(x(t)) = \int_{-\infty}^{+\infty} E\left(x(t + t/2)\, x^*(t - t/2)\right) e^{-i2\pi nt}\, dt \tag{2.16}$$

where

> x^* = conjugate of x for complex signals or Hilbert transform of x for real signals

which, in theory, is a measure of the frequency content of a non-stationary random process, ***x(t)***. However, in practice, it is never possible to compute the ensemble-average function accurately because an infinite number of data are necessary [Chiollaz and Frave, 1993].

One solution to deal with the non-stationary case is to omit the ensemble-average in (2.16):

$$WVD(x(t,n)) = \int_{-\infty}^{+\infty} x(t + t/2)\, x^*(t - t/2)\, e^{-i2pnt}\, dt \tag{2.17}$$

Equation (2.17) represents the Wigner-Ville distribution, which belongs to the class of bilinear frequency distributions defined by Cohen [1989] and given by the equation below [Moss and Hammond, 1994]:

$$C(t,v;f) = \frac{1}{2p} \int_{-\infty}^{+\infty} \int_{-\infty}^{+\infty} \int_{-\infty}^{+\infty} e^{i(xu - tn - xt)}\, f(x,t;t,n)\, x(u + \frac{t}{2}) x^*(u - \frac{t}{2})\, du\, dt\, dx \tag{2.18}$$

where $f(x,t;t,n)$ is the kernel function, u is time, and x and t are the bilinear distribution time delays [Flandrin, 1987]. If the kernel function is set to 1 and equation (2.18) is calculated for a specific time t and frequency f, an equation similar to (2.17) will be obtained. For finite-duration signals, the Wigner-Ville distribution is zero up to the start. This is a desirable feature for avoiding non-zero values for the distribution if the signal is zero. The Wigner-Ville always goes to zero at the beginning and end of a finite-duration signal [Cohen, 1989].

The discrete representation for the equation (2.17) is:

$$WVD(x(T_s,n)) = \frac{T_s}{p} \sum_{k=-\infty}^{+\infty} x^*(t - kT_s)\, x(t + kT_s)\, e^{-2inkT_s} \tag{2.19}$$

where T_s is the sampling period and must be chosen so that $T_s \leq (\pi / 2\omega_{max})$, where ω_{max} is the highest frequency in a random signal [Cohen, 1989].

This distribution exhibits a drawback due to the interference caused by cross-terms. These cross-terms appear when the cross-correlation of the two signals is non-zero. This is caused by the superposition of the Wigner-Ville transform of data arrays in the time-shifting operation. Part of the data of one shift are repeated in the following one, causing redundant information to be used. In general the Wigner-Ville distribution is not zero when the signal is zero, and this causes considerable difficulty in interpretation. In speech, for example, there are silences which are important, but the Wigner-Ville distribution masks them [Cohen, 1989]. Figure 2.5 shows a diagram of a practical calculation of the Wigner-Ville distribution performed on a signal with a 4 Hz sine wave using 16 data samples/s.

If the discrete evaluation of the Wigner-Ville distribution is considered, the frequency resolution, associated with dt and which becomes T_s in equation (2.19), is different from that obtained by Fourier transformation of the original N-point time record in two respects [Shin and Jeon, 1993]. The first difference is that the argument of the time signal and its conjugate contains a factor of 1/2, and the second is that the autocorrelation of the time signal is twice the length of the original record and therefore the discrete Fourier transform is evaluated over $2N$. The result is that the Wigner-Ville distribution frequency resolution is half the resolution of an ordinary power spectrum density function for the same number of points.

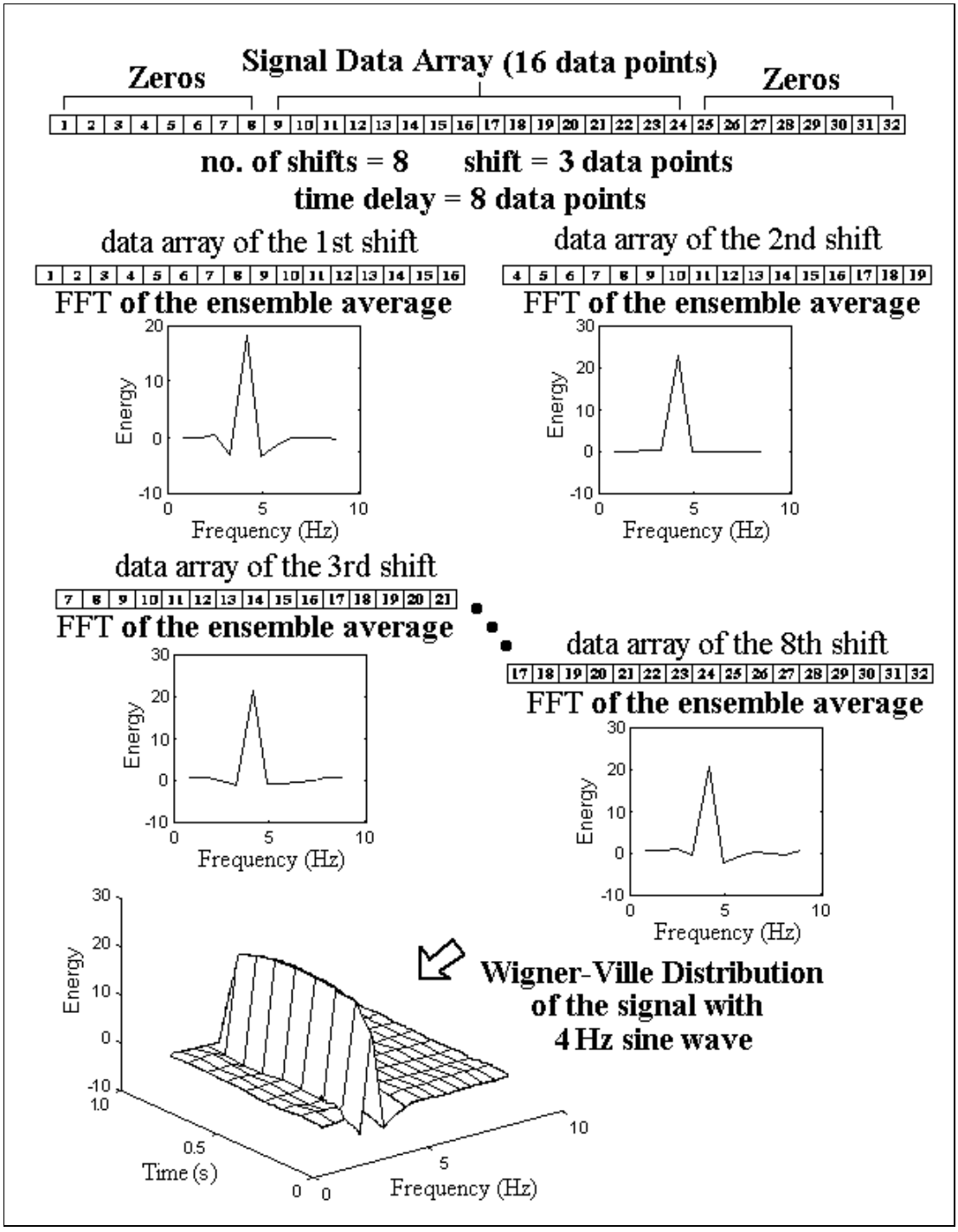

Fig. 2.5 - Wigner-Ville distribution calculation diagram

In the case of signals with multiple frequency components, the Wigner-Ville distribution is very complicated and difficult to interpret due to the interference effect [Shin and Jeon, 1993]. Also, in practice unless the signal ***x(t)*** is a bandlimited signal, it is not possible to calculate the Wigner-Ville distribution as it requires integration over all time or all

frequency [Moss, Hammond, 1994]. Due to these problems, weighting windows are applied to data arrays of each shift in both time and frequency domains, which will lead to the formula of the pseudo-Wigner-Ville distribution (***PWVD***) [Shin and Jeon, 1993, Moss and Hammond, 1994];

$$PWVD(x(t,\nu)) = h(n) \int_{-\infty}^{+\infty} g(t)\, x(t+\frac{t}{2})\, x^*(t-\frac{t}{2})\, e^{-2i\pi\nu t}\, dt \qquad (2.20)$$

where ***h(n)*** and ***g(t)*** are weighting windows applied in the frequency and time domains respectively. As examples, rectangular, Hamming, Gaussian and Kaiser-Bessel weighting windows in the time and frequency domains have been applied in the pseudo-Wigner-Ville distribution [Shin and Jeon, 1993, Chiollaz and Frave, 1993, Moss and Hammond, 1994] (see Appendix D for the Kaiser-Bessel window definition). The application of a weighting window in the time domain is straightforward and requires only a multiplication of data arrays by a specific window. The application of a frequency weighting window may be done through a convolution operation between data arrays and a specific window sliding in the frequency domain.

2.5. Wavelet Transform and Wigner-Ville Distribution Relationship

In a comparison between the two techniques, it is first important to separate the two different concepts of wavelet transforms, the Morlet and the Malat techniques. The Malat technique, due to its random association related to the equations (2.1) and (2.2), presents some inherent difficulties for harmonic component identification. This technique is less related to the harmonic analysis and presents a more confused time-frequency representation than the Morlet technique, based on Bonaldo's algorithm. The Malat technique has proved to be more suitable for data compression in channel transmission due to its capacity to recover the original signal. For example, in a study on signal compression in hearing aids, Drake et al [1993] developed an algorithm based on the Malat wavelet technique that combined standard compression with intensity- level dependent gain

calculation to compensate a common hearing impairment known as “recruitment of loudness”. If a listener suffers from recruitment of loudness, the perceived loudness grows more rapidly with an increase in sound intensity than it does in the normal ear. The proposed technique is applied in a compensation system, in which the impairment is modelled in such a way to develop an attenuator for the sound intensity. The experiments carried out by the authors showed low distortion in the signal compression by the use of Malat wavelet.

The general bilinear class of time-frequency distributions defined by Cohen [1989] are either Fourier transforms or spread versions of the Wigner-Ville distribution, whose major feature is the generation of significant cross-terms for multi-component signals [Moss and Hammond, 1994]. A basic difference between the Morlet wavelet transform and the pseudo-Wigner-Ville distribution, which is a variant of the Wigner-Ville distribution, is the way in which the windows are applied in the signal analysis. In the pseudo-Wigner-Ville distribution the length of the windows are fixed (see equation (2.20)) and in the Morlet wavelet transform they vary according with the centre frequency of the Gaussian window (see equation (2.15)).

As was discussed above, these methods are reported to be inadequate for handling signals containing high levels of noise. It was also shown in the introduction that the original Prony method could be more suitable to analyse non-stationary data, when they are considered as transients (see section 1.6 of Chapter 1). Therefore the theoretical formulations of the original Prony method will now be analysed in greater detail.

2.6. The Original Prony Method

The original Prony method was developed to provided solutions for a deterministic exponential model. When the Fourier transform is applied, the unavailable data or unestimated autocorrelation sequence values outside the window are implicitly zero, which is an unrealistic assumption that leads to distortions in the spectral estimate [Marple, 1987]. Spectral estimates produced with the autoregressive coefficients estimated by the covariance method, used in the autoregressive procedures, usually have less distortion than spectral estimates produced by methods that ensure the filter stability, such as the autocorrelation method [Lang and McClellan, 1980]. To assume that the values outside the window are not zero, an autoregressive procedure has been adopted as represented by the following equation:

$$x(n) = \sum_{k=1}^{p} h_k \; y(n) \tag{2.21}$$

where n is data point number of a discrete time sequence, $x(n)$ is a data vector, p is the order of the autoregressive procedure, h_k is a complex amplitude that represents a time-independent parameter, and $y(n)$ the system response function.

As the sought components in the signal are generally complex exponentials [Marple,1987], the system response $y(n)$ of equation (2.21) may be substituted for exponentials to obtain a clearer representation of the deterministic components and this will lead to the following equation:

$$x(n) = \sum_{k=1}^{p} h_k \; z_k^{n-1} \tag{2.22}$$

where

$$h_k = A_k \exp(i\theta_k)$$

$$z_k = \exp\left((c_k + i2\pi n_k)T_s\right)$$

A_k = amplitude

θ_k = phase

c_k = exponential damping

ν_k = frequency

T_s = sampling interval

p = polynomial order

Note that z_k is a complex exponent that represents a time-dependent parameter.

The original Prony procedure provides solutions for the equation (2.22) by calculating exactly-fitting purely-damped exponentials. This method was first developed in 1795 by Gaspard Riche, Baron de Prony, for interpolating data points in his measurement of gas expansion.

Although it is not a spectral estimation technique, the original Prony method has a close relationship to the least-squares linear prediction algorithms used for the autoregressive (AR) and autoregressive moving average techniques (ARMA). The original Prony method seeks to fit a deterministic exponential model to the data, in contrast to the AR and ARMA models that seek to fit a random model to the second order data statistics. In this way, exact damped exponentials may be fitted to the data considering the p-exponent discrete-time function [Marple, 1987]. In the modern version of the original Prony method, the least-squares and recursive least-squares algorithms have been applied. As a consequence, in some works this technique is called a “least-squares refinement” [DTA Handbook, 1993]. However, this terminology is rather confusing as it does not correspond to the true aspect of the method. For the least-squares algorithm may be applied in the first step of the method as well as the Kalman and eigenvalue analysis techniques (see equations (2.34) to (2.37) and (2.38) to (2.40) below). Figure 2.6 shows the calculation diagram of the original Prony technique.

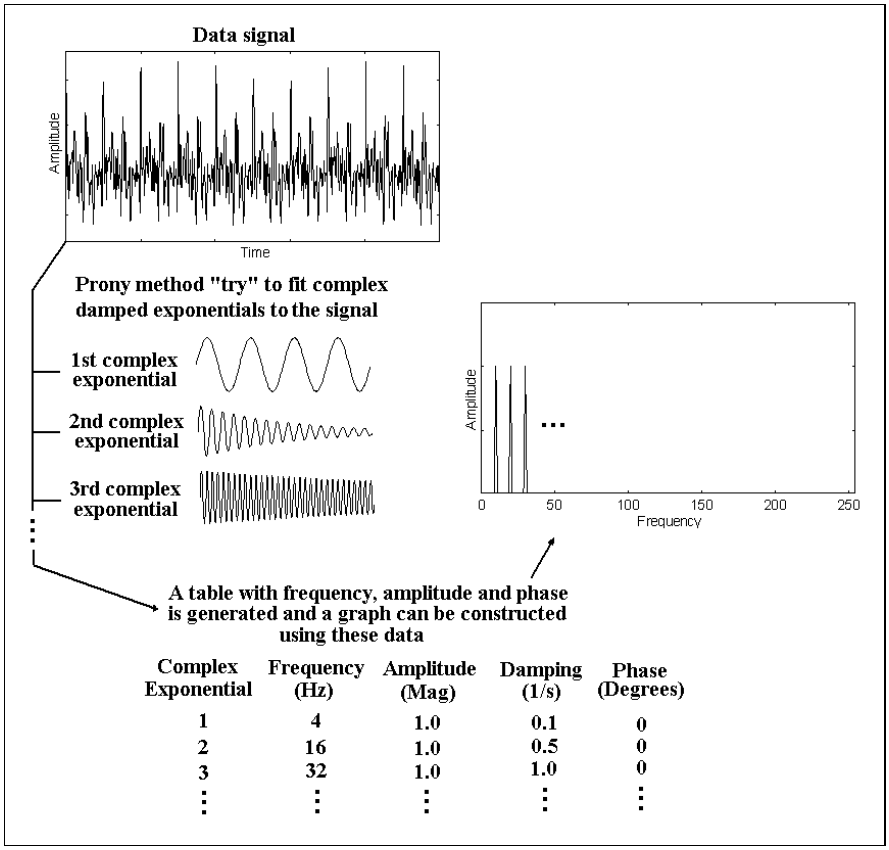

Fig. 2.6 - Original Prony technique calculation diagram

The implicit difficulty associated with exponential fitting using equation (2.22) appears when a minimisation of the squared error over the N data samples is considered. This means minimising:

$$h = \sum_{n=1}^{N} |e(n)|^2 \tag{2.23}$$

where

$$e(n) = x(n) - \hat{x}(n) \tag{2.24}$$

This difficulty can be demonstrated by the single-exponent case of the estimator:

$$\hat{x}(n) = A\exp\left(c(n-1)T\right) \tag{2.25}$$

The minimisation procedure applied to equation (2.25) is obtained setting to zero the derivatives of the estimator, $\hat{x}(n)$, with respect to A and c:

$$\begin{aligned} \frac{\partial r}{\partial A} &= b_1 - b_2 A = 0 \\ \frac{\partial r}{\partial c} &= b_3 - b_4 A = 0 \end{aligned} \tag{2.26}$$

where:

$$\begin{aligned} b_1 &= \sum_{n=1}^{N} x(n) \exp\left(c(n-1)T\right) \\ b_2 &= \sum_{n=1}^{N} \exp\left(2c(n-1)T\right) \\ b_3 &= \sum_{n=1}^{N} (n-1) x(n) \exp\left(c(n-1)T\right) \\ b_4 &= \sum_{n=1}^{N} (n-1) \exp\left(2c(n-1)T\right) \end{aligned} \tag{2.27}$$

From the first equation of (2.26) $A = b_1 / b_2$ can be obtained, and substituted in the second equation (2.26), and this will lead to:

$$b_2 b_3 = b_1 b_4$$

the above equation is a highly non-linear expression in terms of sums involving $\exp\left(c(n-1)T\right)$ which must be solved for c. No analytic solution is available [Marple, 1987].

A procedure was discovered by Baron de Prony to solve equation (2.22) as a set of decoupled linear simultaneous equations, decoupling the variables h and z, and noting that this expression is the solution for some homogeneous linear constant-coefficient difference equation. To this end, a polynomial which has the exponents z_k as its roots may be defined:

$$f(z) = \prod_{k=1}^{p} (z - z_k) = \sum_{d=0}^{p} a(d) z^{p-d} \tag{2.28}$$

where $a[0] = 0$ and d is the data lag.

If the index in equation (2.22) is shifted from n to $n-d$ and a parameter $a(d)$ is multiplied, this produces:

$$a(d)x(n-d) = a(d)\sum_{k=1}^{p} h_k z^{p-l} \tag{2.29}$$

forming similar products and summing:

$$\begin{aligned}
a(0)x(n) &= \sum_{i=0}^{p} h_i z_i^{n-1} \\
a(1)x(n-1) &= \sum_{i=0}^{p} h_i z_i^{n-2} \\
&\cdots\cdots\cdots\cdots\cdots\cdots \\
&\cdots\cdots\cdots\cdots\cdots\cdots \\
a(d)x(n-d) &= \sum_{i=0}^{p} h_i z_i^{n-d-1}
\end{aligned}$$

$$\sum_{d=0}^{p} a(d)\, x(n-d) = \sum_{i=0}^{p} h_i \sum_{d=0}^{p} a(d)\, z_i^{n-d-1} \tag{2.30}$$

and making the substitution into the equation (2.30):

$$z_i^{n-d-1} = z_i^{n-p}\, z_i^{p-d-1} \tag{2.31}$$

will lead to the following decoupled equation:

$$\sum_{d=0}^{p} a(d)\, x(n-d) = \sum_{i=0}^{p} h_i z_i^{n-p} \sum_{d=0}^{p} a(d)\, z_i^{p-d-1} \tag{2.32}$$

Prony noted that the second right hand summation term can be recognised as the polynomial characteristic equation (2.28) yielding a zero result. Equation (2.32) is the linear difference equation whose homogeneous solution is given by equation (2.22). The polynomial depicted by equation (2.28) is the characteristic equation associated with this linear difference equation. The ***p*** equations representing the valid values of ***a(n)*** that satisfy equation (2.32) may be expressed as the ***p*** ´ ***p*** matrix equation:

$$\begin{bmatrix} x(p) & x(p-1) & \cdots & x(1) \\ x(p+1) & x(p) & \cdots & x(2) \\ \vdots & \vdots & \ddots & \vdots \\ x(2p-1) & x(2p-2) & \cdots & x(p) \end{bmatrix} \begin{bmatrix} a(1) \\ a(2) \\ \vdots \\ a(p) \end{bmatrix} = \begin{bmatrix} x(p+1) \\ x(p+2) \\ \vdots \\ x(2p) \end{bmatrix} \tag{2.33}$$

Equation (2.33) represents the first step of the original Prony technique. To conclude, the original Prony procedure may be summarised in three steps [DTA Handbook, 1993, Ewins, 1995]:

(1) Determination of parameters ***a(k)*** utilising ***2 p*** sample data points, using equation (2.33).

(2) Calculation of the roots of the characteristic polynomial defined by (2.28). The damping and frequency of each component may be calculated using the following equations:

$$c_k = \frac{\ln|z_k|}{T_s} \qquad n_k = \frac{\tan^{-1}\left(Im(z_k)/Re(z_k)\right)}{2\pi T_s}$$

where $Im(z_k)$ and $Re(z_k)$ are the imaginary and the real part of z_k.

(3) And finally, the calculation of equation (2.22) using the roots z_k calculated in equation (2.28) and ***p*** sample data points. The amplitude and phase of each component may be calculated using the following equations:

$$A_k = |h_k| \qquad q_k = \tan^{-1}\left(\frac{Im(h_k)}{Re(h_k)}\right)$$

where $Im(h_k)$ and $Re(h_k)$ are the imaginary and the real part of h_k.

Figure 2.7 shows a diagram of the application of the original Prony procedure to a signal with 16 data points.

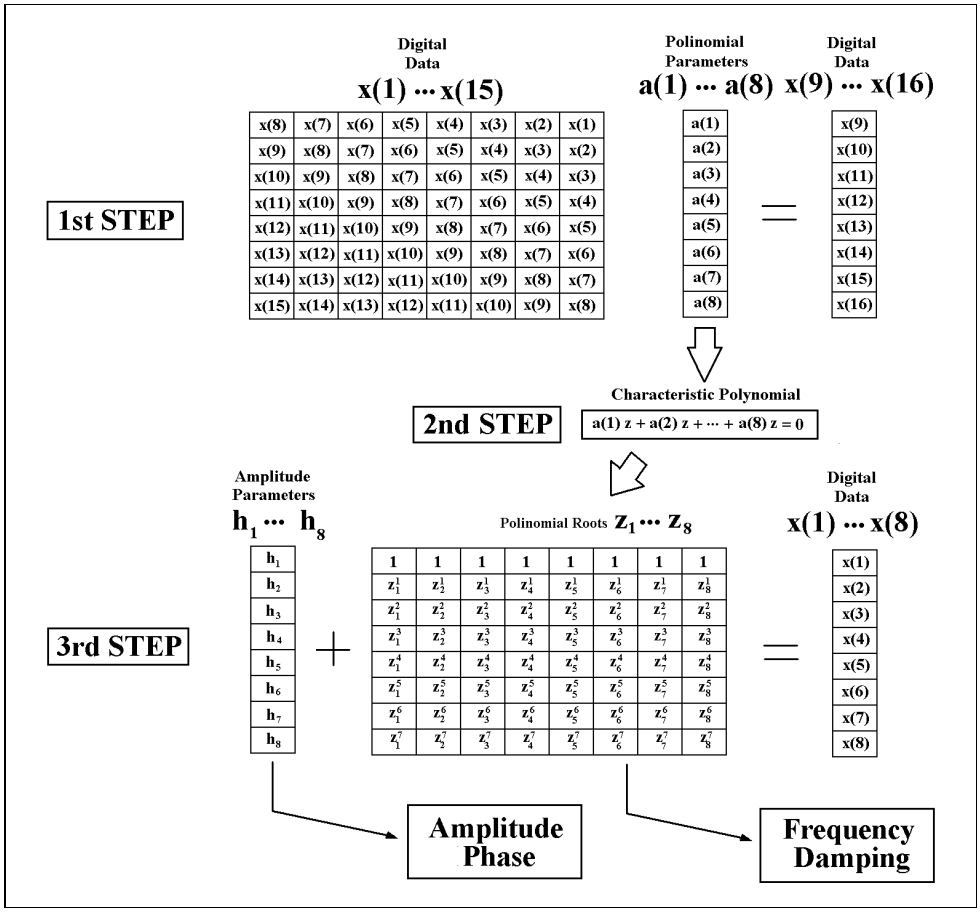

Fig. 2.7 - Original Prony step procedure diagram

In regard to the first step (equation (2.33)), the least-squares linear prediction estimation (covariance) and the recursive least-squares methods can be used to determine the ***a(k)*** parameters.

The starting point for the application of the covariance method in the first step of the original Prony technique is the minimisation of the forward and backward linear prediction errors [Marple, 1987, Kay, 1993]:

$$e_f = x^T(n)a_f \qquad e_b = x^T(n)a_b \tag{2.34}$$

where $x^T(n)$ is the transposed data vector, a_f and a_b are the forward and backward linear prediction coefficient vectors.

Based on the measured data samples, the covariance method minimises, in separate calculations, the forward and backward linear prediction squared errors [Marple, 1987, Kay, 1993]:

$$h_f = \sum_{n=p+1}^{N} \left| e_f \right|^2 \qquad h_b = \sum_{n=p+1}^{N} \left| e_b \right|^2 \tag{2.35}$$

resulting from the normal equations:

$$Ra_f = \begin{Bmatrix} h_f \\ 0_p \end{Bmatrix} \qquad Ra_b = \begin{Bmatrix} h_b \\ 0_p \end{Bmatrix} \tag{2.36}$$

where 0_p is an all-zeros vector and R the vector outer product:

$$R = \sum_{n=p+1}^{N} x^*(n)\, x^T(n) \tag{2.37}$$

In the traditional recursive least-squares estimation, which is another technique that may be used to compute the first step of the original Prony procedure, only the forward linear prediction error is computed by the formula [Marple, 1987]:

$$e_{p,f} = x_p(n) + \sum_{k=1}^{p} x_p(n-k)a_{p,f} \tag{2.38}$$

The squared error and the vector outer product are weighted by a positive real scalar, γ ($0 < \gamma \leq 1$), given all measured data up to time index, N

$$r_f = \sum_{n=1}^{N} \gamma^{N-n} \left| e_f \right|^2 \tag{2.39}$$

$$R_p = \sum_{n=1}^{N} \gamma^{N-n} x_p^*(n)\, x_p^T(n) \tag{2.40}$$

where R_p the vector outer product of order p.

What differentiates the two techniques that can be applied in the first step of the original Prony method is the degree of freedom given to the order and time. The covariance technique is recursive in order but fixed in time, and the recursive least-squares technique is the opposite.

Despite being quite accurate for short-to-medium-length data records, a poor long-term numerical stability is reported for the fast recursive least squares algorithm [Cioffi and Kailath, 1984]. Sometimes this fast algorithm is called "fast Kalman", but this seems inappropriate due to the non-random nature of the deterministic least-squares solution [Marple, 1987].

2.7. Theoretical Formulation for an Extended Prony Time-Frequency Representation

As stated above, several problems have consistently been associated with the wavelet transform and the Wigner-Ville distribution techniques, and hence the need for a new technique that can improve deterministic component detection in the presence of high-

level noise and strong non-stationary processes. In this section, an attempt will be made to demonstrate theoretically that the Prony method is suitable to be extended for the purpose of filtering out strong spurious components and improving the detection of the deterministic ones.

As it is expected that the actual signal to be analysed has an adverse signal-to-noise ratio (SNR), the noise and non-stationary components will be considered as transients, and will be eliminated through a technique extended from the original Prony procedure, on the basis that they may indicate high exponential damping values.

It is argued here that an extended Prony time-frequency plane representation can be developed in a similar way to the one represented in the Wigner-Ville distribution, whose "sliding window in time shifts" approach is closer to the short Fourier transform without its time-frequency resolution drawback. An advantage of the original Prony technique is that it can extract exponentials on a limited amount of data, although the amount of data may influence its performance under some conditions. If only a few data values are used, this tends to induce the method to seek more transient components. In this case, the polynomial order, $\boldsymbol{p}$, has to be decreased and this in turn will reduce the number of exponentials sought. If a large amount of signal data are used, the method will work in a probabilistic sense and tend to "smooth" the transient components, which are represented by short arrays of data. These two outcomes are both due to the correlation between the amount of parameters and data points ($2\boldsymbol{p}$) in the calculations performed by the method.

In order to obtain an extended Prony time-frequency representation, a matrix construction using the equation (2.22) is suggested as follows:

$$\boldsymbol{PTF} = \left[x_1(n) \quad x_2(n) \quad \cdots \quad x_u(n) \right], \quad x_u(n) = \sum_{k=1}^{p} h_k \, z_k^{n-1} \tag{2.41}$$

where $\boldsymbol{u}$ is the starting time point of each data sample shifted each incremental period $\boldsymbol{dT=1/N}$ on the signal data, and $\boldsymbol{x_u(n)}$ is a data vector related to that sample and calculated using the equation (2.22).

As the original Prony method generates results which can be presented in a table defining frequency, amplitude, phase and exponential damping of each component sought by the method (see the table of Appendix A), it is necessary to arrange the generated data in "a non-parametric spectrum graph shape" in order to create a time-frequency plane using data generated from all samples at starting time points, $\boldsymbol{u}$. Figure 2.8 shows a plot of the Prony time-frequency representation generation. If zero values corresponding to the frequencies not sought in each sample at a time point, $\boldsymbol{u}$, from 1 to $\boldsymbol{N}$, of equation (2.41) are inserted within the $\boldsymbol{p}$ frequencies found in order to obtain one spectrum line, $\boldsymbol{q}$, from 1 to $\boldsymbol{N}$/2 (see Figure 2.8 (a)), an extended Prony time-frequency representation matrix may be defined as:

$$\boldsymbol{PTF(u,q)} = \begin{bmatrix} A_{11},c_{11},q_{11} & A_{11},c_{12},q_{12} & \cdots & A_{1u},c_{1u},q_{1u} \\ A_{21},c_{21},q_{21} & A_{22},c_{22},q_{22} & \cdots & A_{1u},c_{2u},q_{2u} \\ \vdots & \vdots & \ddots & \vdots \\ A_{q1},c_{q1},q_{q1} & A_{q2},c_{q2},q_{q2} & \cdots & A_{qu},c_{qu},q_{qu} \end{bmatrix} \tag{2.42}$$

where each column of the matrix of the equation (2.42) is related to one data vector $\boldsymbol{x_u(n)}$ referred to one sample starting at a time point, $\boldsymbol{u}$, which, in turn, corresponds to one calculation using the equation (2.22) (see the diagram of Figure 2.8 (b)).

Each element, $\boldsymbol{A_{qu}}$ of the $\boldsymbol{PTF}$ matrix has its associated values of exponential damping, $\boldsymbol{c_{qu}}$, and phase angle, $\boldsymbol{q_{qu}}$. What is denoted by this is that the $\boldsymbol{PTF}$ is a three-dimensional matrix with $\boldsymbol{N}$/2 lines, $\boldsymbol{N}$ columns and 3 planes corresponding to the amplitude, exponential damping and phase values for each component found by the extended technique.

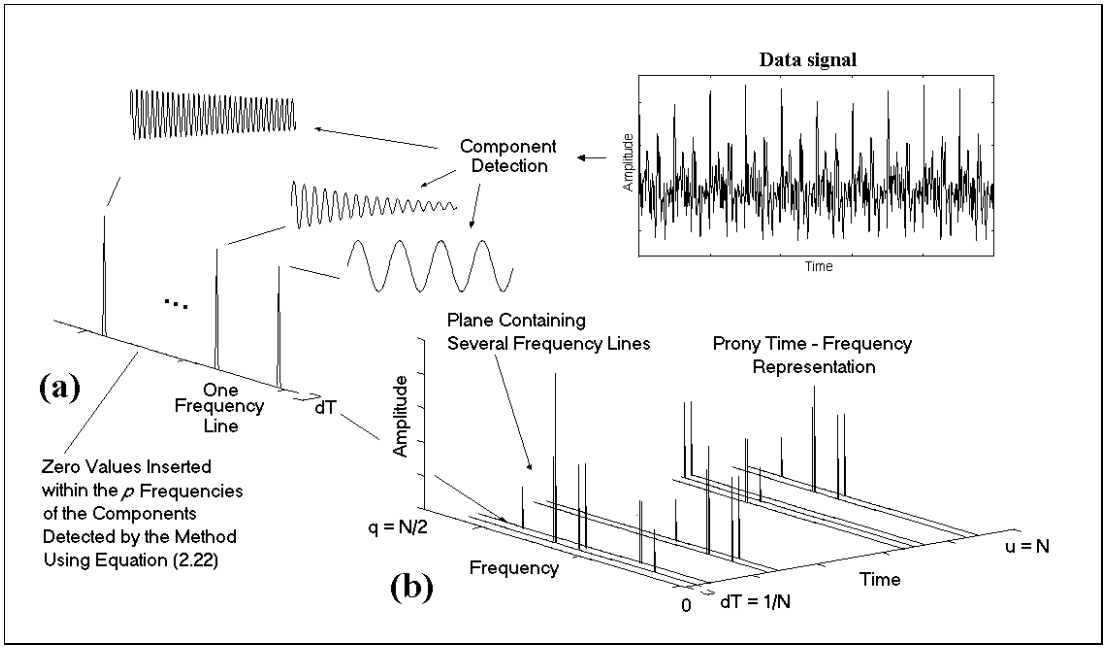

Fig. 2.8 - Schematic diagram of the development procedures of the extended Prony time-frequency representation

If the sampling period ***dT*** is equal to ***1/N***, an extended Prony time-frequency plane projection on the frequency domain ***S(q)*** and the respective recovered signal ***s(u)*** may be defined as:

$$S(q) = \frac{1}{N} \sum_{u=1}^{N} A_{qu} \quad q = 1, 2, \cdots N / 2 \tag{2.43}$$

and,

$$s(u) = \sum_{q=1}^{N/2} A_{qu} \exp(i q_{qu}) \quad u = 1, 2, \cdots N \tag{2.44}$$

Each ***S(q)*** of equation (2.43) represents the average amplitude of a specific line, ***q***, parallel to the time axis projected on the frequency axis and each ***s(u)*** of equation (2.44) represents one recovered data point of the original signal. The recovered time data points evaluated by equation (2.44) are the ones which are being proposed to be filtered from the time-frequency plane by a selection using an exponential damping level.

In relation to the model order choices in the filtering procedure, it is not advisable to determine the best method polynomial "fitting" order ***p*** of equation (2.41) using criteria such as the Akaike criterion. The order selection criteria normally determine the most suitable order related to the number of components "statistically" present in a signal. In the case of weak component detection in the presence of strong spurious components, a statistical criterion will look for the most statistically represented components in the signal. This is not the case of the weak components. The Akaike Information Criterion (***AIC***) is represented by the equation [Tong, 1975 and 1977]:

$$AIC(p) = N \ln(\hat{r}_p) + 2p$$

where ***p*** is the autoregressive order, ***N*** the number of data points, and $\hat{r}_p$ is the input white noise variance estimator of an assumed autoregressive process with order ***p***. The term ***2p*** represents the penalty for the use of extra autoregressive coefficients that do not result in a substantial reduction in the prediction error variance estimator, $\hat{r}_p$. The smaller the ***AIC***, the better the autoregressive parameter fitting obtained for a process which has Gaussian statistics. Many studies have found that the order selected by the AIC is often too low for practical non-autoregressive data sets [Marple, 1986]. Also, Kashyap [1980] has found that the AIC is statistically inconsistent because the probability error does not tend to zero, in the case of the right order choice, and when ***N*** tends to infinity. Furthermore, when setting the order choice for applying the original Prony procedure, a mistake is often made in the right order selection when comparing a different method and the original Prony procedure. Take, for example, the work of Liu [1996] cited in the section 1.5.1 of Chapter 1. Liu applied the state-space method through a singular value decomposition (SVD) and compared it with the original Prony method. The separation of two subspaces in the SVD generates low orders that are associated with the signal subspace matrices. In contrast, the original Prony technique order is associated with a matrix containing both components and noise data. In this case, it is necessary to use higher orders to represent all components in the signal, which includes those associated with noise. For this reason, signals used to compare both

techniques should be analysed through the original Prony technique with a much higher order than that set to perform the SVD method.

With regard to the possible exponential solutions generated throughout the original Prony procedure, it must be pointed out that the maximum number of possible solutions given by the original Prony technique is equal to ***p***, which corresponds to the method order. To apply the original Prony technique, ***2p*** data are used for parameter fitting in the left-hand matrix of equation (2.33). In this study, the first step of the original Prony method, which corresponds to an exact exponential model, is substituted by the least squares linear fitting procedure to perform the extended Prony time-frequency representation. This means that in each data-set of a time point ***u*** of equation (2.41), an over-determined set of equations system case with the number of data points ***N*** is used to generate exponential solutions much greater than the order ***p***. This sub-optimum approach effectively reduces the non-linear exponential problem into a linear factorisation in the first step of the original technique, which is used in the extended Prony time-frequency representation.

A significant advantage with this extended Prony time-frequency representation is that it produces parameters over the entire time-frequency plane, unlike the Wigner-Ville distribution where negative amplitude values may appear, as Cohen [1989] mentioned (see section 1.5.3 of Chapter 1).

A computer program was developed to generate extended Prony time-frequency representations. In this program, the original Prony procedure is carried out in time shifts through an array of data. With regard to the original Prony method exponential detection model used in the program, which is central to the extended technique, it should be noted that extra care is necessary to develop its program routines. The need for precision and robustness to perform the matrix and polynomial evaluations through the steps of the original Prony procedure requires specialised routines, rather than “home-made” ones for developing the program. Examples of these routines are those developed by Jenkins and Traub [1972] to perform complex polynomial

evaluations, and by Marple [1987] to execute Cholesky matrix decomposition, both of which are used in the second and in the third steps of the original Prony procedure (equations (2.28) and (2.22)). Also, a large number of "check-test" program lines are necessary for detecting singular matrices, divisions by zero, and other mathematical abnormalities. This is necessary because the original Prony procedure involves the manipulation of non-linear exponential functions that are not always well behaved.

A problem with the original Prony method has been reported by Poggio and Blaricum [1978] if the number of components, which is correlated to the order of the method, is unknown. If the selected order is greater than the actual number of components present in the signal, singular matrices may appear in the calculations performed by the method. To avoid this problem, a routine is incorporated in the computer program to perform a loop to reduce the order $\boldsymbol{p}$ of the method. This means that, if a routine fault due to floating errors or singular matrices appears in the calculations, the program is reset and the order of the method is reduced. This requires several numerical tests to avoid faulty operations being executed by a particular subroutine of the program. Since the program to execute the extended Prony time-frequency representation is moderately large (close to 2000 FORTRAN lines), an exhaustive task was performed to check every sub-loop of the program. Finally, the debugged extended Prony time-representation program was then applied to the simulated and experimental signals of Chapters 3 and 4. This program generates three matrices, each containing, in separate, the amplitude, exponential damping, and phase values of the components detected in the time-frequency plane. Just what is meant by the "time-frequency plane" is discussed in the next section.

2.8. Time-Frequency Plane Interpretation

For a better visualisation of non-stationary components, it is necessary to show how a specific technique depicts the signal on a time-frequency plane plot. To this end, a signal composed of a 32 Hz sine wave, which is sampled at 512 Hz, will be analysed

by the techniques discussed in this study. The respective time-frequency planes are shown on Figures 2.9, 2.10 and 2.11. Every point in the time-frequency plane represents an amplitude or energy peak perpendicular to the plane. Actually, the plane is a numerical matrix carrying the values of amplitude or energy peaks corresponding to each point of the time-frequency plane. The results of the pseudo-Wigner-Ville distribution are shown in the two graphical views in Figure 2.9, and Figures 2.10 and 2.11 show the time-frequency representations obtained by the Morlet wavelet technique and the extended Prony time-frequency representation with least-squares fitting in the first step. In the three time-frequency representations, the amplitude of the 32 Hz component is projected on the vertical axis and is generally represented in grey scale maps on the time-frequency plane. The frequency scale in the wavelet graph is always represented in $\boldsymbol{log_2}$ scale due to the nature of its evaluation. This can be seen in equation (2.2) where the wavelet coefficients $\boldsymbol{W}$ are scaled $\boldsymbol{2^j x - k}$ in the frequency axis (levels).

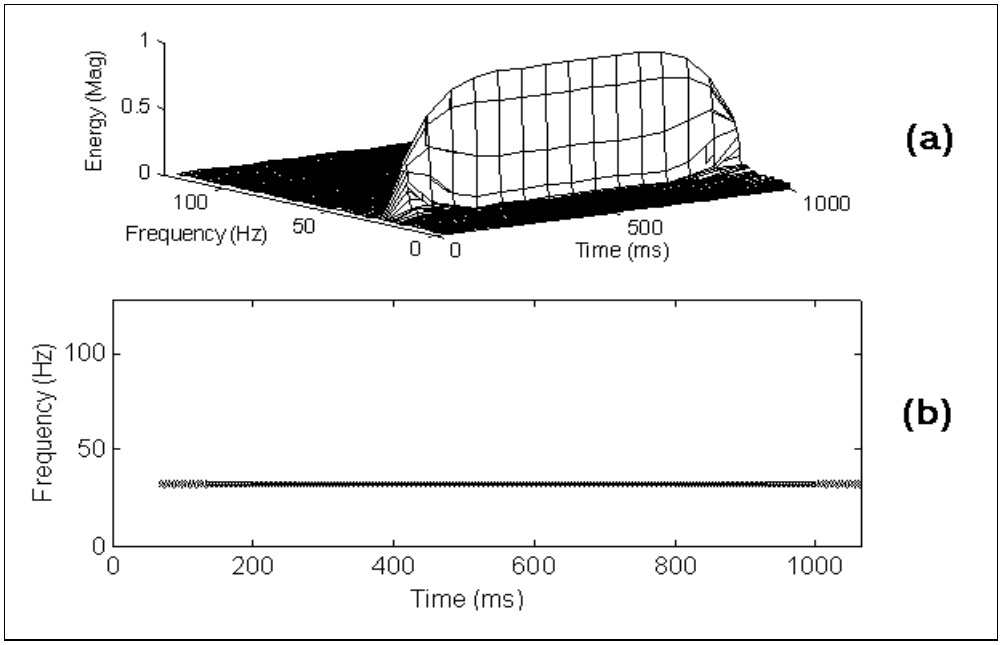

Fig. 2.9 - Pseudo-Wigner-Ville of the 32 Hz signal (perspective view (a) and time-frequency plane view (b))

The original Prony method is a time-fitting method but when extended to generate frequency lines, calculated from data arrays of shifting time windows, defined by

equation (2.41), in order to generate a time-frequency matrix, defined by equation (2.42), the graph representing a time-frequency plane of Figure 2.11 can be mounted.

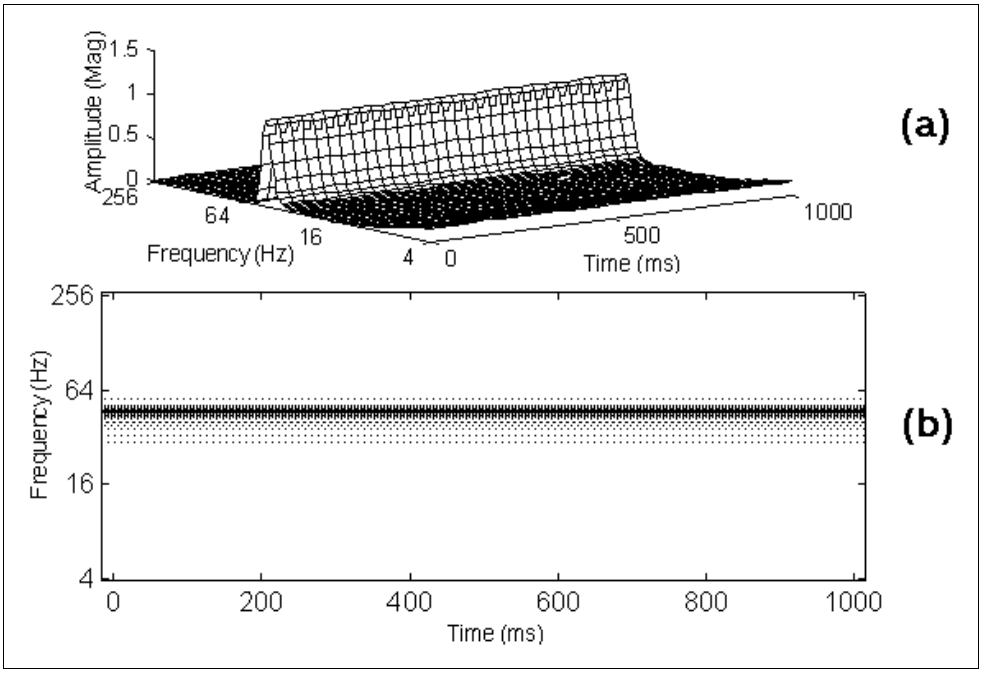

Fig. 2.10 - Wavelet transform of the 32 Hz signal (Morlet technique - perspective view (a) and time-frequency plane view (b))

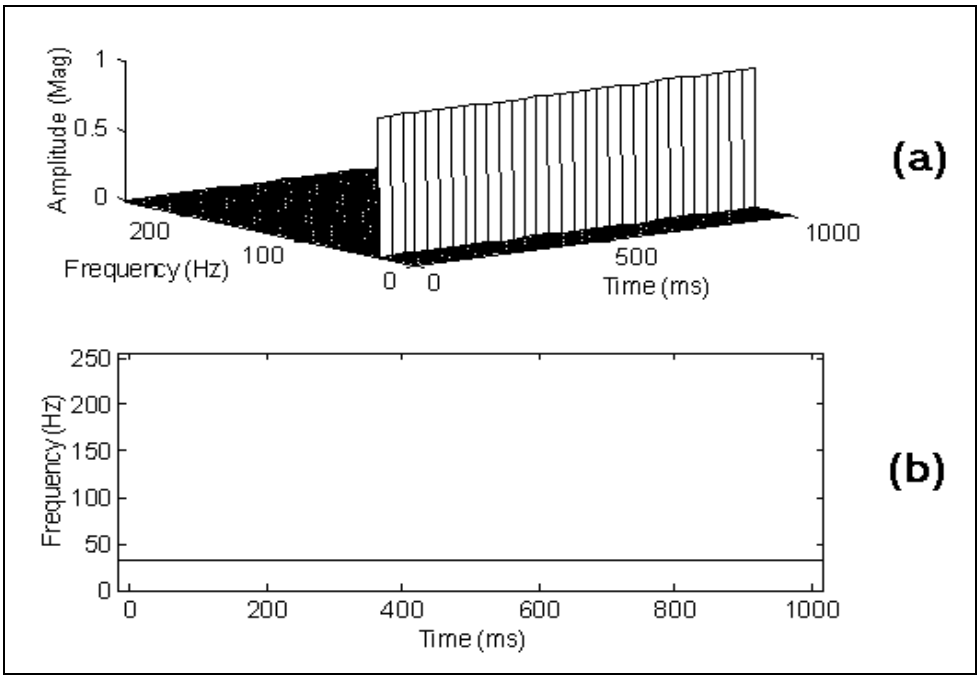

Fig. 2.11 - Extended Prony time-frequency representation of the 32 Hz signal (least-squares in the first step - perspective view (a) and time-frequency plane view (b))

The perspective view graphs (a) in Figures 2.9 to 2.11 are intended to illustrate and help visualise the time-frequency plane graph (b) arrangement. The time-frequency plane represents the “component amplitude or energy distribution” of a signal, and what should be mainly noted in the time-frequency plane is the way in which the points are distributed.

The theoretical work presented above not only deals with stationary components, but also with non-stationary processes. What is in question is the capacity of each technique to depict both stationary and non-stationary components in the presence of noise. The Morlet wavelet transform, the Wigner-Ville distribution, and a variant of the latter, the pseudo-Wigner-Ville distribution, process signals through the use of the Fourier transform and they present some characteristics of this method. The Malat wavelet transform is based on random theory to generate its time-frequency representation and is the most recent technique that has been applied to signal processing analysis. The extended Prony time-frequency representation developed in this study to apply for non-stationary processes represents a new approach which uses the original Prony method. This new approach is based on the idea of considering non-stationary conditions as transients, for which the original Prony method, an autoregressive class technique, is the most suitable mean of representation, and each of these techniques, theoretically described above, will be compared in several specific simulation conditions below, in order to depict their “best” and “worst” signal processing conditions and to select the most suitable one for detecting weak deterministic components in signals containing strong spurious components.

The extended Prony time-frequency representation will be "forced" to seek all components present in the signal before selecting specific components to be filtered in order to reduce the possibility of the elimination of weak components through the filtering procedures. As the extended Prony time-frequency representation will

generate time-frequency planes which may provide signal recovery by projecting plane values in the time axis (equation (2.44)), it is firstly intended to utilise these planes, to limit a specific signal frequency bandwidth directly to the plane rather than applying the convolution technique to the signal. In the following section, the theoretical formulations of the convolution technique, as well a new way of performing bandwidth signal filtering, will be presented.

2.9. Convolution and Time-Frequency Plane Filtering Techniques

As the main components in the vibration signal of an ESP have frequencies between 55 and 62 Hz, a bandwidth frequency window set within these specific limits applied to the signal may improve the detection of the ESP weak components. To improve the weak component detection, the signal may be convolved in the time domain with a bandwidth filter prepared in the frequency domain. This convolution is represented mathematically by the following equation [Ifeachor, E. C. and Jervis, B. W., 1993]:

$$x(n) = IFT(n) \otimes s(n) = \sum_{k=0}^{m-1} IFT(n)s(n-k), n = 0, 1, \ldots, m-1 \qquad (2.45)$$

where

x(n) = signal band filtered

IFT(n) = inverse Fourier transf. of a frequency bandwidth flat window

s(n) = raw signal

n = data sample number of the discrete time sequence

To illustrate this operation, a signal with frequency components each 10 Hz up to 200 Hz is windowed in a frequency bandwidth between 40 to 70 Hz. Figure 2.12 shows the resulting graphs.

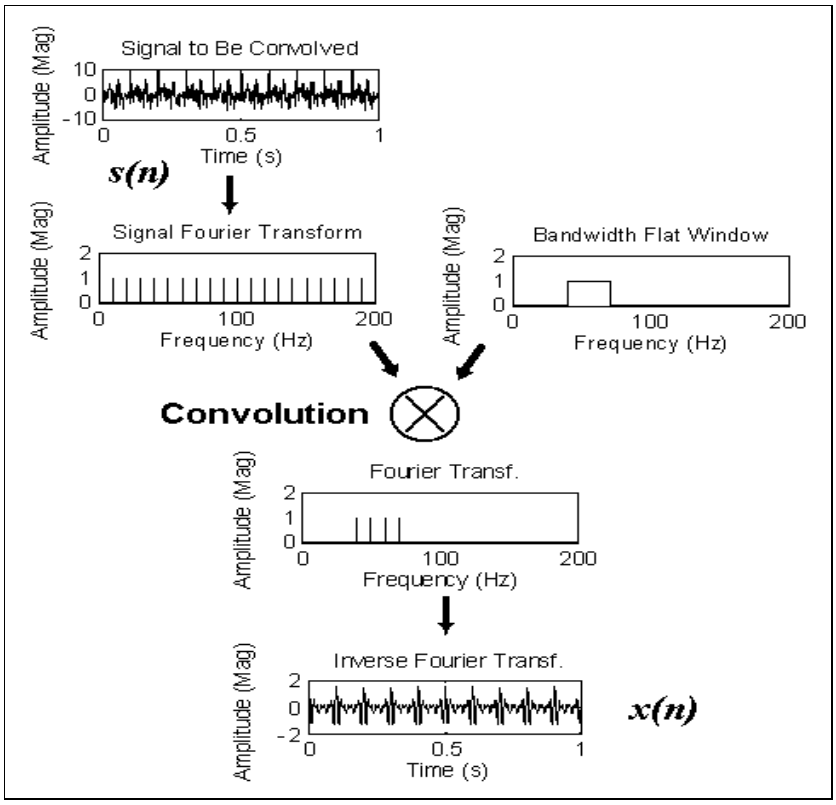

Fig. 2.12 - Convolution applied to a signal limiting the frequency bandwidth to 40 to 70 Hz

As was suggested above, a more convenient frequency bandwidth selection may be achieved by selecting frequency lines in the time-frequency plane, as shown in Figure 2.13. As both stationary and non-stationary components are represented in the time-frequency plane, it may be more convenient to adopt the plane “band-selection” procedure than adopting the traditional convolution filtering.

As the Prony time-frequency representation plane depicts what is "non-stationary" and what is "stationary", the non-stationary components may be eliminated setting to zero

parts of the time-frequency plane in which they are detected. The rest of the components may be recovered by summing the corresponding amplitude values in the frequency bandwidth selection along the time axis of the plane, after multiplying by its respective phase (see equation (2.44)).

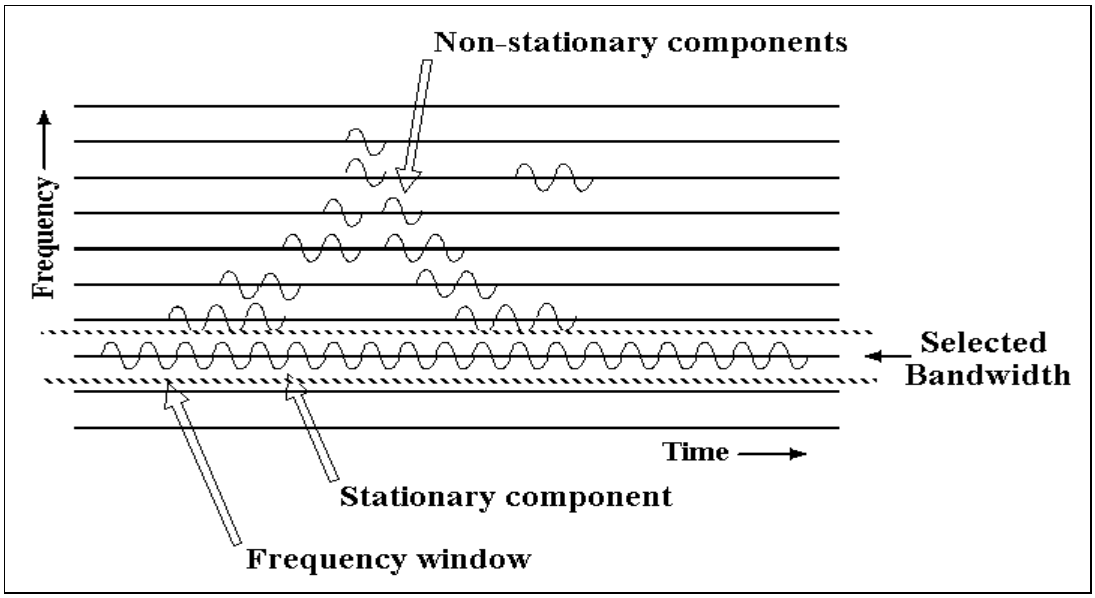

Fig. 2.13 - Separating stationary from non-stationary components
and applying the plane "band-selection" operation

A simple example is given in the diagram of Figure 2.14. The time-frequency filtering and recovering operation described above is applied to a signal containing an 8 Hz component (Figure 2.14 (a)). An extended Prony time-frequency representation of the original signal, which contains amplitude, frequency, phase, and exponential damping is generated. Figure 2.14 (b) shows a plot of the time-frequency plane amplitude values. A "bandwidth slice" is selected from the time-frequency plane (Figure 2.14 (c)), and each amplitude value is then multiplied by its associated phase value to recover the original signal (Figure 2.14 (d)). In this case no exponential damping filtering procedure is applied.

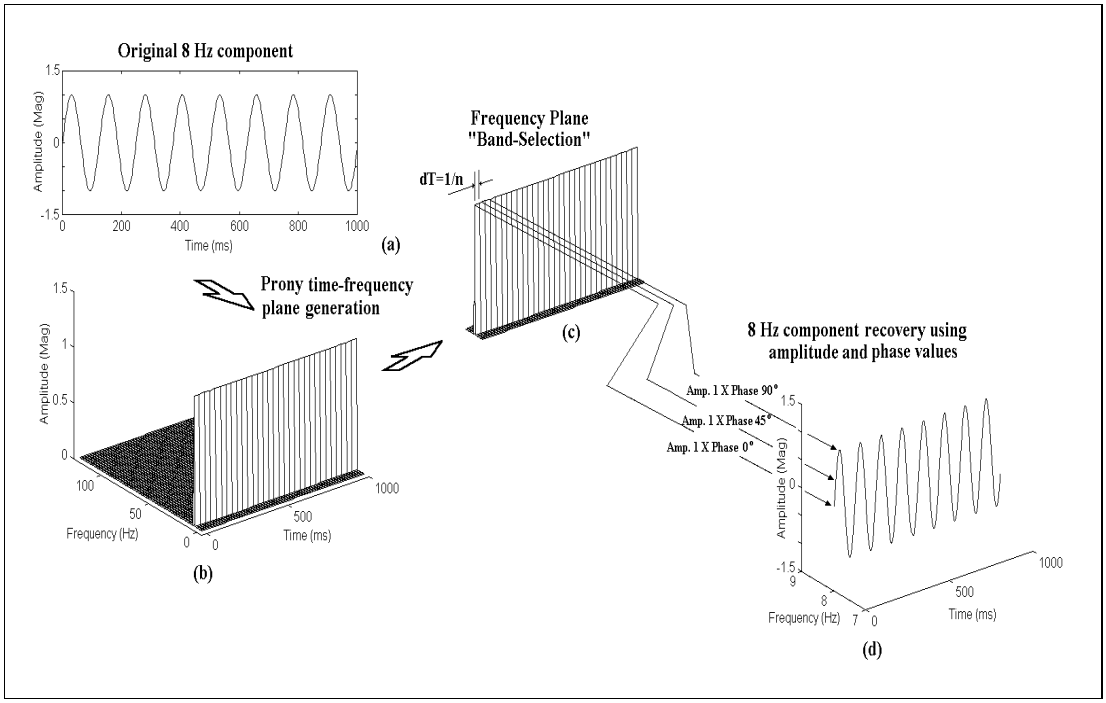

Fig. 2.14 - Time- frequency plane “band-selection” and recovery operation of a signal containing an 8 Hz component

Figure 2.15 shows the graph of the procedure by which a signal is analysed and filtered. This procedure involves the following steps:

(1) The signal is decomposed using the extended Prony time-frequency representation, and the resulting amplitude peaks of all components found by the method are rearranged on the time-frequency plane (Figure 2.15 (a)). The time-frequency plane generated can then be used for filtering purposes.

(2) A bandwidth selection can be made by setting to zero all amplitude values outside the selected frequency bandwidth on the time-frequency plane, as depicted by Figure 2.15 (b).

(3) In this step, all amplitude values of the components which have high exponential damping (transients) are set to zero. The remaining amplitude values of the relevant

components on the bandwidth are multiplied by their respective phase and projected on the time axis generating the signal shown in the graph of Figure 2.15 (c).

(4) To the resulting signal shown in Figure 2.15 (c), which has a high information content of the deterministic weak components, is applied the Fourier transform (Fig. 2.15 (d)). We can now utilise the resulting spectrum to detect weak component amplitude variation.

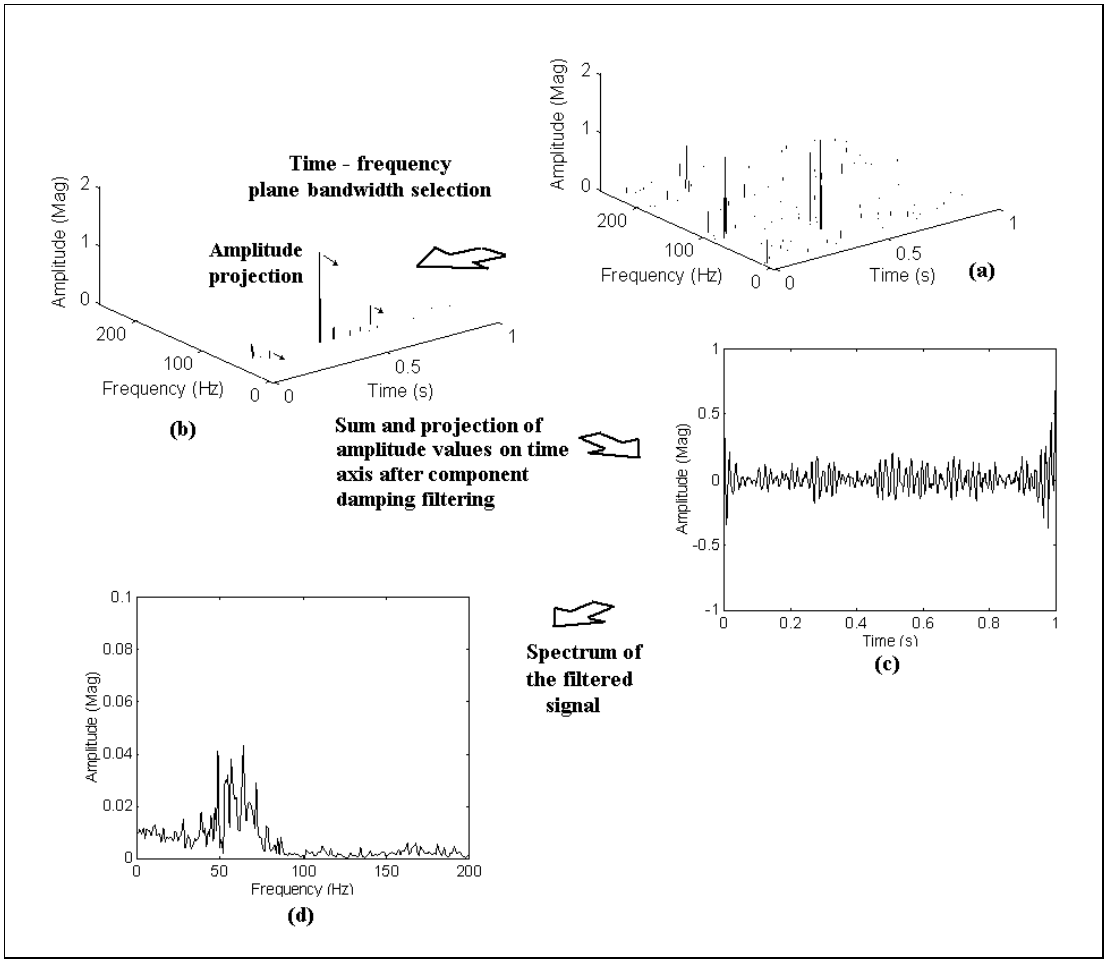

Fig. 2.15 - Time- frequency filtering and recovering operation

2.10. Conclusion of the Signal Processing Theoretical Analysis

It may be noted with the above theoretical analysis of the signal processing techniques that the extended Prony time-frequency representation developed in this study (equations (2.41) and (2.42)) will require much more computational effort than the counterpart wavelet transform and pseudo-Wigner-Ville distribution techniques (equations (2.15) and (2.20)). The reason for this resides in the fact that each time step of the extended Prony time-frequency representation requires two matrix computations (equations (2.22) and (2.33)) and a complex polynomial of order 2***p*** evaluation (equation (2.28)). These matrix computations require more numerical calculations than are required to evaluate the Fourier transform by the use of a fast algorithm (FFT). This may cause some difficulties when implementing the extended Prony time-frequency representation to a real time analysis as implemented in the case of the spectral analysis using Fourier transform through a fast algorithm (FFT). Furthermore, in equations (2.22), (2.28) and (2.33), which are the heart of the original Prony technique calculation, some singular matrices and floating point errors can be expected. To overcome this problem, the order of the original Prony method for each time step has been set with an initial value of 96 (maximum computer program order evaluation) which will automatically reduce if an abnormal error should occur.

The extended Prony time-frequency representation will be regarded throughout this thesis as more of a filtering technique than a technique for observing true spectra of signals. With regards to the time-frequency plane signal recovery (see Figure 2.14), Flandrin [1985] applied this operation to the Wigner-Ville distribution and concluded that this can be reasonably applied to time-frequency distribution results. This can also be stated for the extended Prony time-frequency representation. In Chapter 3, the extended Prony-time-frequency representation will be compared with the Wigner-Ville and pseudo-Wigner-Ville distributions, and Wavelet transform techniques by applying then to simulated signal data.

Chapter 3
Signal Simulation

3.1. Introduction

In this chapter, the theoretical methods described in Chapter 2 will be compared and contrasted under simulated conditions. Simulated signals will be used to test the Fourier and the Morlet wavelet transforms, the Wigner-Ville distribution, the pseudo-Wigner-Ville distribution and the extended Prony time-frequency representation methods for their effectiveness in depicting deterministic and non-stationary components under specific conditions. Once these tests have been completed, multi-component signals will be generated in an attempt to represent the live signal collected at the petroleum wellhead. Since the aim of this study is to develop a method to detect the rotation-related vibration of an electrical submersible pump, with a frequency value close to 58 Hz, the focus will be on detecting signal components with frequencies that are around that value. Finally, additional signals with unknown compositions will be prepared for processing in order to avoid any bias when seeking a specific component in the signal.

3.2. Preliminary Tests of Some Existing Signal Processing Techniques

It will be shown below that preliminary tests carried out in this study using simulated signals revealed basic problems with the average and the autocorrelation (biased and unbiased) filtering techniques, the Fourier and the Malat wavelet transforms, and the extended Prony time-frequency representation with a recursive least squares routine initialisation. These problems were encountered when applying these techniques to detect weak components in signals with high-levels of spurious components and non-stationary characteristics.

3.2.1. Time Average Phase Synchronisation Problem

When using time signal averaging, which is one of the most basic techniques for filtering data from signals, care has to be taken to set the correct frequency phase synchronisation between the averaging time steps of the component to be analysed. If the correct frequency phase synchronisation is not observed, the component to be detected will be eliminated through the averaging process. However, it is difficult to avoid this problem when the frequency of the weak component, or any related trigger, is not known precisely, and high-levels of noise are present in the signal. In this case, the averaging process is not efficient at detecting a weak component present in the signal. Figure 3.1 shows an example in which the wrong phase synchronisation was deliberately used to collect data samples to demonstrate what happens to a 32 Hz time signal component (graphs of Figure 3.1 (a) and (b)). Here it can be seen that the average of only two time traces will eliminate the 32 Hz component (graph of Figure 3.1 (c)).

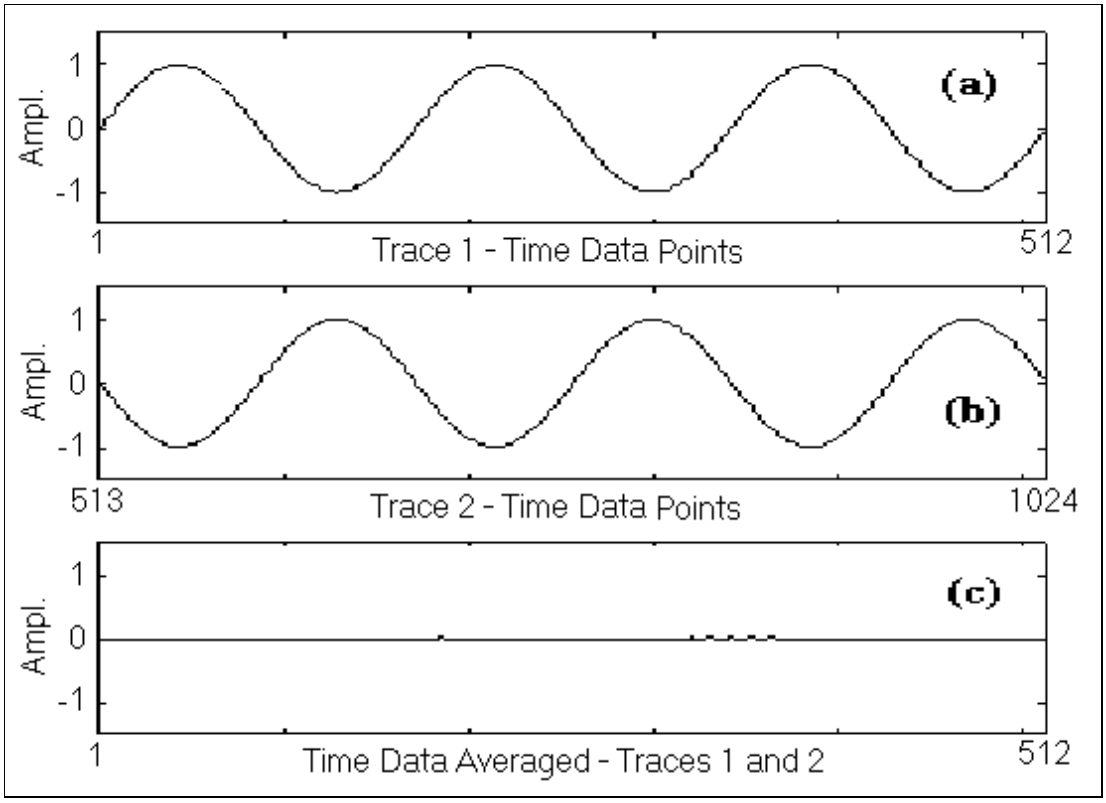

Fig. 3.1 - Average problem (sine wave of 3 Hz, 1 second of data, sampling frequency 512 Hz)

3.2.2. The Autocorrelation Filtering Problems

With regard to autocorrelation filtering techniques, both the biased and unbiased approaches have been found to present problems. The unbiased autocorrelation estimate sequence is defined by the equation [Marple, 1987]:

$$L_u(d) = \frac{1}{N-d} \sum_{n=0}^{N-d-1} x(n+d)\, x^*(n), \quad \text{for } 0 < d < n-1 \tag{3.1}$$

where $L(d)$ is the autocorrelation sequence, d is the lag, N is the number of data points, n is the data point index, and $x^*(n)$ is the complex conjugate of $x(n)$. It must be pointed out that the unbiased autocorrelation estimate may not generate valid autocorrelation sequences. The autocorrelation sequence is defined as [Marple, 1987, Newland, 1993]:

$$L(d) = E\left(x(n+d)\,x(n)\right), \quad for\ 0 < d < n-1 \tag{3.2}$$

If the lag d is zero the autocorrelation will correspond to the mean square value of a random process:

$$L(0) = E\left(x(n)^2\right) = E(x^2) \tag{3.3}$$

If a random process $x(n)$ is uncorrelated to $x(n+d)$, for any lag d greater than zero ($d>0$):

$$L(0) \geq L(d) \tag{3.4}$$

Equation (3.4) represents a property of the true autocorrelation sequence. In the case of the unbiased autocorrelation estimate, if a large lag d is used the reduced denominator $n-d$ of equation (3.1) may generate $L(d)$ values greater than $L(0)$, which is inconsistent with the concept of the autocorrelation sequence.

A biased autocorrelation estimator that has also been applied for signal filtering is defined by the equation [Marple,1987]:

$$L_b(d) = \frac{1}{N}\sum_{n=0}^{N-d-1} x(n+d)\,x^*(n), \quad for\ 0 < d < n-1 \tag{3.5}$$

The problem of the appearance of $L(d)$ values greater than $L(0)$ in the unbiased autocorrelation techniques is not observed in the biased estimate, since the lag is not subtracting the number of data points as in the unbiased estimate (see equation (3.1)). For this reason, the biased autocorrelation is often the preferred estimator. However, it can be demonstrated through a simulation that due to the bias, the biased autocorrelation estimator distorts an existing sinusoid component, gradually reducing its amplitude in the time axis, if a reasonable number of data lags are not used. In the

graph of Figure 3.2, an example of the signal containing a 32 Hz component is shown together with its respective biased autocorrelation. In this case, only two signal traces of 512 data samples were used to generate the autocorrelation sequence, and a decay can be seen in the amplitude values of the 32 Hz component. This problem may be reduced if a large number of data samples are used [Marple, 1987]. Due to this decay, if a biased autocorrelation is applied to filter a signal, followed by the extended Prony-time-frequency representation, the results may depict false exponential damping values for the detected components and, as a consequence, the proposed "exponential damping filtering" mask in that representation will be distorted.

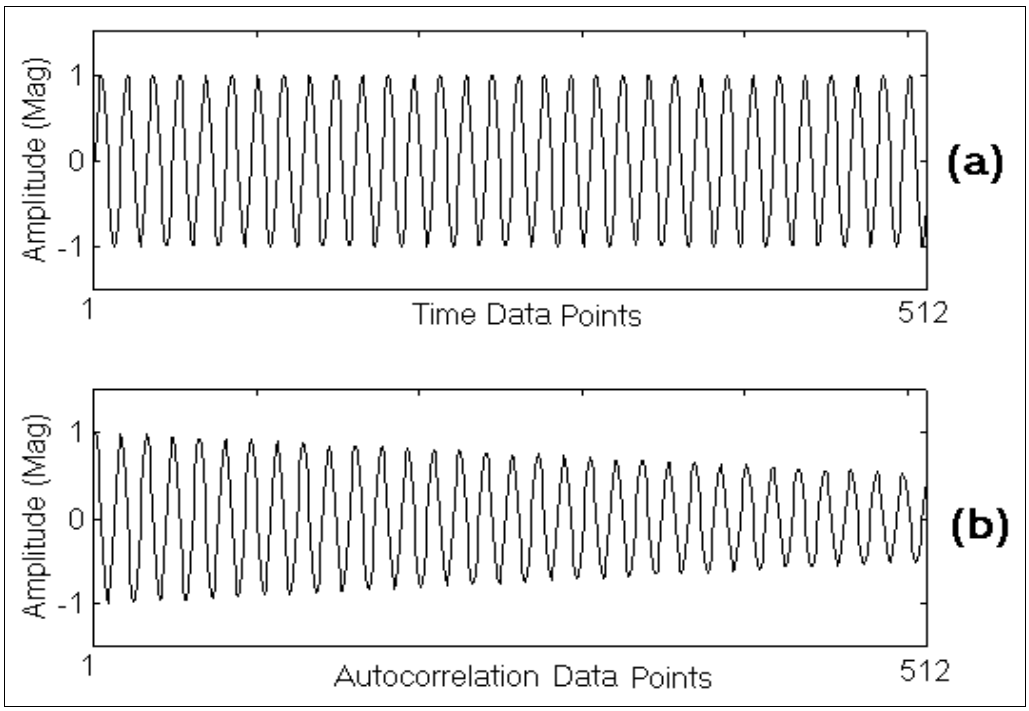

Fig. 3.2 - Example of autocorrelation damping effect ((a) signal containing a 32 Hz component, (b) the biased autocorrelation sequence - sampling frequency 512 Hz)

It must be also be pointed out that if an autocorrelation operation (either biased or unbiased) is applied to a signal, the information about the component phase will be lost. To demonstrate this problem, a signal with a 32 Hz component was processed using the unbiased autocorrelation equation (3.1) (see Figure 3.3). It may be noted in the graph that the original signal phase of 0 degrees (graph of Figure 3.3 (a) - t = 0) was changed to 90 degrees (graph of Figure 3.3 (b) - t = 0). This is embedded in the intrinsic definition of the autocorrelation sequence, the maximum value of the autocorrelation sequence corresponds to an element correlated with itself (100 % correlated). As a consequence, the autocorrelation has no real phase information.

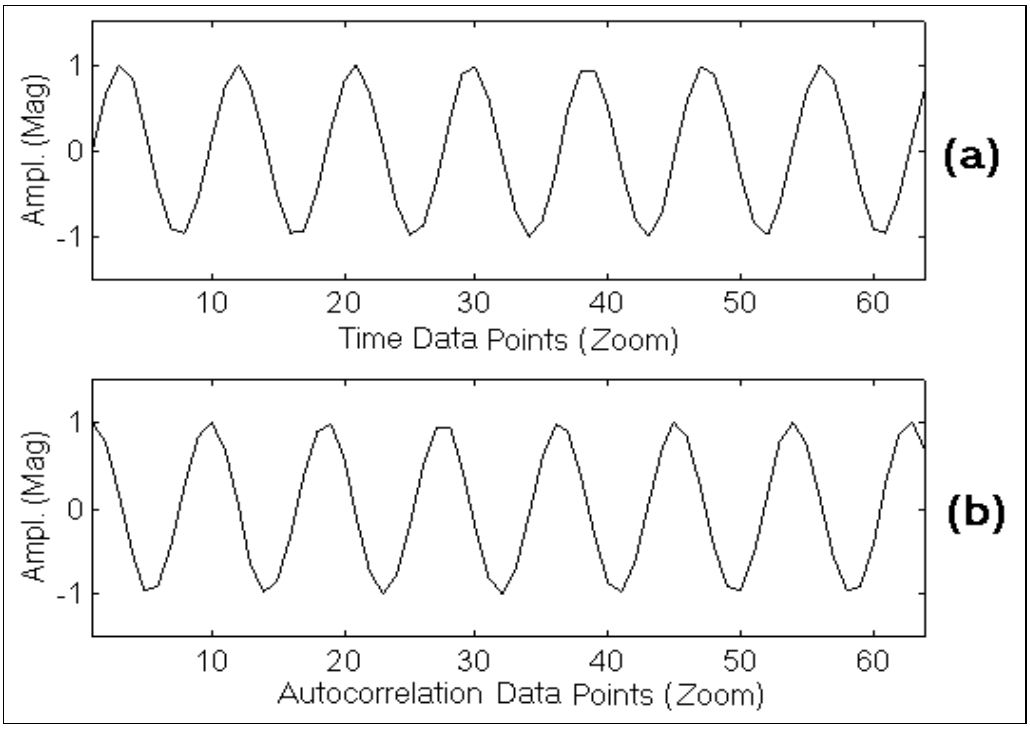

Fig. 3.3 - Example of phase loss in the autocorrelation technique (original signal (a) and the autocorrelated signal (b), calculated using two lags - sampling frequency 512 Hz)

3.2.3. The Fourier Transform Resolution Problem

One problem associated with the Fourier transform method is that due to the resolution limitation related to the uncertainty principle. To demonstrate this problem, a comparison can be made with the original Prony method. As mentioned above, the original Prony method is an autoregressive type of procedure, and due to the nature of its calculations, a high resolution may be obtained when using limited signal data (see section 2.6 of Chapter 2), which is not possible when the Fourier transform is used.

The resolution of the Fourier transform and the original Prony technique were compared by using a signal with a single 32 Hz component. The results shown in Figure 3.4. reveal clearly the difference in resolution. In the graph obtained using the original Prony procedure, only one point in the frequency scale is exactly associated with the 32 Hz component, whereas in the graph obtained using the Fourier transform technique several points represent that component (see Figure 3.4). The shape of the peak corresponding to the 32 Hz component presents a wide base in the graph of the Fourier transform, and this induces the idea of the existence of some components around the 32 Hz component. This phenomenon is known as “leakage”, and is commonly associated with the Fourier transform.

The results from the original Prony method involved the least squares routine in the first step of the algorithm, and used 256 signal data samples for exponential fitting purposes. To generate the Fourier transform results, 512 signal data samples were used. The graph of Figure 3.4 is an adapted form to represent the only exponential found by the original Prony technique. All other graph points were set to zero value. The graph of the original Prony procedure of Figure 3.4 corresponds to one frequency line of the extended Prony time-frequency representation, which corresponds to one calculation of equation (2.22) (see section 2.7 of Chapter 2). As can be seen in the Figures 3.4, to obtain an equivalent resolution using the Fourier transform method a

greater number of data points would be necessary due the leakage problem (Uncertainty Principle).

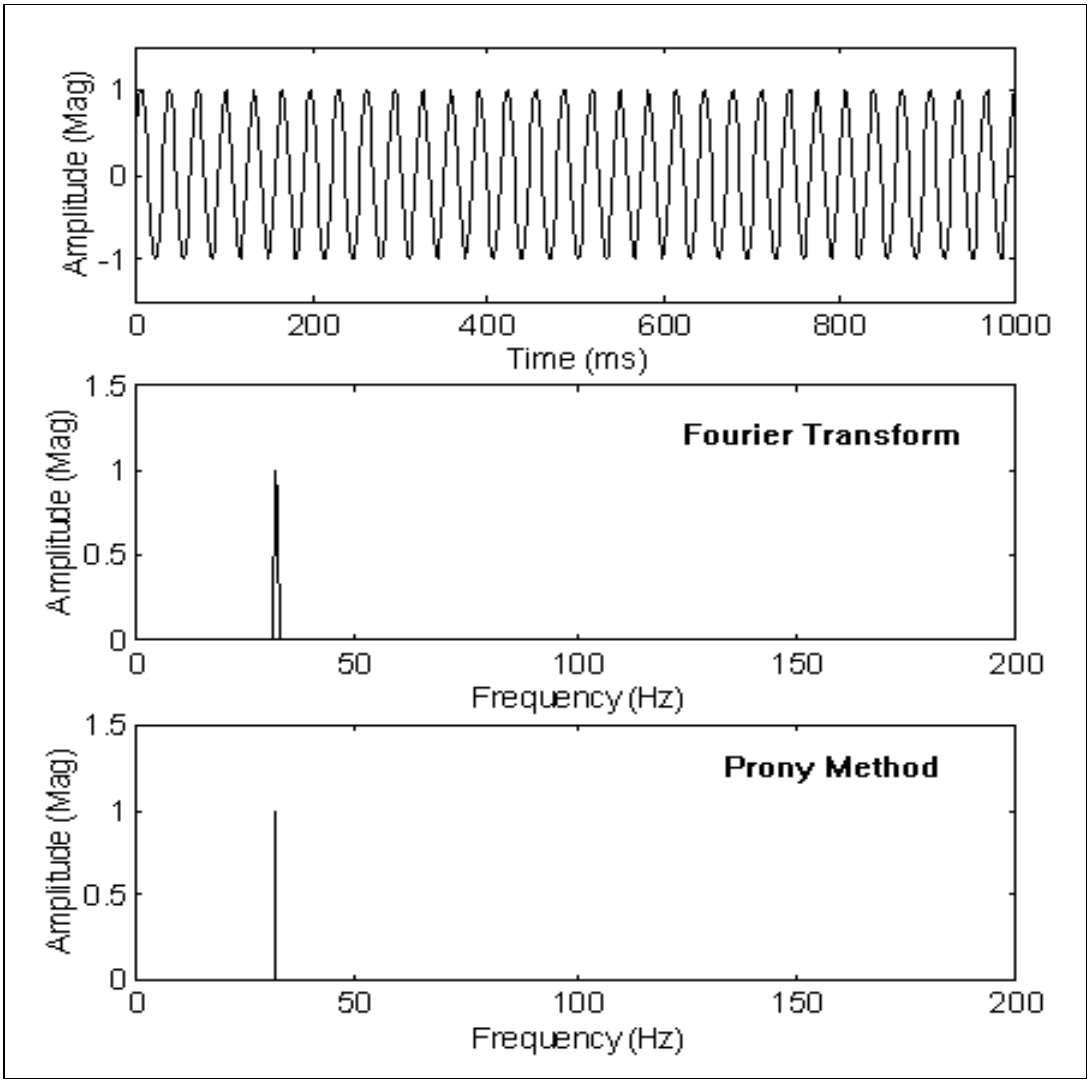

Fig. 3.4 - 32 Hz sine wave signal (512 samples/s) with its Fourier Transform (frequency resolution = 1 Hz) and original Prony method graphs

3.2.4. The Malat Interpretation Problem

A problem found to be associated with the Malat wavelet technique, when attempting to detect weak components in the presence of strong spurious ones, is the basic difficulty of interpreting the results generated by this method. To demonstrate this problem, a signal consisting of two deterministic components and modulations was

generated and processed by this technique. The signal's composition is described in Table 3.1 and the results of the Malat wavelet transform are shown in Figure 3.5.

Components	Time length (s)	No. of data points	Frequency (Hz)	Amplitude (Mag.)	Phase (degrees, t = 0)
sine wave	1.0	512	58	0.1	0
sine wave	1.0	512	60	0.3	90
modulated sine waves (3)*	1.0	90	initial = 6 centre = 24 final = 6	5.0	---

Table 3.1 - Composition of the signal with deterministic components and modulations (* 3 non-stationary local modulations with 90 data points approximately)

The 58 and 60 Hz deterministic components (sine waves) used in several signals throughout of this study were generated according with the following formula:

$$x(n) = A \sin\left(2\pi n t \left(\frac{n}{N}\right) + q\right)$$

where,

n = data sample number of a discrete time sequence ($0 \leq n \leq N - 1$)

$x(n)$ = sine wave discrete data point

A = amplitude (Magnitude)

N = number of data points per time interval

n = frequency (Hz) (58 and 60 Hz)

t = time (s)

q = phase (rad - fixed value)

The modulation components used in this signal were generated according to the following formula:

$$x(n) = A \sin\left(2\pi n_{var} t \left(\frac{n}{N}\right) + q\right)$$

where the frequency ν_{var} is varied according with the formula:

$$\nu_{var} = \nu_{min} + n\Delta\nu, \quad for\ t_1 \rightarrow t_2$$
$$\Delta\nu = (\nu_{max} - \nu_{min})\sin(\theta_V)$$

and where,

ν_{min} = minimum frequency (6 Hz)

ν_{max} = maximum frequency (24 Hz)

t_1 = initial modulation time point (s) (initial frequency 6 Hz)

t_2 = final modulation time point (s) (final frequency 6 Hz)

θ_V = angle varying from 0 to π for $t_1 \rightarrow t_2$

Figure 3.5 (a) shows a plot of this signal, and its time domain Malat wavelet transform is shown in the graph of Figure 3.5 (b). The original signal is decomposed into several Malat wavelet levels representation (level 0 - (c), level 2 - (d), level 4 - (e), level 6 - (f), level 8 - (g)), and the signal can be reconstructed again through the sum of the levels (Figure 3.5 (h)). The Malat wavelet decomposition has a similar meaning as the harmonic decomposition in the Fourier transform. As is shown in Figure 3.5 (h), in spite of a good reconstruction of the signal by adding the wavelet levels, the wavelet representation through levels 0 to 8 (graphs from (c) to (g) in Figure 3.5) has no comparable association between the levels and the physical phenomena as would be expected from a harmonic analysis. It is difficult to make any association with the deterministic components presented in the original signal (58 and 60 Hz). The computer program used to apply the Malat wavelet technique is taken from Newland [1993].

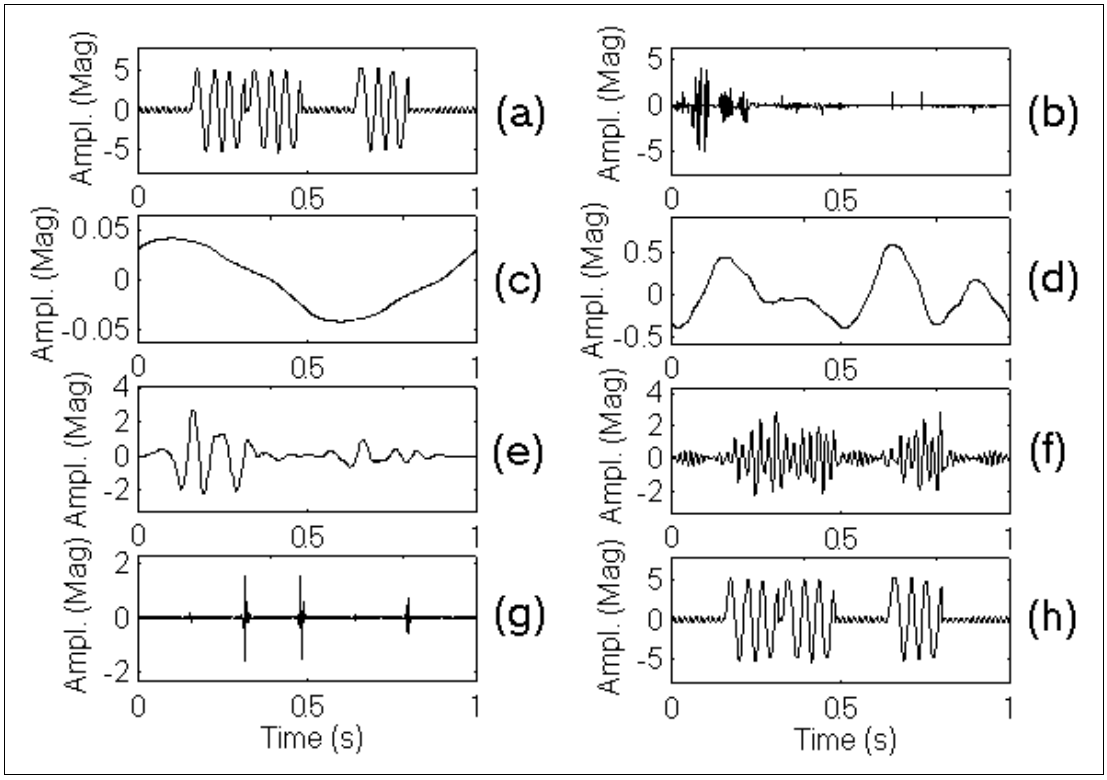

Fig. 3.5 - Wavelet Transform based on Malat method applied to the signal with 58 Hz component (sampling rate of 512 data points per second, (a) original signal, (b) Malat wavelet transform, (c) level 0, (d) level 2, (e) level 4, (f) level 6, (g) level 8, (h) reconstructed signal)

The main point to mention about the graphs in Figure 3.5 is the problem with interpretation that will occur if one tries to interpret the levels as the counterparts of harmonics in the Fourier transform. The wavelet levels have to be regarded as a completely new representation of vibration signals and the Malat wavelet transform should not be compared with an harmonic time-frequency based technique. If the signal contains noise, this difficulty is increased because numerous noise-related components will appear in the Malat wavelet levels generating more confusing graph results. For this reason, the Malat wavelet technique is not considered suitable for this study.

3.2.5. Noise Filtering Problems in the Extended Prony Time-Frequency Representation with Recursive Least Squares Initialisation Routine in the First Step

With regard to the extended Prony time-frequency representation, which has two initialisation routines: recursive least-squares (RSL) and least-squares (covariance), problems were found in the simulation when the RSL routine was used to start up the calculations of this technique. The extended Prony time-frequency representation, with the recursive least-squares initialisation in the first step, was applied to a signal containing a single 58 Hz component of amplitude 1 both with and without high-level white noise of amplitude of magnitude 50 (SNR -34 dB - see section of 3.3.3 of Chapter 3 for white noise definition and Appendix C for SNR assumption). To process the signal without noise, a quantity of 64 data points per time-shift, order 2 with no exponential damping limit was used. The slight variation around the 58 Hz frequency line is due to the instabilities with the calculations of the method (see Figure 3.6).

The extended Prony time-frequency representation with the recursive least-squares routine initialisation in the first step, which has a close relationship with the Kalman filtering technique, is recognised to be appropriate for non-stationary components due to the degree of freedom given to the time parameter (see equations (2.38) to (2.40)). In the case of a slow-time-varying signal, Kalman filtering shows how the incoming raw measurements can be processed to produce more effective autoregressive parameter estimates as a function of time [Press et al, 1992]. However, this method presents problems due to instabilities in the calculations. The weighting window of the recursive time-shifting operation in the first step of this procedure generates a slight variation in the frequency component results (see equations (2.39) and (2.40)). The instability problem of the calculations observed in the graphs of Figures 3.6 (the calculated frequency values are varying) and 3.7 (great number of points randomly

scattered in the plane) would suggest that this method is not suitable for the simulated signals.

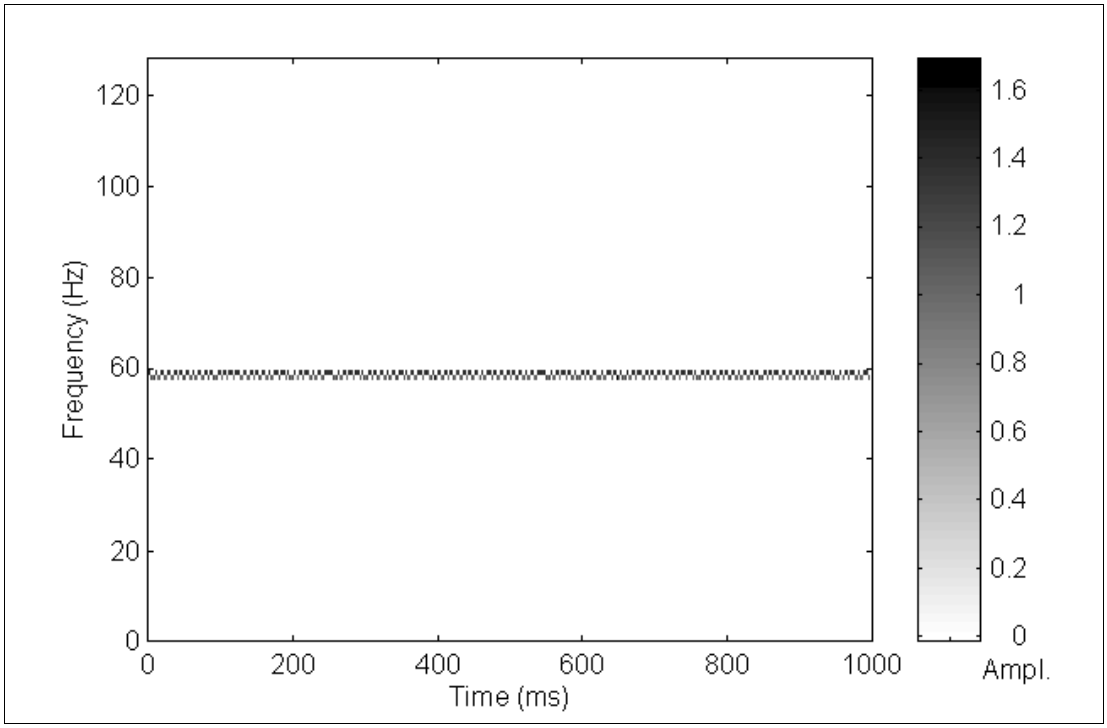

Fig. 3.6 - Extended Prony time-frequency representation with recursive least-squares initialisation in the first step applied to the signal with the 58 Hz component, no noise was added (64 data points per time-shift, order 2 and no exponential damping limit)

If a signal with high-level noise is processed, the inherent calculation instabilities are stressed. This may be noted in the graph of Figure 3.7, which was obtained by applying the extended Prony time-frequency representation, with RSL routine in the first step, to a signal with high-level noise (maximum amplitude 50 times greater than the 58 Hz component, SNR -34dB), where data arrays with 64 data points per time-shift, of order 62 and a exponential damping limit of 0.05 s^{-1} were set to generate the results shown. As may be noted in the plot of Figure 3.7, the recursive based technique seems to present difficulties when operating with noise. Its respective time-frequency plane representation presents points that are randomly scattered (see Figure 3.7) and no information about the 58 Hz component present in the analysed signal is given.

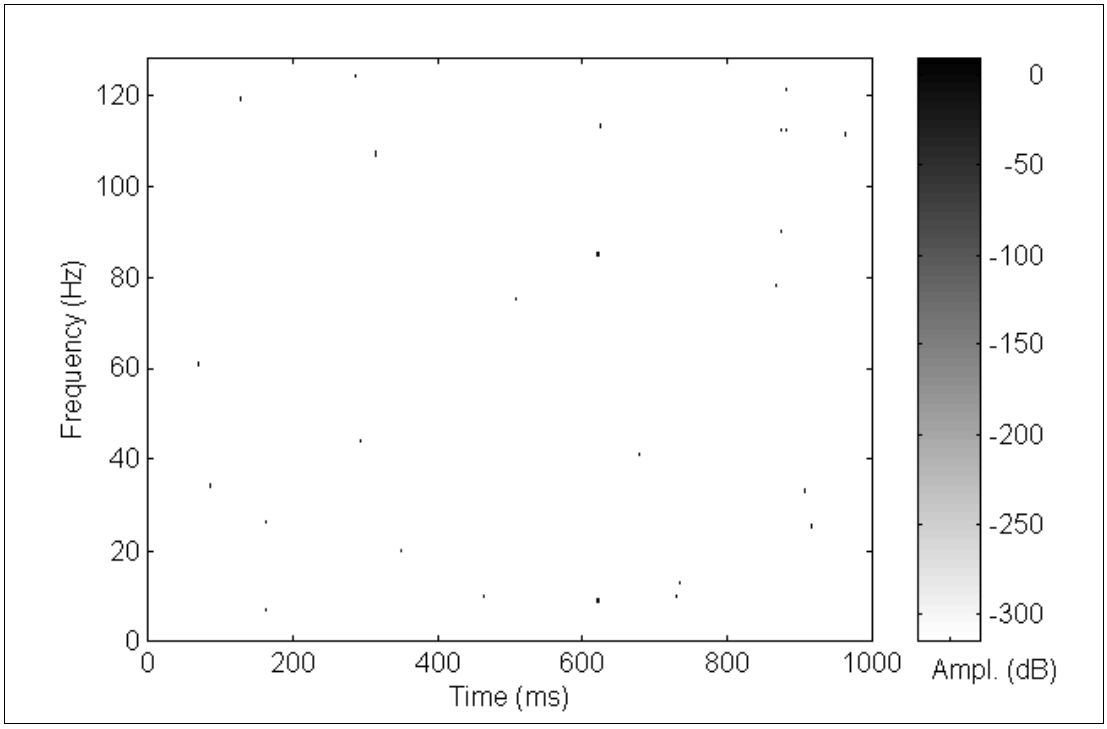

Fig. 3.7 - Extended Prony time-frequency representation with recursive least-squares initialisation in the first step applied to the signal with the 58 Hz component embedded in high-level noise (64 data points per time-shift, order 62 and exponential damping limit set to 0.05 s^{-1})

As a consequence of the problems presented in the preliminary testing simulation, the average and the autocorrelation (biased and unbiased) filtering techniques, the Malat wavelet transform, and the extended Prony time-frequency representation with a recursive least squares routine initialisation will not be considered in the detailed simulations set below. As the Fourier transform resolution problem may be overcome in certain signal processing conditions, for example in the analysis of stationary components by using a large number of data points, this method has been chosen for more detailed tests in the next section. As the Wigner-Ville and the pseudo-Wigner-Ville distributions, the Morlet wavelet transform and the extended Prony time-frequency representation with least-squares initialisation in the first step, did not present any basic problems to analyse non-stationary processes and signals containing noise, they have also been selected for tests with several simulation signals in the next section.

3.3. Signal Processing Techniques: Basic Simulation

In this section, the Fourier and the Morlet wavelet transforms, the Wigner-Ville and the pseudo-Wigner-Ville distributions, and the extended Prony time-frequency representations will be tested with some basic signal conditions. However, first a critique will be made of the programs used to perform each signal processing technique.

What distinguishes the Wigner-Ville from the pseudo-Wigner-Ville distribution is that the latter uses weighting windows applied to each data array in both the time and the frequency domains. This is used to reduce the interference caused by superposition of the extremities of the signal sets. Rectangular, Hamming, Gaussian and Kaiser-Bessel weighting windows in the time and frequency domains have been applied in the pseudo Wigner-Ville distribution [Shin and Jeon, 1993, Chiollaz and Frave, 1993, Moss and Hammond, 1994] (see Appendix D for Kaiser-Bessel window definition). Because it has good selectivity, the Kaiser-Bessel window has been applied to obtain a good two-tone separation of closely-spaced frequency components with widely different levels [Flandrin, 1989], and, for this reason it will be adopted in this study. A MATLAB program has been developed for the purpose of calculating the Wigner-Ville and the pseudo-Wigner-Ville distributions of the signals to be tested.

The program used to apply the Morlet wavelet transform algorithm, where a temporal Gaussian window with variable width is used, is based on the work of Bonaldo [1993]. This latter program involves an algorithm to execute the Morlet wavelet transform via the fast Fourier transform to improve the speed of the calculations.

The original Prony procedure with the least-squares linear prediction estimation (covariance), that is used in the extended Prony time-frequency representation in this simulation, involves a modified least-squares algorithm with computational improvements [Marple, 1981]. It is used in place of the original version to solve the covariance normal equations made by Morf et al [1977]. As the original Prony technique is

considered an autoregressive (AR) process, a loss of resolution can be expected due to the fact that the estimated AR poles are drawn towards the origin of the Z plane due to the noise [Kay, 1979]. Noise only affects the zero-lag autocorrelation term. Covariance and correlation are similar concepts, the correlation is covariance of a process with the mean removed. Take, for example, an uncorrelated noise process, according to the autocorrelation sequence concept (see section 3.2.2 of this Chapter) a large value will be set to the zero-lag term and very low values will be set to the rest of the lags. To reduce this problem, an alternative noise compensation method is offered by Kay [1980] to reduce noise effects on the computational routine that evaluates the covariance for fitting data purpose in the autoregressive techniques. The noise compensation proposed by Kay [1980] is simply accomplished by subtracting all autocorrelation terms by the value obtained in the calculation of the autocorrelation zero-lag term. This alternative has been incorporated in the computational program which uses covariance in the first step of the original Prony procedure, for use in the extended Prony time-frequency representation.

The least-squares routine used in the computational program of the extended Prony time-frequency representation has been modified to accelerate the calculation and to reduce the possibility of obtaining singular matrices. This was accomplished through the insertion of several command lines to check dependent vectors, divisions by zero etc.

Finally, to execute test simulations with the processing methods, a FORTRAN subroutine has been developed to generate signals with a variety of sought and spurious components. The true time-frequency representation graphs, given below, refers to the exact time-frequency representation of the instantaneous components of a simulated signal.

3.3.1. Signal with two Deterministic components (Signal S1)

For this basic simulation phase, three signals were prepared: signal S1 with two deterministic components (58 and 60 Hz); signal S2 comprising a 58 Hz component with amplitude variation, and signal S3 containing a 58 Hz weak component embedded in high-level noise. By using such a basic signal as each of these it is possible to see how each technique involved in this study depicts deterministic components separately. Table 3.2 describes the composition of signal S1 and Figures 3.8 to 3.10 show the signal, its true time-frequency representation, and its Fourier transform. The signal processing results of each time-frequency representation method are shown in Figures 3.11 to 3.14.

Component	Time length (s)	No. of data points	Frequency (Hz)	Amplitude (Mag)	Phase (degrees, t = 0)
sine wave	1.0	512	58	0.1	0
sine wave	1.0	512	60	0.3	90

Table 3.2 - Signal S1 with deterministic components (see section 3.2.4 for component definition)

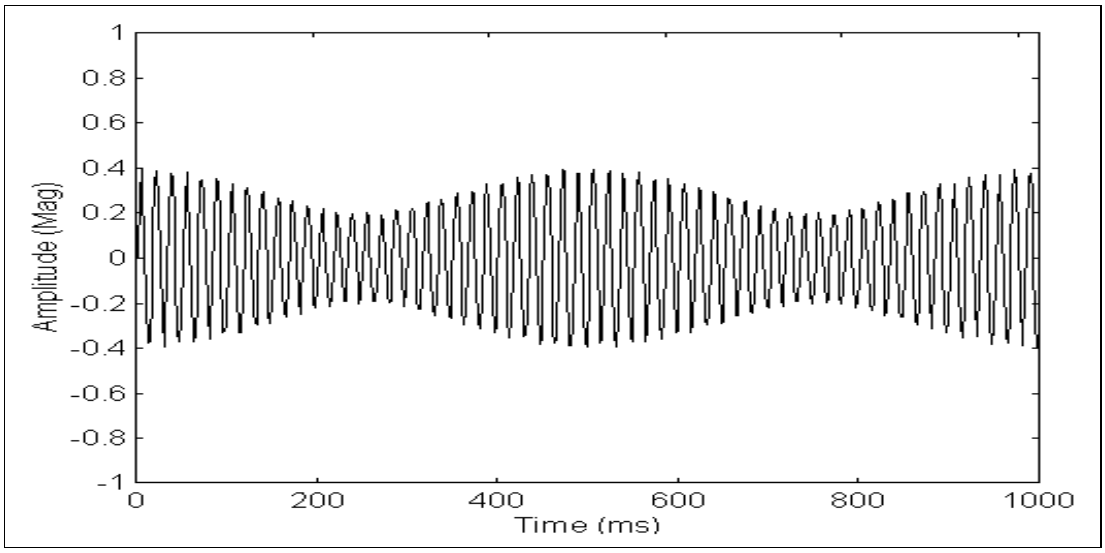

Fig. 3.8 - Signal S1with 58 and 60 Hz deterministic components

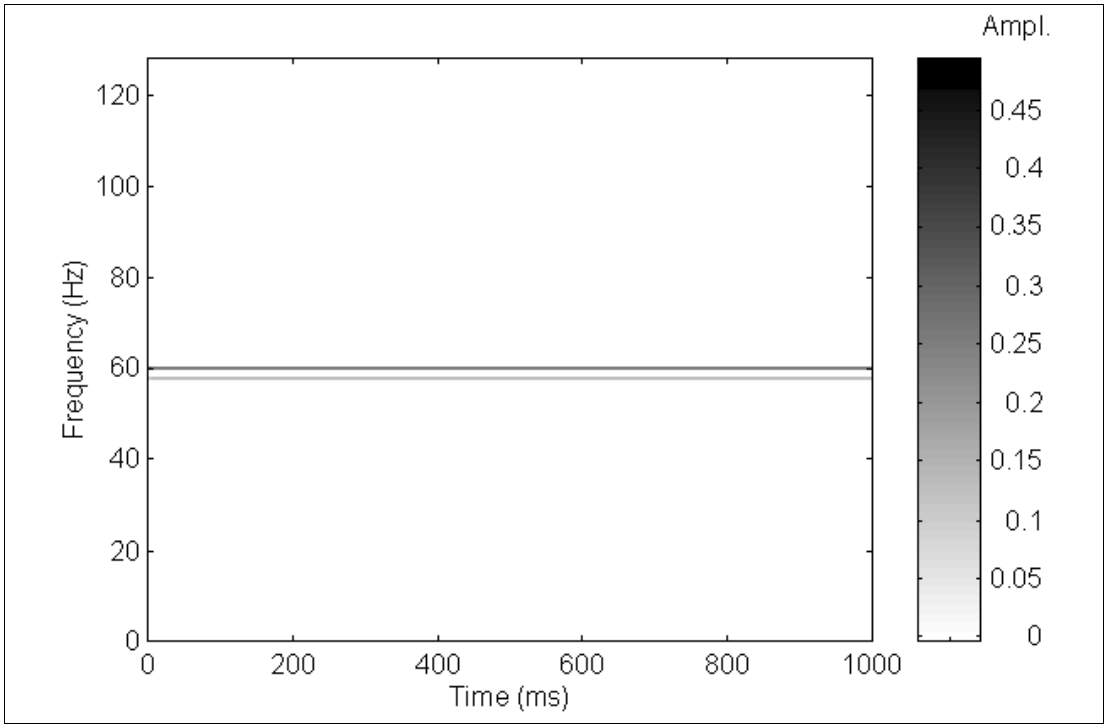

Fig. 3.9 - True time frequency representation of signal S1

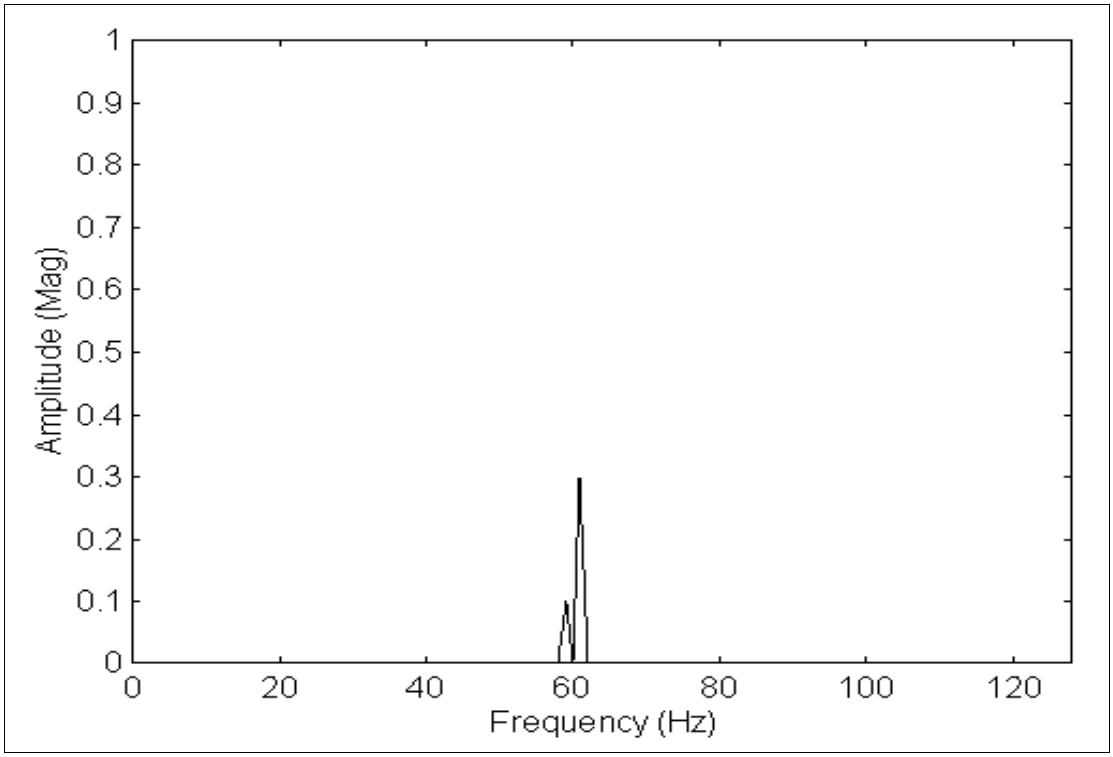

Fig. 3.10 - Fourier transform of signal S1 (frequency resolution = 1 Hz, no window)

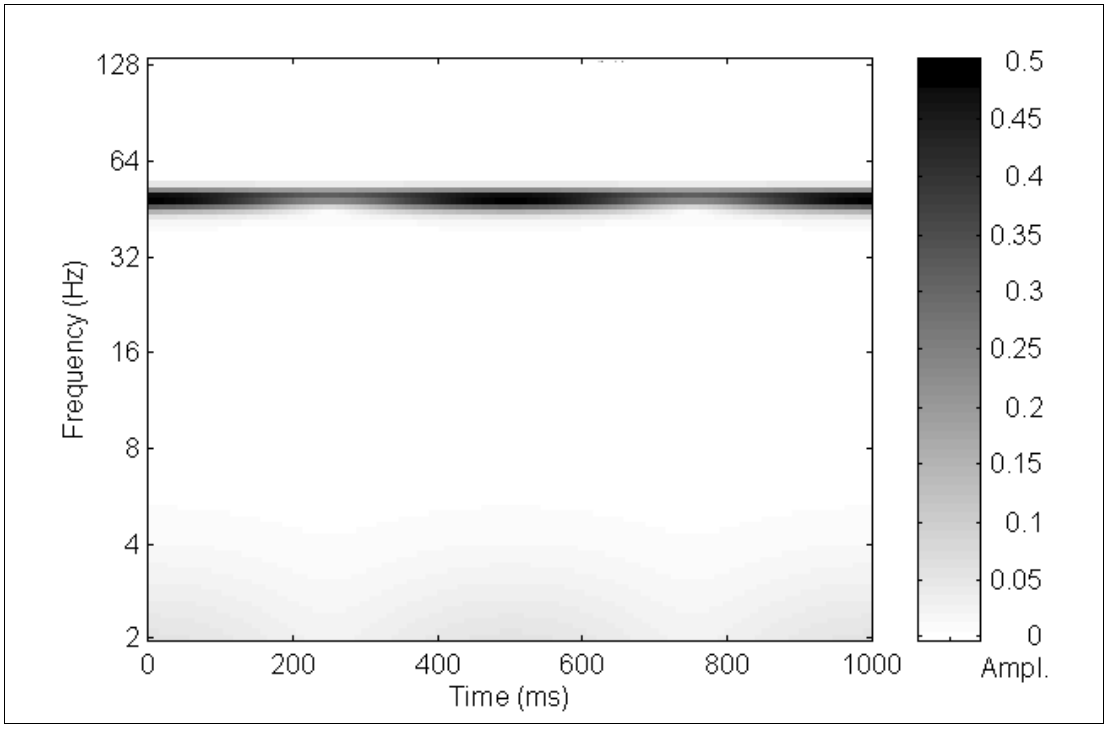

Fig. 3.11 - Morlet wavelet transform of signal S1 (8 octaves & 20 voices per octave)

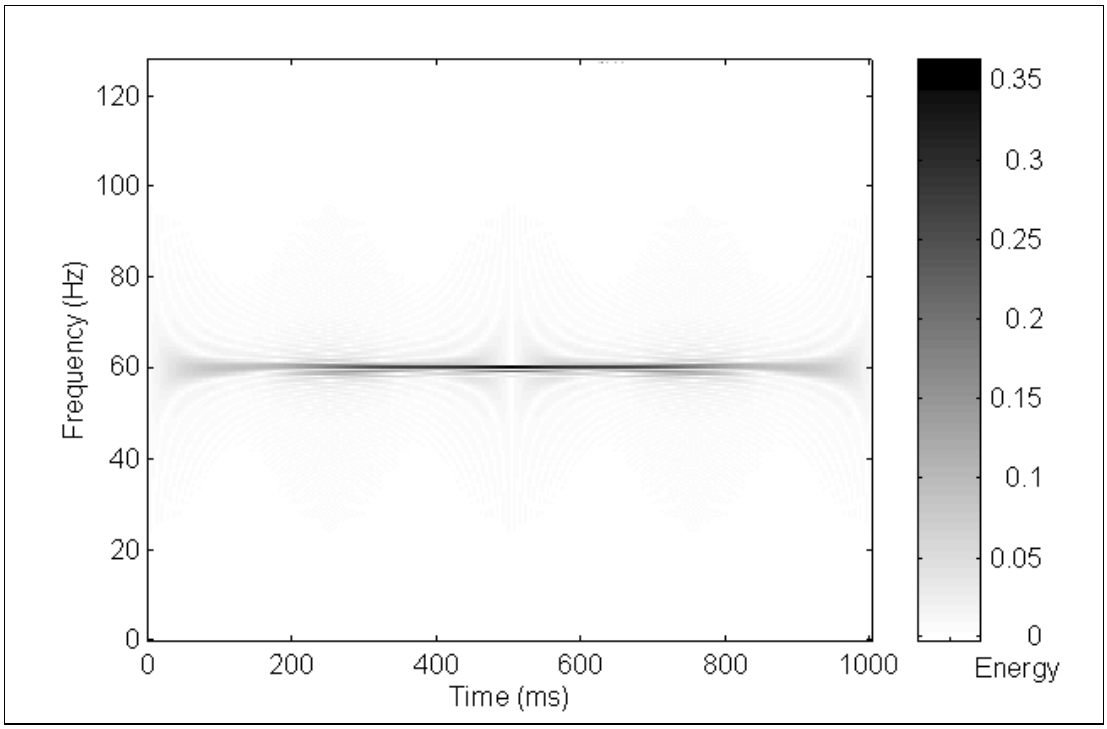

Fig. 3.12 - Wigner-Ville distribution of signal S1 (time-shift = 1 data point)

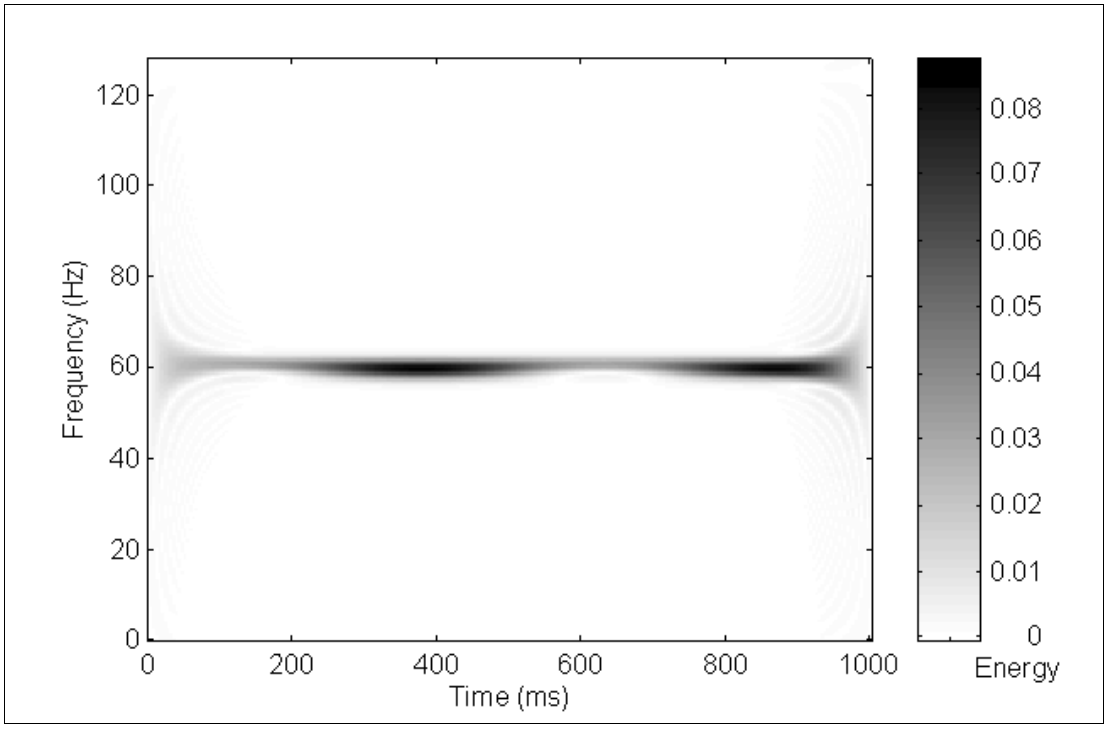

Fig. 3.13 - Pseudo-WV distribution of signal S1 (KB time window exponential argument 70, no frequency window - time-shift = 1 data point)

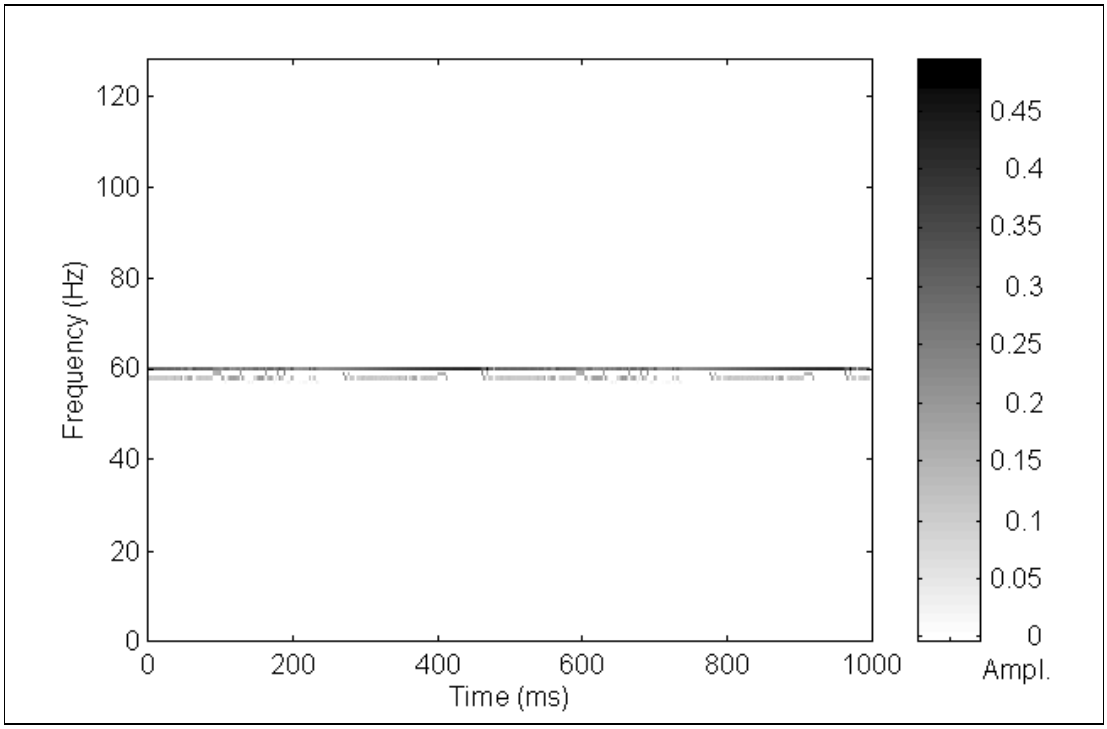

Fig. 3.14 - Extended Prony time-frequency representation of signal S1 (128 data points per sample - total data points used = 639, order 16 and no exponential damping limit)

As expected, the two deterministic components were clearly (though not perfectly) represented when analysed by the Fourier transform (see Figure 3.10). It can be seen that the 60 Hz deterministic component is reasonably depicted by the Wigner-Ville distribution and by the extended Prony time-frequency representation, but the 58 Hz component is not depicted so clearly (see Figures 3.12 and 3.14). The graphs generated by the Morlet wavelet transform and the pseudo-Wigner-Ville techniques do not discriminate adequately the two components. Furthermore, it should be noted that the variation in the tone of the trace of the graph may mistakenly be interpreted as an amplitude or frequency modulation (see Figures 3.11 and 3.13). Due to the windowing effect the pseudo-Wigner-Ville distribution may present different energy peak values from the Wigner-Ville distribution (see Figures 3.12 and 3.13).

3.3.2. Signal Containing a 58 Hz Component with Random Amplitude Variation (Signal S2)

The results of applying each time-frequency representation method to a signal containing a single 58 Hz component with random amplitude variation are shown in Figures 3.18 to 3.21. Table 3.3 describes the composition of this signal and the graphs of Figures 3.15 to 3.17 show the respective signal, its true time-frequency representation, and its Fourier transform.

Component	Time length (s)	No. of data points	Frequency (Hz)	Amplitude (Mag)	Phase (degrees, t=0)
sine wave	1.0	512	58	min. = 0.0 max. = 1.0	0

Table 3.3 - Signal S2 with deterministic component whose amplitude varies randomly

The 58 Hz deterministic component whose amplitude varies randomly (sine wave) used in this signal was generated according with the following formula:

$$x(n) = A_R \sin(2\pi n t (n/N) + q)$$

where,

n = data sample number of a discrete time sequence ($0 \leq n \leq N - 1$)

$x(n)$ = deterministic component discrete data point

A_R = amplitude randomly varied using a random generator computational routine (Magnitude, 0 - 100%)

N = number of data points per time interval

n = frequency (58 Hz)

t = time (s)

q = phase (rad - fixed value)

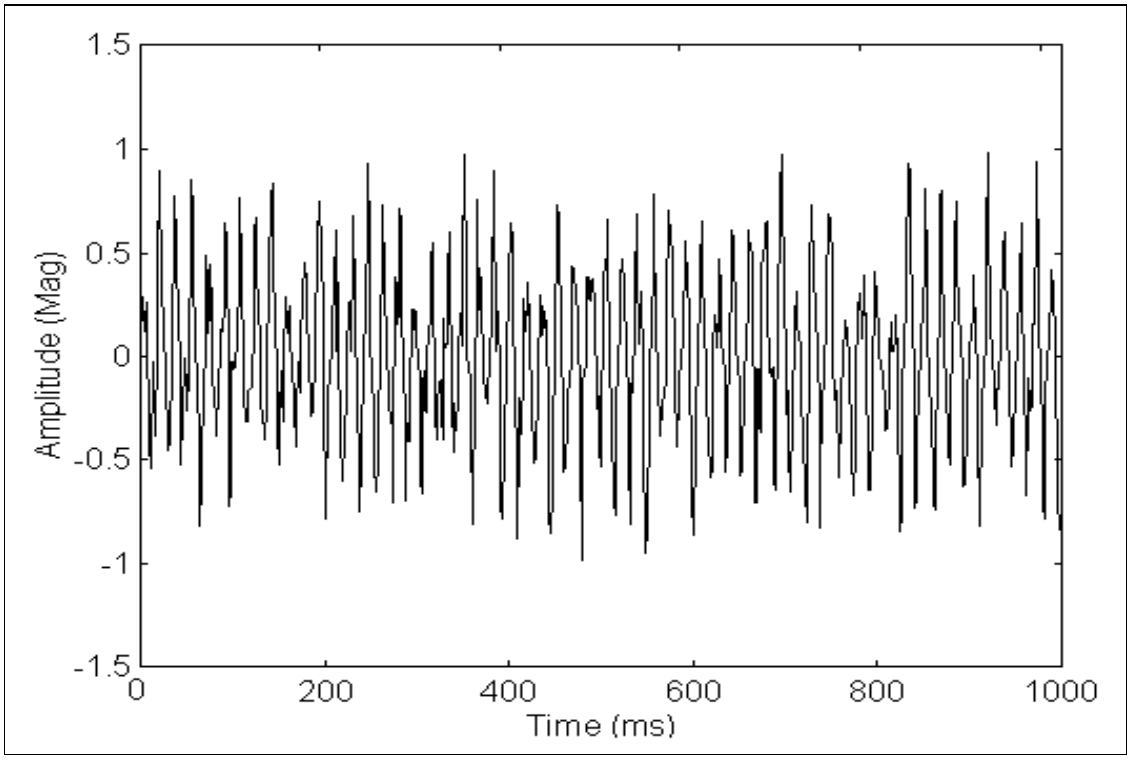

Fig. 3.15 - Signal S2 with deterministic component whose amplitude varies randomly

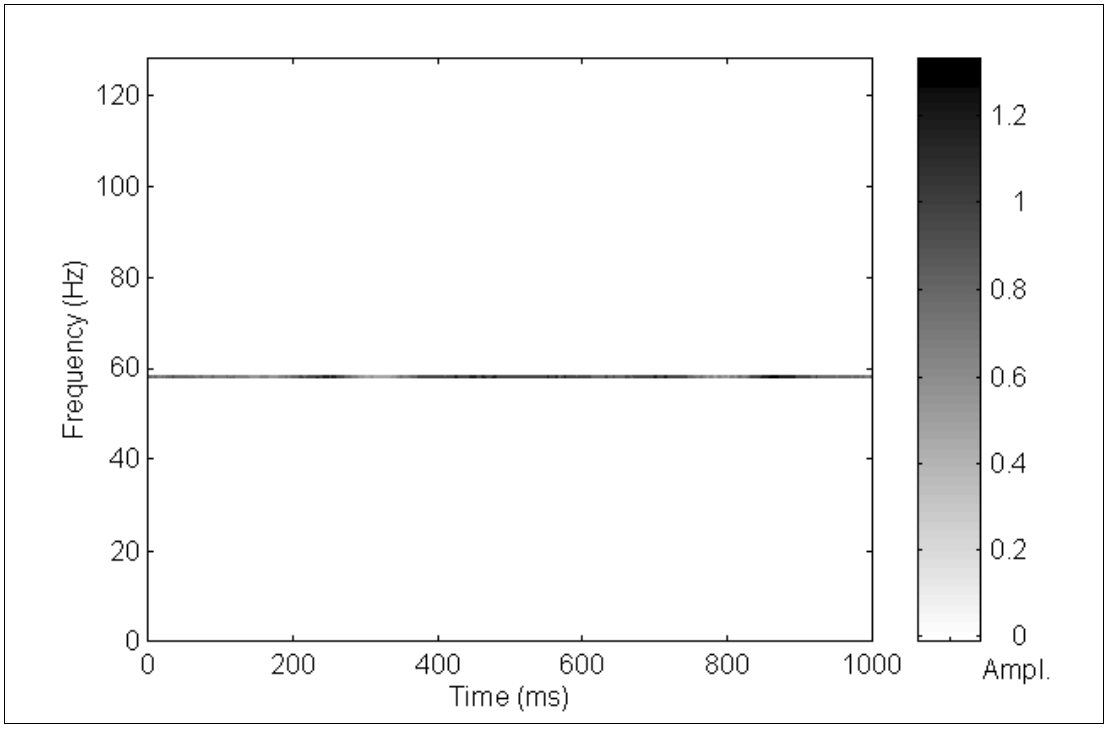

Fig. 3.16 - True time-frequency representation of signal S2

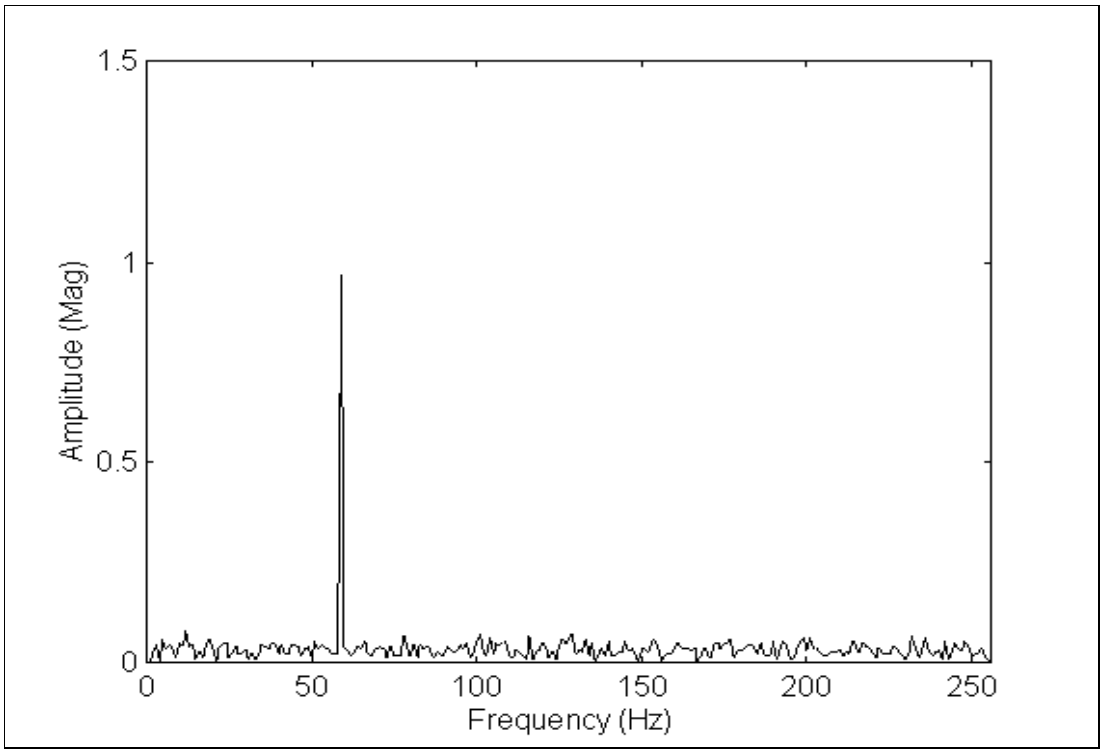

Fig. 3.17 - Fourier transform of signal S2 (frequency resolution = 1 Hz, no window)

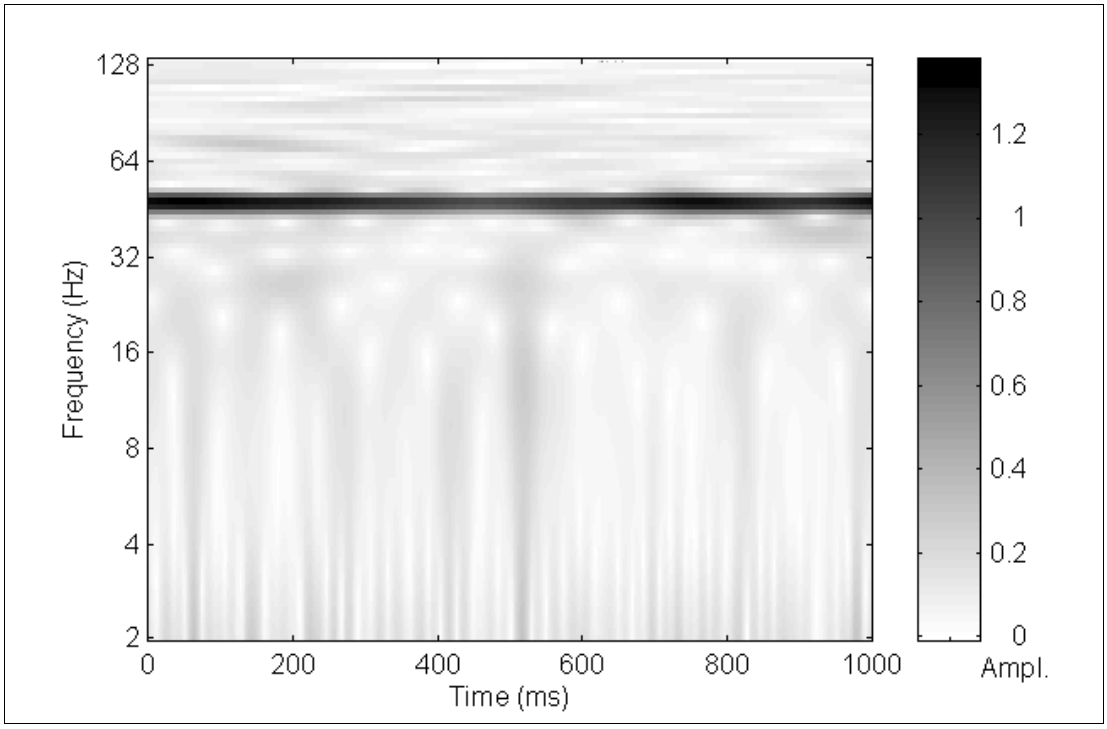

Fig. 3.18 - Morlet wavelet transform of signal S2 (8 octaves & 20 voices per octave)

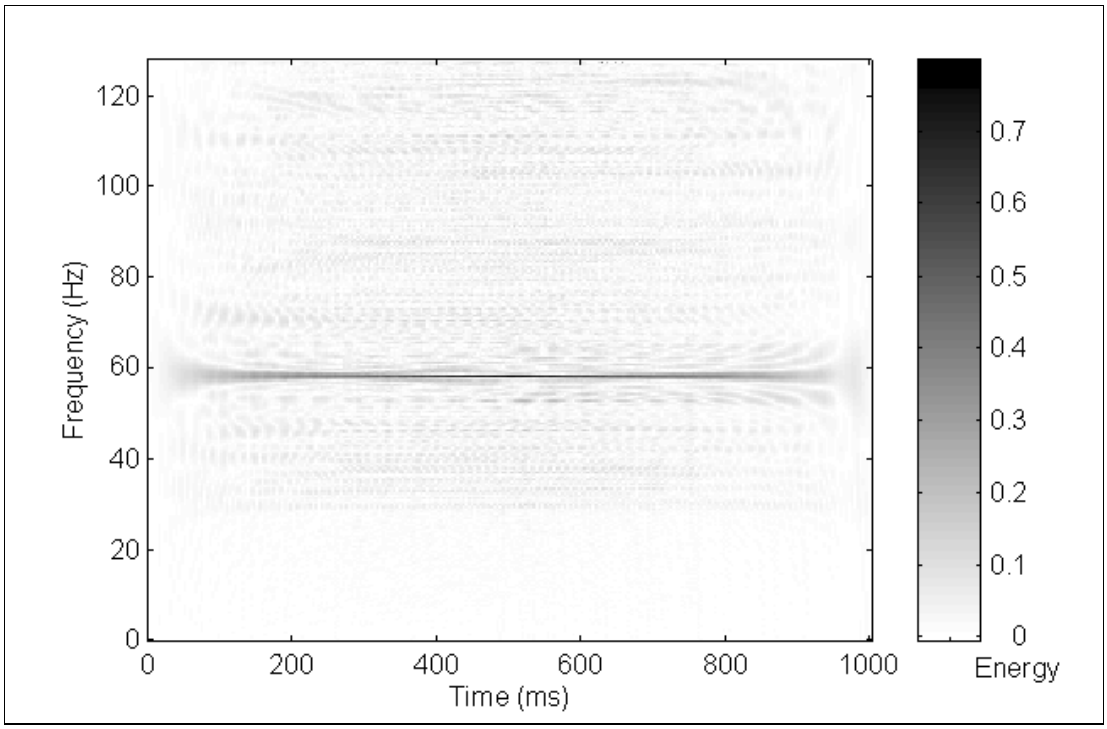

Fig. 3.19 - Wigner-Ville distribution of signal S2 (time-shift = 1 data point)

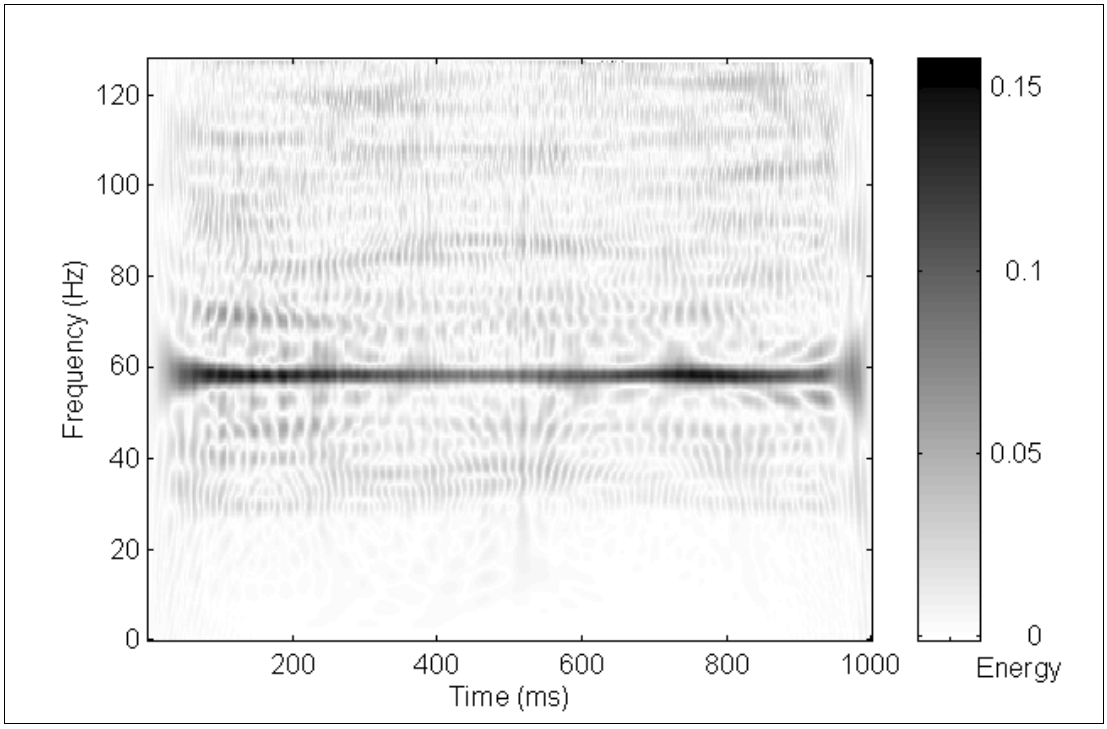

Fig. 3.20 - Pseudo-WV distribution of signal S2 (KB time window exponential argument 70, no frequency window - time-shift = 1 data point)

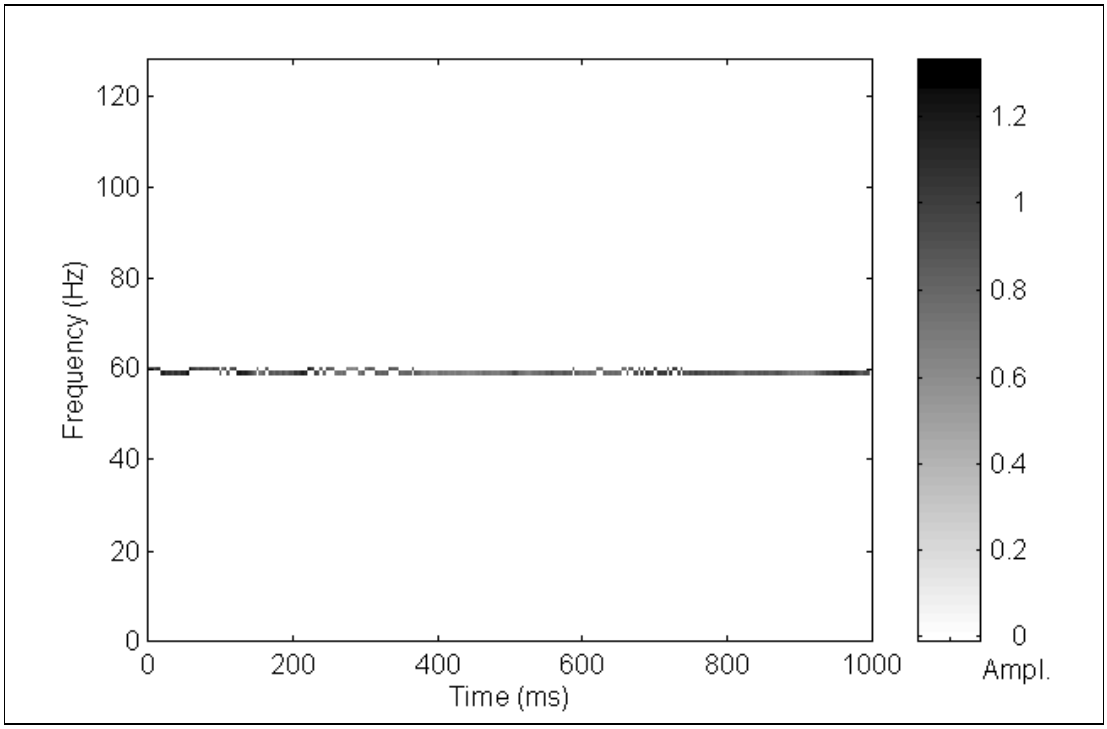

Fig. 3.21 - Extended Prony time-frequency representation of signal S2 (256 data points per sample - total data points used = 767, order 4, no exponential damping limit)

As may be noted in the above Figures 3.17, 3.19, and 3.21, the Fourier transform, the Wigner-Ville distribution and the extended Prony time-frequency representation do not depict well the amplitude variation of the 58 Hz component. In regards to the Wigner-Ville distribution and the extended Prony time-frequency representation, the low sensitivity to amplitude variation is due to the data arrays with large quantity of data points used to calculate the time-frequency planes (see Figures 3.19 and 3.21). In the case of the extended Prony time-frequency representation, the data arrays with large quantity of data points are necessary to "force" the method to detect deterministic components, and, as a consequence, the amplitude values will be averaged. In the numerical evaluations performed to generate the extended Prony time-frequency representation, exponentials are fitted to depict the most representative components of a specific data set. If large data sets are used, the method tends to detect deterministic components because there are more data associated with them. As a matter of fact, the exponential fitting of the original Prony calculations essentially "forces" the method to "search" components which are represented by the greatest number of data points. The pseudo-Wigner-Ville distribution depicts the amplitude variation of the deterministic component due to the windowing effect (see Figure 3.20), the narrow time window applied to data arrays in the time-shifting operation (KB time window exponential argument 70) "forces" the method to detect the local amplitude variation. However, it is difficult to discern in the graph generated by the pseudo-Wigner-Ville distribution if the variations in the graph spots is due to the amplitude or frequency variation. This also applies to the Morlet wavelet transform technique (see Figure 3.18).

3.3.3. Signal Containing a Weak Component Embedded in High-Level Noise (Signal S3)

In this section the weak signal component detection performance of the Fourier and the Morlet wavelet transforms, the Wigner-Ville and pseudo-Wigner-Ville

distributions, and the extended Prony time-frequency representation methods will be assessed using simulated signals containing high-level noise.

The white noise used in the simulation was generated through a FORTRAN subroutine [Press et al, 1992], where a minimal random number generator of Park and Miller, with Bays-Durham shuffle and added safeguards, is generated. This routine returns a uniform random number between 0.0 and 1.0 (exclusive of the point end values). The authors do not know of the existence of any statistical test this routine fails to pass, except when the number of calls starts to become greater than 10^8. This routine generates a white noise which is fairly uncorrelated. Figure 3.22 shows a signal composed of pure pseudo-white noise with maximum amplitude 1 generated by this routine and its autocorrelation. The autocorrelation applied to the signal depicted in Figure 3.22 (b) is the biased one and is defined by the equation (3.5) above. It was performed with 15 data lags with 512 data samples each. The Fourier transform of this signal with pure white noise presents a broadband spectrum in the 200 Hz bandwidth (see Figure 3.23).

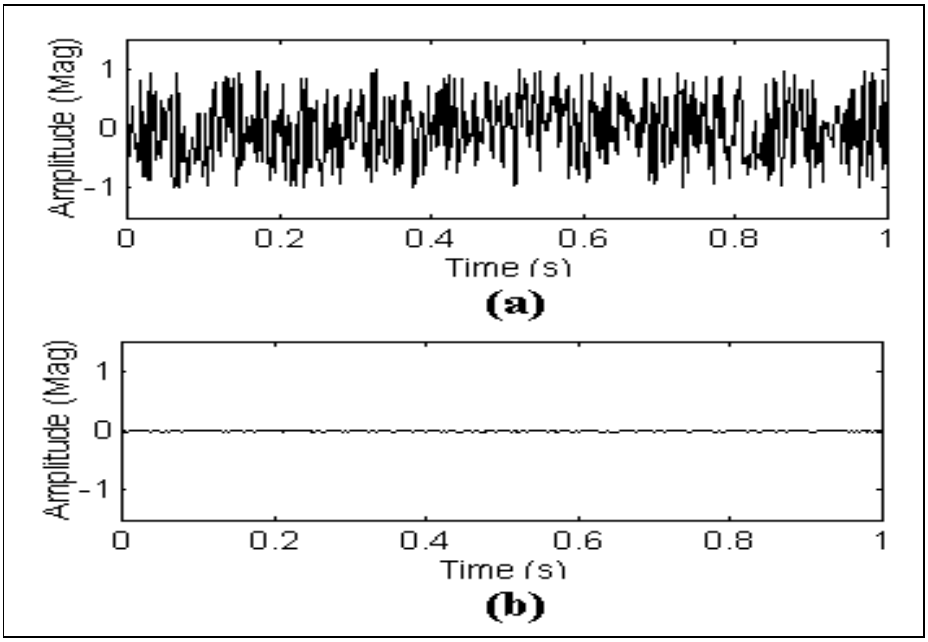

Fig. 3.22 - Signal with pure pseudo white noise (a) and its autocorrelation (b)

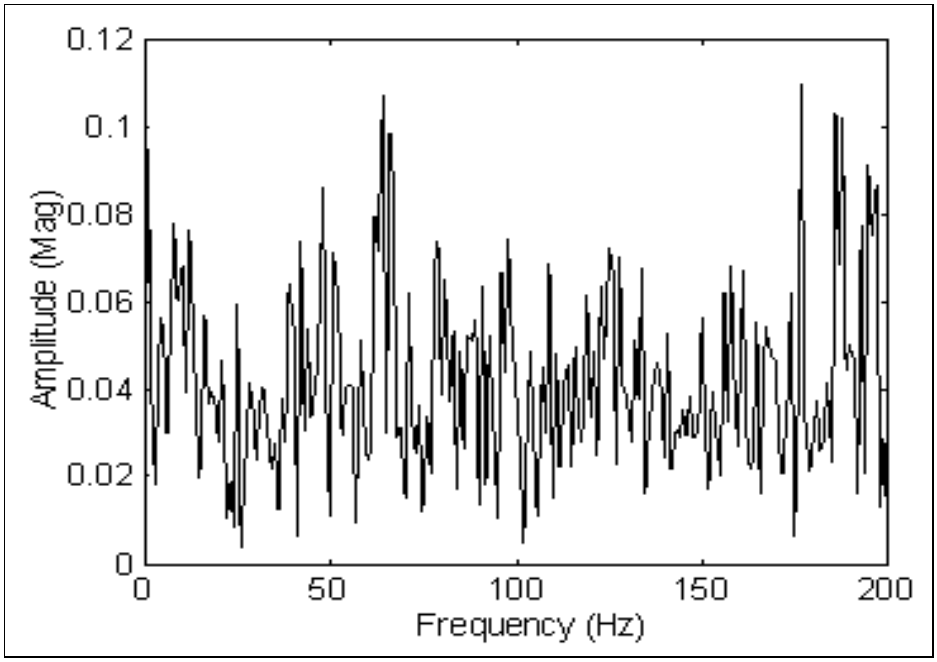

Fig. 3.23 - Fourier transform of signal with pure pseudo white noise (maximum amplitude peak of the time signal = 1, frequency resolution = 1 Hz, no window)

In order to test the method's ability to identify a weak component embedded in white noise, a signal was prepared according to the composition described in Table 3.4. Figures 3.24 and 3.25 show the respective signal S3 and its Fourier transform. For comparative purposes, the Fourier transform method was applied to two different sets of signal data samples, one containing 512 data points and another containing 524288 data points (see Figure 3.25). The figures 3.26 to 3.29 show the results generated by each time-frequency representation method.

Component	Time length(s)	No. of data points	Frequency (Hz)	Amplitude (Mag)	Phase (degrees, t = 0)
sine wave	1.0	512	58	0.1	0
white noise	1.0	512	---	5.0 (max.)	---

Table 3.4 - Signal S3 with deterministic component embedded in high-level noise (see section 3.2.4 for component definition and Appendix C for SNR assumption)

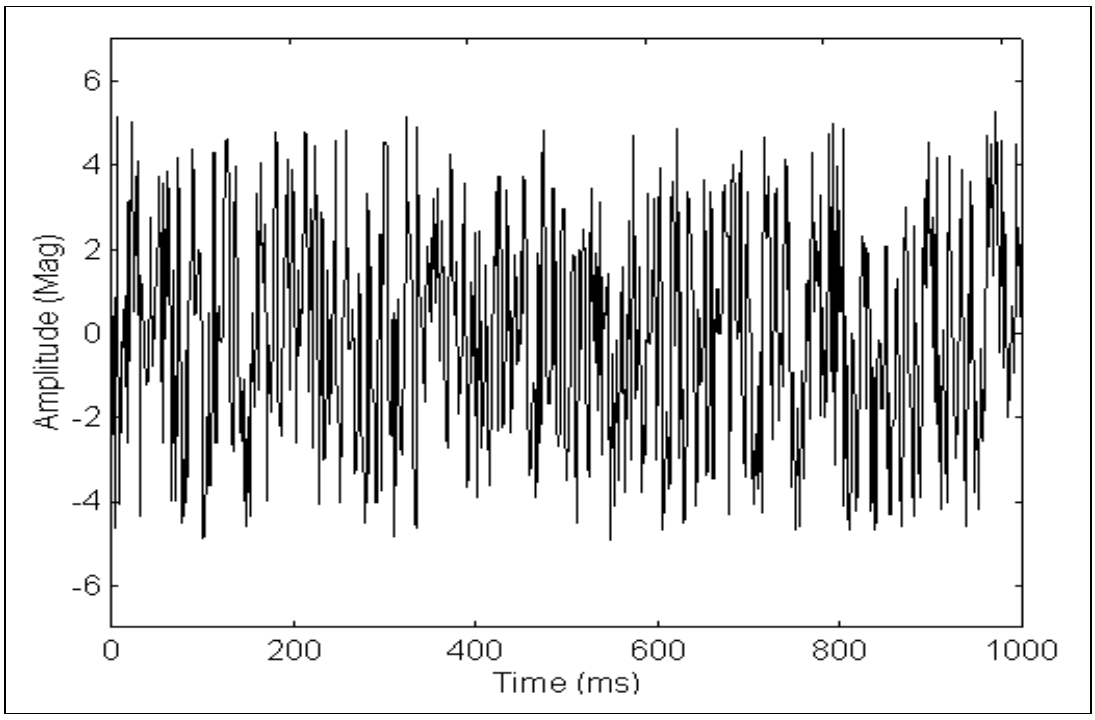

Fig. 3.24 - Signal S3 with a weak component embedded in high-level noise

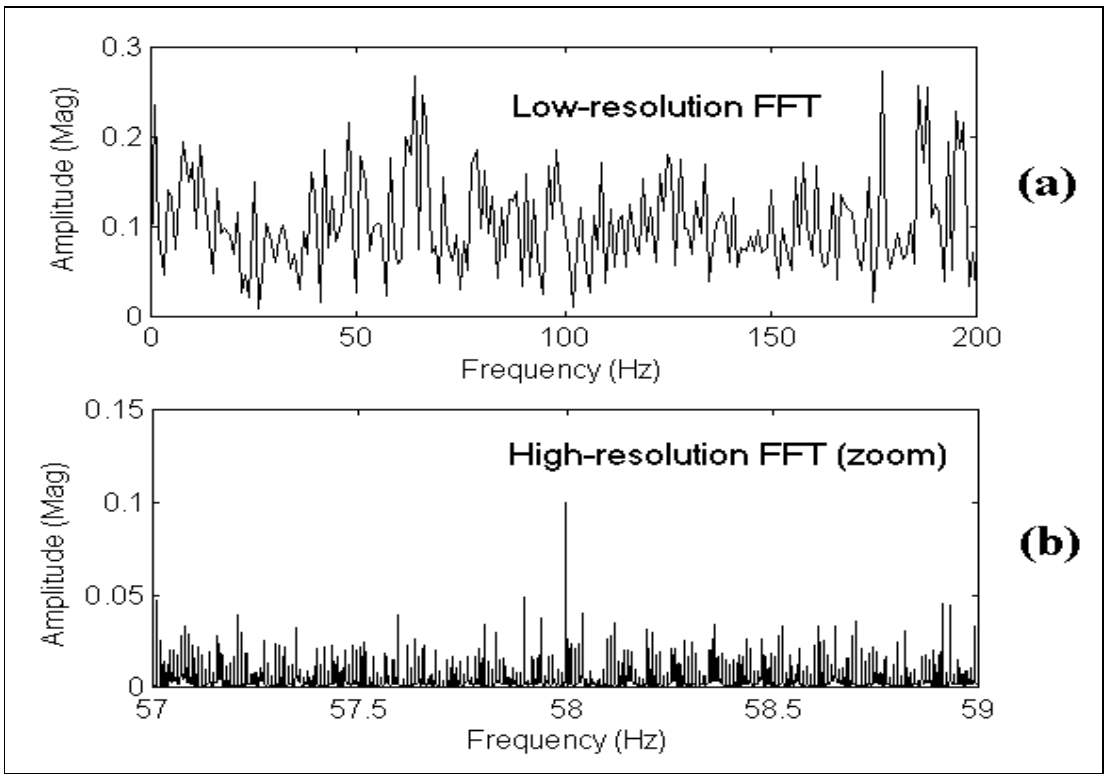

Fig. 3.25 - Fourier transform of signal S3 ((a) 512 data points, 1 second, freq. resolution = 1 Hz, (b) 524288 data points, 1024 seconds, freq. resolution = 0.001 Hz - no averaging, no window)

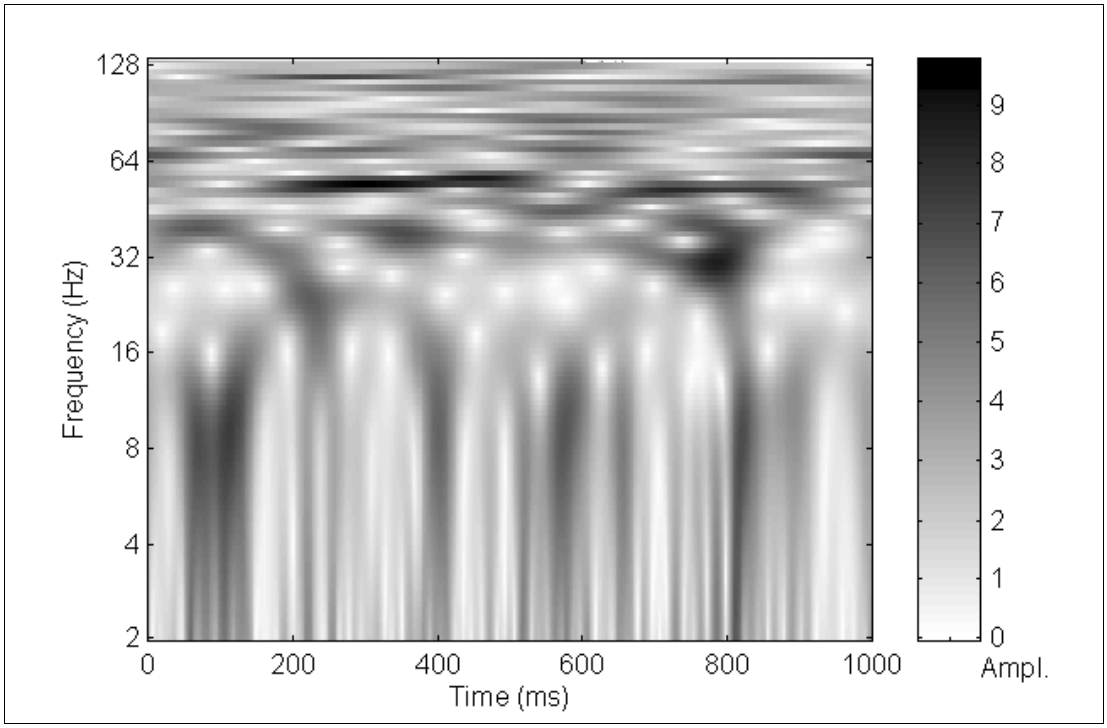

Fig. 3.26 - Morlet wavelet transform of signal S3 (8 octaves & 20 voices per octave)

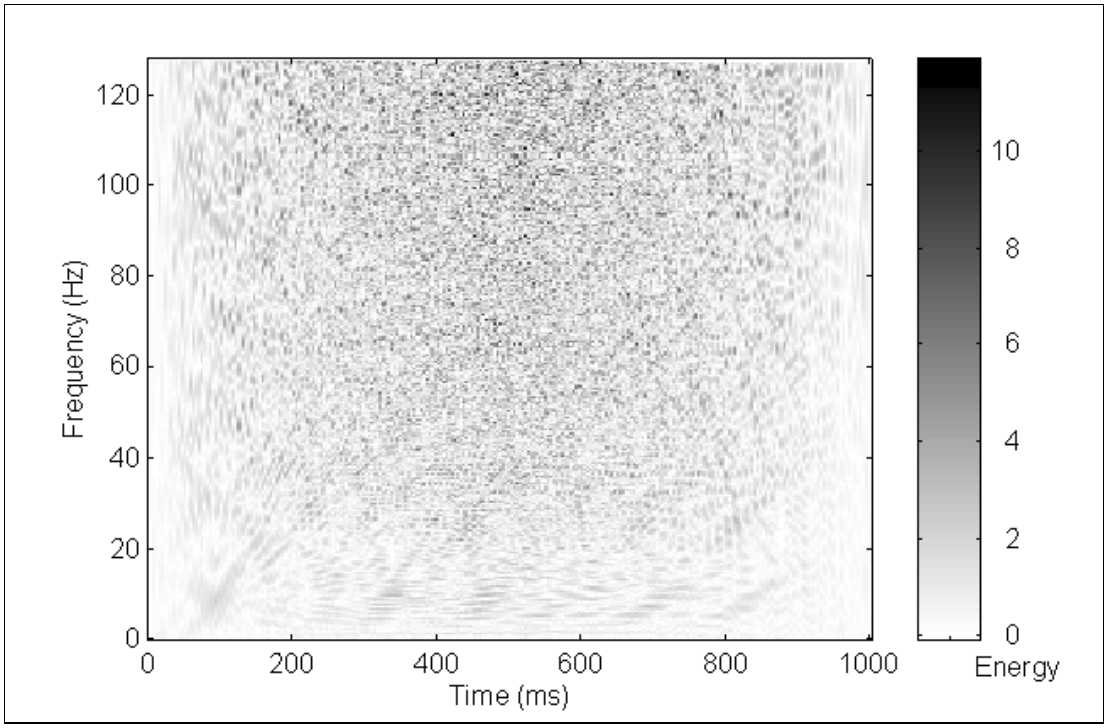

Fig. 3.27 - Wigner-Ville distribution of signal S3 (time-shift = 1 data point)

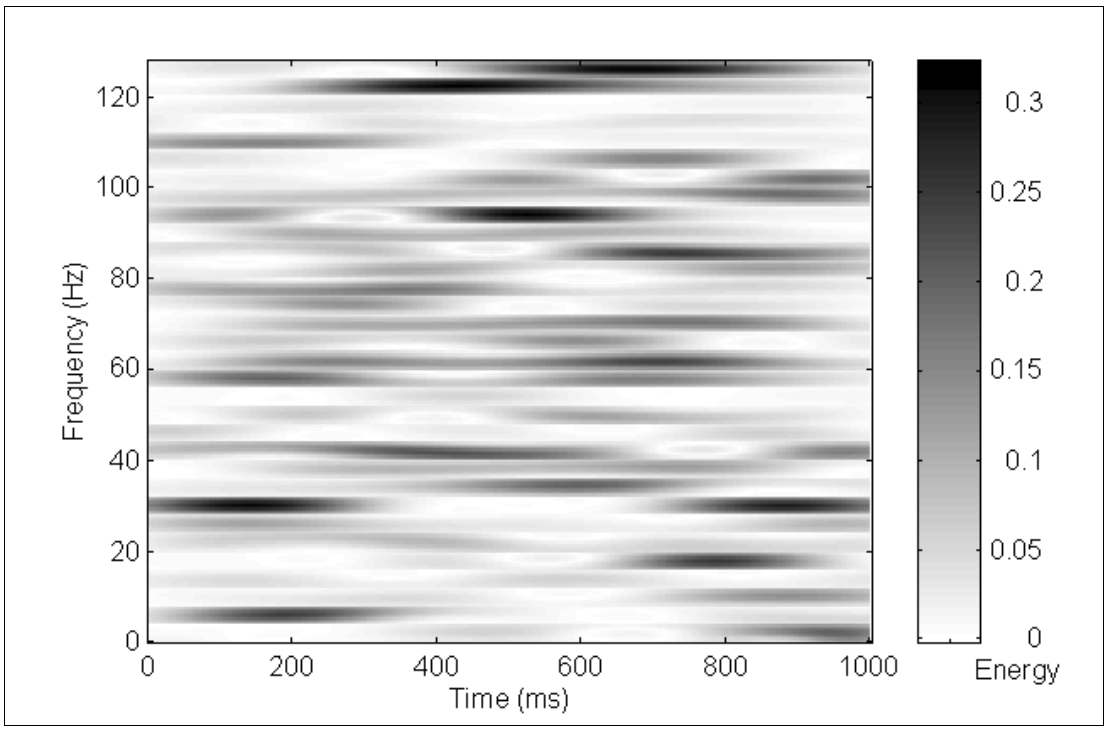

Fig. 3.28 - Pseudo-WV distribution of signal S3 (KB time and frequency window exponential arguments 70, 2 - time-shift = 1 data point, frequency shift = 8 Hz)

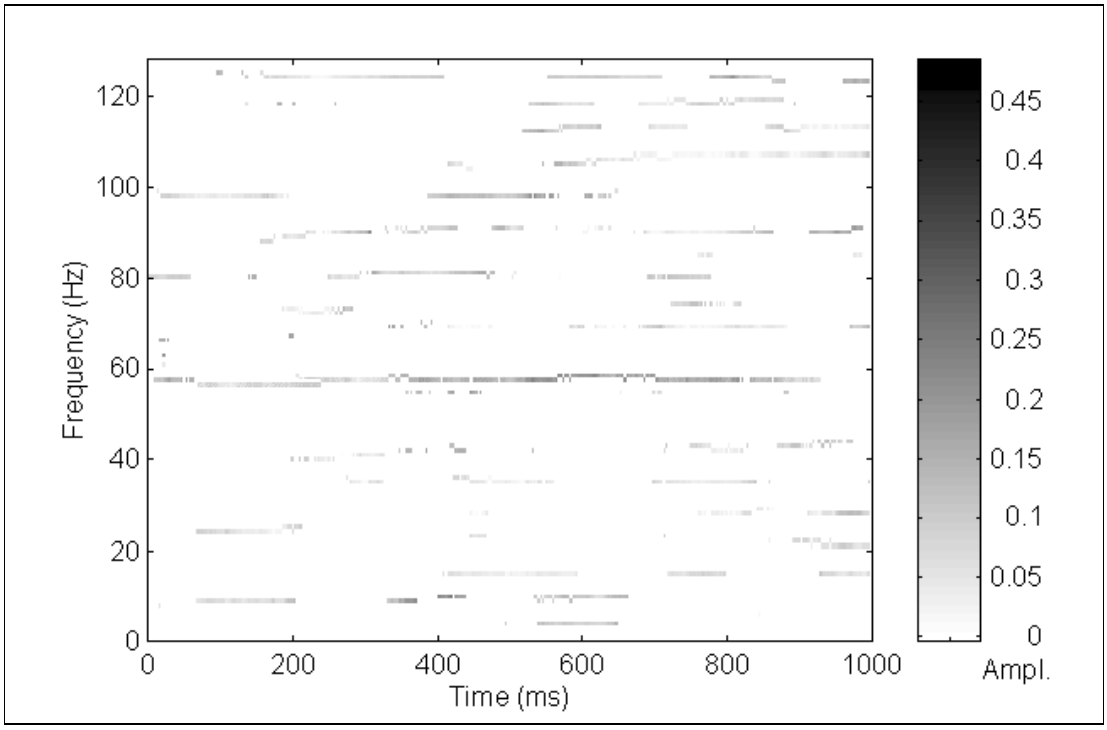

Fig. 3.29 - Extended Prony time-frequency representation of signal S3 (512 data points per sample - total data points used = 1023, maximum order 96, maximum exponential damping 0.02 s^{-1})

For the case of weak components embedded in high-level white noise, the Fourier transform depicts the weak component quite well if a very large number of data points is used (see Figure 3.25 (b)). However, long data arrays are not always available. The Morlet wavelet transform does not depict any deterministic component clearly (see Figure 3.26). The Wigner-Ville distribution does not depict these components due to the cross-term drawback, as mentioned above, which propagates the noise (see Figure 3.27). Although windows were applied to reduce the appearance of cross-terms in the pseudo-Wigner-Ville distribution, no improvement is observed when attempting to detect weak components in the presence of high-level noise (see Figure 3.28). However, in the graph of the extended Prony time-frequency representation (see Figure 3.29), the weak component is depicted fairly well.

Table 3.5 is a summary of the results obtained using the techniques involved in this study applied to the signals S1, S2, and S3.

Signal feature (basic simulation)	Technique				
	FT	MWT	WVD	PWVD	PTFR
Two deterministic components (signal S1)	D >B<	NC	NC	NC	D
Amplitude variation (signal S2)	ND	NC	ND	NC >B<	ND
Weak component embedded in high-level noise (signal S3)	D >B<*****	NC	ND	NC	D

ABBREVIATIONS

**** for long data arrays***

FT - Fourier transform
MWT - Morlet wavelet transform
WVD - Wigner-Ville distribution
PWVD - Pseudo-Wigner-Ville distribution
PTFR - Extended Prony time-frequency rep.

ND - not detected
NC - not clear
D - detected
>B<- best method

Table 3.5 - Method component detection performance

3.4. Signal Processing Techniques: Depicting Non-Stationary Processes

To test the performance of the Fourier transform and the Morlet wavelet transform methods, the Wigner-Ville and the pseudo-Wigner-Ville distributions, and the extended Prony time-frequency representation for handling non-stationary components, the following signals were prepared:

- A signal containing two sine sweeps (signal S4).
- A signal containing a component whose frequency varies with the time (signal S5).
- A signal with modulations (signal S6)
- A signal with three Gaussian waves (signal S7).

3.4.1. Signal with 2 Sine Sweeps (Signal S4)

A signal with two simultaneous sine sweeps was prepared to demonstrate the capacity of each time-frequency representation method to depict component frequency linear variation. Table 3.6 describes the composition of this signal, and Figures 3.30 to 3.32 show the signal, its true time-frequency representation, and its Fourier transform. Figures 3.33 to 3.36 show the results generated by each method.

Component	Time length (s)	No. of data points	Frequency (Hz)	Amplitude (Mag)	Phase (degrees, t=0)
sine sweep	1.0	512	min. = 20 max. = 40	1.0	0
sine sweep	1.0	512	min. = 30 max. = 90	1.0	90

Table 3.6 - Signal S4 with two sine sweeps

The sine sweep components used in this signal were generated according with the following formula:

$$x(n) = A \sin\left(2\pi n_{var}\, t \left(\frac{n}{N}\right) + \varphi\right)$$

where the frequency n_{var} varies according with the formula:

$$n_{var} = n_1 + n\Delta n, \quad \Delta n = \frac{n_2 - n_1}{N}$$

and where,

n = data sample number of a discrete time sequence ($0 \leq n \leq N - 1$)

$x(n)$ = sine sweep discrete data point

A = amplitude (Magnitude)

N = number of data points per time interval

n_1 = initial frequency (Hz) (20 Hz in the first sine sweep and 30 Hz in the second)

n_2 = final frequency (Hz) (40 Hz in the first sine sweep and 90 Hz in the second)

t = time (s)

φ = phase (rad - fixed value)

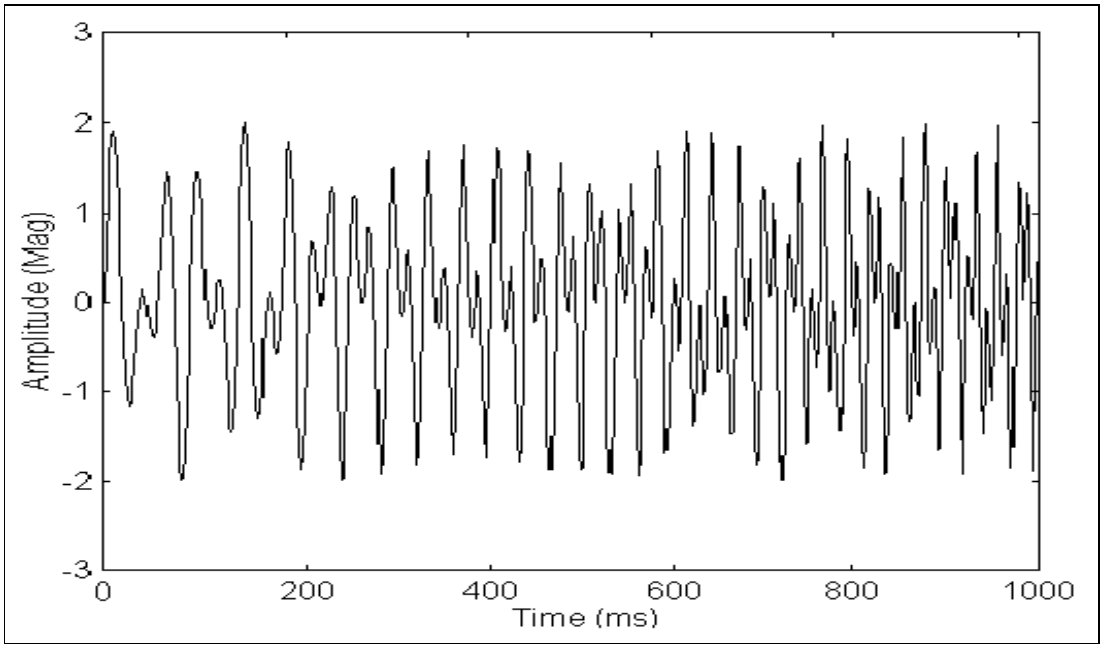

Fig. 3.30 - Signal S4 containing two sine sweeps

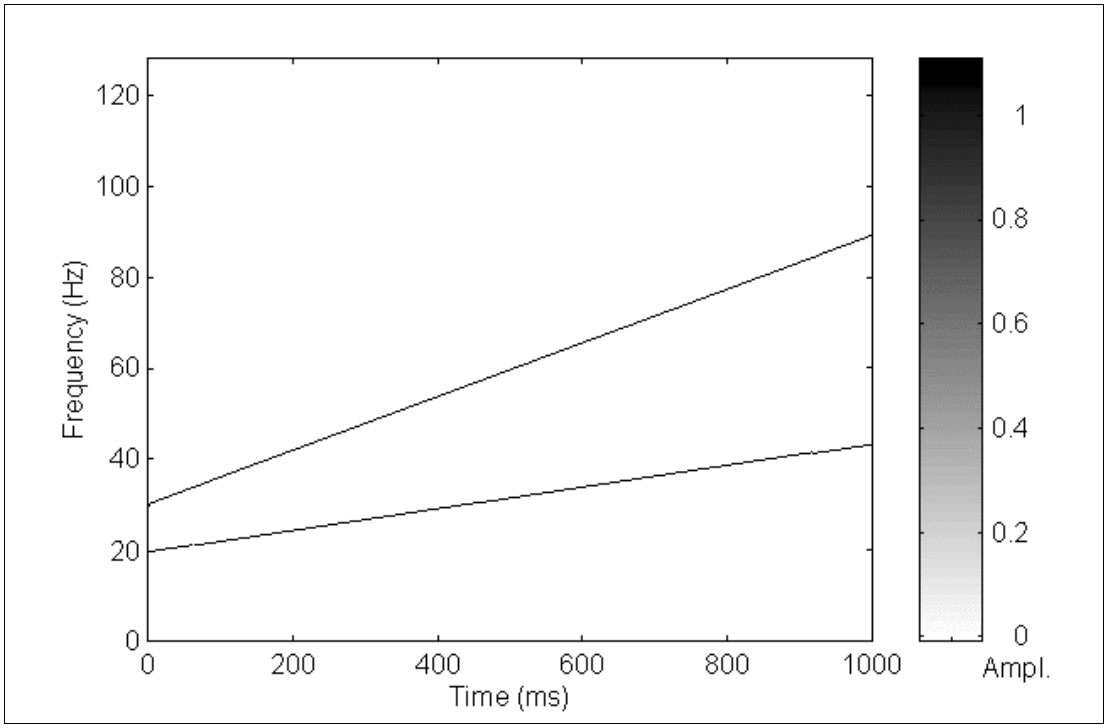

Fig. 3.31 - True time-frequency representation of signal S4

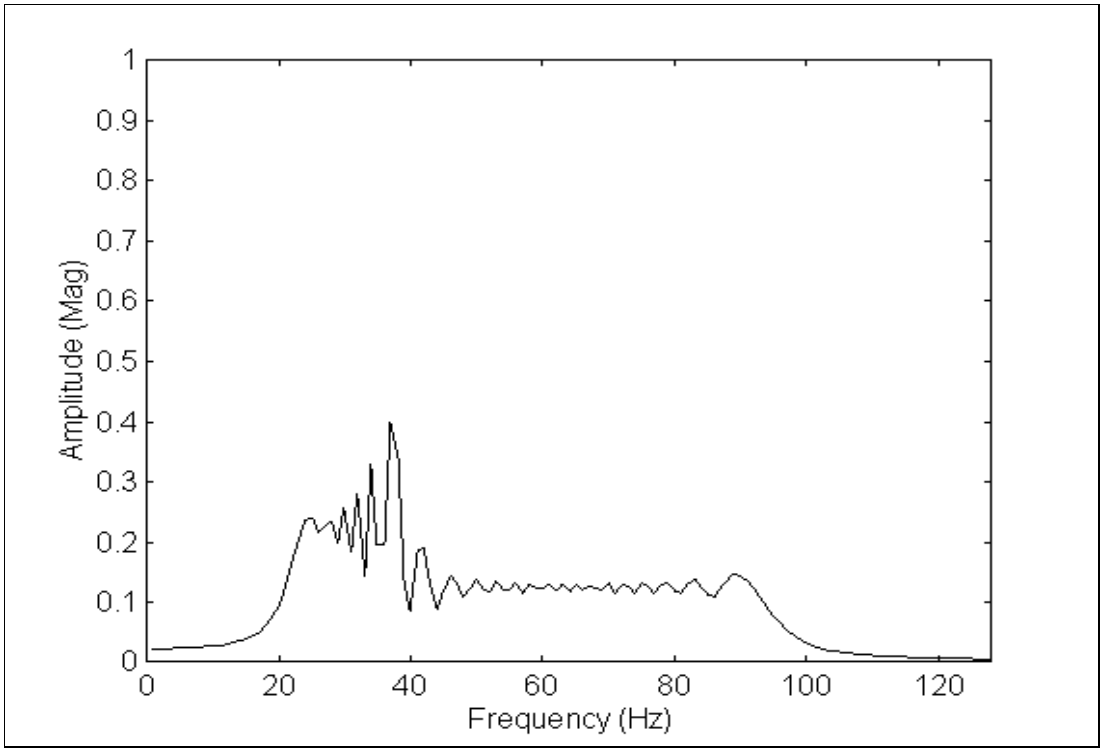

Fig. 3.32 - Fourier transform of signal S4 (frequency resolution = 1 Hz, no window)

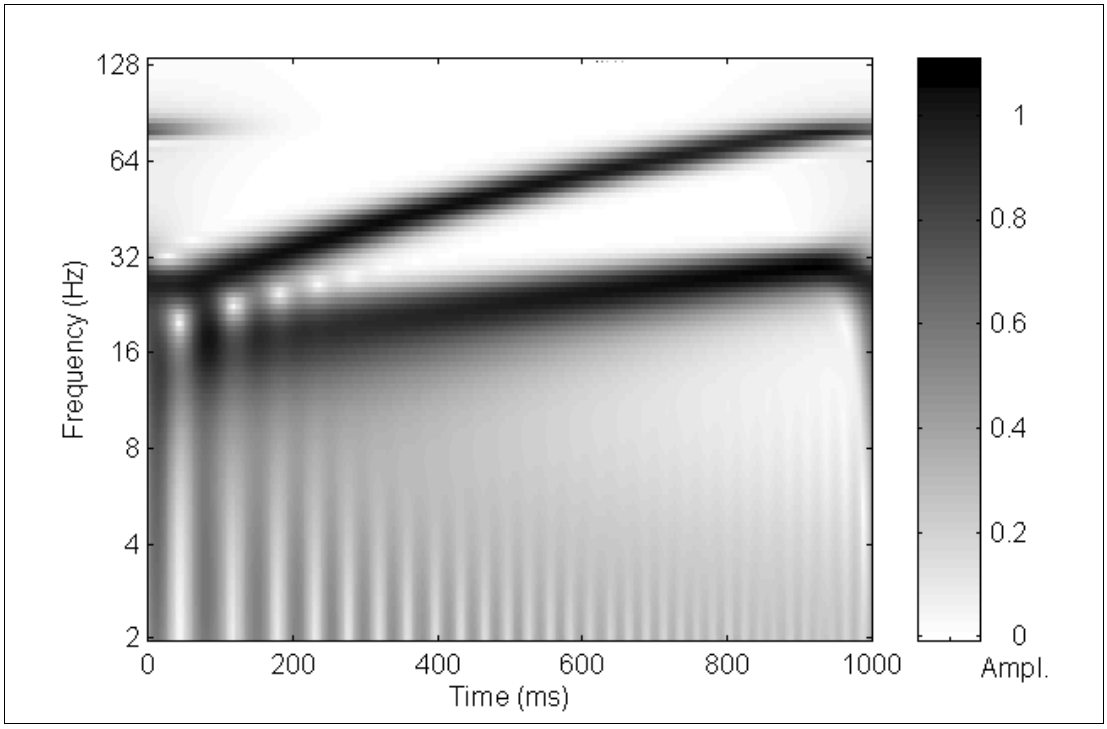

Fig. 3.33 - Morlet wavelet transform of signal S4 (8 octaves & 20 voices per octave)

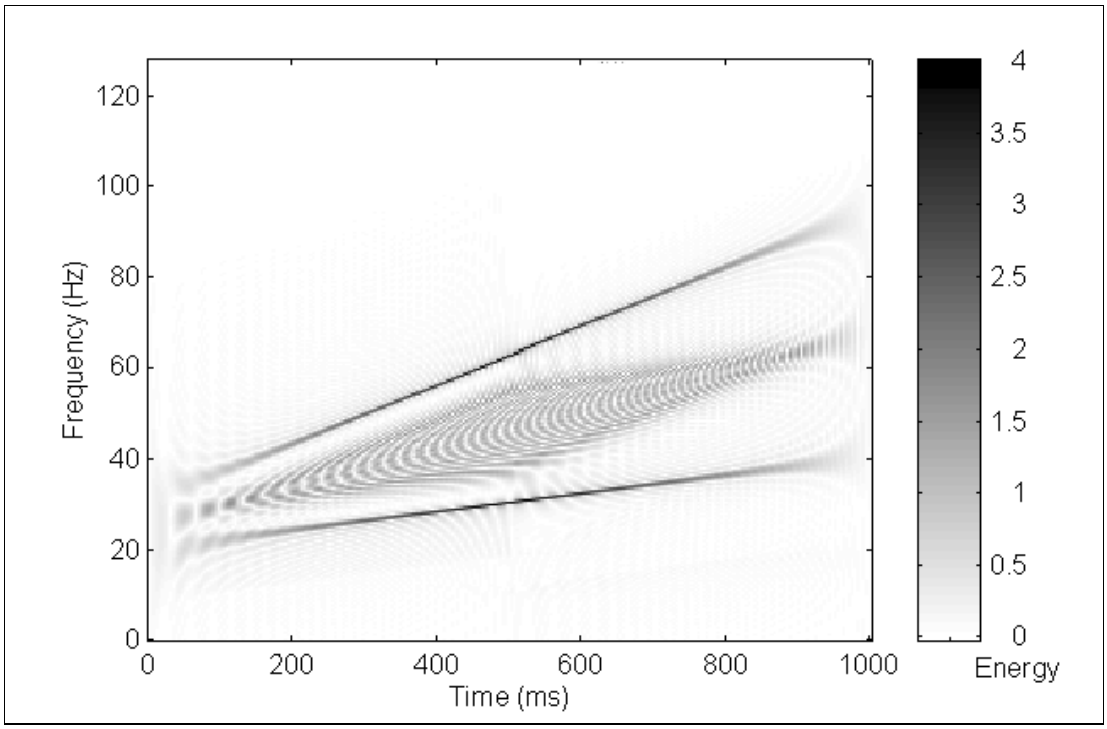

Fig. 3.34 - Wigner-Ville distribution of signal S4 (time-shift = 1 data point)

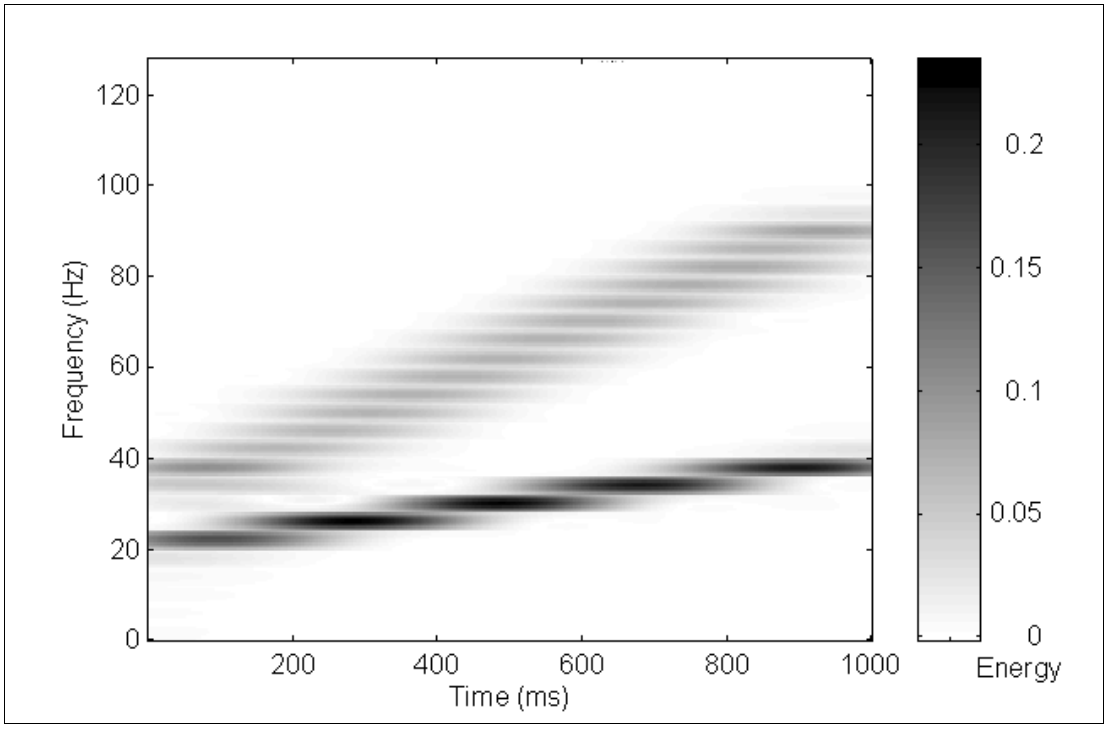

Fig. 3.35 - Pseudo-WV distribution of signal S4 (KB time and frequency window exponential arguments 70 and 2 - time-shift = 1 data point, frequency shift = 8 Hz)

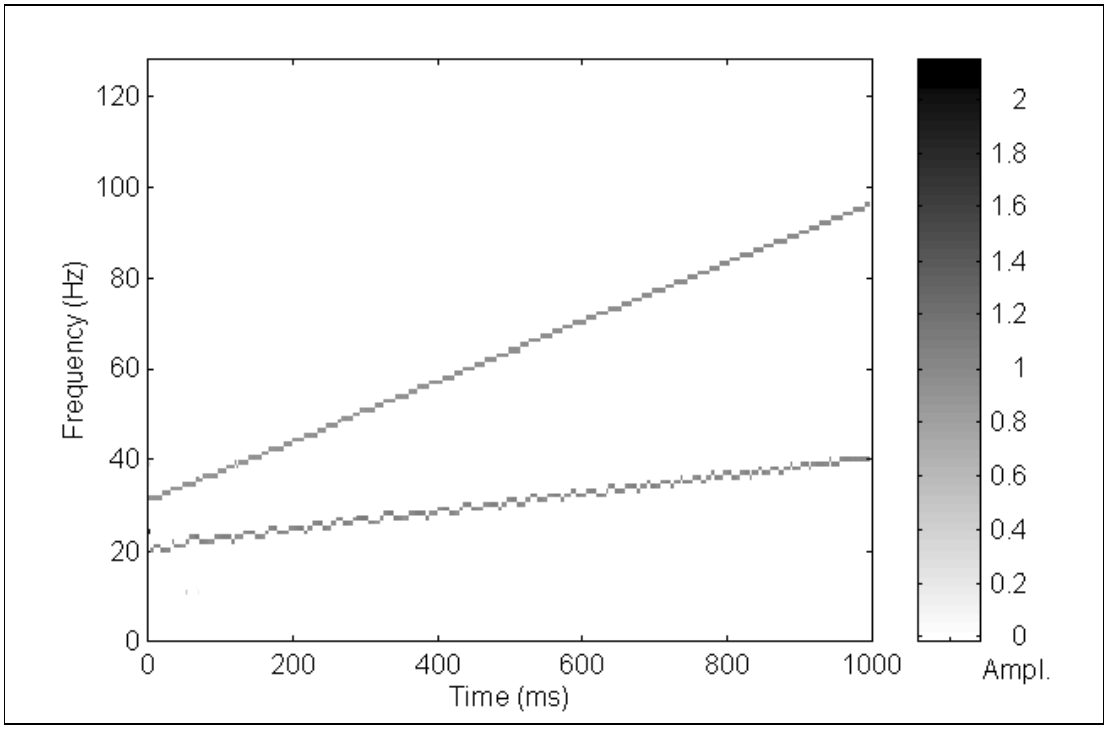

Fig. 3.36 - Extended Prony time-frequency representation of signal S4 (16 data points per sample - total data points used = 527, order 4, no exponential damping limit)

As may be noted in Figures 3.32 to 3.36, all techniques except the Fourier transform (see Figure 3.32) depict the sine sweeps. As shown in the graph of Figure 3.32, the Fourier transform cannot be considered an appropriate technique to process signals with non-stationary processes. The Morlet wavelet and the pseudo-Wigner-Ville distribution present low resolutions due to the windowing effect of their calculations (see Figures 3.33 and 3.35). However, the Wigner-Ville distribution shows a good resolution, although it has the disadvantage of generating cross-terms in its calculations, which are clearly depicted by the large spot located in the middle of the two sine sweeps (see Figure 3.34). The extended Prony time-frequency representation is shown to have the best graphical results for this signal (see Figure 3.36).

3.4.2. Signal with a Component with Frequency Variation (Signal S5)

This second signal was used to test the methods for their capacity to analyse another non-stationary condition. The signal is composed of a single component whose frequency varies with time. The component frequency is varied sinusoidally between 56 to 59 Hz. This signal is designed to represent variations in the rotation speed of the ESP, which in turn are caused by variations in the load to which the ESP is subjected. The fluid pumped by the ESP varies in density, and this may be also reflected in the rotation speed. This signal is intended to test the capacity of the methods to depict small variations in a component frequency in the 56/59 Hz frequency bandwidth.

The signal composition is described in Table 3.7 below, and Figures 3.37 to 3.39 show the signal S5, its true time-frequency representation, and its Fourier transform. Figures 3.40 to 3.43 show the results generated by each method.

Component	Time length(s)	No. of data points	Frequency (Hz)	Amplitude (Mag)	Phase (degrees, t = 0)
sine wave (frequency varied sinusoidally)	1.0	512	min. = 56 max. = 59	0.1	0

Table 3.7 - Signal S5 with a component whose frequency varies sinusoidally with time

The sine wave whose frequency varies sinusoidally used in this signal was generated according with the following formula:

$$x(n) = A \sin\left(2\pi \nu_c \, t \left(n/N\right) + \varphi_{var}\right)$$

where

$x(n)$ = sine wave discrete data point

n = data sample number of a discrete time sequence ($0 \leq n \leq N - 1$)

A = amplitude (Magnitude)

ν_c = central frequency (57.5 Hz)

t = time (s)

N = number of data points per time interval

φ_{var} = variable phase (rad)

The central frequency ν_c of a component may be varied through a phase addition or subtraction as the frequency of this component is increased or reduced. Thus, the phase φ_{var} may be varied according with the formula:

$$\varphi_{var} = \varphi_{max} \sin\left(2\pi \nu_{mod} \, t \left(n/N\right)\right)$$

where ν_{mod} is the modulated variation frequency along the time axis (3.5 Hz) and the maximum phase variation φ_{max} is calculated by the formula:

$$\varphi_{max} = \frac{\pi}{4} \frac{\nu_r}{\nu_{mod}}$$

where ν_r is the frequency range variation (3 Hz).

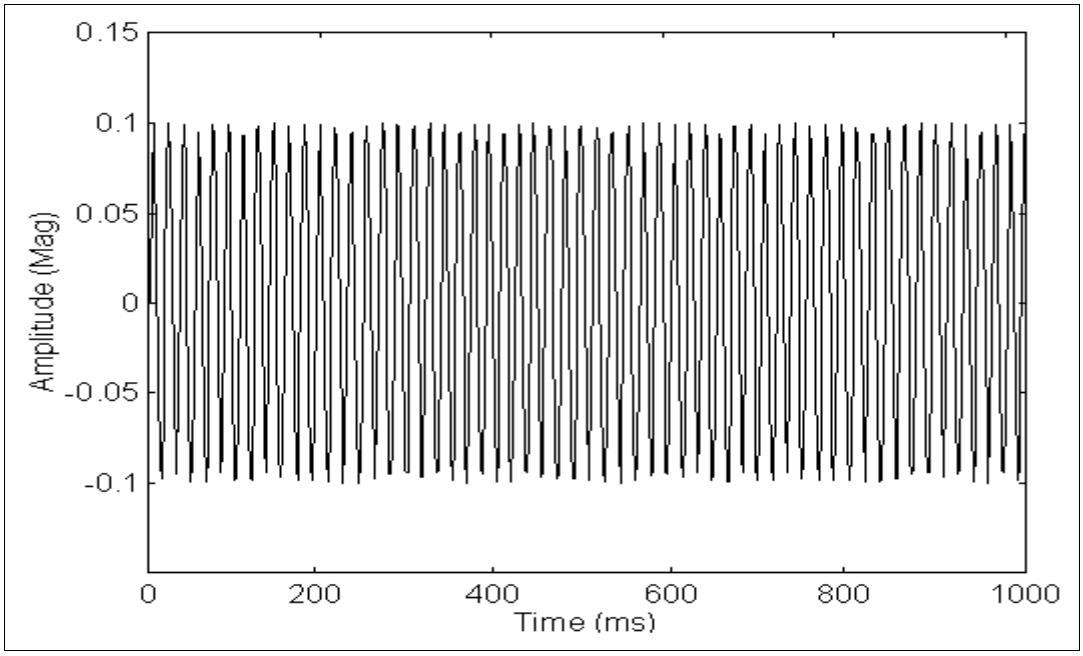

Fig. 3.37 - Signal S5 containing a single component whose frequency varies sinusoidally between 56 to 59 Hz

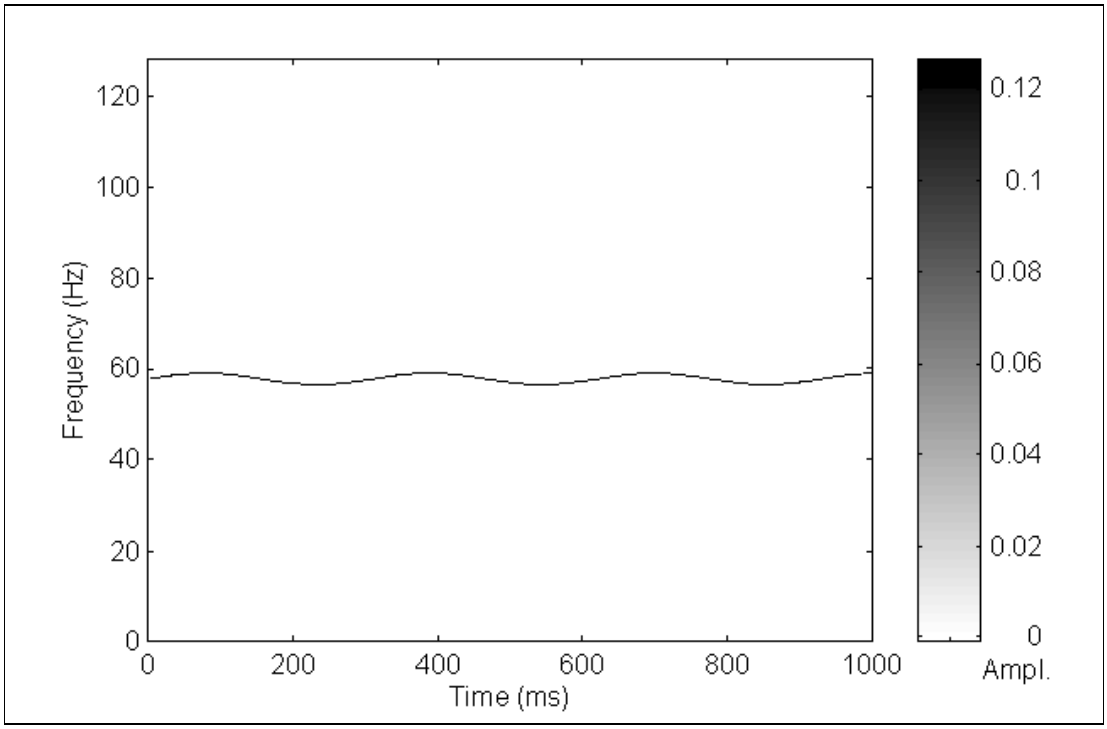

Fig. 3.38 - True time-frequency representation of signal S5

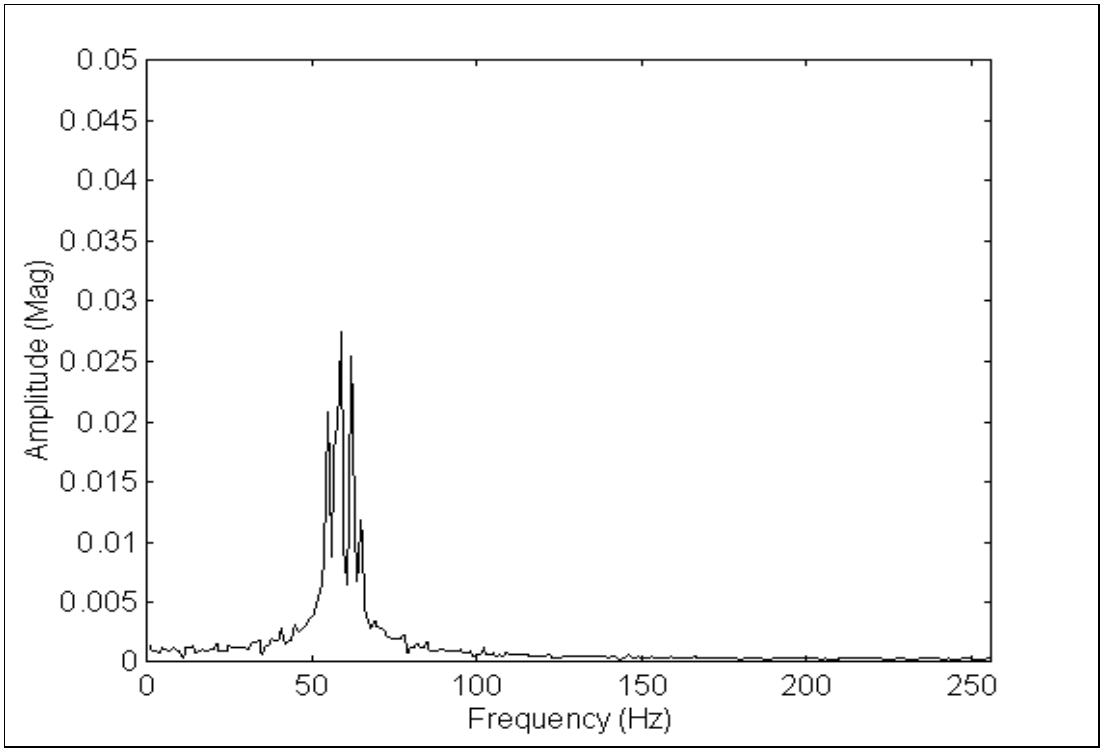

Fig. 39 - Fourier transform of signal S5 (frequency resolution = 1 Hz, no window)

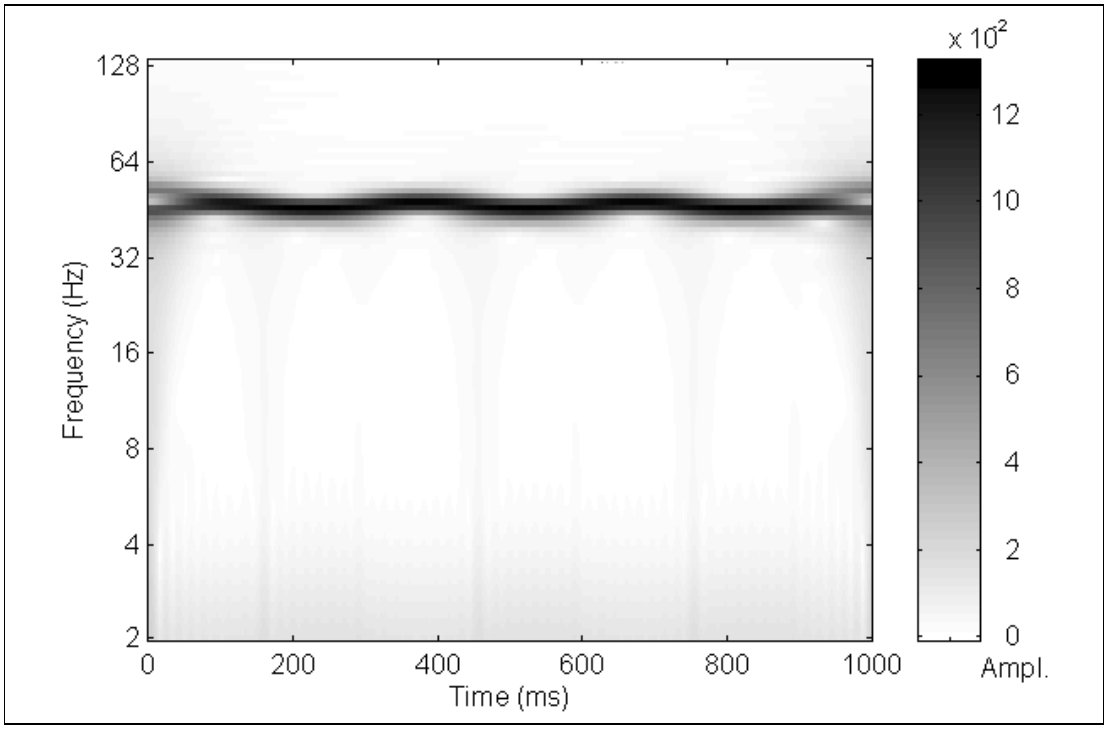

Fig. 3.40 - Morlet wavelet transform of signal S5 (8 octaves & 20 voices per octave)

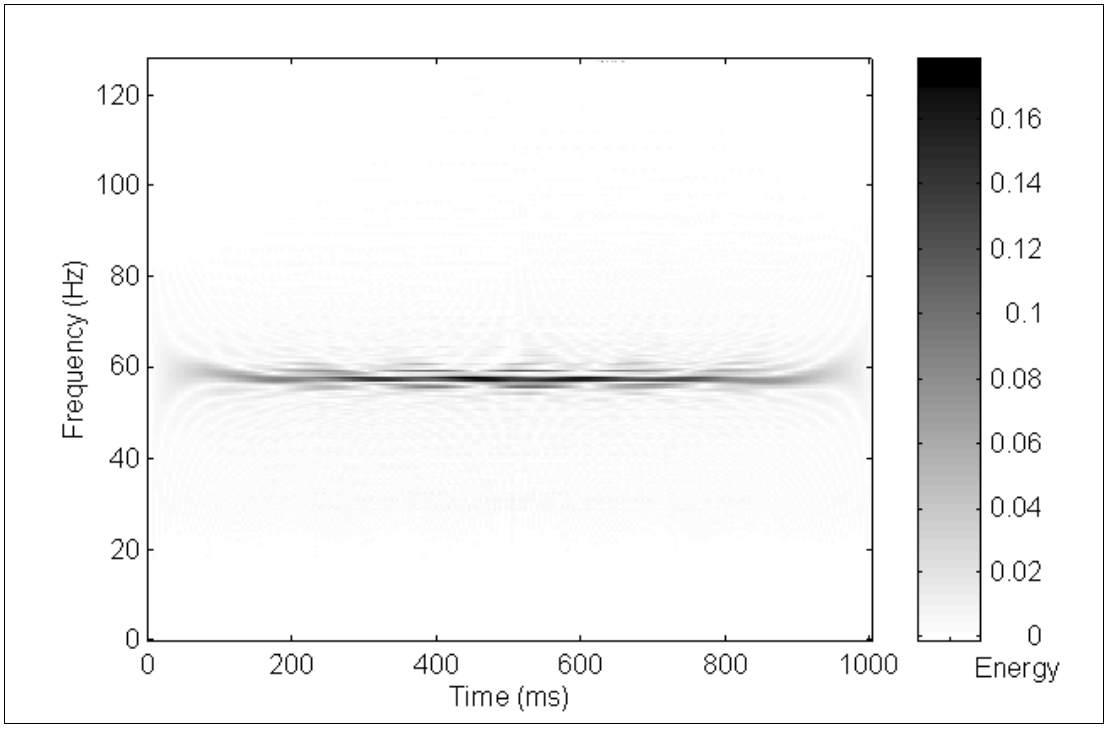

Fig. 3.41 - Wigner-Ville distribution of signal S5 (time-shift = 1 data point)

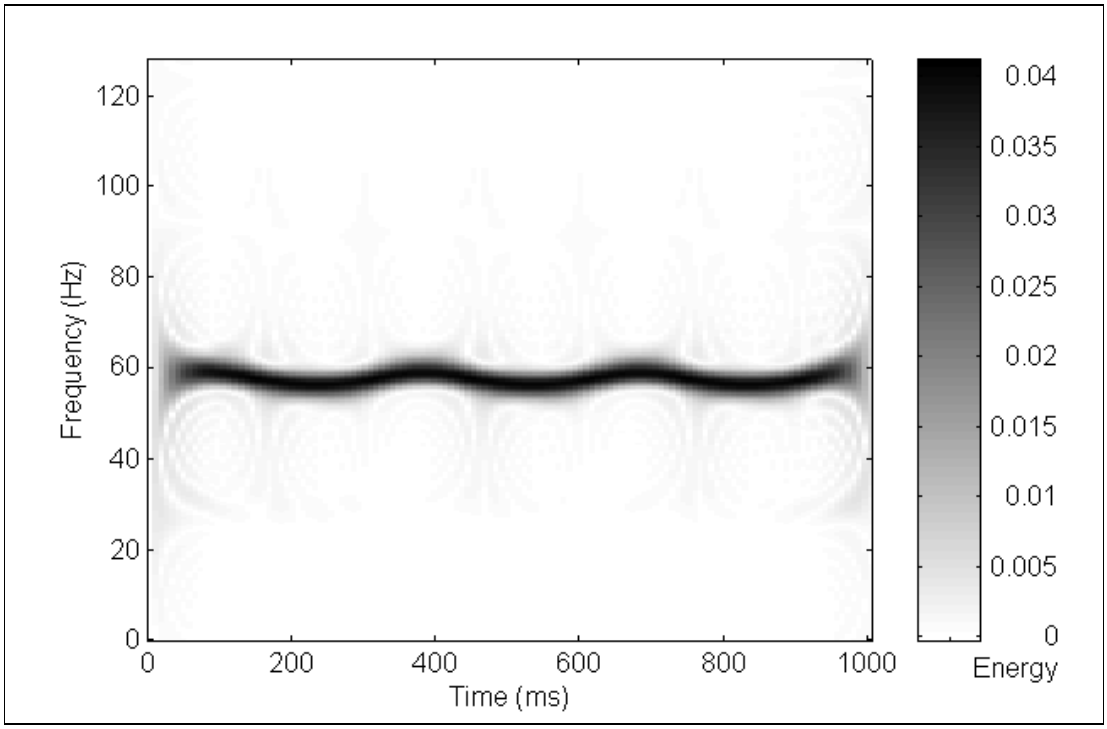

Fig. 3.42 - Pseudo-WV distribution of signal S5 (KB time window exponential argument 150, no frequency window - time-shift = 1 data point)

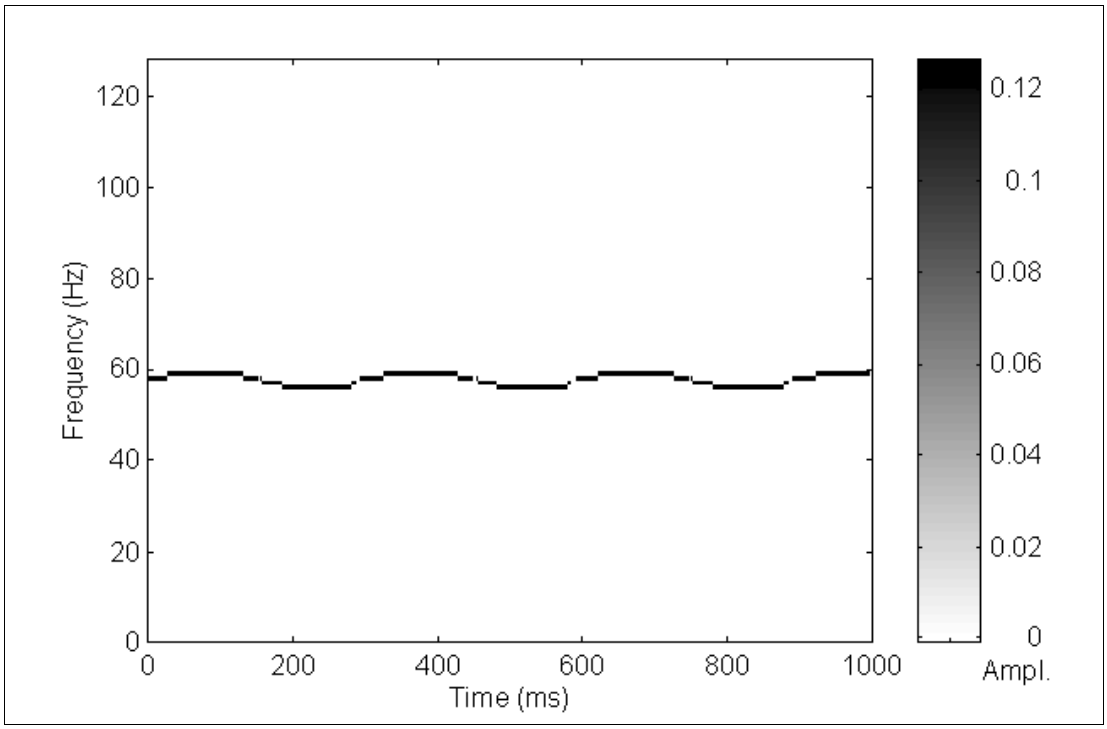

Fig. 3.43 - Extended Prony time-frequency representation of signal S5 (4 data points per sample - total data points used = 515, order 2, no exponential damping limit)

It can be seen in Figures 3.39 to 3.43 that the technique which best depicts the signal containing a single component whose frequency varies between 56 to 59 Hz is the extended Prony time-frequency representation. The Fourier transform of this signal again, does not represent the frequency variation properly (see Figure 3.39) and the graph generated by the Wigner-Ville distribution does not depict the signal correctly due to the existence of the cross-terms (see Figure 3.41). The frequency variations in the graphs generated by the pseudo-Wigner-Ville distribution and the Morlet wavelet transform, on the other hand, can be clearly seen. However, in these cases the component is “smoothed” due to the windowing effect (see Figures 3.40 and 3.42) and is not as clearly identified as in the extended Prony time-frequency representation.

3.4.3. Signal with Modulations (Signal S6)

The third signal of this simulation (signal S6) is designed to test the methods' capacity for detecting fluid slug vibration components. It contains a component whose frequency varies from 6 to 24 Hz. and represents the fluid slug vibration present in the petroleum wellhead. Fluid slug vibration has been studied by Leducq and Hervieu [1991] through the Morlet wavelet analysis and it has been shown that generally the component frequency varies from 6 to 24 Hz. It has been also shown that this fluid slug vibration also presents some higher frequency components caused by moderate shocks between the fluid slug and pipe deviations or connections. In these signals, the values used to represent the modulation frequency correspond to the experimental values obtained by Leducq and Hervieu [1991].

Table 3.8 describes the composition of signal S6, and Figures 3.44 to 3.46 show the signal, its true time-frequency representation, and its Fourier transform. The graphs in Figures 3.47 to 3.50 show the results generated by each time-frequency representation method involved in this study.

Component	Time length (s)	No. of data points	Frequency (Hz)	Amplitude (Mag)	Phase (degrees, t = 0)
modulations (2)*	1.0	512	initial = 6 centre = 24 final = 6	5.0	0

Table 3.8 - Signal S6 with frequency modulations (each modulation has 90 data points approximately, see section 3.2.4 for modulation component definition)

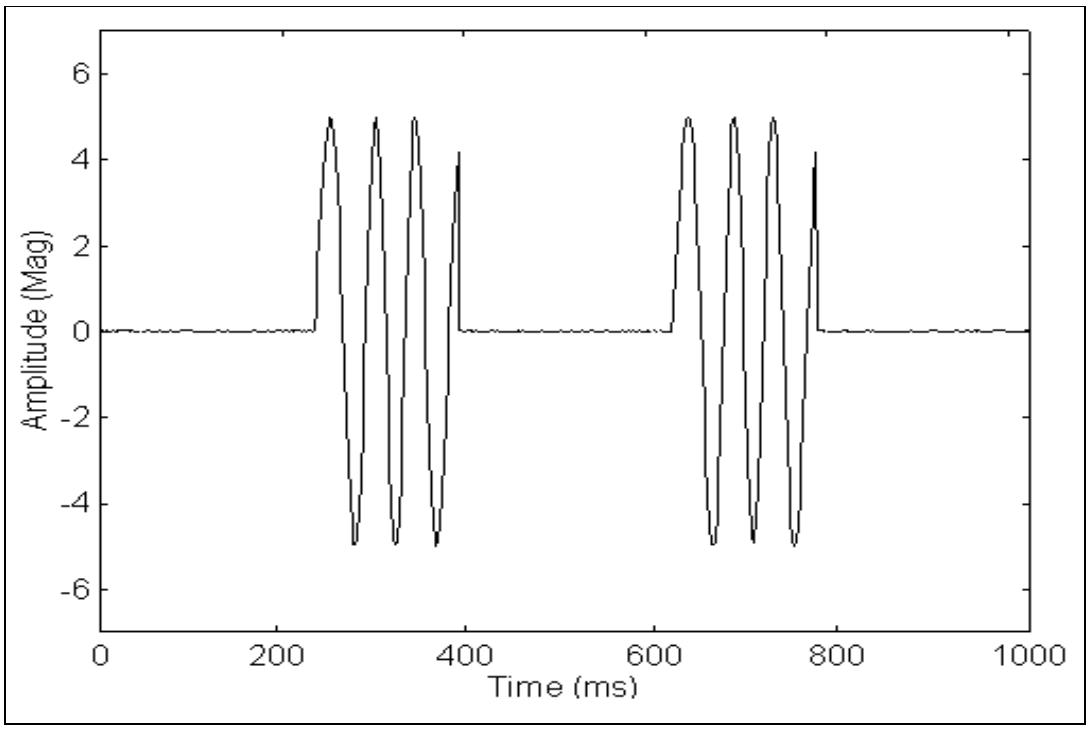

Fig. 3.44 - Signal S6 containing frequency modulated components

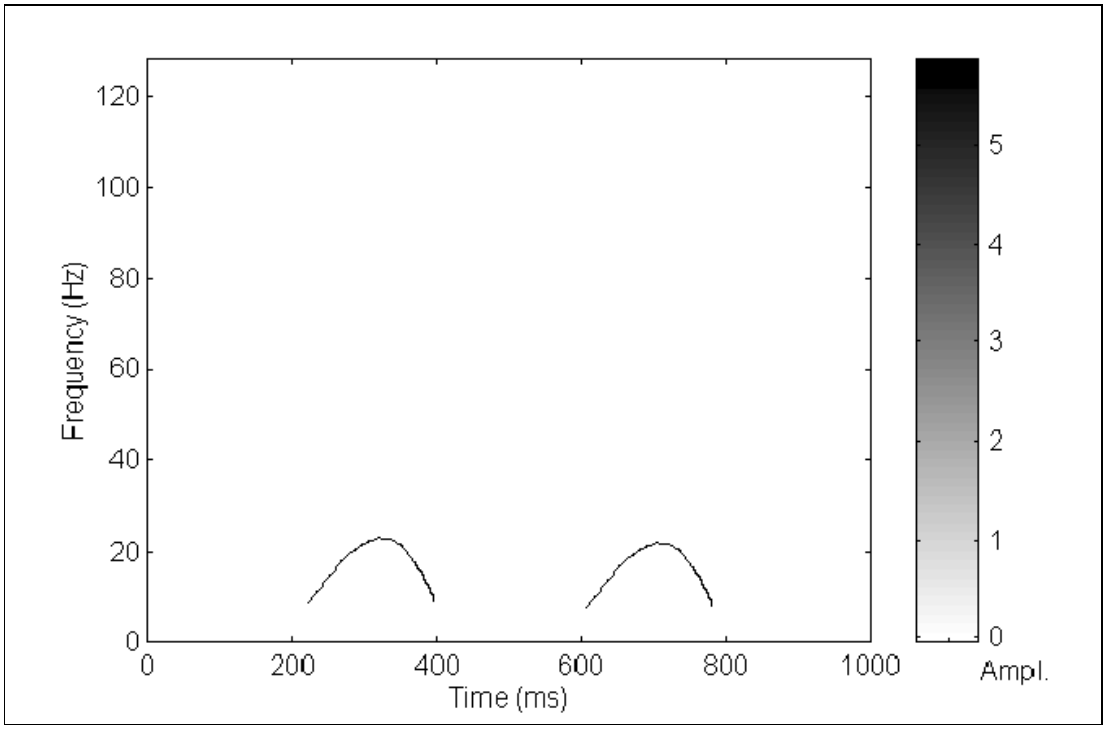

Fig. 3.45 - True time-frequency representation of signal S6

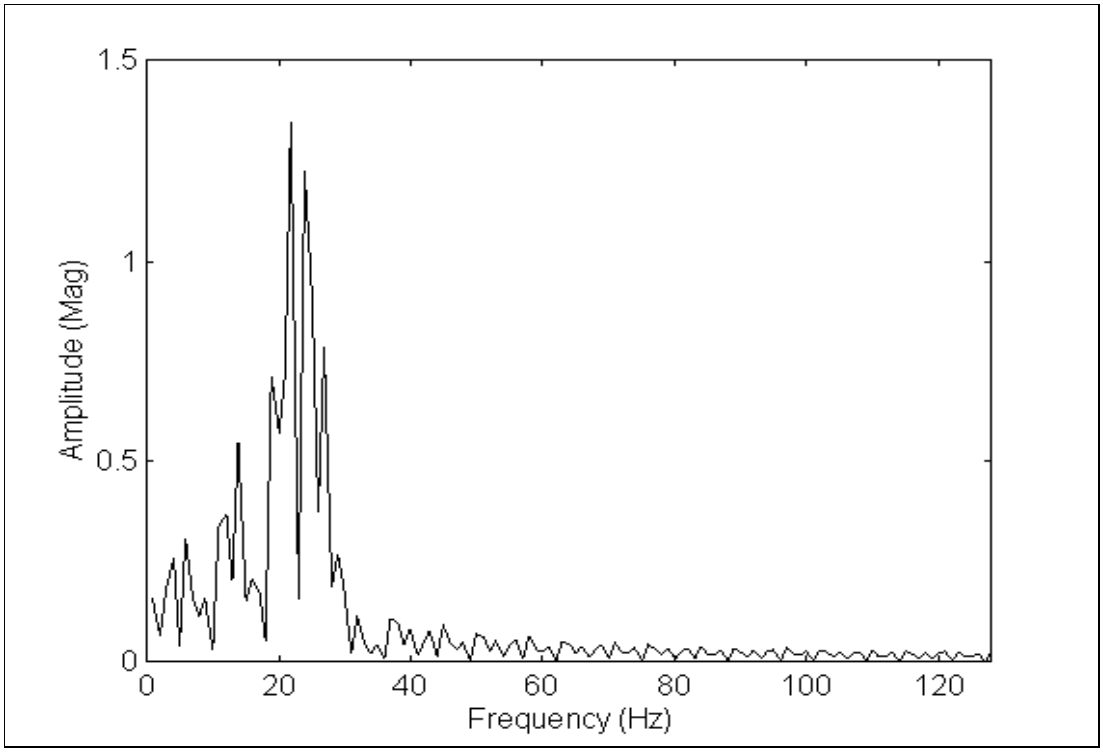

Fig. 3.46 - Fourier transform of signal S6 (frequency resolution = 1 Hz, no window)

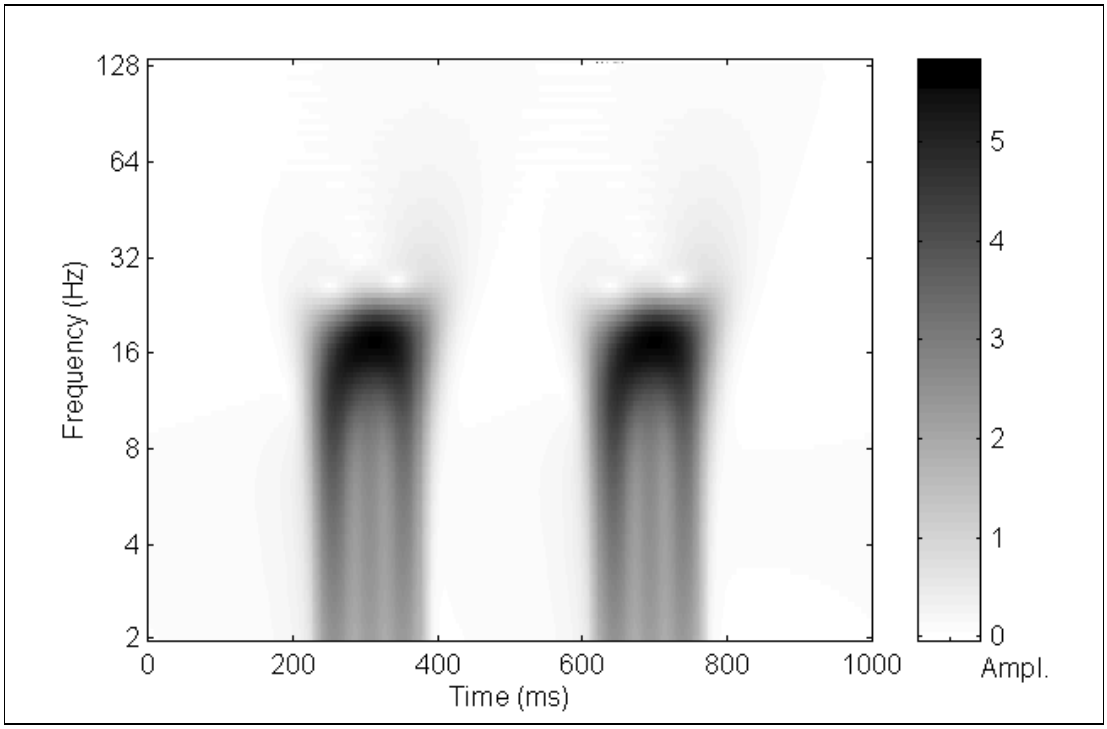

Fig. 3.47 - Morlet wavelet transform of signal S6 (8 octaves & 20 voices per octave)

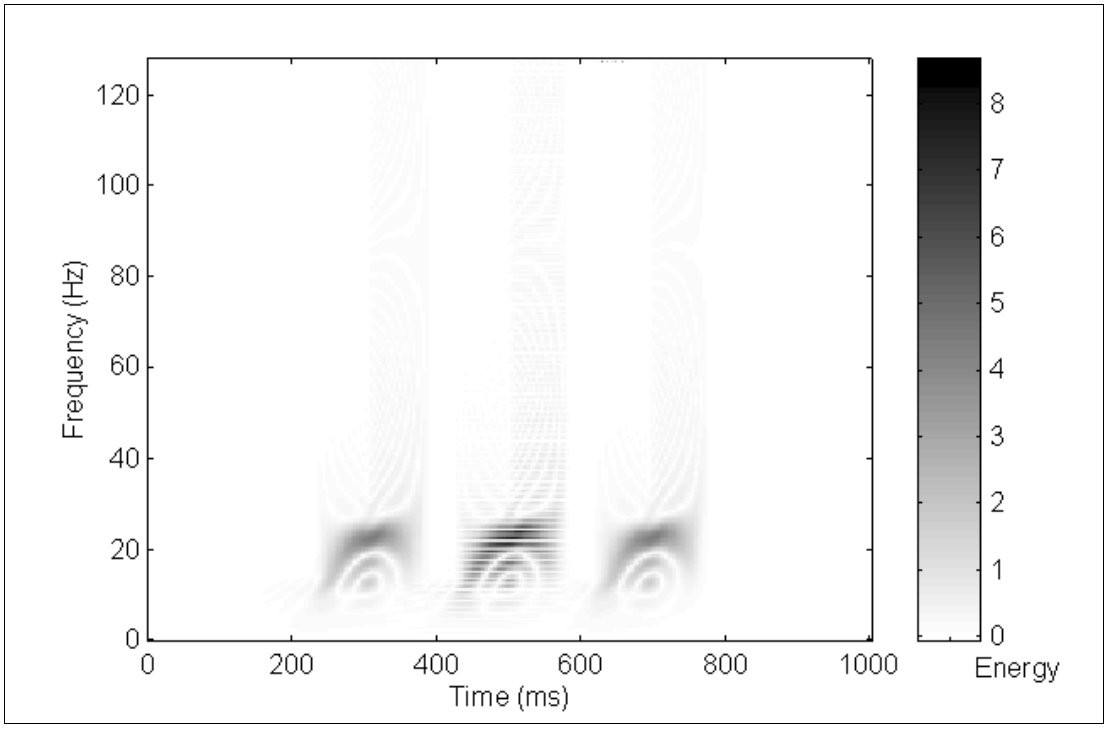

Fig. 3.48 - Wigner-Ville distribution of signal S6 (time-shift = 1 data point)

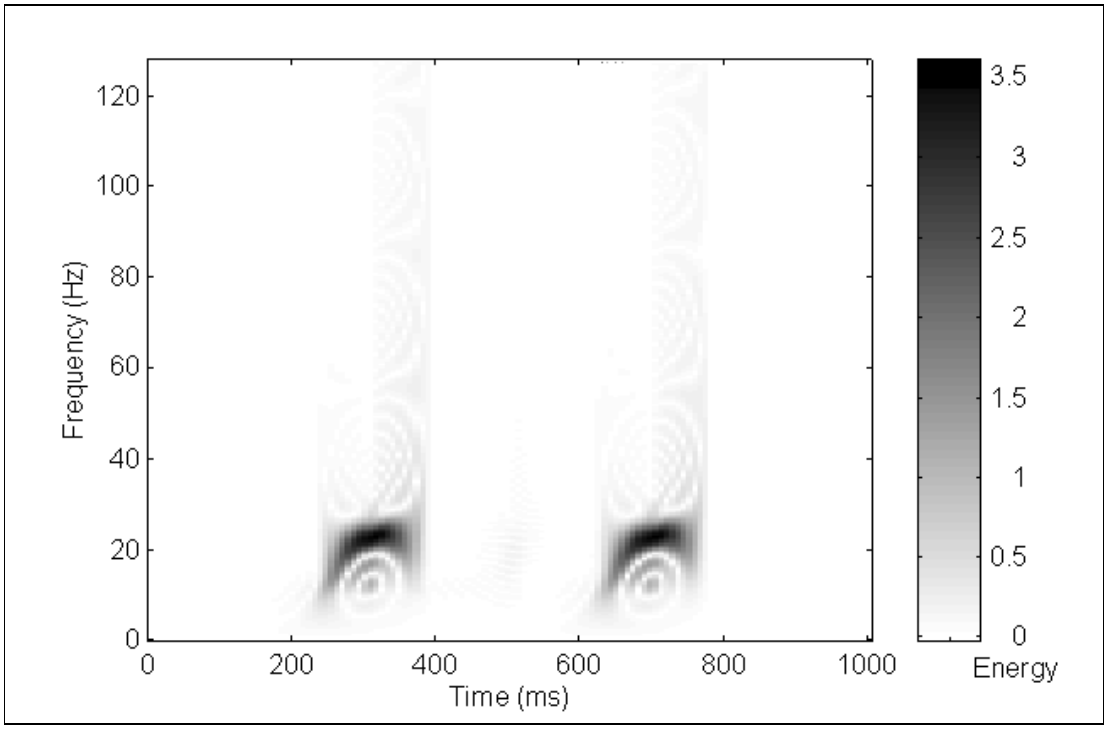

Fig. 3.49 - Pseudo-WV distribution of signal S6 (KB time window exponential argument 70, no frequency window - time-shift = 1 data point)

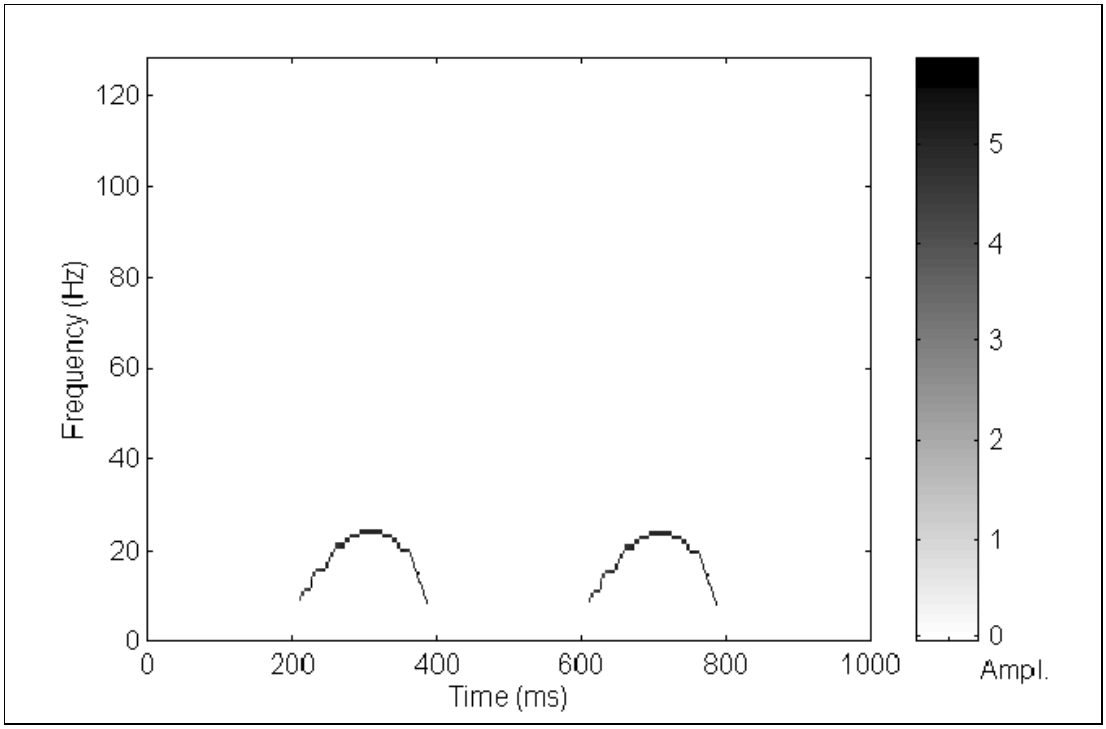

Fig. 3.50 - Extended Prony time-frequency representation of signal S6 (4 data points per sample - total data points used = 515, order 2, no exponential damping limit)

The composition of signal S6 is best depicted by the extended Prony time-frequency representation (see Figures 3.46 to 3.50). The Fourier transform of this signal does not represent the frequency variation properly (see Figure 3.46). The graph generated by the Wigner-Ville distribution depicts the modulations, but it also shows cross-terms that result from its calculations (see the spot between the two true modulations in the graph of Figure 3.48). The modulations are not depicted clearly in the graphs generated by the pseudo-Wigner-Ville distribution or the Morlet wavelet transform (see Figures 3.47 and 3.49). In the Morlet wavelet transform, the "smoothed" results due to the windowing effect make it difficult to infer the true nature of the components (see Figure 3.47). The results also show non-existent components between 2 and 6 Hz (see Figure 3.47). Normally, in the Morlet wavelet transform the windowing effect is less prominent in the low-frequency bandwidth than in the high-frequency bandwidth. This is because, as a feature of the method, the size of the Gaussian time windows set for low frequencies is larger than those set for high-frequencies (see equation (2.15)).

3.4.4. Signal with Gaussian Waves (Signal S7)

The fourth signal containing non-stationary components to be analysed (signal S7) was generated by adopting the same components as those described in the work of Chiollaz and Frave [1993]. It contains three Gaussian waves disposed in such a way as to depict the cross-terms problem in the Wigner-Ville distribution and the subsequent elimination of these terms by the windowing operation performed in the pseudo-Wigner-Ville distribution. Signals containing only Gaussian components have been commonly used to demonstrate the capacity of the Wigner-Ville distribution to depict non-stationary conditions, because they will always generate positive results in the distribution time-frequency plane [Cohen, 1989, Chiollaz and Frave, 1993].

Table 3.9 shows the composition of signal S7, and Figures 3.51 to 3.53 show the signal, its true time-frequency representation, and its Fourier transform respectively.

The graphs in Figures 3.54 to 3.57 show the results generated by of each time-frequency representation method involved in this study.

Component	Time length (s)	No. of data points	Frequency (Hz)	Amplitude (Mag)	Phase (degrees, t = 0)
1st Gaussian	1.0	512	initial = 24 centre = 32 final = 40	1.0	---
2nd Gaussian	1.0	512	initial = 40 centre = 48 final = 56	1.0	---
3rd Gaussian	1.0	512	initial = 88 centre = 96 final = 104	1.0	---

Table 3.9 - Signal S7 with Gaussian waves

To obtain the right Gaussian shape in the frequency domain, each Gaussian component of this signal was generated from the frequency domain according with the following formula:

$$x_f(n) = A\frac{1}{s\sqrt{2p}}exp\left(-1\right)\frac{n(n)+N/2}{2s^2}^2$$

where,

- n = data sample number of a discrete time sequence (minimum frequency $\leq n \leq$ maximum frequency)
- $x_f(n)$ = Gaussian wave discrete data point in the frequency domain
- A = amplitude (Magnitude)
- s = standard deviation (value set to 4 for all Gaussian waves)
- N = number of data points per time interval
- $n(n)$ = frequency data point (varied from 24 to 40 Hz to generate the 1st Gaussian, from 40 to 56 Hz to generate the 2nd Gaussian, and from 88 to 104 Hz to generate the 3rd Gaussian)

After generating the Gaussian waves according with the above formula in the frequency domain, the inverse Fourier transform was applied to the data $x_f(n)$ in order to obtain the temporal signal containing the Gaussian waves as shown in the graph of Figure 3.51.

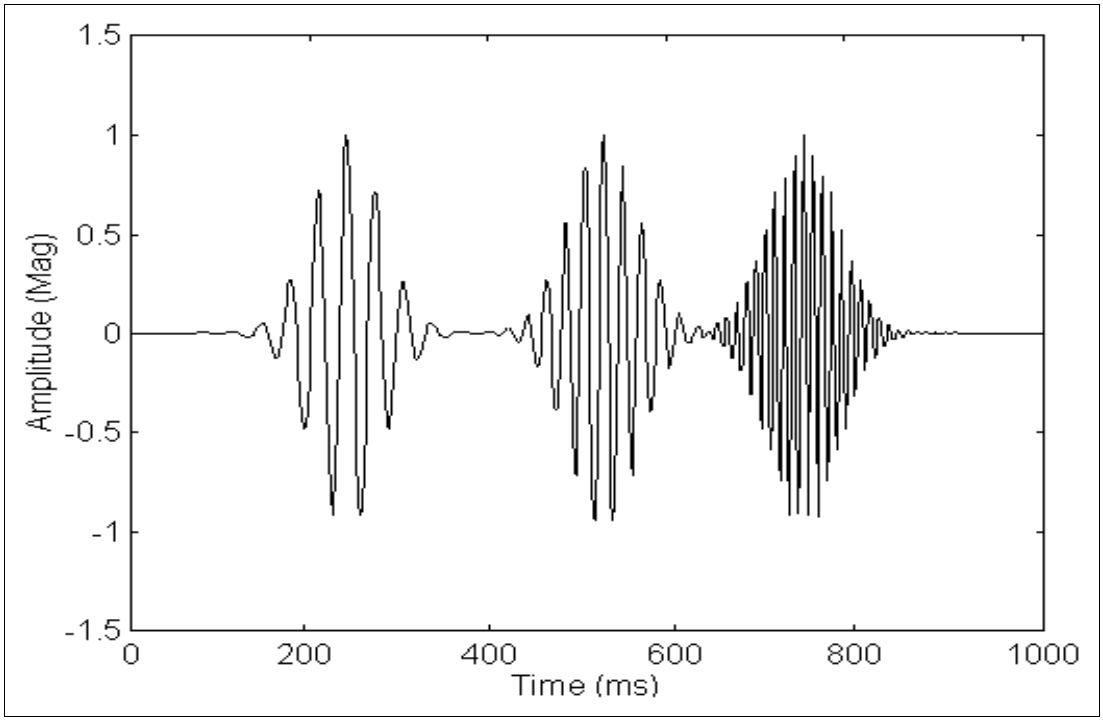

Fig. 3.51 - Signal S7 with Gaussian waves

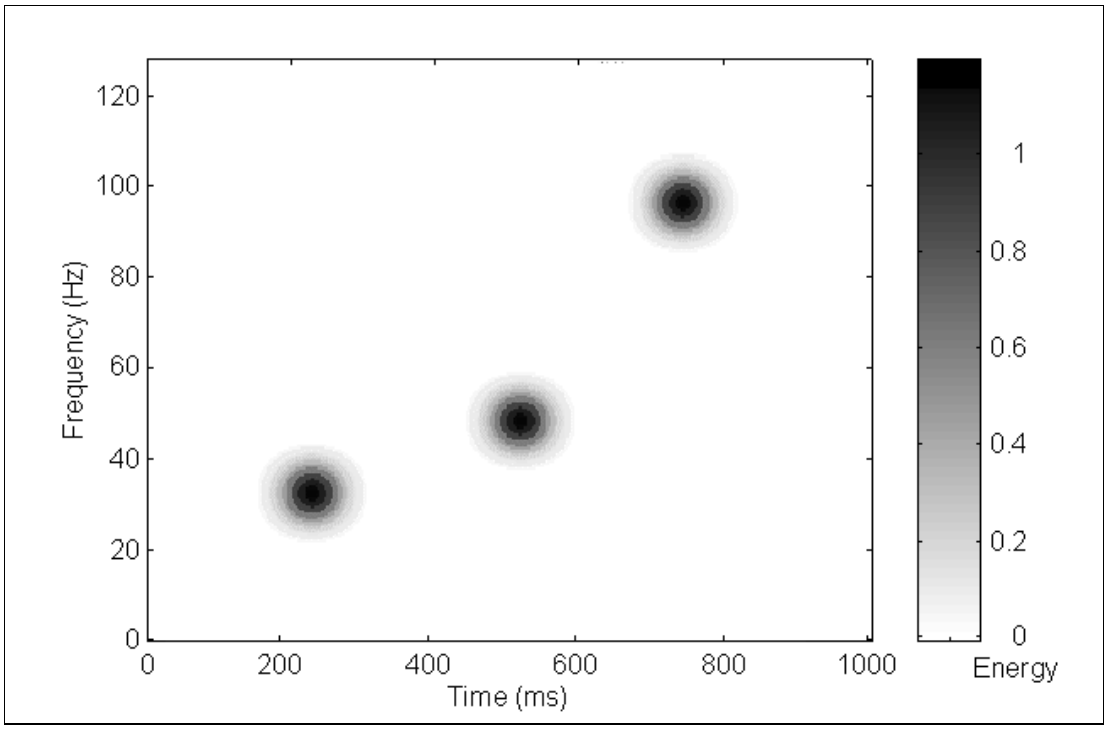

Fig. 3.52 - True non-stationary time-frequency representation of signal S7

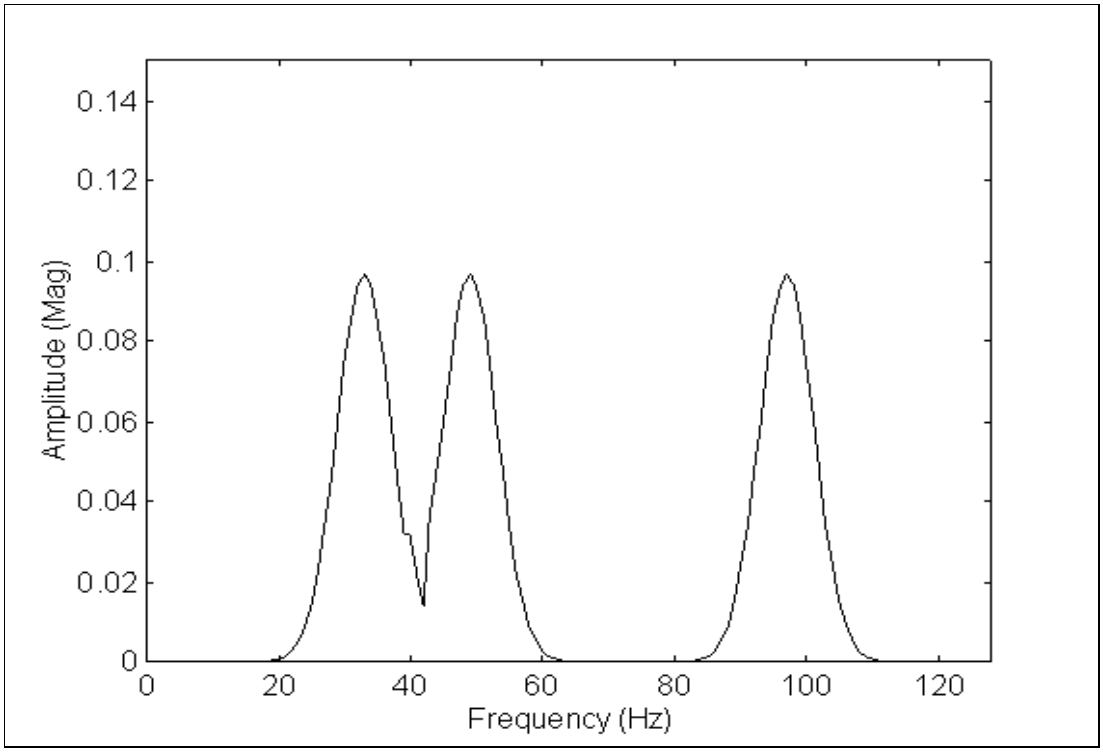

Fig. 3.53 - Fourier transform of signal S7 (frequency resolution = 1 Hz, no window)

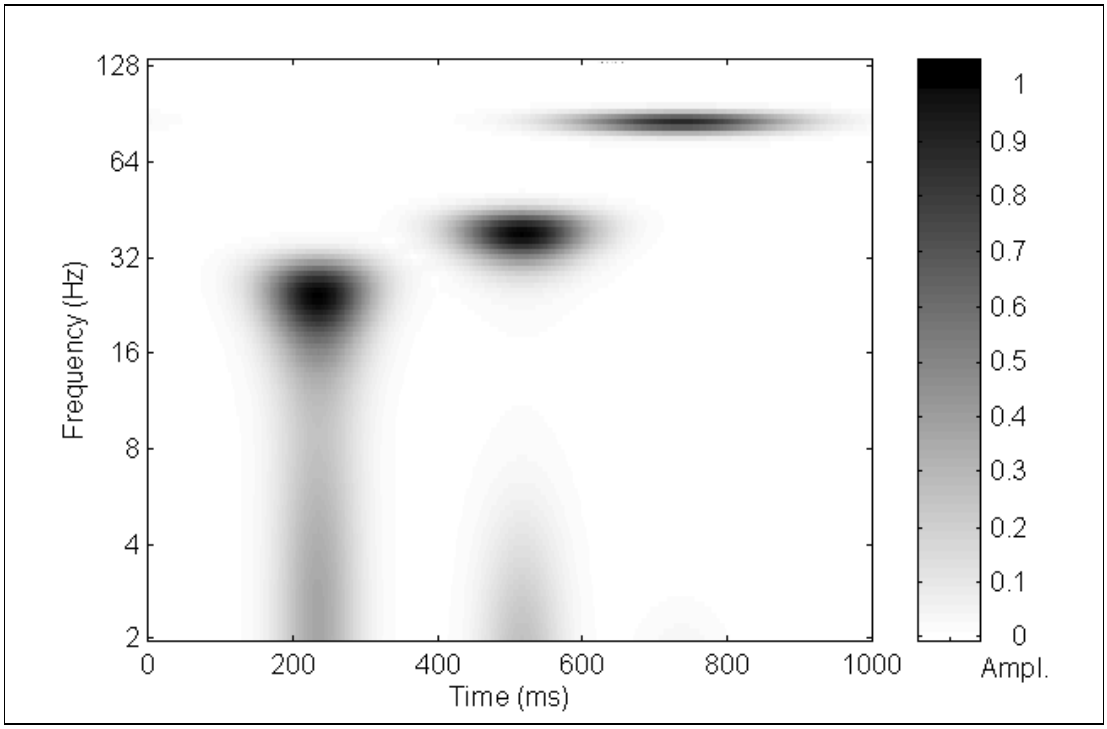

Fig. 3.54 - Morlet wavelet transform of signal S7 (8 octaves & 20 voices per octave)

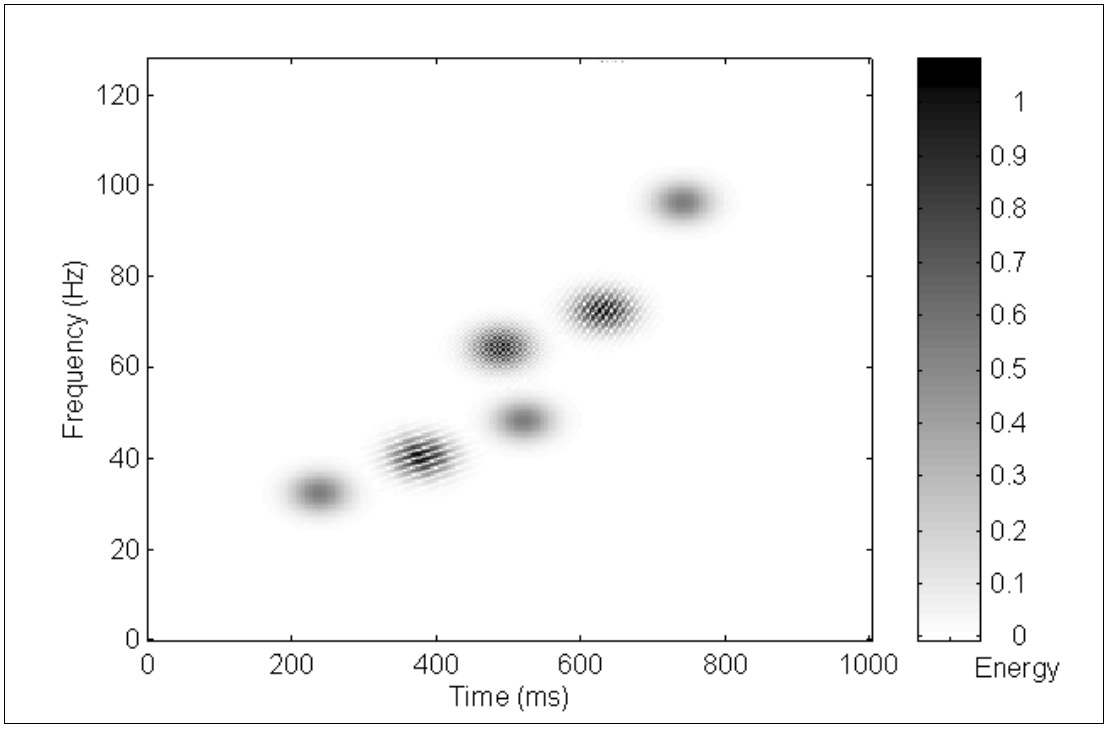

Fig. 3.55 - Wigner-Ville distribution of signal S7 (time-shift = 1 data point)

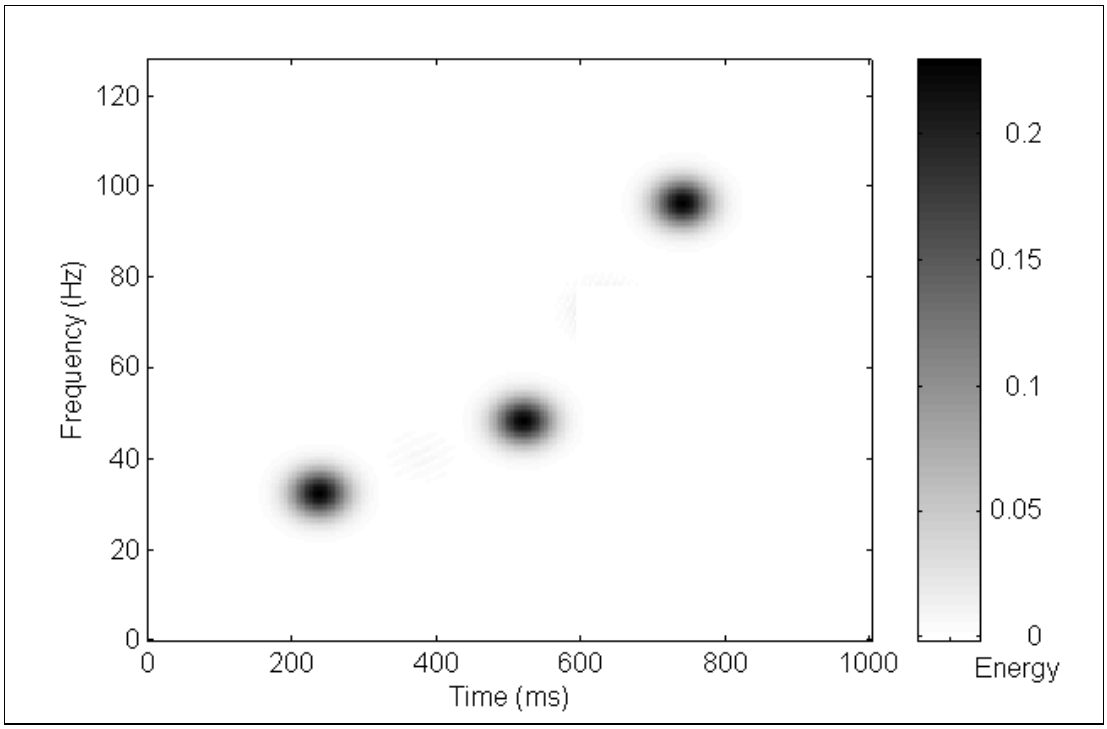

Fig. 3.56 - Pseudo-WV distribution of signal S7 (KB time window exponential argument 150, no frequency window - time-shift = 1 data point)

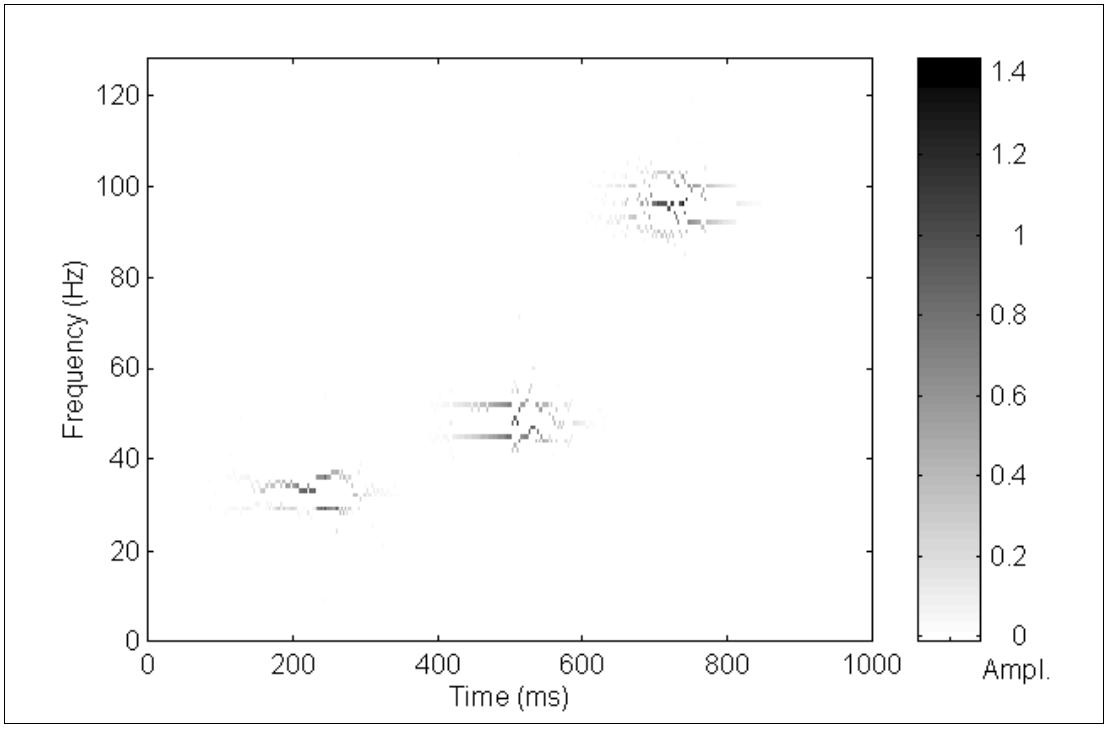

Fig. 3.57 - Extended Prony time-frequency representation of signal S7 (48 data points per sample - total data points used = 559, order 46, no exponential damping limit)

It can be seen in the graphs of Figures 3.53 to 3.57, that the best representation for the signal with Gaussian waves was obtained using the pseudo-Wigner-Ville distribution, which also corresponds closely to the true representation of this signal. The same results were obtained in the work of Chiollaz and Frave [1993], who suggested the use of time and frequency windows in order to reduce the interference effect that appears in the results of the Wigner-Ville distribution. This interference, caused by the cross-terms problem, can be seen in the graph of Figure 3.55 which was generated using the Wigner-Ville distribution. This graph also shows a second-order cross-term generated by propagation, which is depicted by the spot in the middle of the two first-order cross-terms generated by this distribution. The distortion in the graph generated by the Morlet wavelet transform (see Figure 3.54), is caused by the logarithm frequency scale of its results. In this test the extended Prony time-frequency representation does not depict the Gaussian waves properly (see Figure 3.57). A large order (46) is necessary to force the extended Prony time-frequency representation to represent the large number of points that exists in the centre of the Gaussian waves.

Table 3.10 summarise the results obtained using the techniques involved in this study applied to the signals S4, S5, S6, and S7.

Signal feature (non-stationary simulation)	Technique FT	MWT	WVD	PWVD	PTFR
Sine sweeps (signal S4)	NC	D	D	D	D >B<
56/59 Hz component (signal S5)	NC	D	NC	D	D >B<
Modulations (signal S6)	NC	D	D	D	D >B<
3 Gaussians (signal S7)	NC	D	D	D >B<	D

ABBREVIATIONS

FT - Fourier transform
MWT - Morlet wavelet transform
WVD - Wigner-Ville distribution
PWVD - Pseudo-Wigner-Ville distribution
PTFR - Extended Prony time-frequency rep.

ND - not detected
NC - not clear
D - detected
>B<- best method

Table 3.10 - Method component detection performance

3.5. Signal Processing Techniques: Analysis of Multi-Component Signals

In this section the components of basic signals analysed in the previous section will be combined in order to obtain more complex signals for testing the processing techniques involved in this study.

3.5.1. Signal with a Deterministic Component and a Component with Frequency Variation (Signal S8)

This signal S8 consists of two components that are commonly found in the signals of ESP vibrations. The first component, whose frequency varies between 56 to 59 Hz is

associated with the rotation of an ESP pump subjected to load variation. A second 60 Hz deterministic component is associated with the electrical torque of the motor due the magnetic field. This signal is difficult to analyse due to a combination of the proximity of the component frequencies (56/59 and 60 Hz) and the non-stationary condition of the 56/59 Hz component. Table 3.11 shows the composition of this signal, and Figures 3.58 to 3.60 show the signal, its true time-frequency representation, and its Fourier transform. Figures 3.61 to 3.64 show the results generated by of each time-frequency representation method involved in this study.

Component	Time length (s)	No. of data points	Frequency (Hz)	Amplitude (Mag)	Phase (degrees, t = 0)
sine wave	1.0	512	min. = 56 max. = 59	0.1	0
sine wave	1.0	512	60	0.3	90

Table 3.11 - Signal S8 containing a component whose frequency varies between 56 to 59 Hz and a 60 Hz deterministic component (see sections 3.2.4 and 3.5.2 respectively for component definitions)

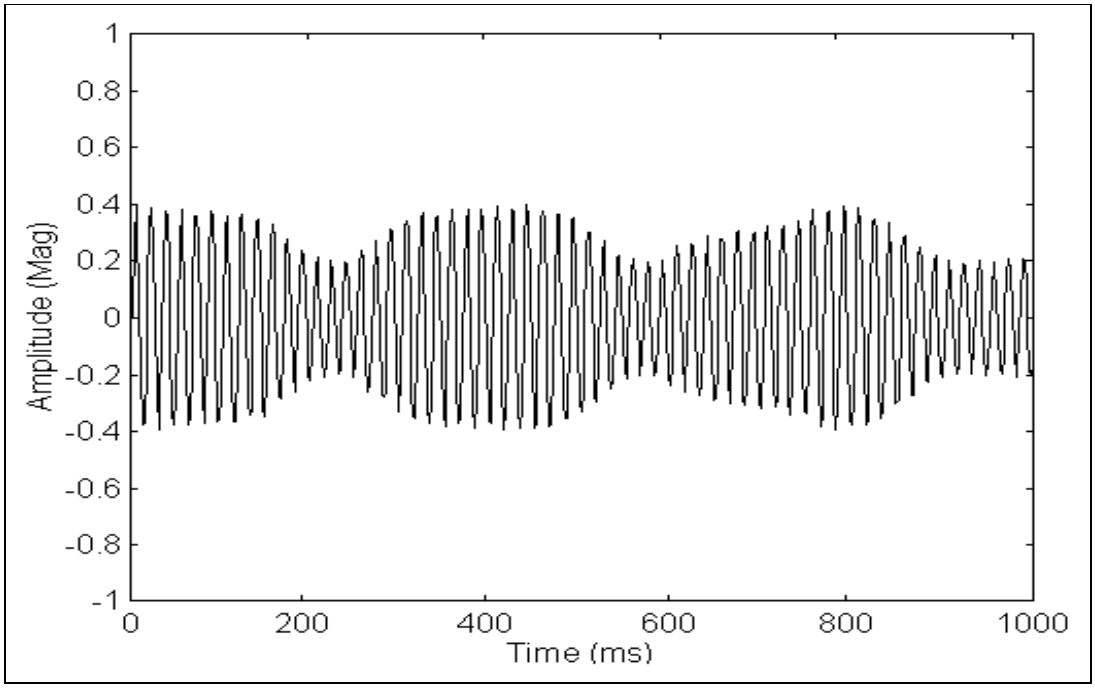

Fig. 3.58 - Signal S8 containing a component whose frequency varies between 56 to 59 Hz and a 60 Hz deterministic component

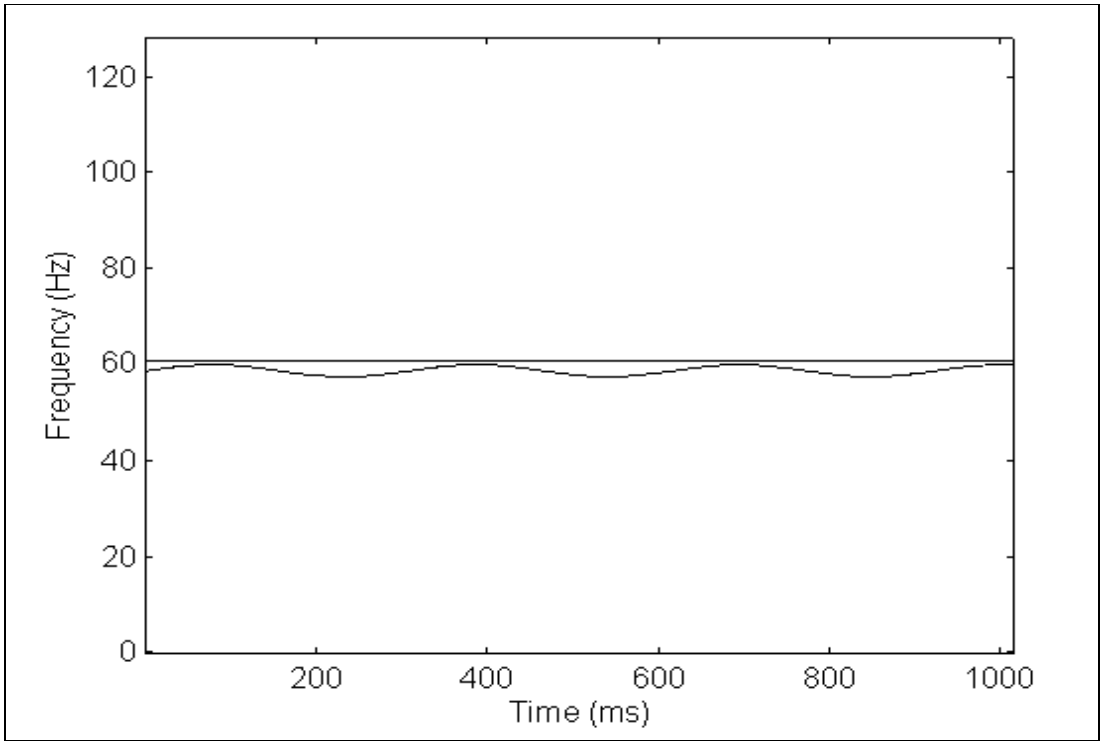

Fig. 3.59 - True time-frequency representation of signal S8

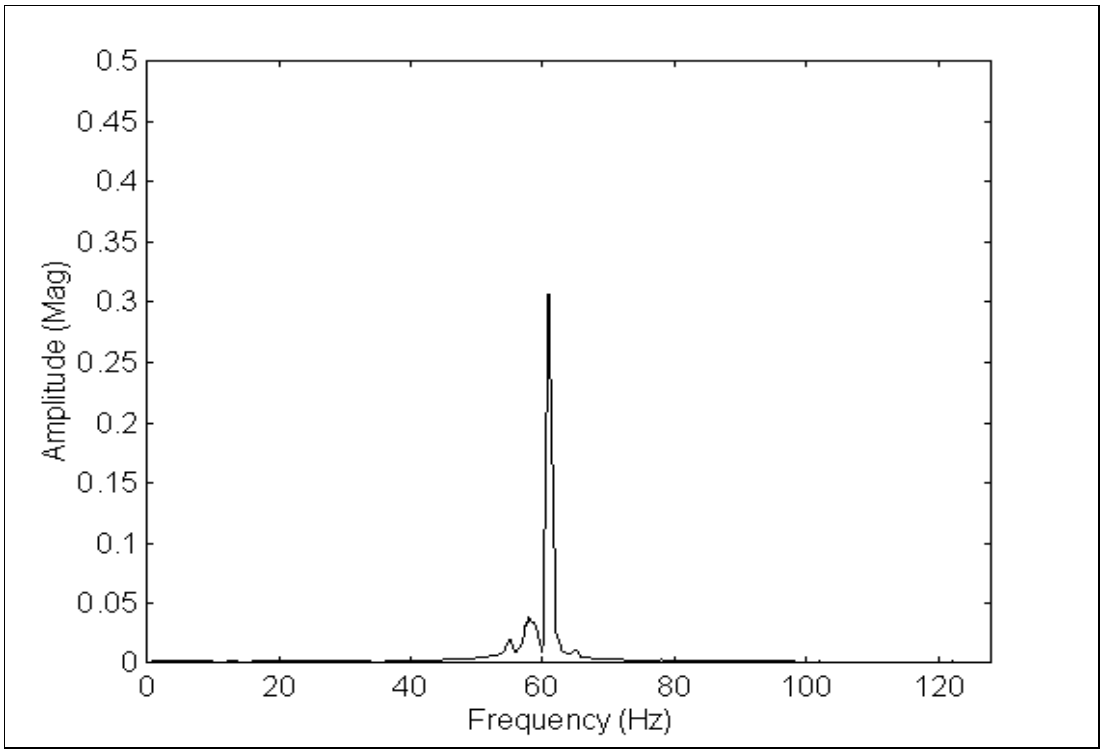

Fig. 3.60 - Fourier transform of signal S8 (frequency resolution = 1 Hz, no window)

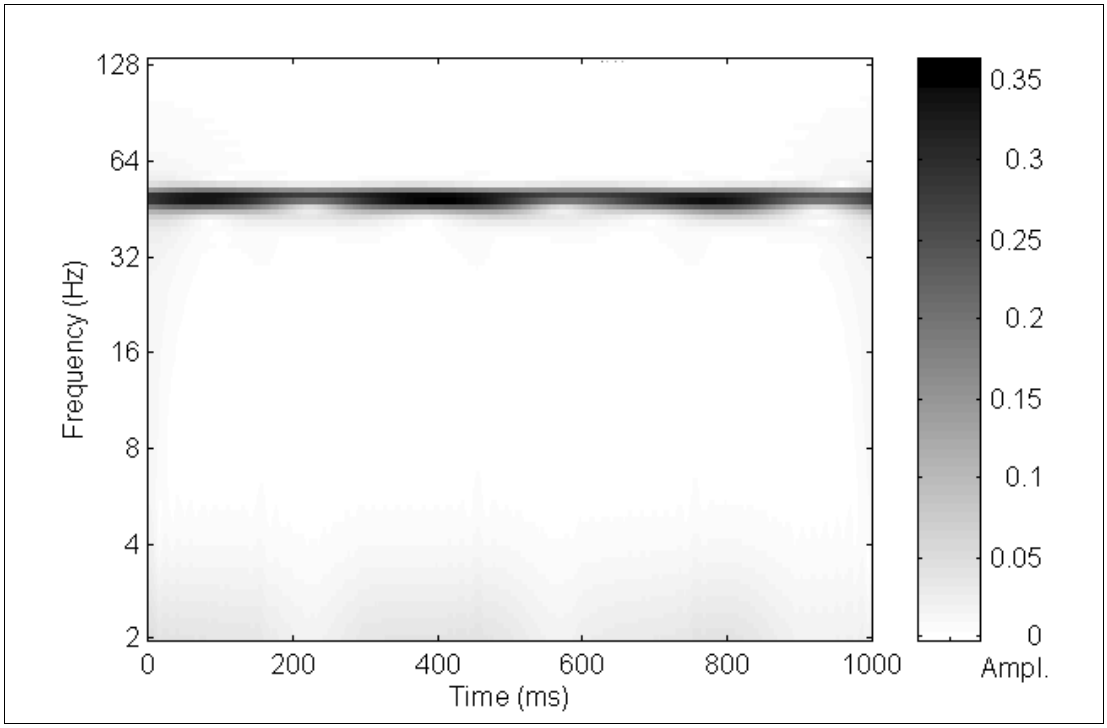

Fig. 3.61 - Morlet wavelet transform of signal S8 (8 octaves & 20 voices per octave)

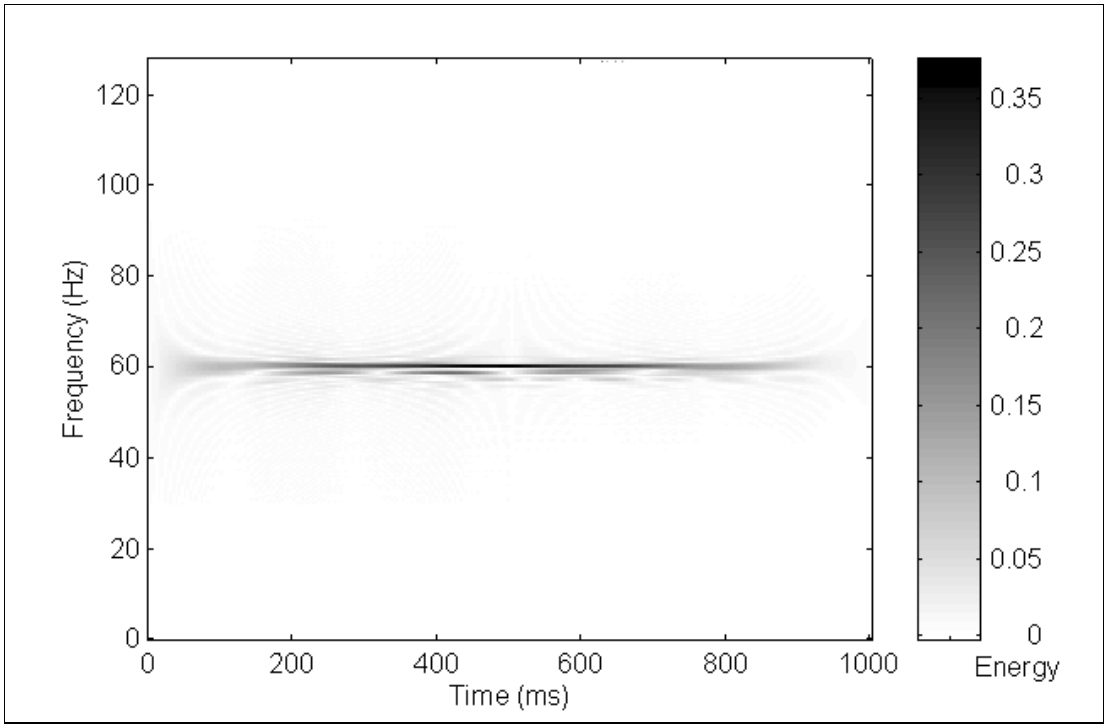

Fig. 3.62 - Wigner-Ville distribution of signal S8 (time-shift = 1 data point)

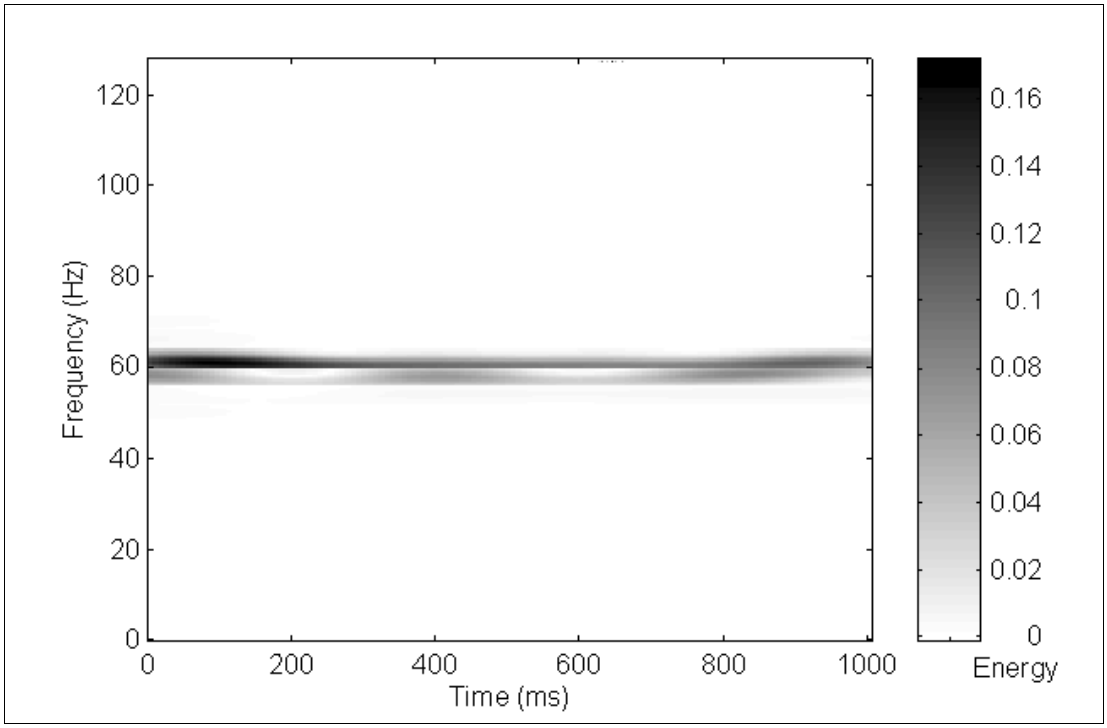

Fig. 3.63 - Pseudo-WV distribution of signal S8 (KB time and frequency window exponential arguments 70 and 2 - time-shift = 1 data point, frequency shift = 8 Hz)

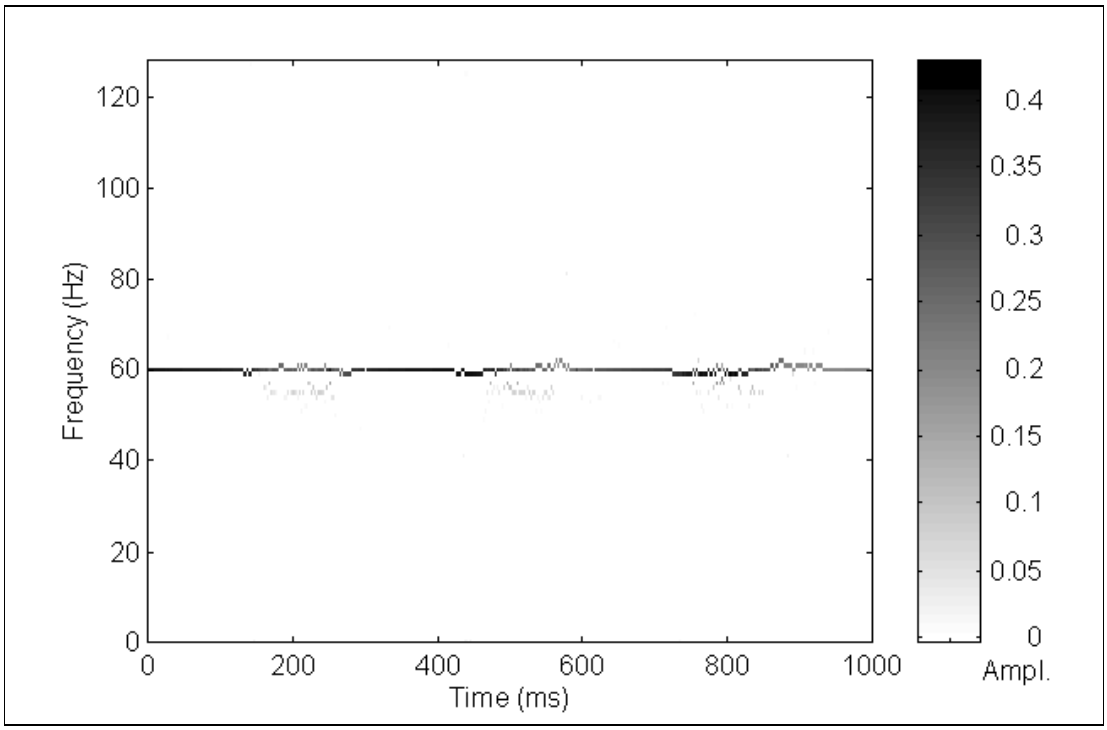

Fig. 3.64 - Extended Prony time-frequency representation of signal S8 (16 data points per sample - total data points used = 527, order 8, no exponential damping limit)

None of the time-frequency representations show the composition of the signal described in Table 3.9 properly (see Figures 3.60 to 3.64). It is only in the results of the Fourier transform technique that there is some indication that there are two definite components in the signal (see Figure 3.60).

3.5.2. Signal with Deterministic Components and Modulations (Signal S9)

This signal S9 is designed to test the methods capability to analyse strong non-stationary conditions, which represent the fluid slug vibration (modulations), together with deterministic components. This signal is described in Table 3.12, and Figures 3.65 to 3.67 show the signal, its true time-frequency representation, and its Fourier transform. For comparative purposes, the Fourier transform method was applied to two different sets of signal data samples, one containing 512 data points and another containing 524288 data points (see Figure 3.67). The results of the application of each time-frequency representation method to the signal S9 are shown in Figures 3.68 to 3.72 in logarithmic vertical scale (dB) due to the great disparity between the amplitude values of the 58 and 60 Hz components and the frequency modulations.

Components	Time (s)	No. of data points	Frequency (Hz)	Amplitude (Mag)	Phase (degrees, t=0)
sine wave	1.0	512	58	0.1	0
sine wave	1.0	512	60	0.3	90
modulations (3)	1.0	90	initial = 6 centre = 24 final = 6	5.0	---

Table 3.12 - Signal S9 with stationary and non-stationary component data (see section 3.2.4 for component definition)

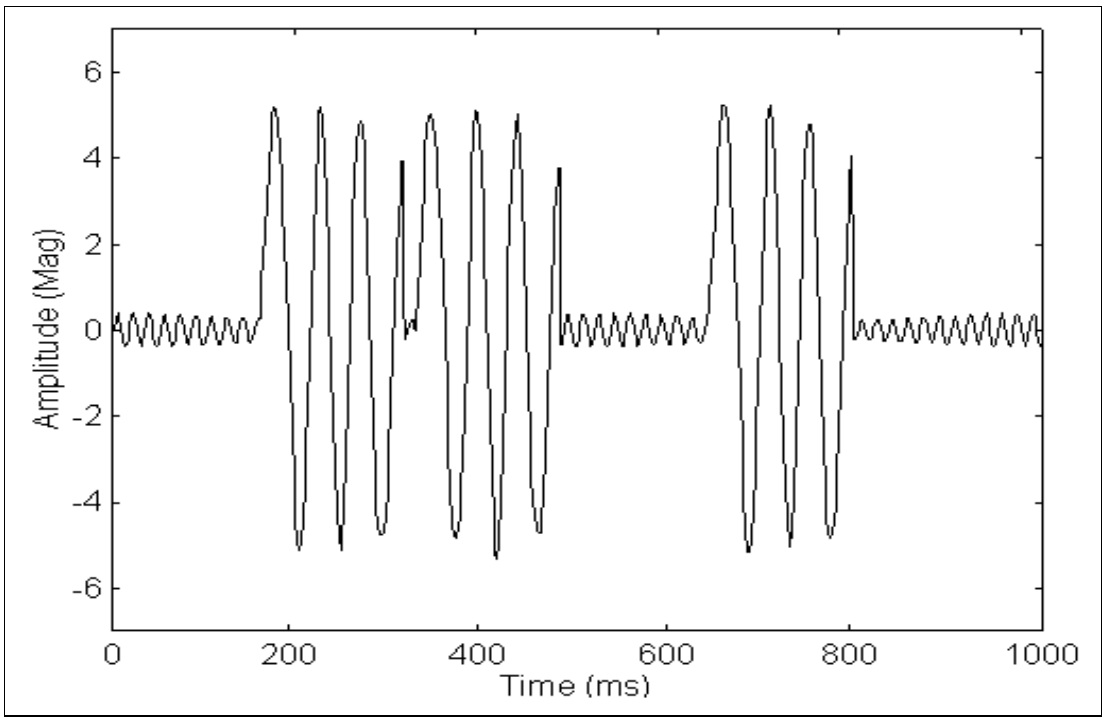

Fig. 3.65 - Signal S9 containing modulations and two deterministic components with frequencies of 58 and 60 Hz each

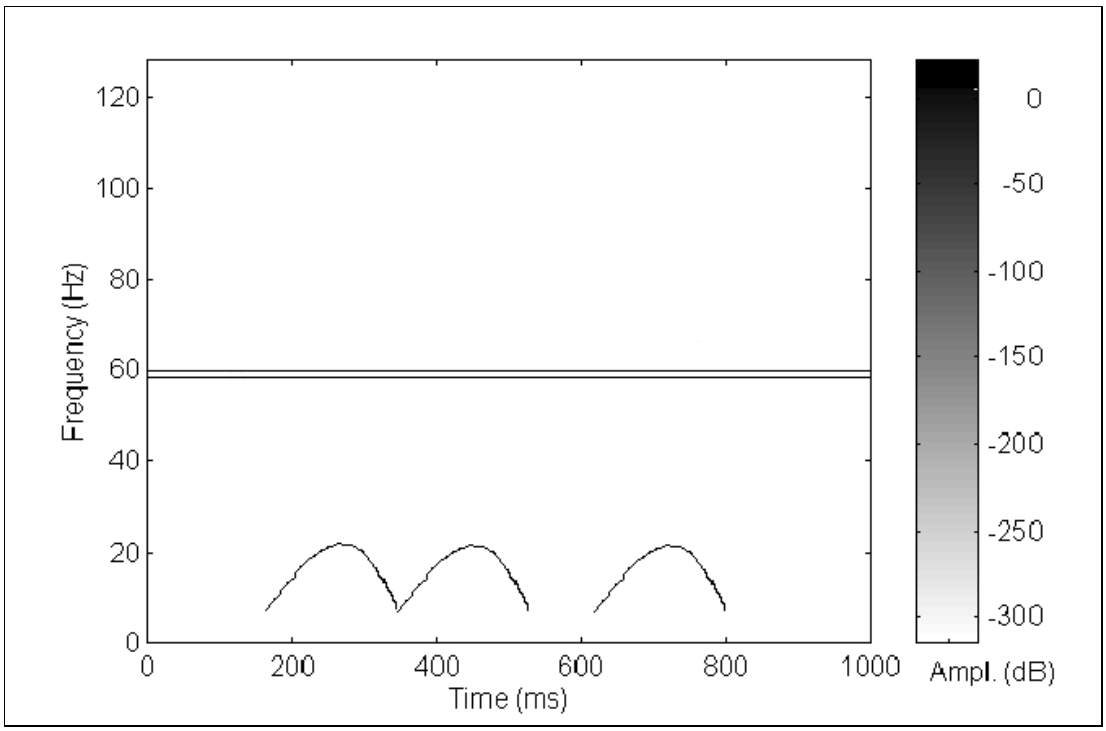

Fig. 3.66 - True time-frequency representation of signal S9 (dB Magnitude)

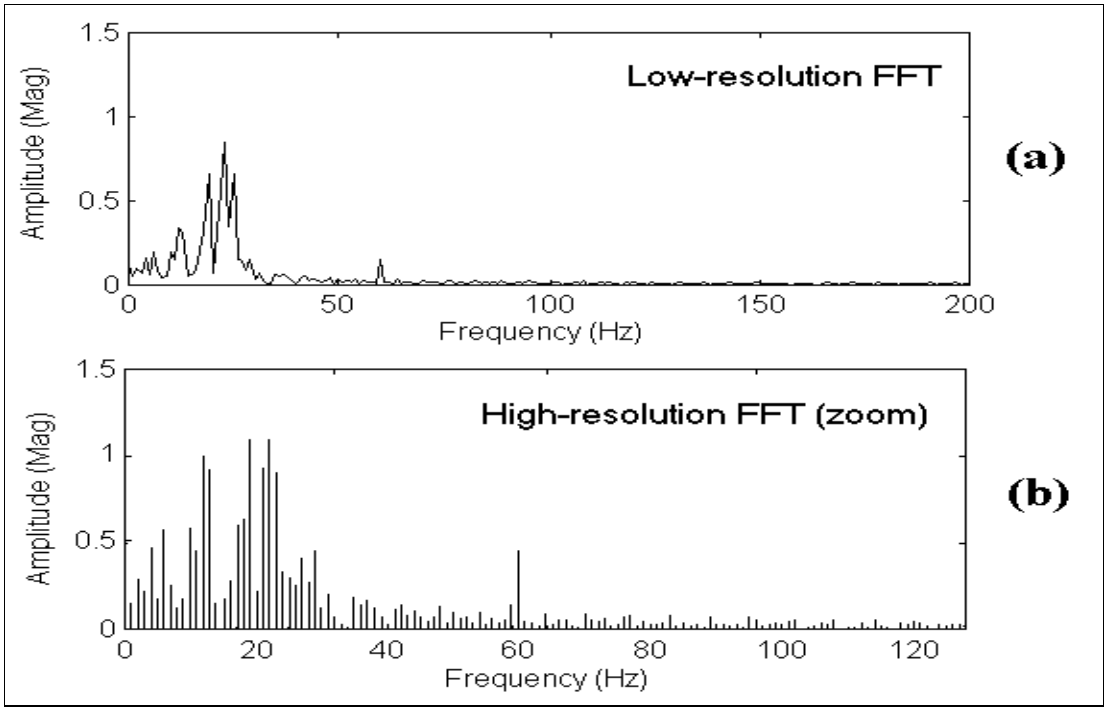

Fig. 3.67 - Fourier transform of signal S9 ((a) 512 data points, 1 second, freq. resolution = 1 Hz, (b) 524288 data points, 1024 seconds, freq. resolution = 0.001 Hz - no averaging, no window)

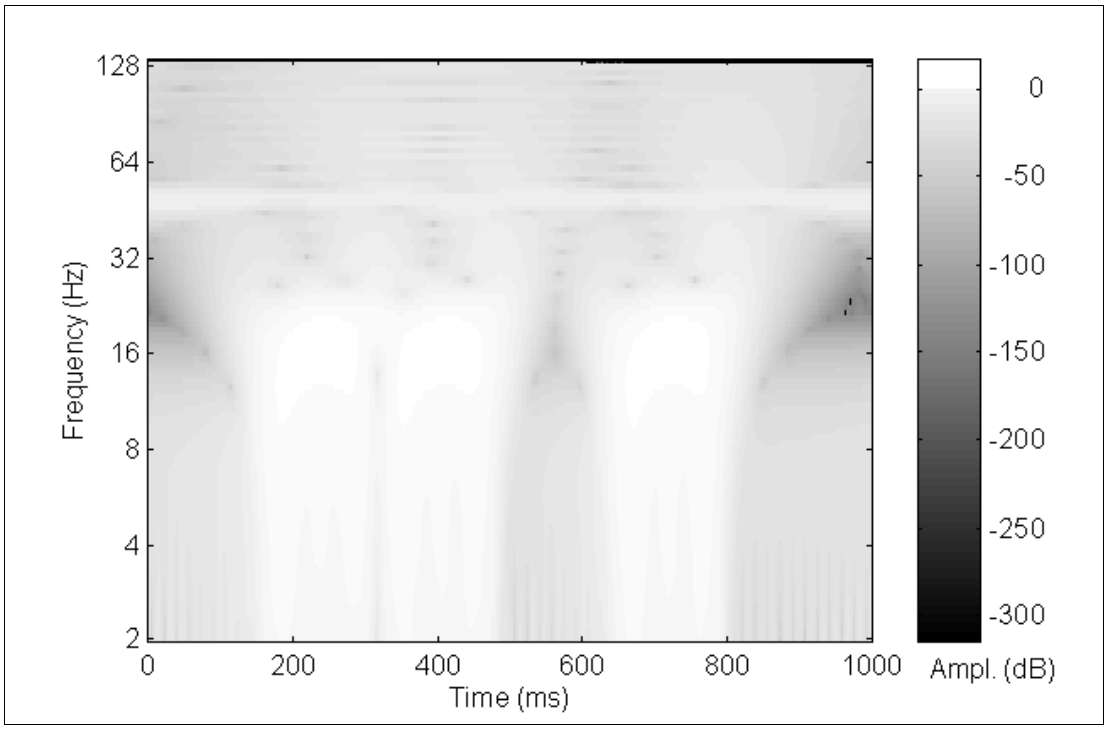

Fig. 3.68 - Morlet wavelet transform of signal S9 (8 octaves & 20 voices per octave - note that the grey-scale is inverted in order to provide a clear depiction of the weak component)

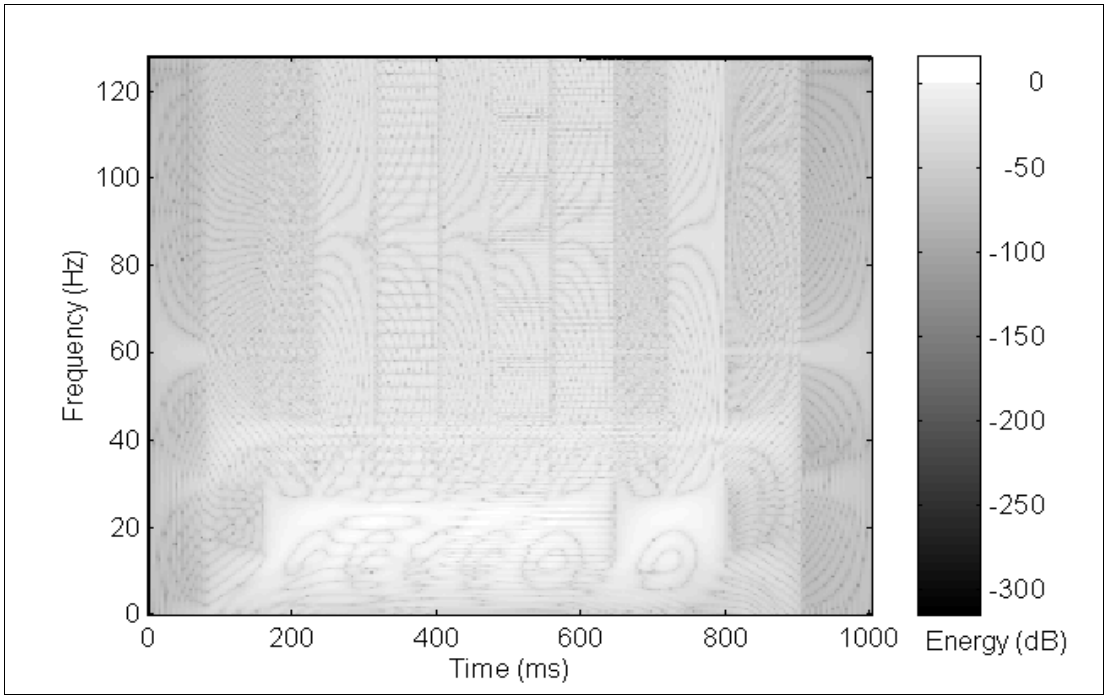

Fig. 3.69 - Wigner-Ville distribution of signal S9 (time-shift = 1 data point - note that the grey-scale is inverted in order to provide a clear depiction of the weak component)

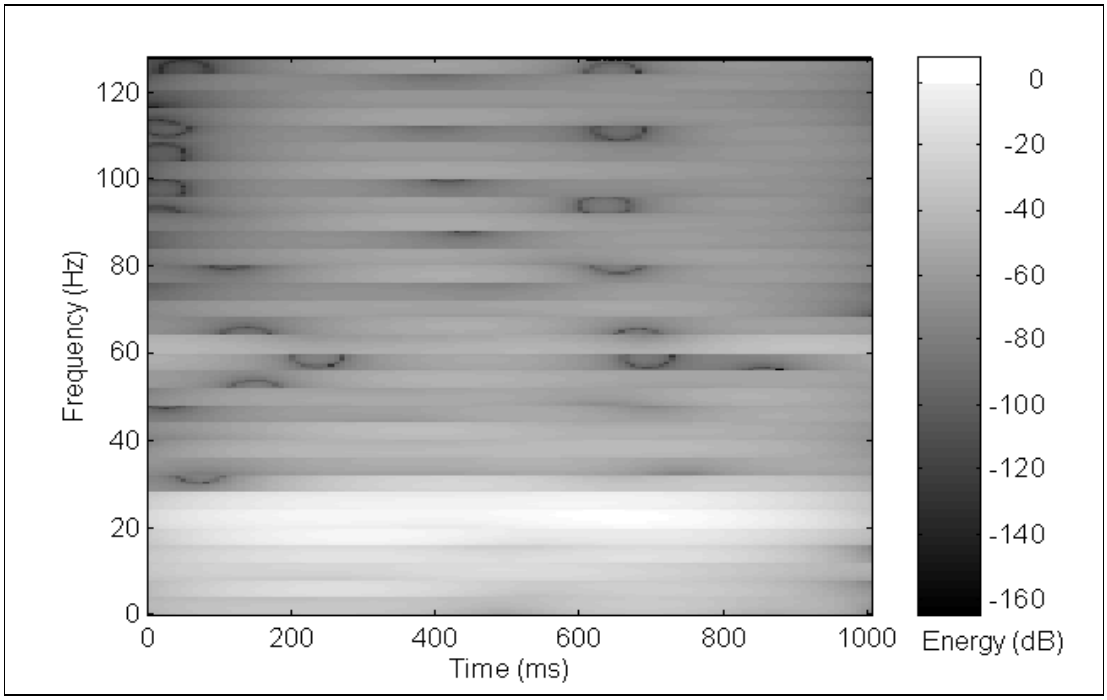

Fig. 3.70 - Pseudo-WV distribution of signal S9 (KB time and frequency window exponential arguments 70 and 2 - time-shift = 1 data point, frequency shift = 8 Hz - note that the grey-scale is inverted in order to provide a clear depiction of the weak component)

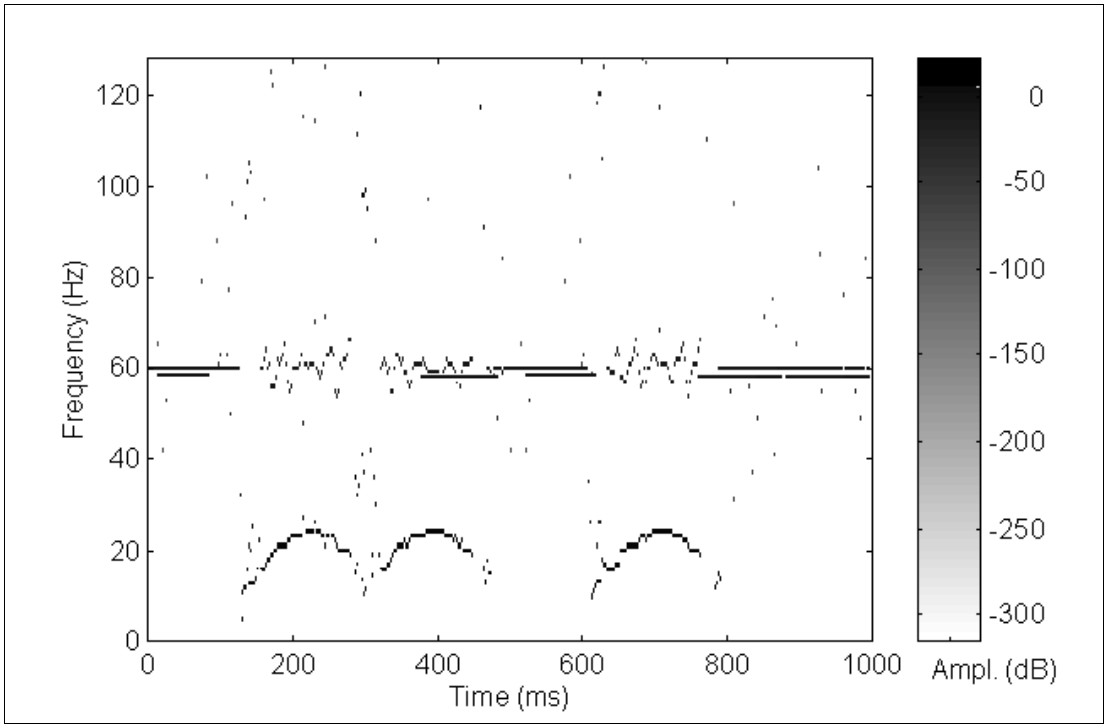

Fig. 3.71 - Extended Prony time-frequency representation of signal S9 (16 data points per sample - total data points used = 527, order 14, no exponential damping limit)

The deterministic components are clearly depicted by the graph of the Fourier transform shown in Figure 3.67, but the modulations are not represented properly due to the difficulty in performing non-stationary analysis with this method. The modulations are represented in a more precise way, in terms of component frequency composition, by the Wigner-Ville distribution (Figure 3.69), the pseudo-Wigner-Ville distribution (Figure 3.70), the Morlet wavelet transform (Figure 3.68) and the extended Prony time-frequency representation (Figure 3.71). Only in the graph generated by the extended Prony time-frequency representation are the signal components fairly depicted.

It is possible to adjust the exponential damping limit of the extended Prony time-frequency representation in order to "extract" deterministic components to the detriment of the non-stationary ones. The graph in Figure 3.72 demonstrates this operation, where the method was set to calculate the time-frequency representation with reduced amplitude and exponential damping limits, which caused the elimination

of the modulations values. This filtering procedure of non-stationary elimination is what is referred to above as time-frequency exponential damping filtering obtained using the exponential damping values calculated by the original Prony method and associated with each component depicted in the time-frequency plane (see equation (2.22)).

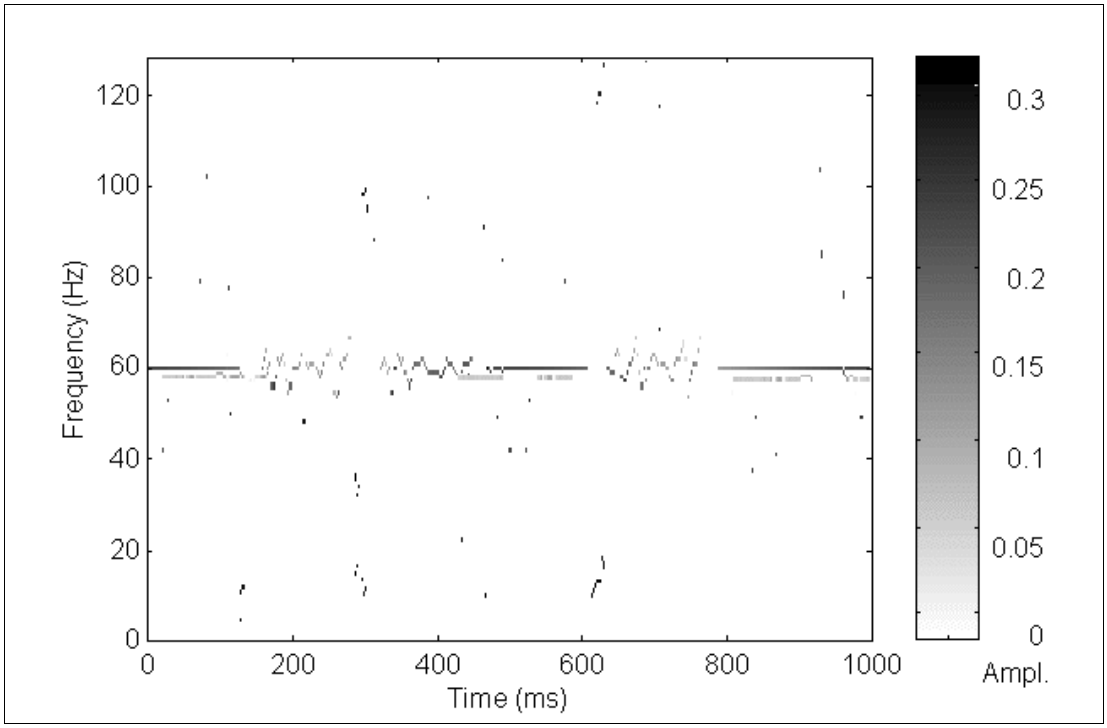

Fig. 3.72 - Extended Prony time-frequency representation of signal S9 (16 data points per sample - total data points used = 527, order 14, exponential damping limit set to 0.02 s^{-1})

3.5.3. Signal with Deterministic Components, High-Level Noise, and Modulations (Signal S10)

The first signal to represent a live signal collected in a petroleum wellhead is composed of deterministic components corresponding to the rotation of the ESP equipment (58 Hz) and to the electrical power supply (60 Hz), white noise and

modulations corresponding to the fluid-slugs as defined in the work of Leducq and Hervieu [1991]. Table 3.13 describes this signal, and Figures 3.73 and 3.74 show the signal and its Fourier transform. For comparative purposes, the Fourier transform method was applied to two different sets of signal data samples, one containing 512 data points and another containing 524288 data points (see Figure 3.74). Figures 3.75 to 3.78 show the results generated by the methods applied in this study.

Components	Time length (s)	No. of data points	Frequency (Hz)	Amplitude (Mag)	Phase (degrees, t = 0)
sine wave	1.0	512	58	0.1	0
sine wave	1.0	512	60	0.3	90
white noise	1.0	512	---	5.0	---
modulations (2)	1.0	90	initial = 6 centre = 24 final = 6	5.0	---

Table 3.13 - Signal S10 containing deterministic components, high-level white noise and non-stationary modulations (see section 3.2.4 for deterministic and modulation component, 3.3.3 for white noise definition, and Appendix C for SNR level assumption)

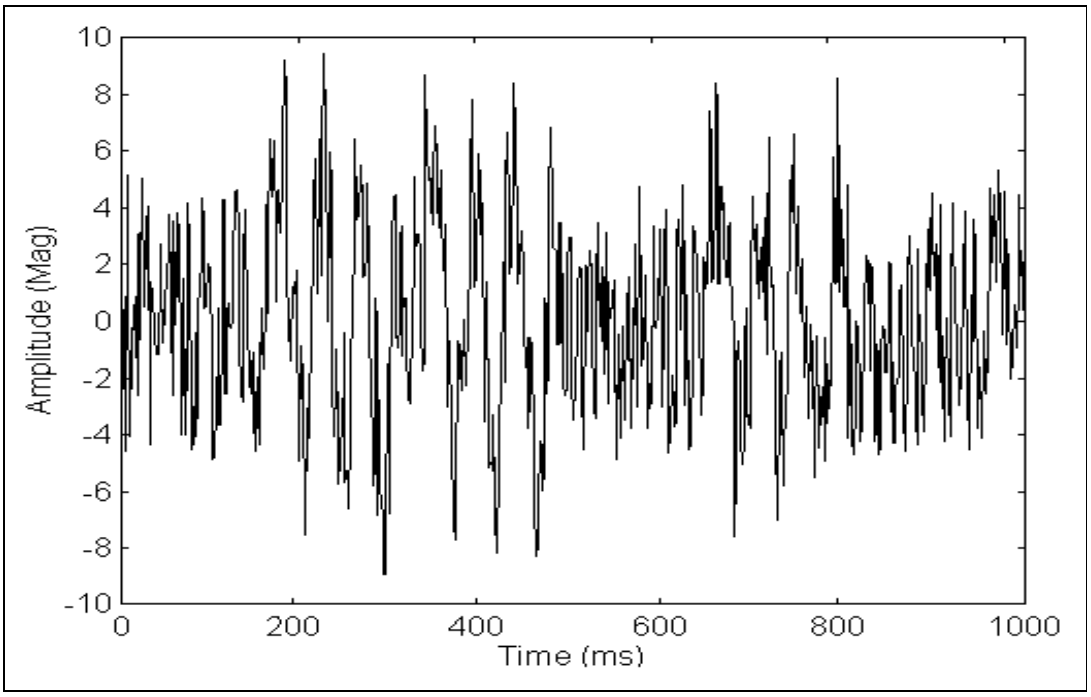

Fig. 3.73 - Signal S10 containing deterministic components, high-level white noise and non-stationary modulations

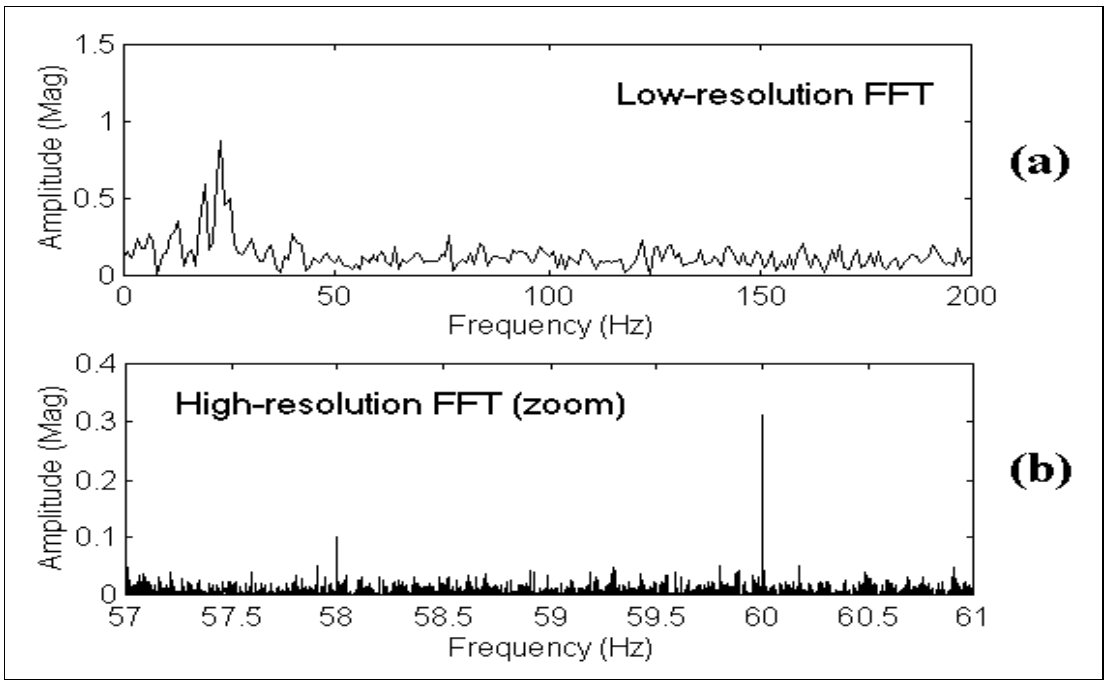

Fig. 3.74 - Fourier transform of signal S10 ((a) 512 data points, 1 second, freq. resolution = 1 Hz, (b) 524288 data points, 1024 seconds, freq. resolution = 0.001 Hz - no averaging, no window)

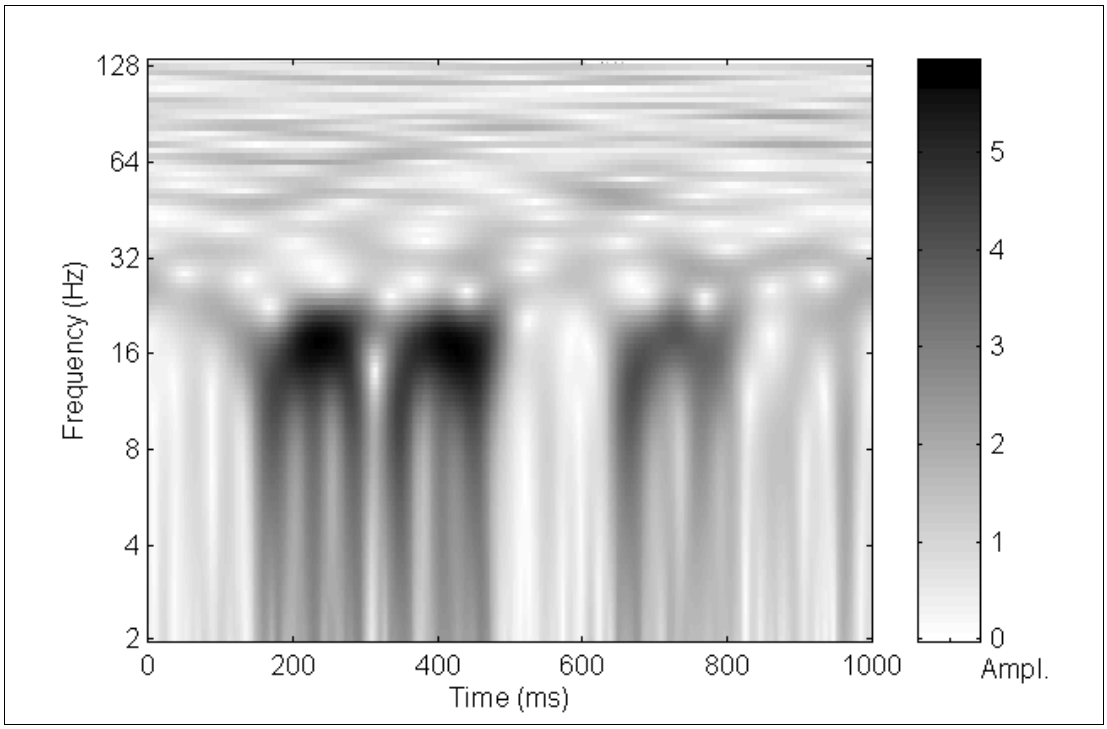

Fig. 3.75 - Morlet wavelet transform of signal S10 (8 octaves & 20 voices per octave)

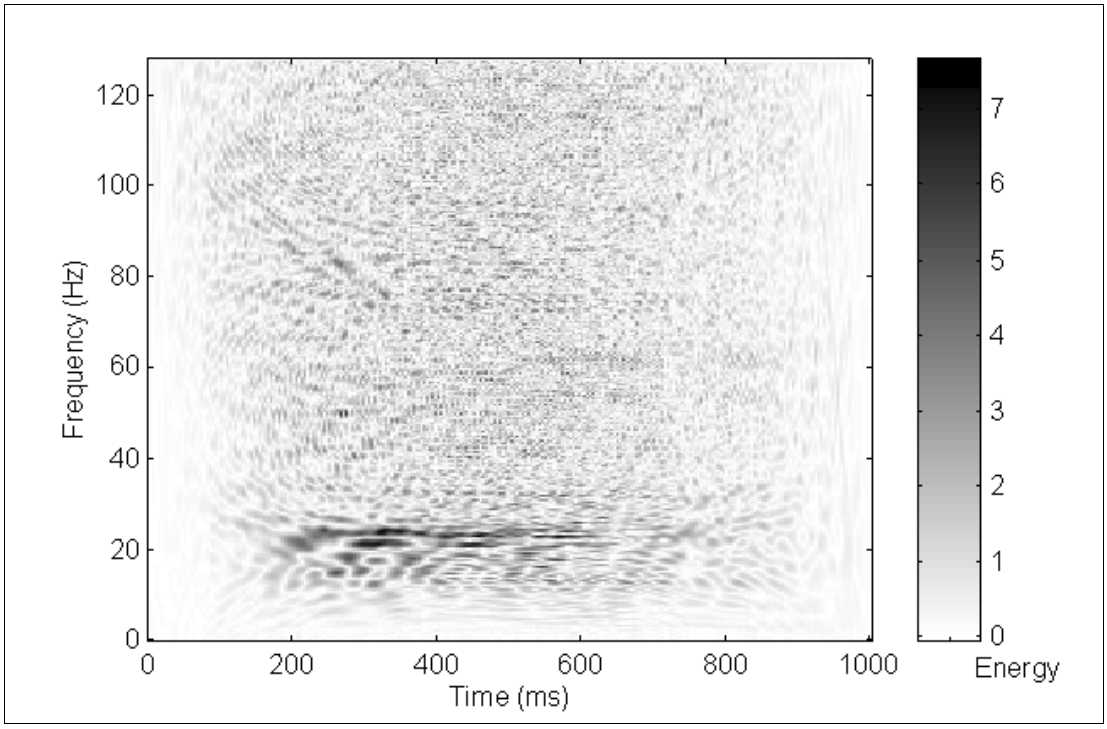

Fig. 3.76 - Wigner-Ville distribution of signal S10 (time-shift = 1 data point)

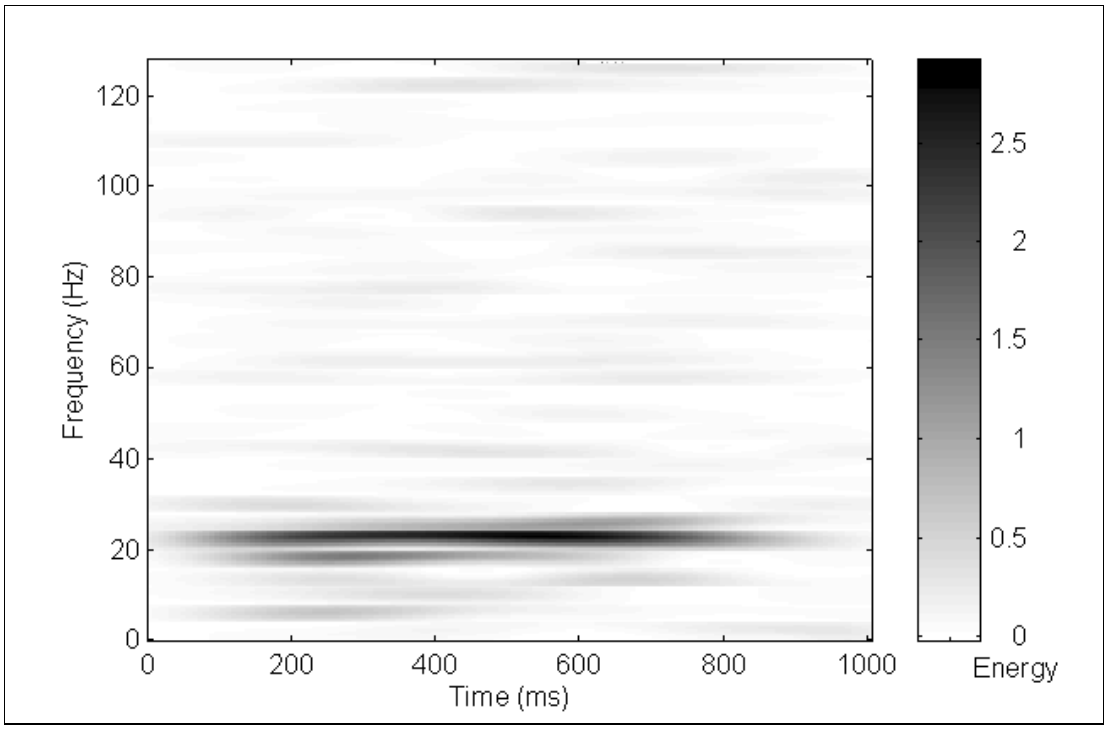

Fig. 3.77 - Pseudo-WV distribution of signal S10 (KB time and frequency window exponential arguments 70 and 2 - time-shift = 1 data point, frequency shift = 8 Hz)

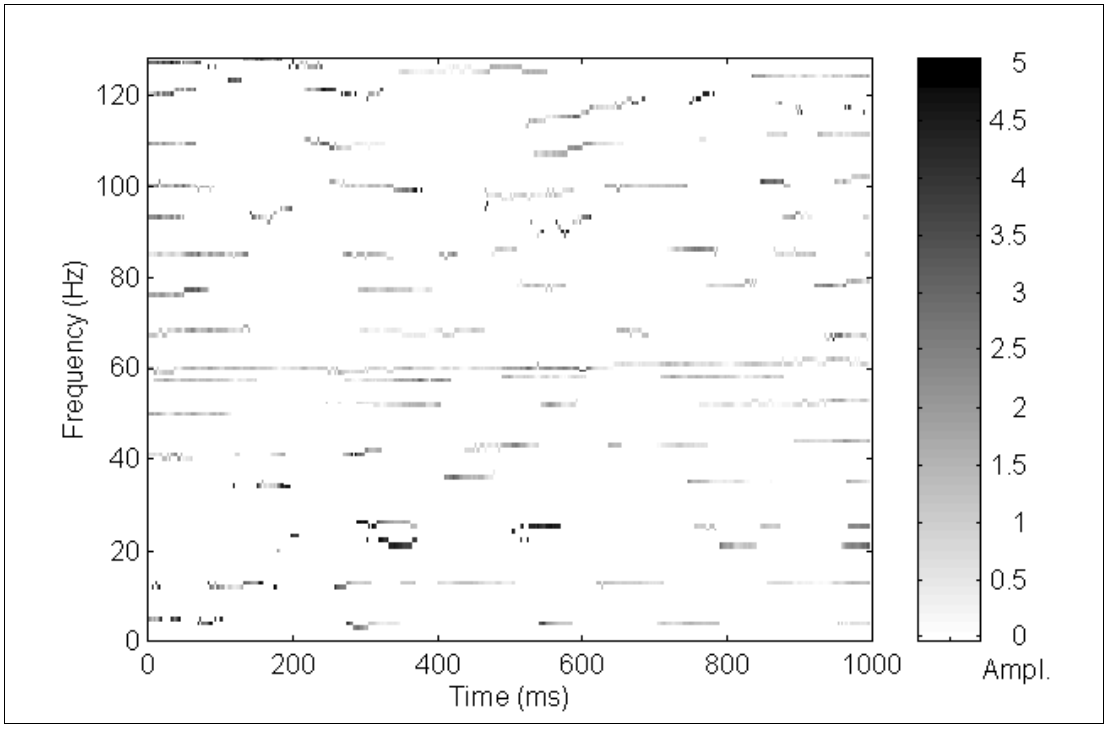

Fig. 3.78 - Extended Prony time-frequency representation of signal S10 (512 data points per sample - total data points used = 1023, order 64, maximum exponential damping 0.02 s^{-1})

In the graphs generated by the Morlet wavelet transform, the Wigner-Ville distribution and the pseudo-Wigner-Ville distribution, only the modulations are depicted (see Figures 3.75 to 3.77). In the graph of Figure 3.78 are shown the results obtained when the extended Prony time-frequency representation is applied to a simulated signal with a 512-data-point-shift. In this case the exponential damping was limited to 0.02 s^{-1}.

The modulation components shown in Figure 3.74 are not properly depicted because the Fourier transform is not appropriate to analyse non-stationary conditions. Also, some signal sample processed using the extended Prony time-frequency representation (see section 2.7) does not depicts the modulation components (see Figure 3.79). However, for the detection of deterministic components in the presence of high-level noise and strong non-stationary conditions, one signal sample processed using the extended Prony time-frequency representation is more efficient than the Fourier transform. For an adequate depiction of the deterministic components using the

Fourier transform, a very large number of data points are necessary to process the signal. It can be seen that the results generated by one signal sample processed using the extended Prony time-frequency representation are less confusing than that processed by the Fourier transform (see Figures 3.74 and 3.79). This is a consequence of the way that this technique processes the signal. The signal sample processed using the extended Prony time-frequency representation, which is related to the original Prony method, is not a transformation with consequent domain change, as is the Fourier transform, when an exponential is "found" on the time domain, that may really correspond to one deterministic component which may be damped, or not. The graph in Figure 3.79 shows another useful advantage of the signal samples processed using the calculation of the extended Prony time-frequency representation, in that there are fewer detected components, and the probability of one of them being a sought component is higher than in the Fourier transform spectrum. In a 200 Hz range, 200 peaks were registered in the Fourier spectrum as a trivial characteristic of this non-parametric method (see Figure 3.74), while only 21 peaks were found in one signal sample processed using the extended Prony time-frequency representation (see Figure 3.79), resulting in a "less confusing" spectrum.

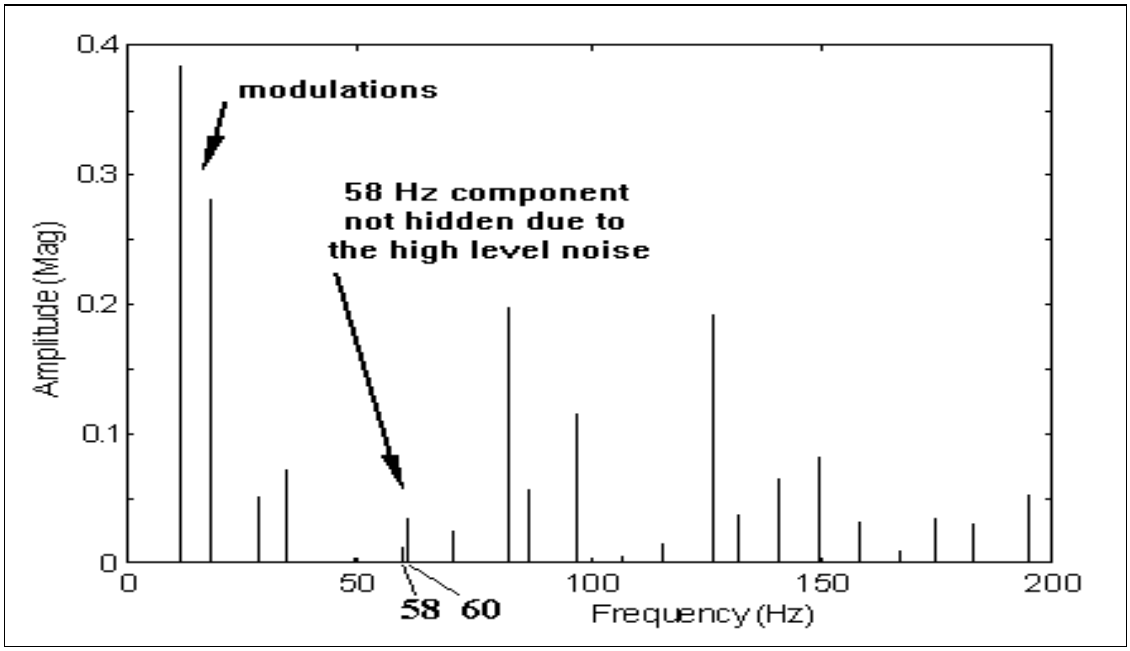

Fig. 3.79 - One signal sample processed using the extended Prony time-frequency representation of signal S10 (order 64, 512 data points, 1 second)

If the number of data points per sample is reduced to 128, the resulting Prony time-frequency plane does not show properly the deterministic component (see Figure 3.80). This suggests that when deterministic components need to be detected, a larger number of data points per sample has to be used. In fact, the larger the quantity of data points per sample used, the stronger is the tendency to find more lightly-damped exponentials (deterministic components). However, this will lead to a greater sacrifice of computational evaluation, because the method will handle large matrices in the equations (2.22) and (2.33) (see section 2.6 of Chapter 2).

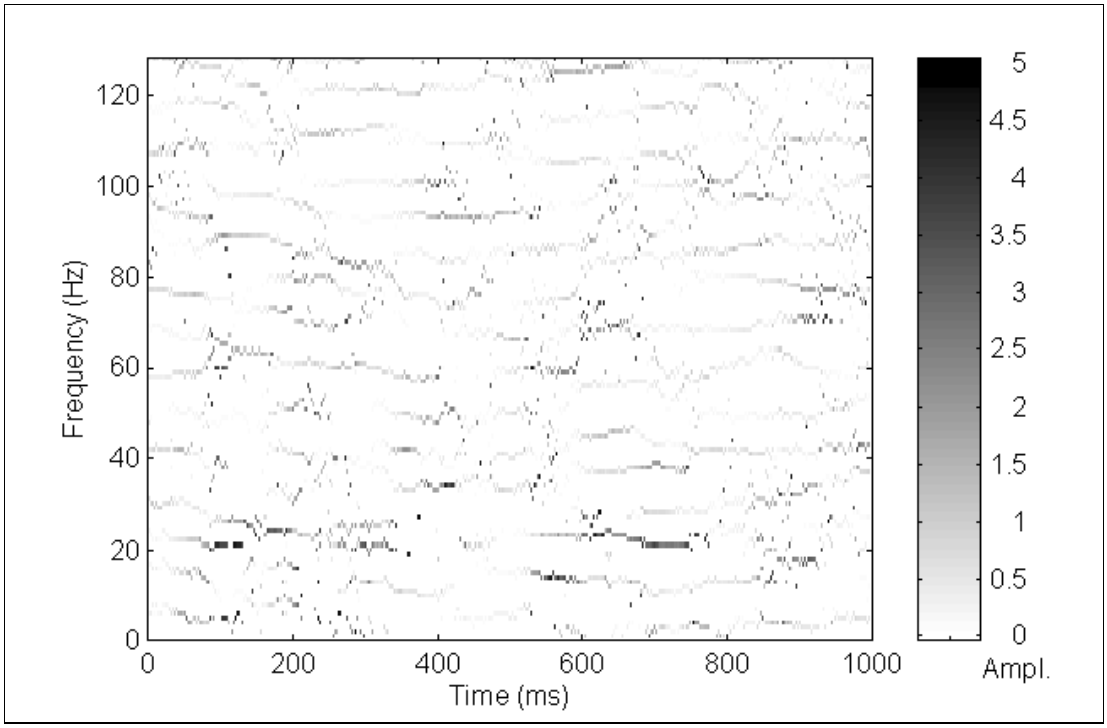

Fig. 3.80 - Extended Prony time-frequency representation of signal S10 (128 data points per sample - total data points used = 639, order 64, maximum exponential damping 0.02 s^{-1})

3.5.4. Main Component with Frequency Variation Embedded in High-Level Noise (Signal S11)

The second signal used to represent a live signal collected in a petroleum wellhead is composed of a component whose frequency varies from 56 to 59 Hz, corresponding to the rotation of the pump under fluid loads, and a 60 Hz deterministic component corresponding to the electrical power supply. White noise was added to the signal, as described in Table 3.14, and the graphs of Figures 3.81 and 3.82 show the signal and its Fourier transform respectively. For comparative purposes, the Fourier transform method was applied to two different sets of signal data samples, one containing 32768 data points and another containing 524288 data points (see Figure 3.82). The graphs of Figures 3.83 to 3.86 show the results generated by the methods applied in this study.

Components	Time length (s)	No. of data points	Frequency (Hz)	Amplitude (Mag)	Phase (degrees, t = 0)
sine wave	1.0	512	min. = 56 max. = 59	0.1	0
sine wave	1.0	512	60	0.3	90
white noise	1.0	512	---	5.0	---

Table 3.14 - Signal S11 containing 56/59 and 60 Hz components, and high-level white noise (see sections 3.2.4 for deterministic component, 3.3.3 for white noise, 3.5.2 for 56/59 Hz component definitions, and Appendix C for SNR level assumption)

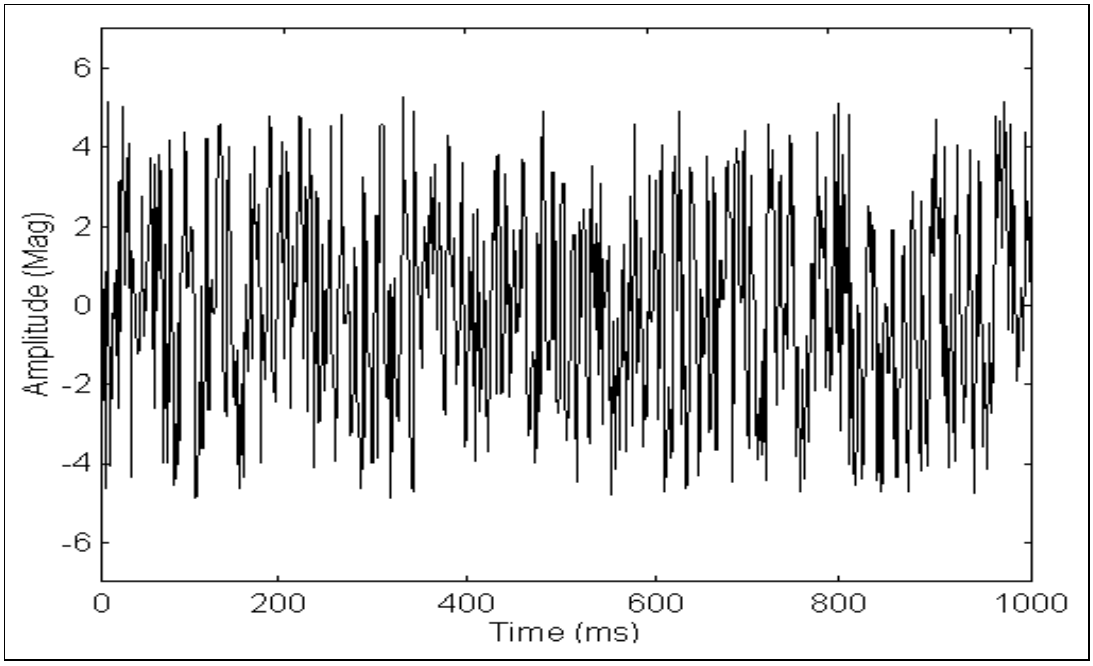

Fig. 3.81 - Signal S11 containing 56/59 and 60 Hz components, and high-level white noise

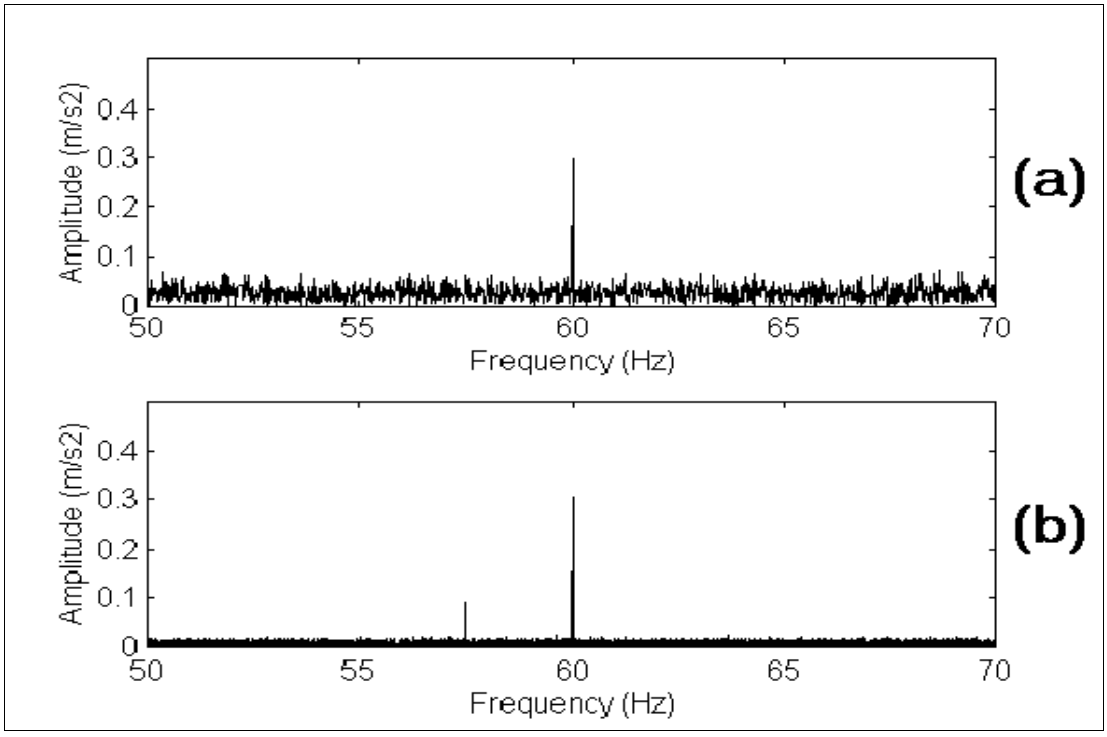

Fig. 3.82 - Fourier transform of signal S11 ((a) 32768 data points, 64 seconds, frequency resolution = 0.016 Hz, no window, (b) 524288 data points, 1024 seconds, frequency resolution = 0.001 Hz, no window)

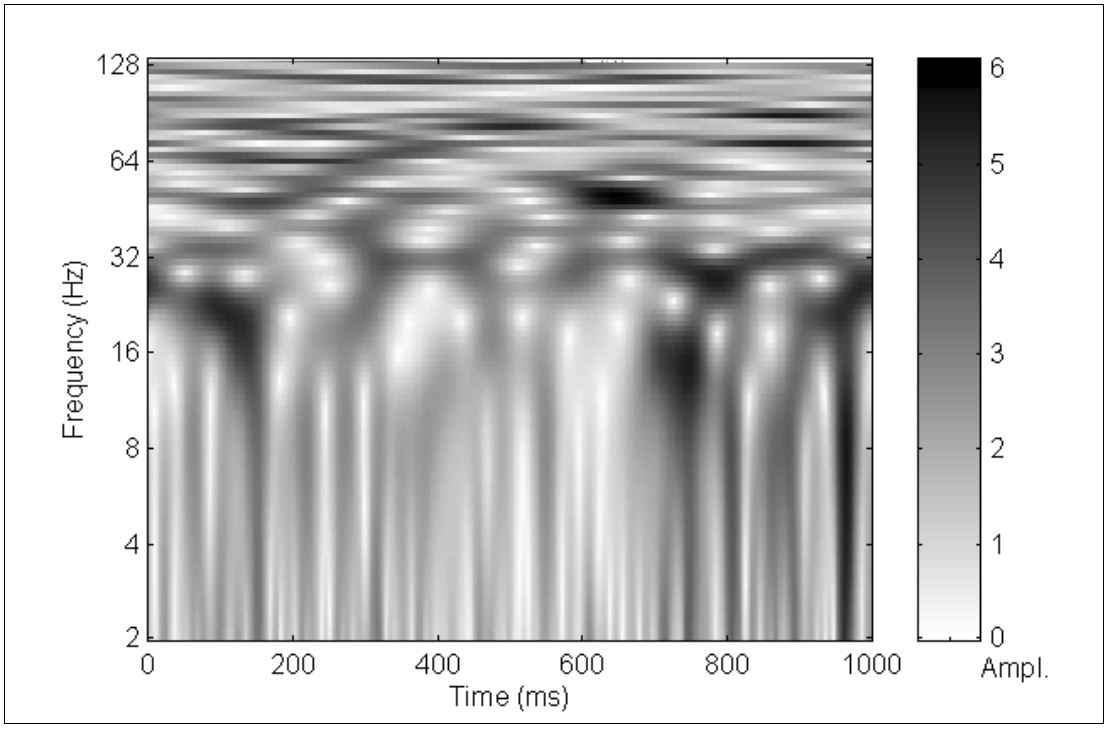

Fig. 3.83 - Morlet wavelet transform of signal S11 (8 octaves & 20 voices per octave)

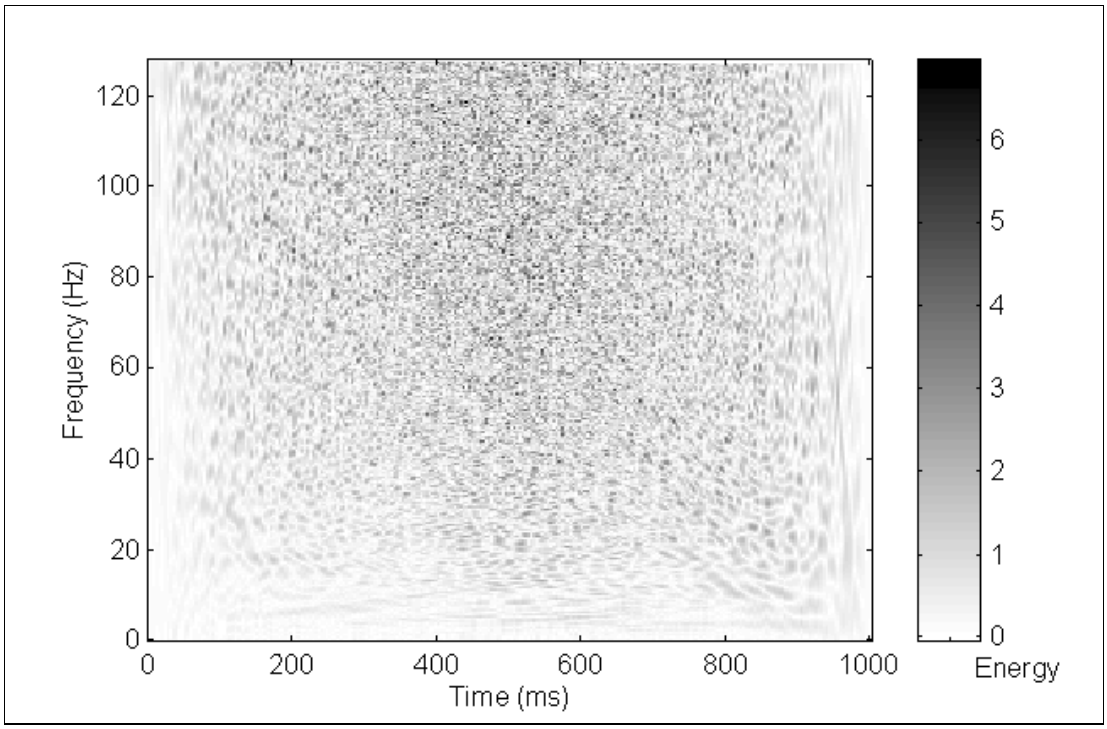

Fig. 3.84 - Wigner-Ville distribution of signal S11 (time-shift = 1 data point)

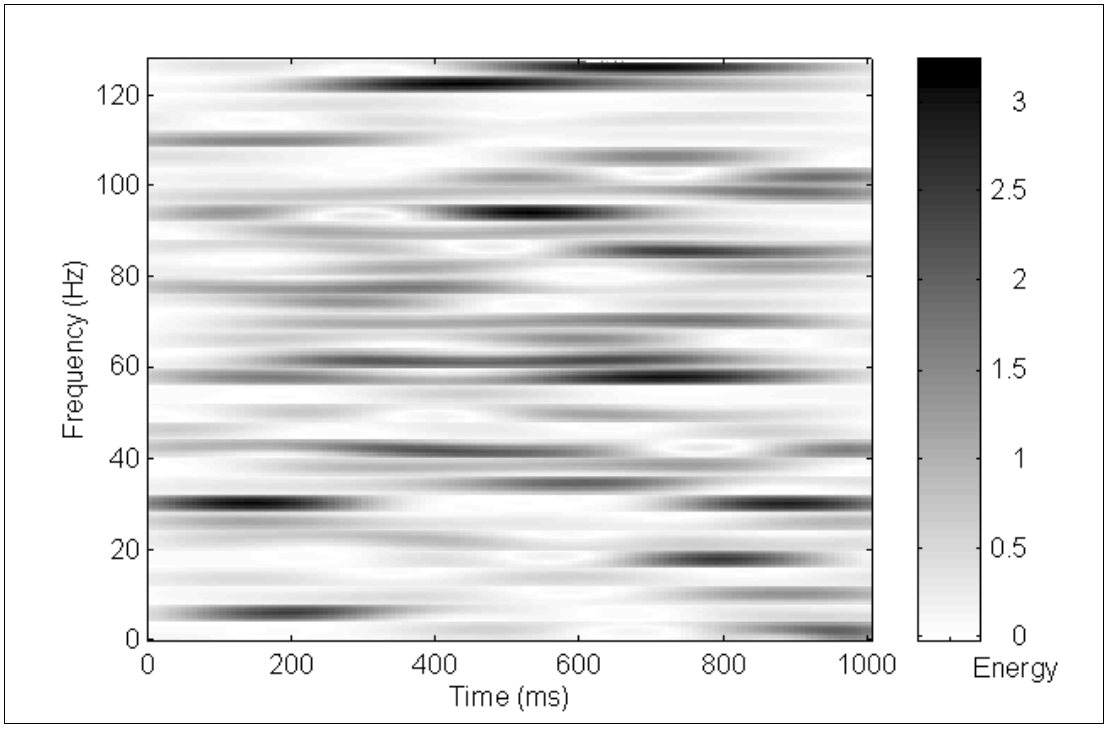

Fig. 3.85 - Pseudo-WV distribution of signal S11 (KB time and frequency window exponential arguments 70 and 2 - time-shift = 1 data point, frequency shift = 8 Hz)

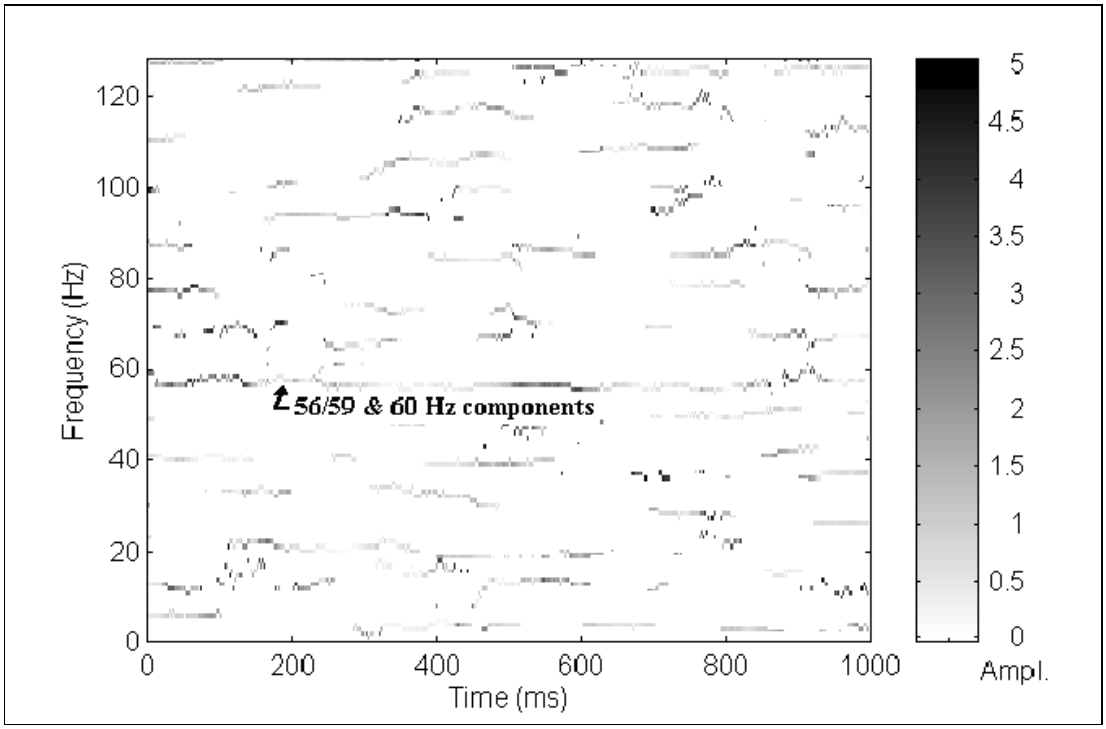

Fig. 3.86 - Extended Prony time-frequency representation of signal S11 (256 data points per sample - total data points used = 767, order 4, maximum exponential damping 0.02 s^{-1})

It can be seen that when the Fourier transform method is applied to the signal no detection of the 56/59 Hz component can be made using a long data array (32768 data points - see Figure 3.82 (a)). However, when the Fourier transform is applied to a very long data array (524288 data points) it is possible to infer that there is a component with a frequency of 57.5 Hz, although it is not possible to infer about the true nature of the component (see Figure 3.82 (b)). This is due to the non-stationary condition of the 56/59 Hz component. When the Morlet wavelet transform, the Wigner-Ville, and the pseudo-Wigner-Ville distribution is applied to this signal, no noticeable result is found for the 56/59 Hz and the 60 Hz components (see Figures 3.83 to 3.85). When the extended Prony time-frequency representation is applied to the signal S11 the 56/59 and the 60 Hz components are detected, albeit not well (see Figure 3.86).

3.5.5. Main Component with Frequency Variation Embedded in High-Level Noise and with Modulations (Signal S12)

This signal is similar to the one in 3.6.2, except for the addition of the non-stationary conditions representing the fluid slugs (modulations). Table 3.15 describes this signal, and the graphs in Figures 3.87 and 3.88 show the respective signal and its Fourier transform. For comparative purposes, the Fourier transform method was applied to two different sets of signal data samples, one containing 32768 data points and another containing 524288 data points (see Figure 3.88). Figures 3.89 to 3.92 show the results generated by the methods applied in this study.

Components	Time length (s)	No. of data points	Frequency (Hz)	Amplitude (Mag)	Phase (degrees, t = 0)
sine wave	1.0	512	min. = 56 max. = 59	0.1	0
sine wave	1.0	512	60	0.3	90
white noise	1.0	512	---	5.0	---
modulations (2)	1.0	90	initial = 6 centre = 24 final = 6	5.0	---

Table 3.15 - Signal S12 containing 56/59 and 60 Hz components, high-level white noise and non-stationary modulations (signal S12, see sections 3.2.4 for deterministic and modulation component, 3.3.3 for white noise, 3.5.2 for 56/59 Hz component definitions, and Appendix C for SNR level assumption)

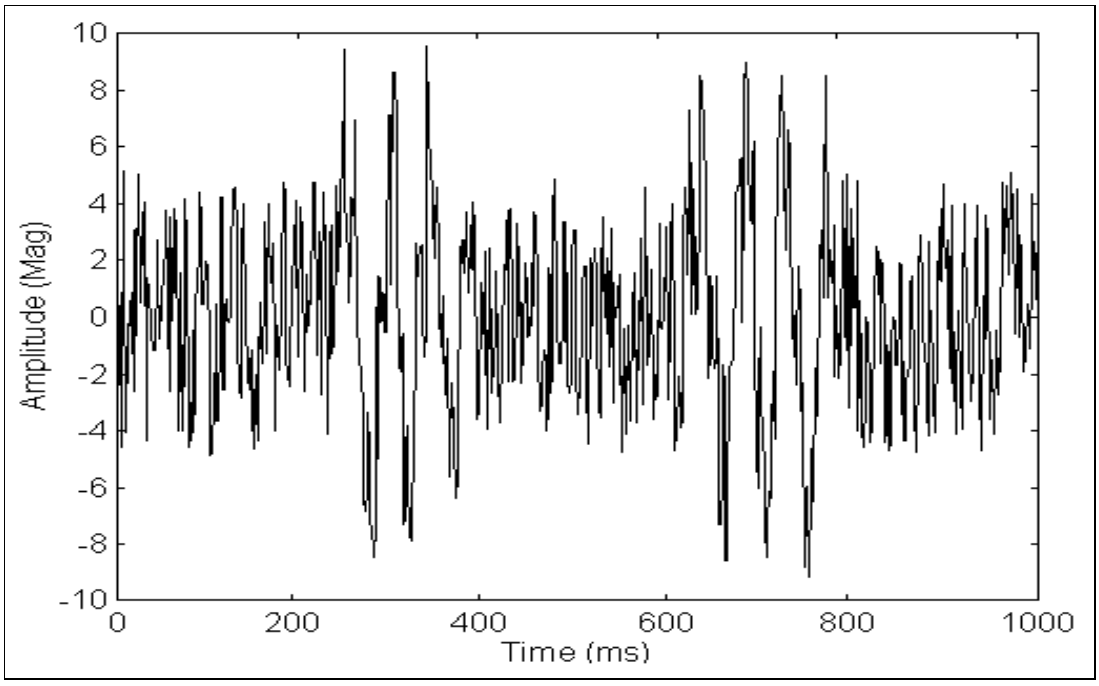

Fig. 3.87 - Signal S12 containing 56/59 and 60 Hz components, high-level white noise and non-stationary modulations

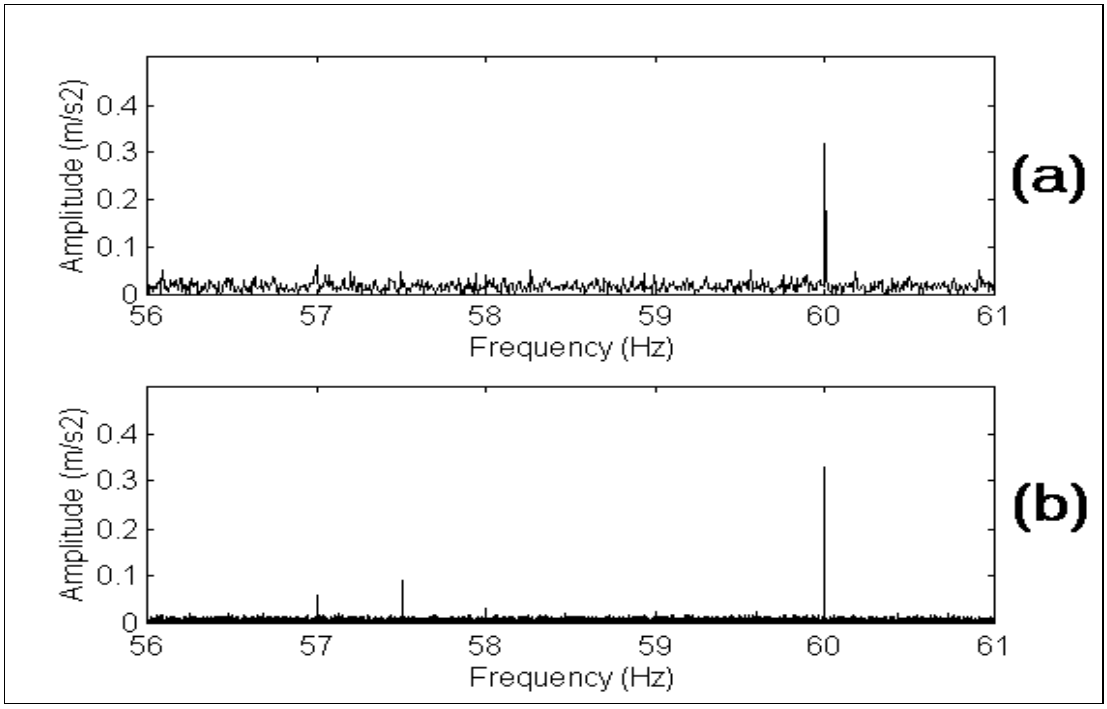

Fig. 3.88 - Fourier transform of signal S12 ((a) 32768 data points, 64 seconds, frequency resolution = 0.016 Hz, no window, (b) 524288 data points, 1024 seconds, frequency resolution = 0.001 Hz, no window)

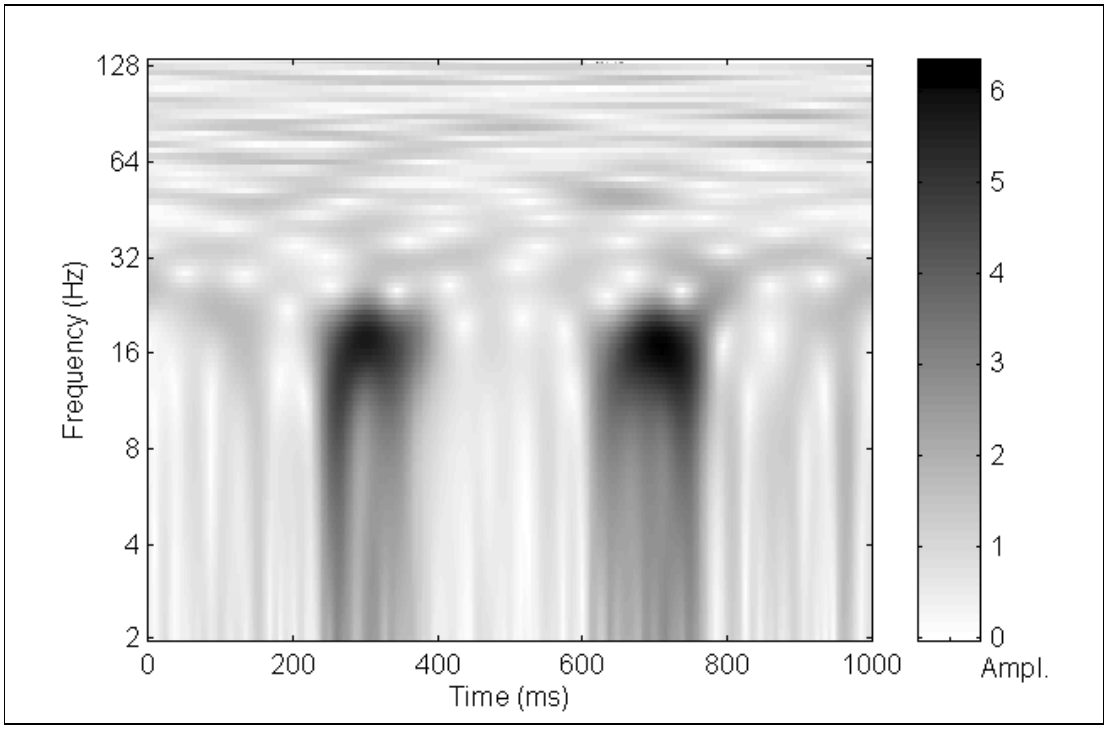

Fig. 3.89 - Morlet wavelet transform of signal S12 (8 octaves & 20 voices per octave)

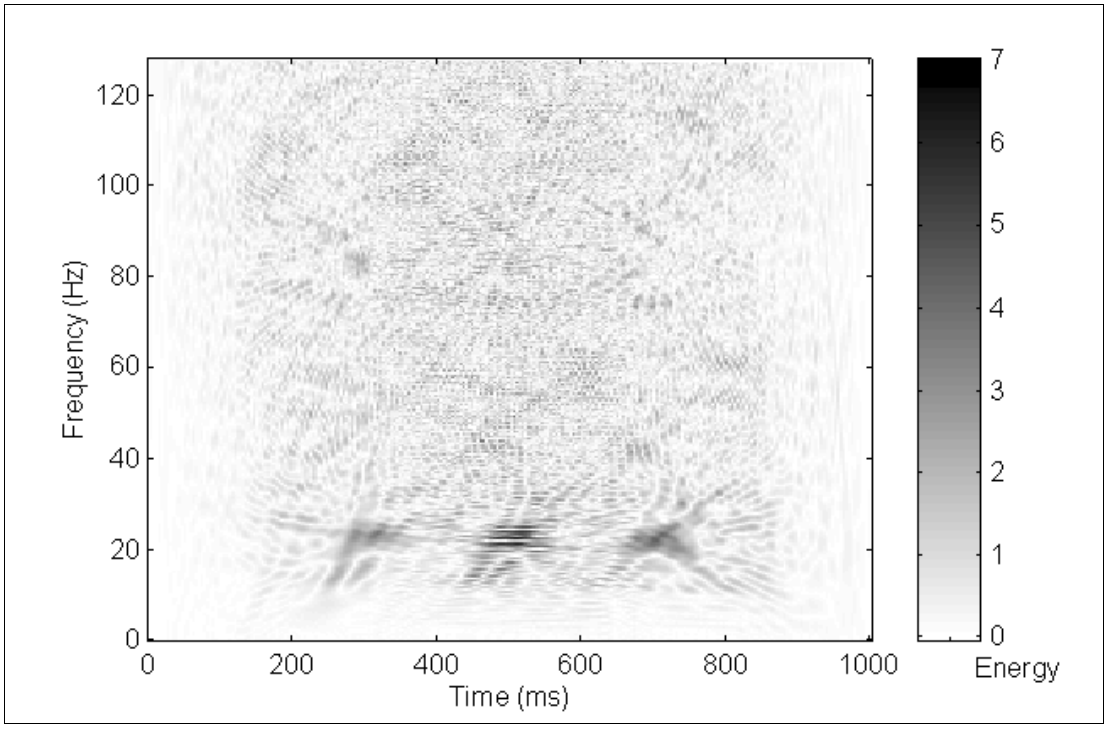

Fig. 3.90 - Wigner-Ville distribution of signal S12 (time-shift = 1 data point)

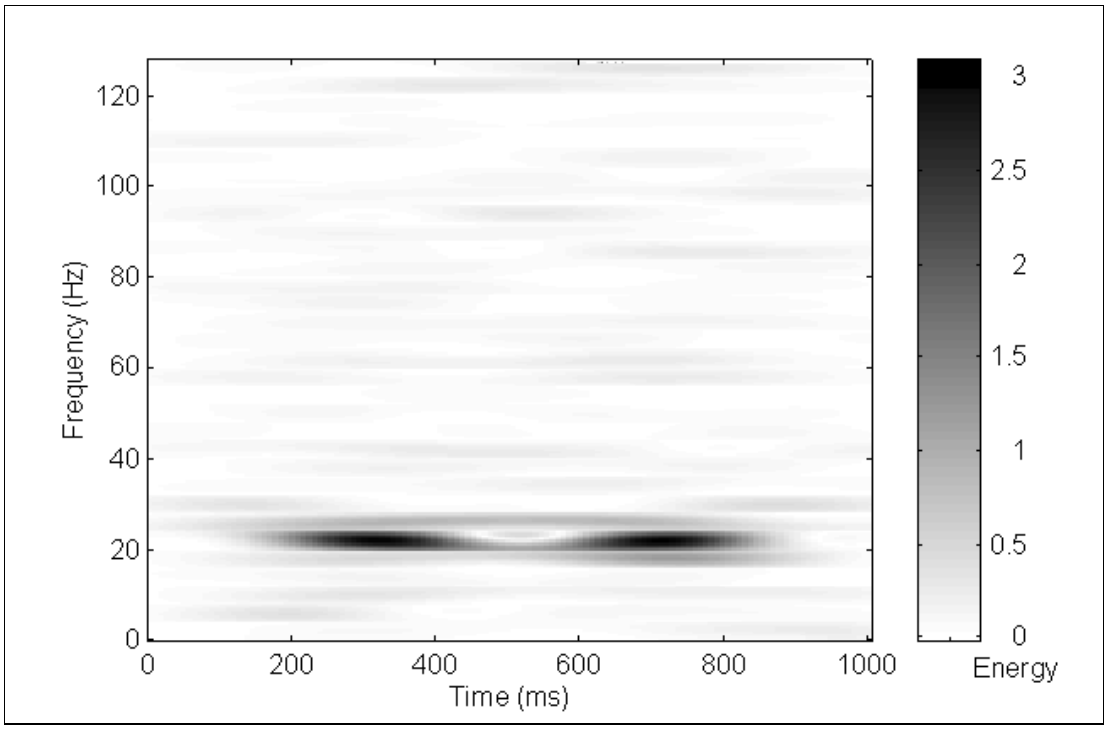

Fig. 3.91 - Pseudo-WV distribution of signal S12 (KB time and frequency window exponential arguments 70 and 2 - time-shift = 1 data point, frequency shift = 8 Hz)

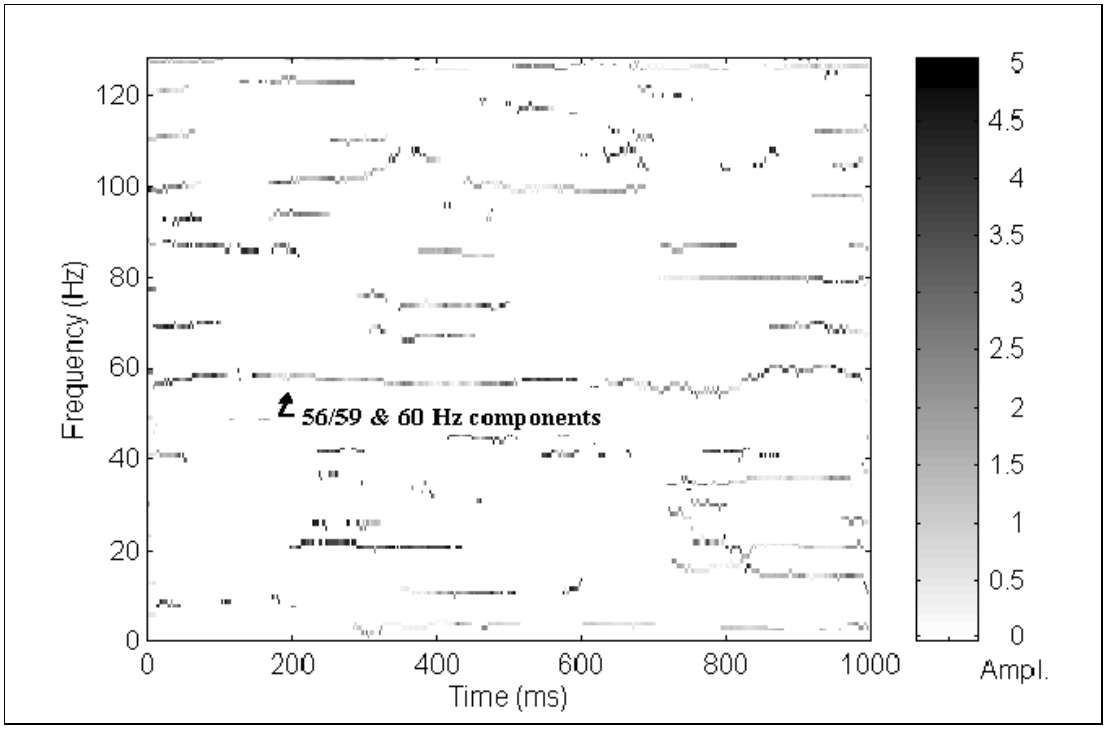

Fig. 3.92 - Extended Prony time-frequency representation of signal S12 (256 data points per sample - total data points used = 767, order 62, maximum exponential damping 0.02 s^{-1})

It may be noted in the graphs of Figures 3.88 to 3.92 that practically the same results were obtained as in the previous test, except for the fact that the Morlet wavelet, the Wigner-Ville and the pseudo-Wigner-Ville distributions show the modulations. When using a very long data array (524288 data points) the Fourier transform gives an indication of the 56/59 Hz and the 60 Hz component, but the true nature of the 56/59 Hz component is not shown in the graph (see Figure 3.88 (b)). In the case of the extended Prony time-frequency representation (see Figure 3.92), is shown only one component in the 55/65 Hz frequency bandwidth. The 60 Hz component is not properly represented in the plane. This corruption may be caused by the strong spurious components (noise and modulations).

A summary of the results obtained from the techniques applied to the signals S8 to S12 is shown in Table 3.16.

Signal feature (multi-component simulation)	Technique FT	MWT	WVD	PWVD	PTFR
56/59 and 60 Hz components (signal S8)	NC	NC	NC	NC	NC >B<
58 and 60 Hz components in the presence of modulations (signal S9)	NC	ND	ND	ND	D >B<
58 and 60 Hz comps. in the presence of white noise+modulations (signal S10)	D	NC	ND	ND	D >B<
56/59 and 60 Hz comps. in the presence of white noise (signal S11)	NC	NC	ND	NC	NC >B<
56/59 and 60 Hz comps. in the presence of white noise+modulations (signal S12)	NC	NC	ND	ND	NC >B<

ABBREVIATIONS

FT - Fourier transform
MWT - Morlet wavelet transform
WVD - Wigner-Ville distribution
PWVD - Pseudo-Wigner-Ville distribution
PTFR - Extended Prony time-frequency rep.

ND - not detected
NC - not clear
D - detected
>B<- best method

Table 3.16 - Method component detection performance

The results of the simulations above have shown that a better systematic detection of the components that have frequencies in the 56 to 60 Hz bandwidth has been obtained using the extended Prony time-frequency representation (see Figures 3.71, 3.79, 3.86, and 3.92). Only in four simulation signals did the extended Prony time-frequency representation not achieve the best result: signal S1 and S3 - where the best result was obtained using the Fourier transform due to its graph and computation simplicity (see Figures 3.10, 3.14 and 3.25); and signals S2 and S7 - where the best results were obtained using the pseudo-Wigner-Ville distribution (see Figures 3.20 for signal S2, and 3.56 for signal S7). The extended Prony time-frequency representation, therefore, may be considered the most appropriate technique for processing the live signal collected in the petroleum wellhead. In the following sections additional simulations will be carried out in order to show, in more detail, certain features and the capacity this method has for detecting variations of weak components present in signals containing strong spurious components within the 56 to 60 Hz frequency bandwidth.

3.6. Signal Processing Techniques: Plane "Band-Selection" Filtering Technique

In section 2.9 of Chapter 2 we saw that an important feature of the extended Prony time-frequency representation is its capacity to perform a convolution filtering directly on the results of the time-frequency plane. Here an attempt is made to demonstrate, this time-frequency plane "band-selection" operation via a signal simulation. As mentioned above, some components of a specific frequency bandwidth may be filtered using the results generated in the time-frequency plane. This corresponds to a convolution performed on the signal and has the advantage of being able to analyse a selected frequency bandwidth directly in the time-frequency plane. To demonstrate this operation, the signal defined in Table 3.17 was generated. Figure 3.93 shows the signal and its Fourier transform. The graph in Figure 3.94 shows the extended Prony time-frequency representation of the raw signal, Figure 3.95 shows the results of this frequency plane "band-selection" operation by zeroing the plane values out of the 55/60 Hz frequency bandwidth, and Figure 3.96 shows the recovered signal and its Fourier transform.

Frequency (Hz)	Amplitude (Mag)	Phase (degrees, t = 0)
50	1.0	40
55	1.0	90
60	1.0	10
65	1.0	130
white noise	0.1	---

Table 3.17 - Signal component composition (see sections 3.2.4 and 3.4 respectively for component and white noise formula definition)

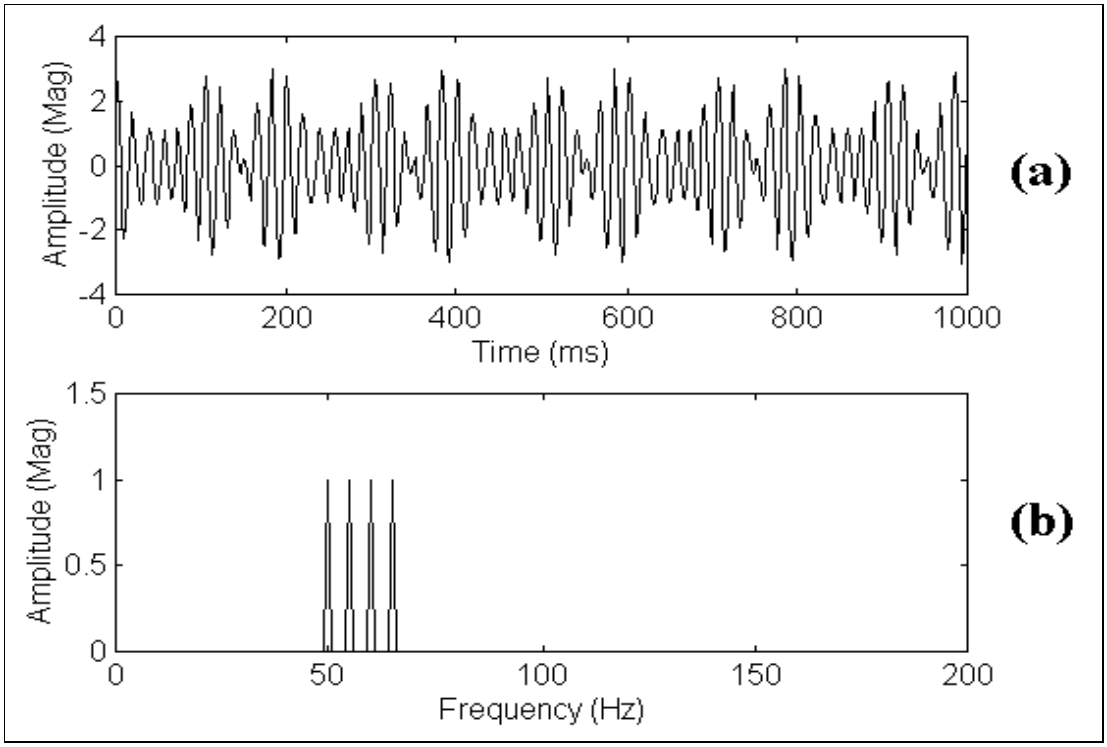

Fig. 3.93 - Signal and its respective Fourier transform (frequency resolution = 1 Hz, no window)

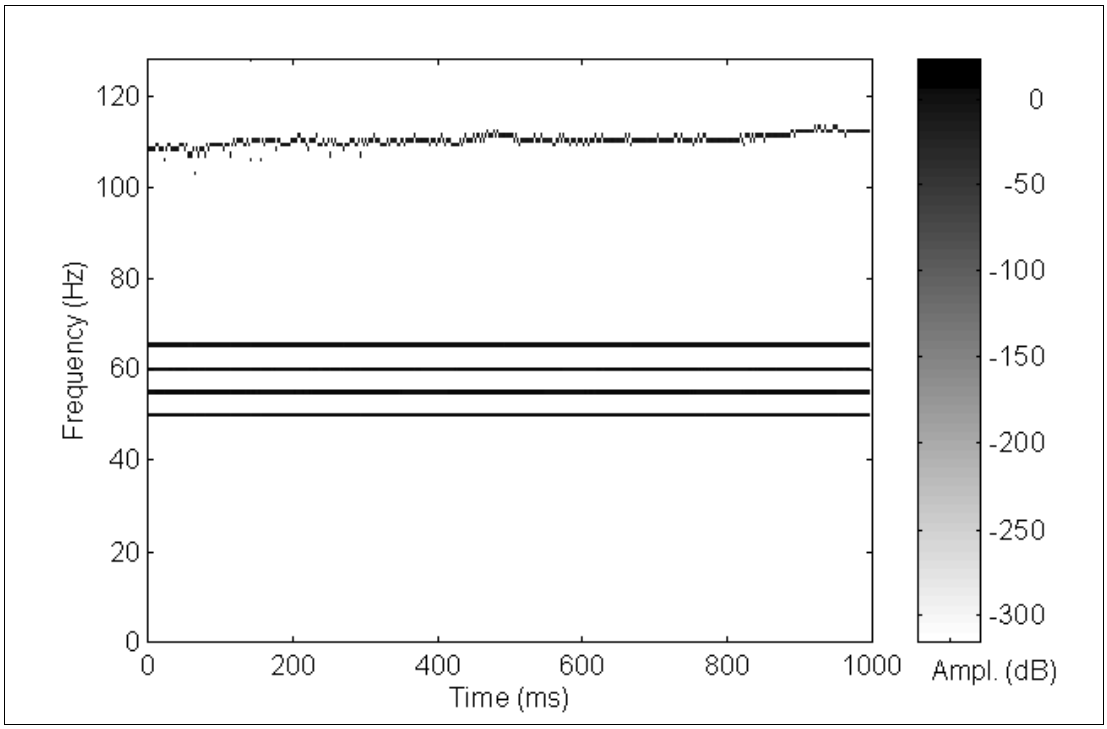

Fig. 3.94 - Extended Prony time-frequency representation (512 data points per sample - total data points used = 1023, order 24, no exponential damping limit)

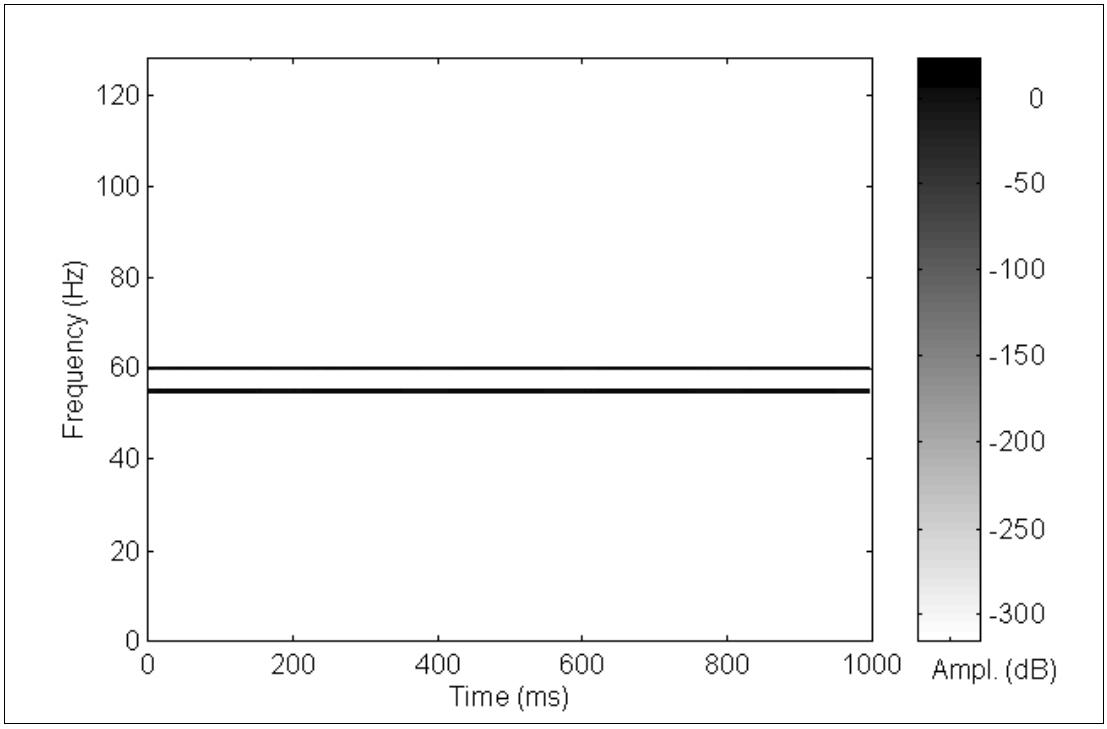

Fig. 3.95 - Extended Prony time-freq. representation, 55/60 Hz "band-selection" in the plane (values outside the 55/60 Hz bandwidth set to zero)

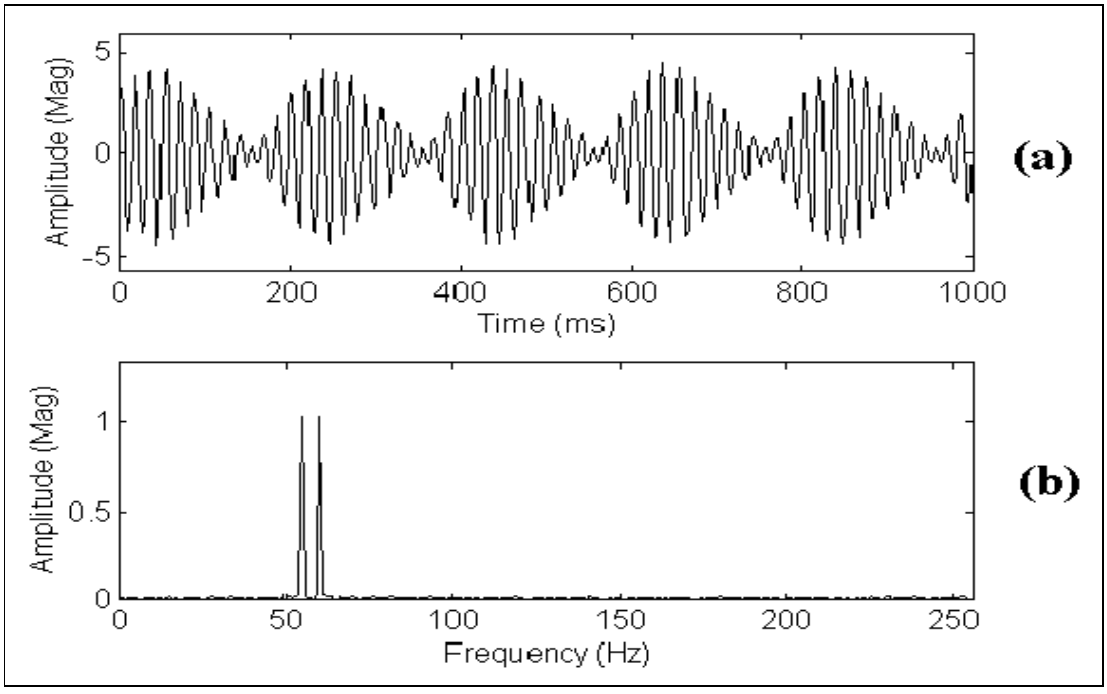

Fig. 3.96 - Filtered signal recovered from the time-frequency plane values and its respective Fourier transform (frequency resolution = 1 Hz, no window)

It can be seen by the simulation above that it is possible to apply a frequency bandwidth selection in the extended Prony time-frequency representation and to recover a filtered signal. However, some low-level corruption may be expected in the component results when this operation is performed. It may be noticed in the graphs of the recovered signal and its respective Fourier transform (see Figure 3.96 (a) and (b)), that some level of noise will result. This noise is not present in the results obtained from the application of the Fourier transform method in the signal with low-level noise (see the graph of Figure 3.93 (b)). As in some time-shifts the order does not correspond to the number of components present in a signal, some spurious components with low amplitude values are generated in the calculation of the extended Prony time-frequency representation, and noise appears when these values are used in the recovering operation. Also, due to non-exact values obtained in the exponential fitting process of the extended Prony time-frequency representation, the amplitude and phase values may present slight differences between the evaluated and real values of a component along the time axis. As a consequence of this non-exact fitting process, different phase values may be obtained in the signal recovery operation, which may be associated with the difference that exists between the shape of the graph of the recovered signal (Figure 3.96 (a)) and the shape of the graph of the signal resulting from the convolution with the bandwidth frequency flat window (Figure 3.97 (a)). If a frequency "band-selection" is performed in the signal using the convolution with a bandwidth frequency flat window, a more efficient frequency "band-selection" operation is obtained (see the Figure 2.12 of item 2.9 of Chapter 2). The plot of Figure 3.97 (b) shows the results of the frequency "band-selection" operation performed on the signal described in Table 3.17 using a convolution with a 57/62 Hz bandwidth frequency flat window filter.

If a signal is previously convolved with a bandwidth frequency flat window it will present less noise than the signal bandwidth filtered and recovered from the Prony time-frequency representation, and the necessary order for the characteristic polynomial to be evaluated in each sample of the extended Prony time-frequency representation is reduced. A consequence of this polynomial order reduction is that

less processing computational effort will be required. The efficiency of the frequency "band-selection" operation using the convolution is also apparent when the signal S10, analysed in the section 3.5.3 and described by Table 3.13, is previously convolved with a 57/62 Hz bandwidth frequency flat window, and analysed through the extended Prony time-frequency representation. Due to the elimination of most of the spurious components present in the signal, the weak 58 and 60 Hz signal components are more easily detected and, as consequence, they are more clearly depicted (see Figure 3.98).

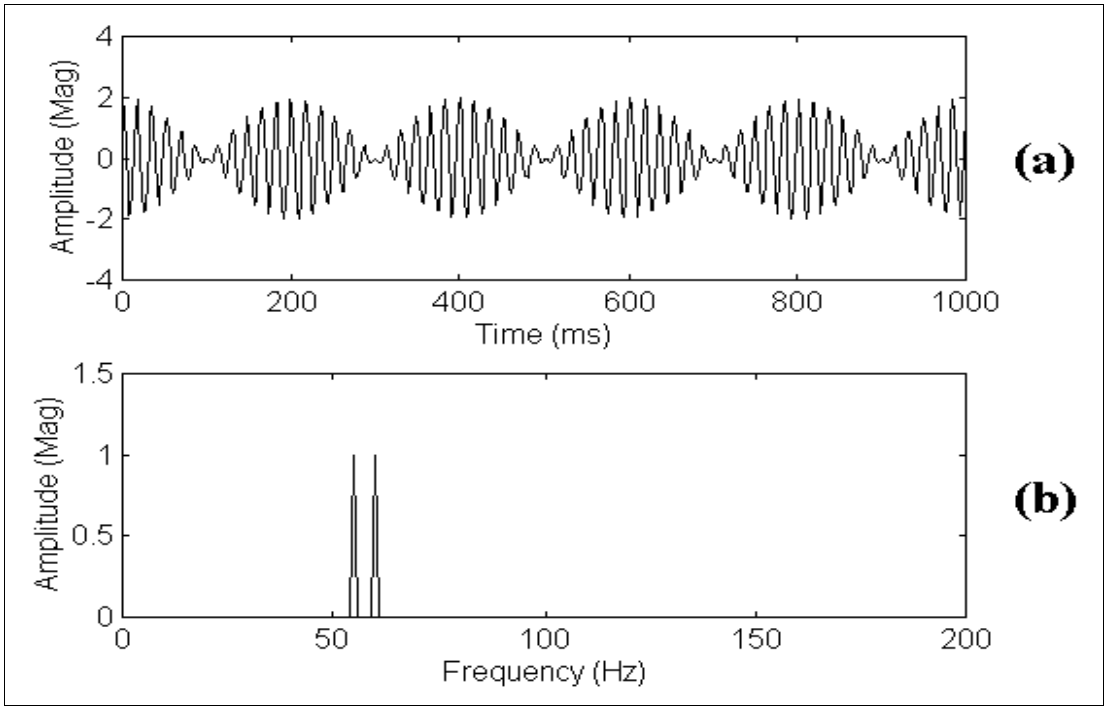

Fig. 3.97 - Signal recovered from the convolution filtering and its respective Fourier transform (frequency resolution = 1 Hz, no window)

Although an improvement is obtained when the convolution with a frequency-bandwidth window is applied, the frequency bandwidth limiting to be used in this study will be the "band-selection" performed in the plane of the extended Prony time-frequency representation. This is because this technique represents an additional feature of the extended Prony time-frequency representation, and it needs to be tested more rigorously in order to determine if it can generate acceptable results (see next section).

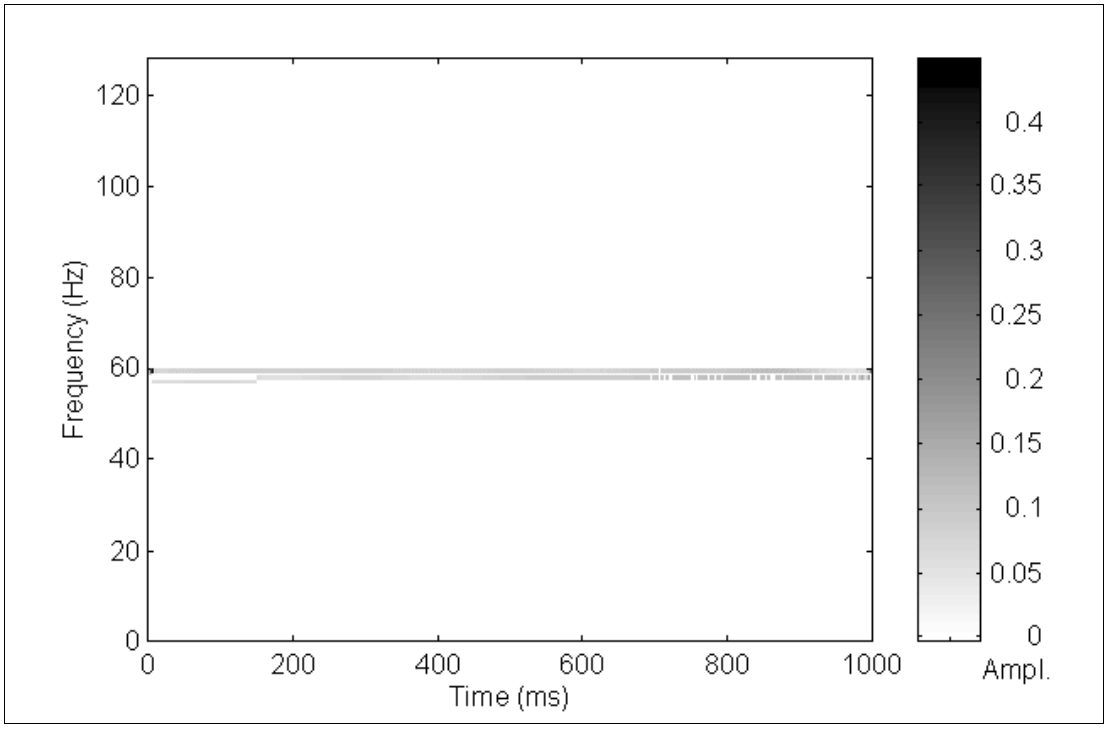

Fig. 3.98 - Extended Prony time-frequency plane of the signal S9 defined above convolved with a bandwidth frequency flat window between 57 to 62 Hz (512 data points per sample - total data points used = 1023, order 8, maximum exponential damping filtering set to 0.02 s^{-1})

3.7.Extended Prony Time-Frequency Representation: Filtering Systematic Simulations (Signals S13 to S22)

From this point systematic filtering of simulated signals will be performed using the extended Prony time-frequency representation. The aim here is: (a) to test the capacity of filtering out spurious components more extensively; and, (b) to determine if the weak component amplitude variations can be detected by applying the Fourier transform to filtered and recovered signal samples. Ten signals with weak components at different amplitude levels, embedded in strong spurious components, will be generated (signals S13 to S22). A difference of two times in the magnitude of amplitude level of the sought component will be set for each signal pair. An analysis will be made of the 20 tests for each signal generated. In each step the amplitude of the sought component will be compared in the two pairs of signals. The composition of the first two signals (S13 and S14) were previously known to this author, and are

described in Table 3.18. However, the composition of the other eight signals, from S15 to S22, were unknown prior to their analysis in order to avoid a "predisposition" to seek a specific component in the signals. The main aim is to detect the amplitude level of the weak component in filtered and recovered signals using the extended Prony time-frequency representation. A frequency bandwidth containing the weak component to be detected (58 Hz) will be selected in the resulting time-frequency plane ("band-selection") and a filtering operation will be performed using the exponential damping associated with each component sought by the extended Prony time-frequency representation. The Fourier transform will be applied to signal samples filtered and recovered from the extended Prony time-frequency representation (see section 2.9 of Chapter 2).

	Deterministic Component Data						6-24 Hz Modulations Amplitude	White Noise Amplitude
	Component 1			Component 2				
	Freq (Hz)	Amp (Mag)	Pha (t=0)	Freq (Hz)	Amp (Mag)	Pha (t=0)		
Signal S13	58	0.1	0 ^{o}	60	0.3	90 ^{o}	5.0	5.0
Signal S14	58	0.2	0 ^{o}	60	0.3	90 ^{o}	5.0	5.0

Table 3.18 - Signals S13 and S14 (see sections 3.2.4 for deterministic and modulation component, 3.3.3 for white noise definitions, and Appendix C for SNR level assumption)

The results of the systematic simulation applied to the signals S13 and S14 are shown in the graphs of Figures 3.99 and 3.100. Samples of both signal S13 and S14 were filtered by using the extended Prony time-frequency representation. This operation was performed by projecting the component amplitudes with the associated phase values, in a frequency bandwidth between 55 and 65 Hz (see section 2.9 of Chapter 2 for more detailed explanation of this operation).

For this systematic simulation, 20 samples of signal S13 and 20 samples of signal S14 were filtered by using the extended Prony time-frequency representation (512 data points per time-shift - total data points of each sample = 1023, order 64, maximum exponential damping 0.02 s^{-1}). Figure 3.99 shows waterfall plots of 20 Fourier

transforms (frequency resolution = 1 Hz) applied to that filtered and recovered data arrays (signal S13 Figure 3.99 (a) and signal S14 Figure 3.99 (b)).

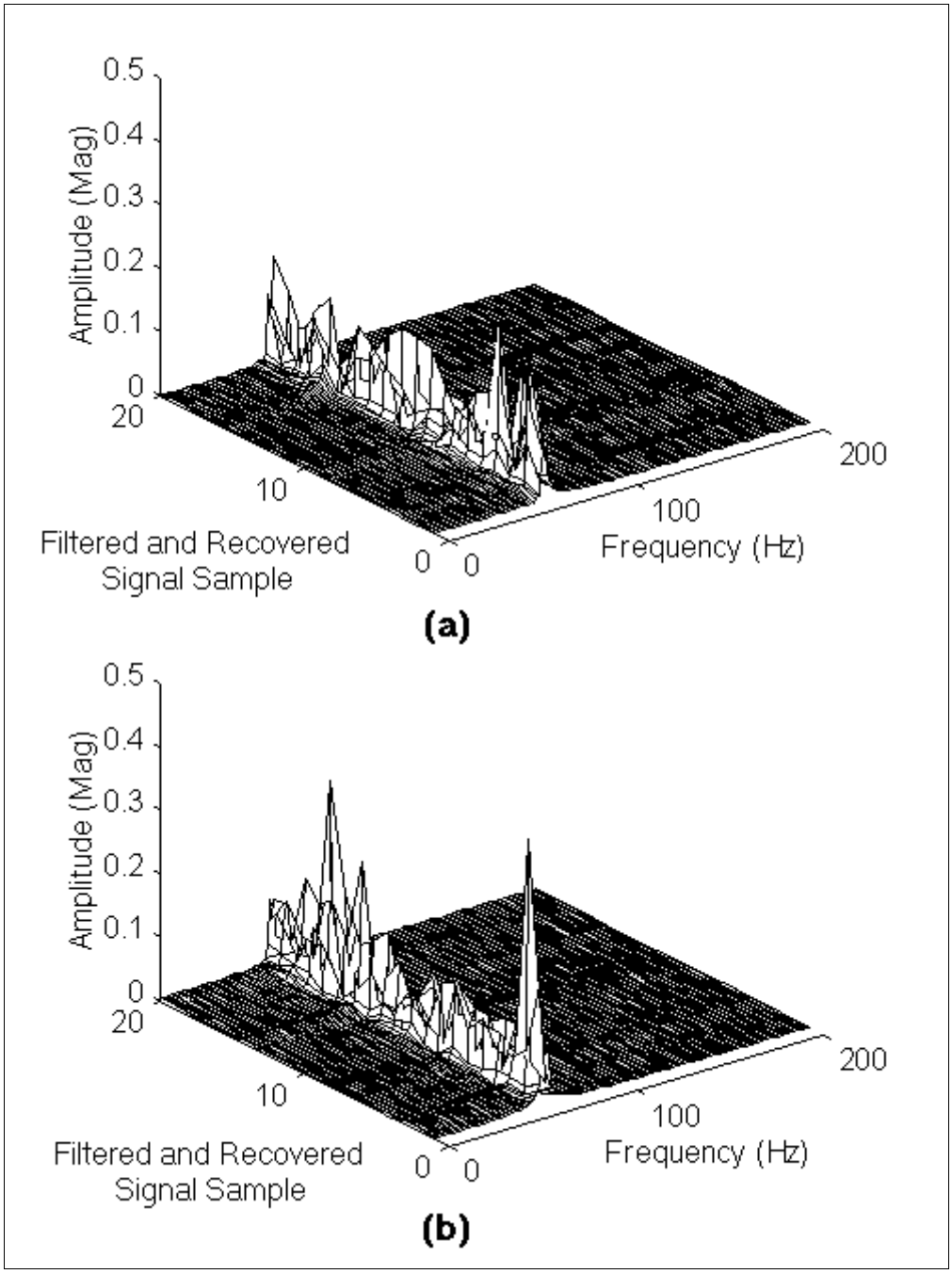

Fig. 3.99 - Waterfall graph of Fourier transforms of signal data arrays filtered and recovered by using the extended Prony time-frequency representation ((a) 20 samples of signal S13 and (b) 20 samples of signal S14, sampling frequency 512 Hz, frequency resolution = 1 Hz)

As shown in the waterfall graphs of Figure 3.99, it is not possible to observe the amplitude variation of the 58 Hz component in every array of filtered and recovered signal data using the extended Prony time-frequency representation. Only in 68 % of the Fourier transforms of the filtered samples show the correct amplitude relationship, i. e., amplitude values of the 58 Hz component of signal S14 greater than the amplitude values of the 58 Hz component of signal S13. For the purpose of comparing both S13 and S14 signals an average of several spectra is still necessary. Figure 3.100 shows the results of averaging the spectra of each signal group of Fourier transforms shown in the waterfall graph of Figure 3.99.

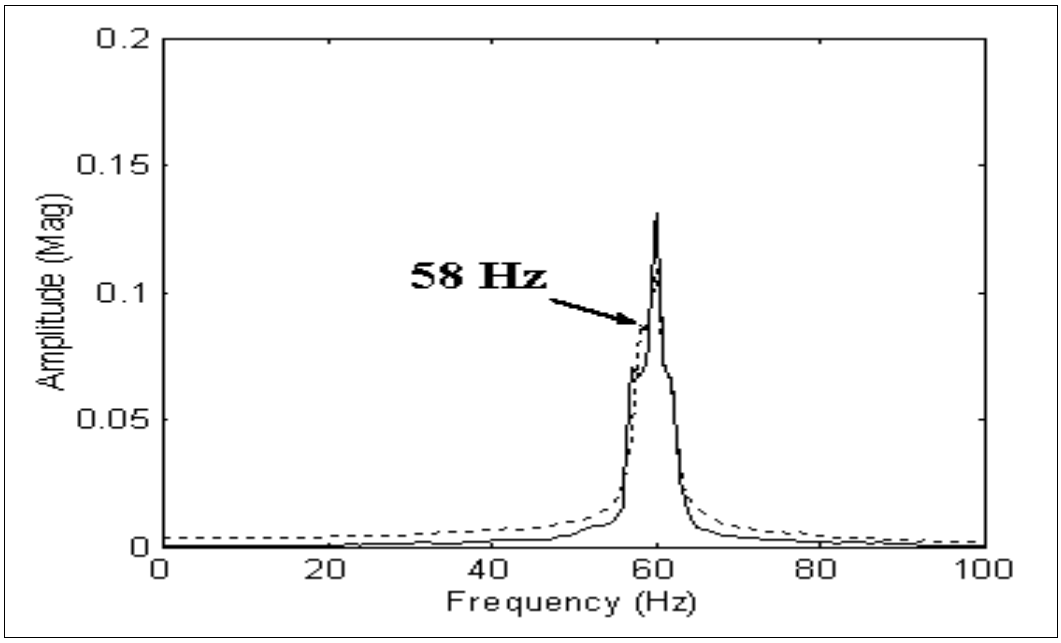

Fig. 3.100 - Spectra average of the filtered signals S13 and S14
(solid line - signal S13, dashed line- signal S14)

In the results of an average of the 20 Fourier transforms performed in filtered data arrays with 512 samples of both recovered signals (see Figure 3.100) there is an amplitude difference corresponding to the greater amplitude of the 58 Hz in signal S14. This is what will be used for detecting equipment failure. Normally, when an ESP pump is going to fail, an increase in the amplitude peak on the rotation frequency is expected.

If one set of filtered signal data is compared with another after applying the extended Prony time-frequency representation and the time-frequency plane "band-selection", it will still be difficult to detect any variation in a signal with strong spurious components (see Figure 3.99). This leads to the assumption that an average of the resulting transformed of each set of filtered signal data are still necessary if a more reliable detection is required.

In a second stage designed to test the capacity of the extended Prony time-frequency representation for detecting the weak components in the signal, eight additional 1024 data-sample computer simulated signals were prepared containing weak components with different frequencies. First, six signals (S15 to S20) were generated with different frequency gaps between each deterministic component inside the 55-65 Hz frequency bandwidth. Then, two more signals (S21 and S22) were generated to detect weak component variations in the 0-200 Hz frequency bandwidth. The sampling frequency of the simulated signals was set to 512 Hz. As stated above, the composition of signals S15 to S22 was unknown to the author at the time of the analysis in order to avoid a "predisposition" to seek specific components in the signals. These signals were generated by another researcher at Imperial College through a computer program. In the generation of the signals S15 to S22, the same component amplitude relationships of the signals S13 and S14 was maintained, i. e., amplitude of the spurious components 50 times greater than the weakest component in one signal and 25 greater in another signal. A 55/65 Hz frequency bandwidth was limited for placing the weak components in the signals S15 to S20 and a 0/200 Hz bandwidth was limited for placing the weak component in he signals S21 and S22. No previous information was given about which component had its amplitude varied or in which signal it was increased.

Figures 3.101 through 3.104 show the average of the 20 Fourier transforms of data arrays taken from each signal S15 to S22 and filtered by using the extended Prony time-frequency representation. This methodology is the same that was applied to the signals S13 and S14 to generate the graph of Figure 3.100. A 55/65 Hz frequency

bandwidth of time-frequency plane "band-selection" was applied to signals S15 to S22. The graphs in Figures 3.101 through 3.104 show the results of an average of 20 Fourier transforms performed in filtered data arrays with 512 samples of signals S15 to S22.

The graphs of Figures 3.101 and 3.103 show that the amplitude level of the 63 Hz component was increased, and the graph of Figure 3.102 shows that the amplitude level of the 57 Hz component was increased.

As no frequency bandwidth window filtering was applied before recovering the filtered signals S21 and S22, numerous peaks appeared in the spectrum, as can be seen in the graph in Figure 3.104. It is difficult to determine which amplitude variation corresponds to the sought weak component in the 0/200 Hz frequency bandwidth.

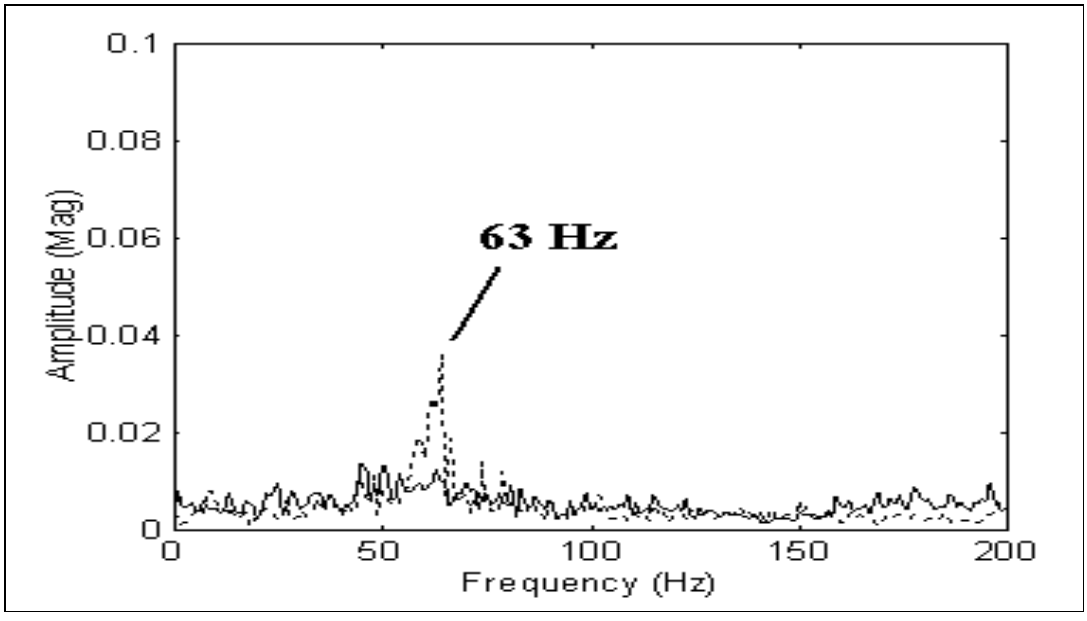

Fig. 3.101 - Spectra average of the filtered signals S15 and S16
(solid line - signal S16, dashed line - signal S15)

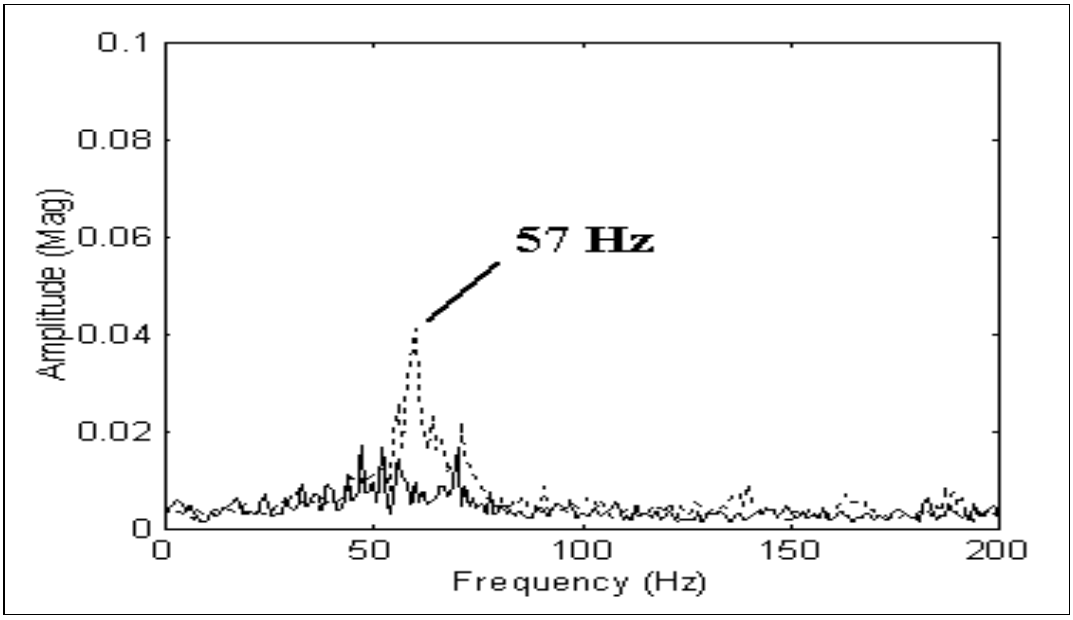

Fig. 3.102 - Spectra average of the filtered signals S17 and S18
(solid line - signal S17, dashed line - signal S18)

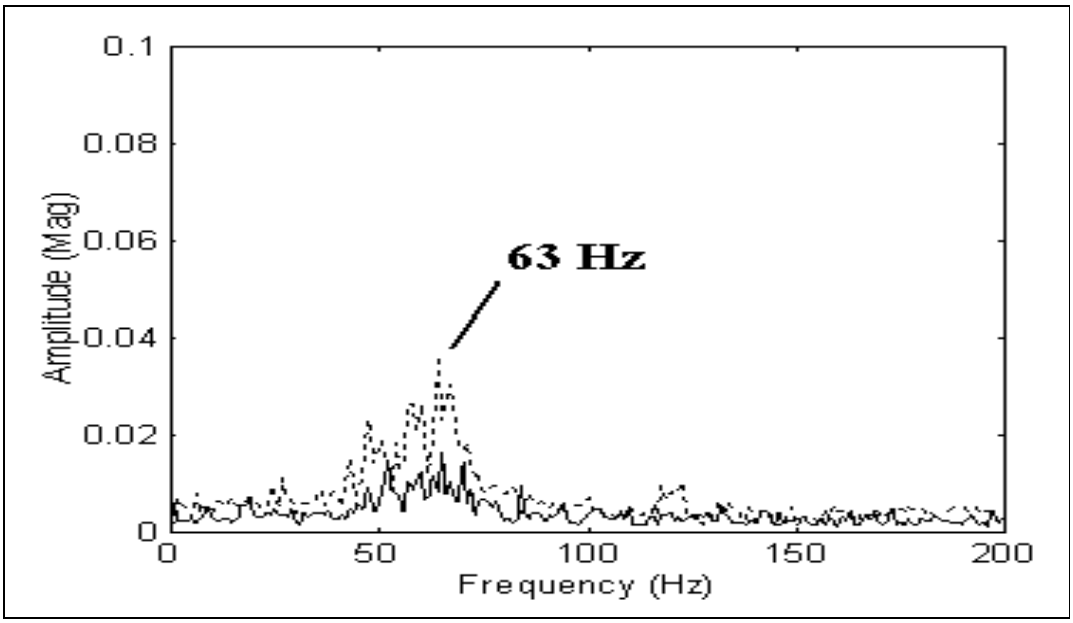

Fig. 3.103 - Spectra average of the filtered signals S19 and S20
(dashed line - signal S19, solid line - signal S20)

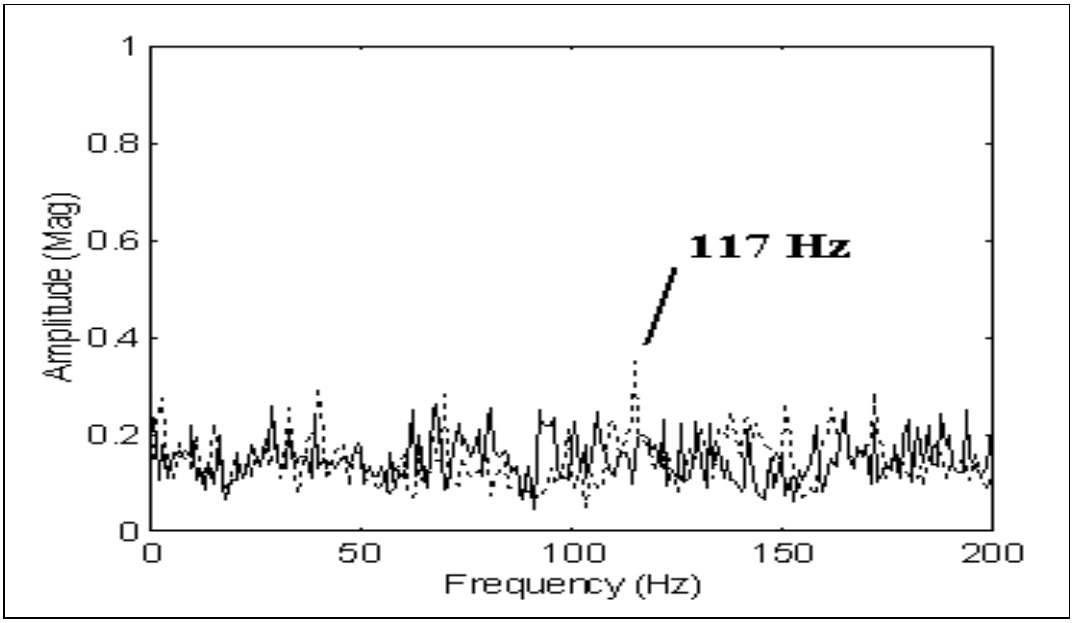

Fig. 3.104 - Spectra average of the filtered signals S21 and S22
(solid line - signal S21, dashed line - signal S22)

The unknown signals were generated in accordance with the data depicted in Table 3.19.

	Deterministic Component Data						6-24 Hz Modulations Amplitude	White Noise Amplitude
	Component 1			Component 2				
	Freq (Hz)	Amp (Mag)	Pha (t=0)	Freq (Hz)	Amp (Mag)	Pha (t=0)		
Signal S15	61	0.3	70 ^{o}	63	0.2	20 ^{o}	5.0	5.0
Signal S16	61	0.3	70 ^{o}	63	0.1	20 ^{o}	5.0	5.0
Signal S17	57	0.1	40 ^{o}	63	0.3	90 ^{o}	5.0	5.0
Signal S18	57	0.2	40 ^{o}	63	0.3	90 ^{o}	5.0	5.0
Signal S19	59	0.3	10 ^{o}	63	0.2	80 ^{o}	5.0	5.0
Signal S20	59	0.3	10 ^{o}	63	0.1	80 ^{o}	5.0	5.0
Signal S21	117	0.15	15 ^{o}	---	---	---	7.3	7.3
Signal S22	117	0.3	15 ^{o}	---	---	---	7.3	7.3

Table 3.19 - Additional signals for simulation (see sections 3.2.4 for deterministic and modulation component, 3.3.3 for white noise definitions, and Appendix C for SNR level assumption)

Comparing the components amplitudes depicted in the graphs of Figures 3.101 to 3.103 with the true component amplitudes depicted in Table 3.19, it may be noted

that the amplitude values are significantly reduced. This may be due to the spurious component filtering process, which incorrectly eliminates some component points.

It can be seen in Figure 3.104 that it is still difficult to determine which amplitude variation corresponds to the sought weak component in a 200 Hz frequency bandwidth. This leads to the assumption that it is still necessary to set a narrow frequency bandwidth to detect variation in a specific weak component.

3.8. Signal Simulation Conclusions

In this Chapter, our objective has been to test five signal processing techniques using numerically-simulated signals in order to determine which technique is the most appropriate to detect weak components in signals with strong spurious components. Of these techniques, particular attention has been given to the extended Prony time-frequency representation, and to how this technique compares with the others.

To conclude this chapter, the main findings of the simulations can be summarised as follows:

a) The extended Prony time-frequency representation developed in this study has been shown to be generally the most effective of the 5 techniques studied in detecting weak deterministic components in signals containing strong spurious components, when using few data points (maximum 1023 data points - 512 data points per sample - sampling frequency of 512 Hz - see Figures 3.26, 3.79, 3.86, and 3.92);

b) The extended Prony time-frequency representation can also handle non-stationary components reasonably well. This may be seen in Figures 3.33, 3.40, 3.47, and 3.54 and 3.18, where the non-stationary processes are represented in the graphs with the correct frequency composition;

c) When an analysis of certain specific non-stationary components, such as the ones that need a large amount of data points to be represented in a small area of the time-frequency plane, the pseudo-Wigner-Ville distribution and the Morlet wavelet transform may be better choices than the extended Prony time-frequency representation. See, for example, the case of the time-frequency representation of the Gaussian waves in the section 3.4.4 (see Figure 3.53);

d) When using the extended Prony time-frequency representation, a narrow frequency bandwidth time-frequency plane "band-selection" is necessary for component level comparison (see Figure 3.104); and

e) It is necessary to average the Fourier transforms of the signals, which have been filtered and recovered from the extended Prony time-frequency representation, in order to depict better weak component peak variations.

Based on the above findings, the extended Prony time-frequency representation was considered to be a good option for filtering technique to be developed for the objective of monitoring variations in the amplitude of weak components, within a 10 Hz frequency bandwidth, in signals containing high levels of noise and with non-stationary components. As a consequence, the extended technique was tested with signals generated in the experimental apparatus described in the following Chapter 4.

Chapter 4
Experimental Analysis

4.1. Introduction

In this Chapter, an experimental apparatus is described which was designed and constructed to generate data with which to test the filtering capacity of the extended Prony time-frequency representation formulated in Chapter 2. The purpose of the experimental apparatus was to generate vibration data which is representative of that produced by ESP equipment operating in a real petroleum well. Therefore, the experimental apparatus was designed to replicate an ESP installation as closely as possible, although using a very small-scale model.

As was mentioned above, the first major systematic vibration analysis of ESP equipment operating under controlled conditions was performed by Moore [1990] (see section 1.4 of Chapter 1). In that research, accelerometers were placed on the pump and at the wellhead 38 meters above. Several types of wear, such as to the bearings and the pump's coupling, were simulated and the collected data processed through the Fourier transform. Moore states that before the ESP failed, data gathered from the transducer attached to the pump revealed an increase of between 30 and 60 times in the amplitude of the rotational vibration. However, Moore also reports

a delay of two weeks in detecting when the ESP failed - that is, the time lag between identifying the failure using the data gathered by an accelerometer installed in the pump and the failure identified by the data gathered from the accelerometer installed in the wellhead 38 meters above the equipment. One possible explanation for this delay in identifying the problem could be the use of inadequate filtering techniques associated with the Fourier transform. Since in this study the extended Prony time-frequency representation, based on the original Prony method, has been developed to improve the signal filtering operation, the task in this section is to test and to validate this new extended representation with experimental signals focusing on the relevant ESP vibration signal components, generated experimentally at a distance between the vibration source and accelerometer close to the distance used in the Moore experiment (38 metres).

As stated above, a complete ESP assembly is generally 15 to 20 metres (50 to 65 ft) long and needs to be erected vertically. This equipment is fixed in a pipe composed of several sections and installed in wells which are normally more than 1 km deep. In this study, the large size of the ESP installation is reduced to a scale model in an experimental apparatus where it is possible to generate data resembling that collected under real conditions. Figure 4.1 depicts a comparison between a schematic diagram of the intended experimental apparatus and the real ESP installation.

As shown in Figure 4.1, the vibration data is generated by a lower shaker, which is then corrupted by strong spurious components generated by an upper shaker and fluid-induced vibrations, the resulting data is then collected through a remote accelerometer close to the upper shaker. The scale model used approximately a 40 m length of wire to represent a petroleum pipe of 1000 m long, installed in the Queen’s Tower of Imperial College.

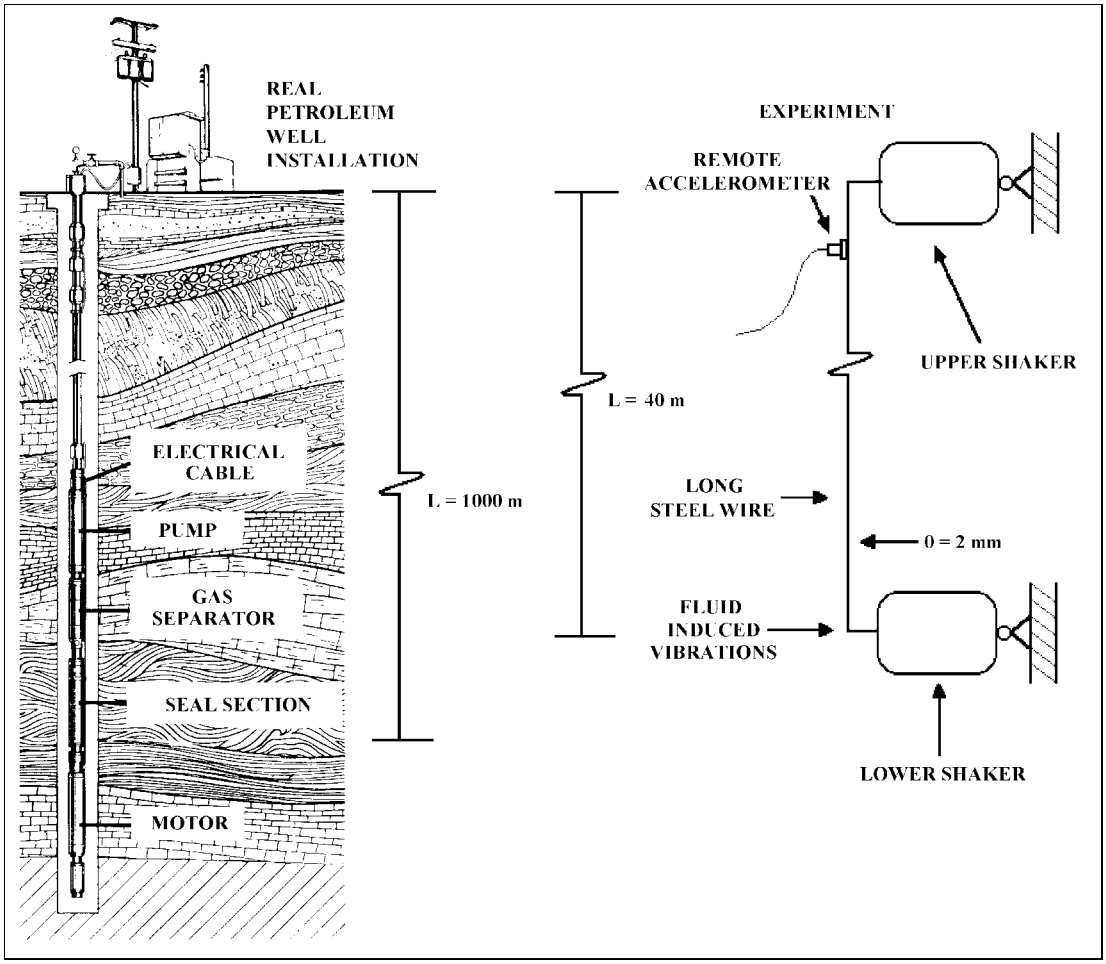

Fig. 4.1 - Comparison between a schematic diagram of the intended experimental apparatus and the real ESP installation

It should be noted that because of the location of the experimental apparatus, a three-week time constraint was placed on the period allowed to undertake the experiment, and this restricted the quantity of data which could be collected. However, sufficient experimental data was gathered to fulfil the statistical requirements of the programme, with the minimum of 200 signal samples for each signal comparison (100 sets per 58 Hz component amplitude condition) for each of the three noise conditions. The experimental results described above represent a total of 600 signal samples. A further problem was that, due to the precarious nature of the experimental environment, an assistant had to be in attendance in the Tower at all times in case of an accident.

4.2. Design and Construction of the Experimental Apparatus

The experimental apparatus was designed to represent the conditions of ESP installations such as those normally found in petroleum wells. The pumps in such ESP installations generate two main vibration components, one at 58 Hz, corresponding to the rotation frequency of the pump and containing information about the state of the pump, and the other at 60 Hz, which corresponds to the electrical power supply. The 60 Hz signal is generated by oscillating magnetic fields in wires, transformers etc that exist in the ESP installations. Analysis of these vibrations has shown that the 60 Hz frequency component is very strong compared with the pump rotation vibration signal at 58 Hz which is transmitted and attenuated through a long tubing that supports the ESP assembly located downhole in the well. Also present in the signal are vibrations caused by non-stationary fluid slugs (gas-liquid fractions pumped through the pipe) and high levels of noise (general platform equipment vibration, sea noise, structural resonances etc.), which corrupt the pump vibration signal.

To represent the above conditions, a model with a 25 to 1 scale of a real ESP installation was constructed. Figure 4.2 shows a schematic diagram of the installation inside the Tower and Figures 4.3 to 4.6 show the configuration of each support. The design of the apparatus involved two wire supports: a lower one (Figures 4.5 and 4.6), which represents the ESP itself and an upper one (Figures 4.3 and 4.4), which represents the wellhead. On each support a shaker was mounted to generate the vibrations at 58 Hz (lower support) and 60 Hz (upper support). Accompanying each shaker was an accelerometer which was fixed to the support plate to measure the vibrations generated, together with a force gauge to verify the data. The force gauge measured the force on a 0.360 kg rigid mass, which included the accelerometer mass, and the deduced acceleration values could then be compared with the acceleration values collected by the accelerometer. A support plate held in alignment the

accelerometer (Figure 4.5), the force gauge and the shaker, as well as transmitting the generated one-dimensional transverse vibration waves to the wire. The combined weight of the lower support, with the force gauge, the mass to activate the force gauge and the dead weight, was 55 N. Technical drawings of the experimental supports are included in Appendix B.

To represent a 1000 m pipe leading from the ESP to the wellhead, commonly found in full-scale offshore exploration installation, a 2 mm diameter, 39.15 m long stainless steel wire, with a self-weight of 10 N, was fixed to each support of the experimental test rig. The wire was tensioned by the weight of the lower support (55 N).

The experimental facility also included a fluid-slug simulation rig, built to generate non-stationary vibration (fluid turbulence) signals in order to corrupt the signal generated by the lower shaker (see Figures 4.7 and 4.8). The aim here was to test the capacity of the extended Prony time-frequency representation to detect small deterministic components which are contained in signals corrupted by these non-stationary vibrations. A centrifugal pump was incorporated in the slug simulation rig to generate air slugs through a hose. One section of this hose was fixed to the lower support of the experimental apparatus. The vibration generated by the fluid slug was transmitted to the plate which supported the wire (see Figures 4.5 and 4.6).

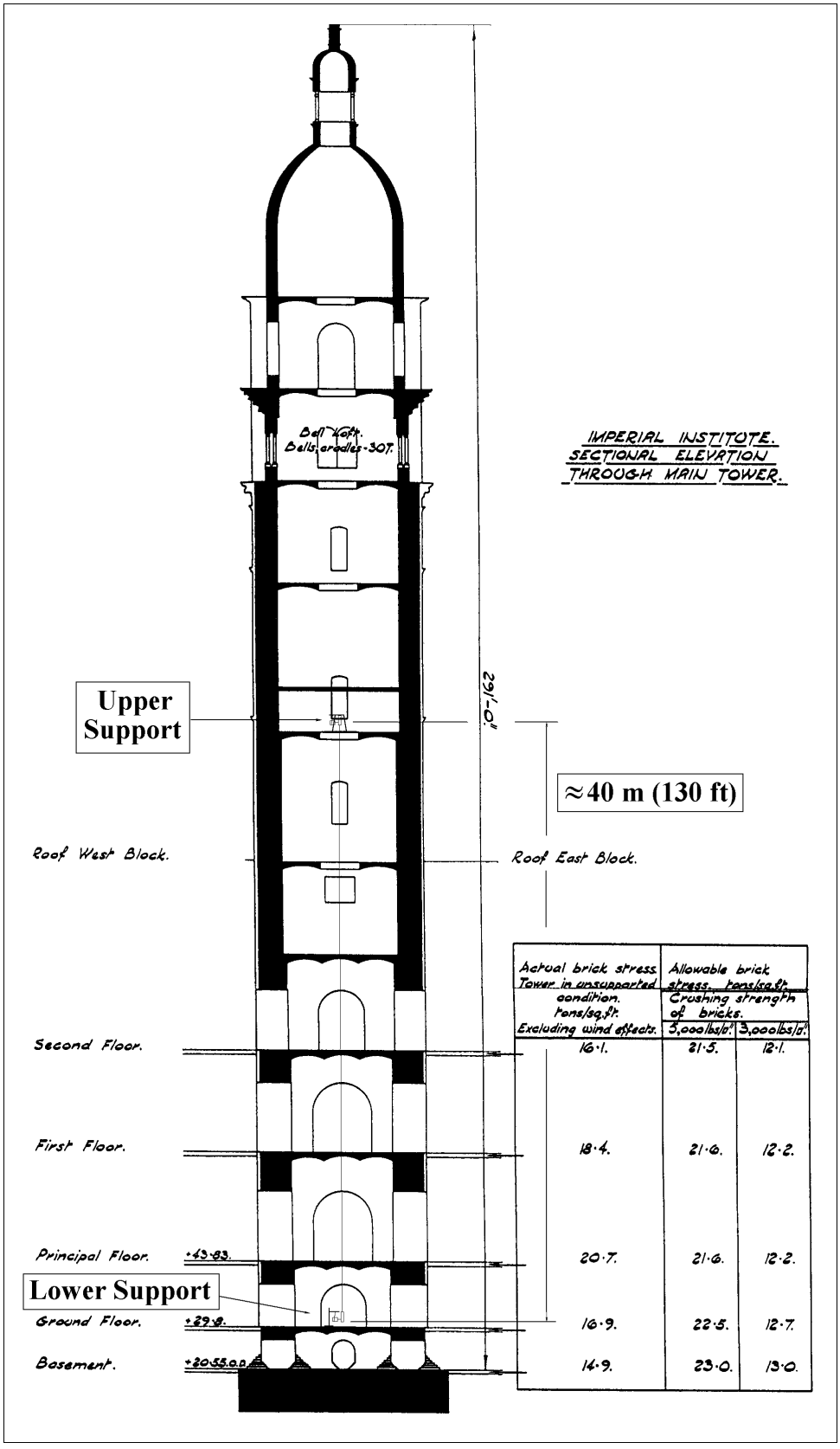

Fig. 4.2 - Experimental facility installation in the Queen's tower

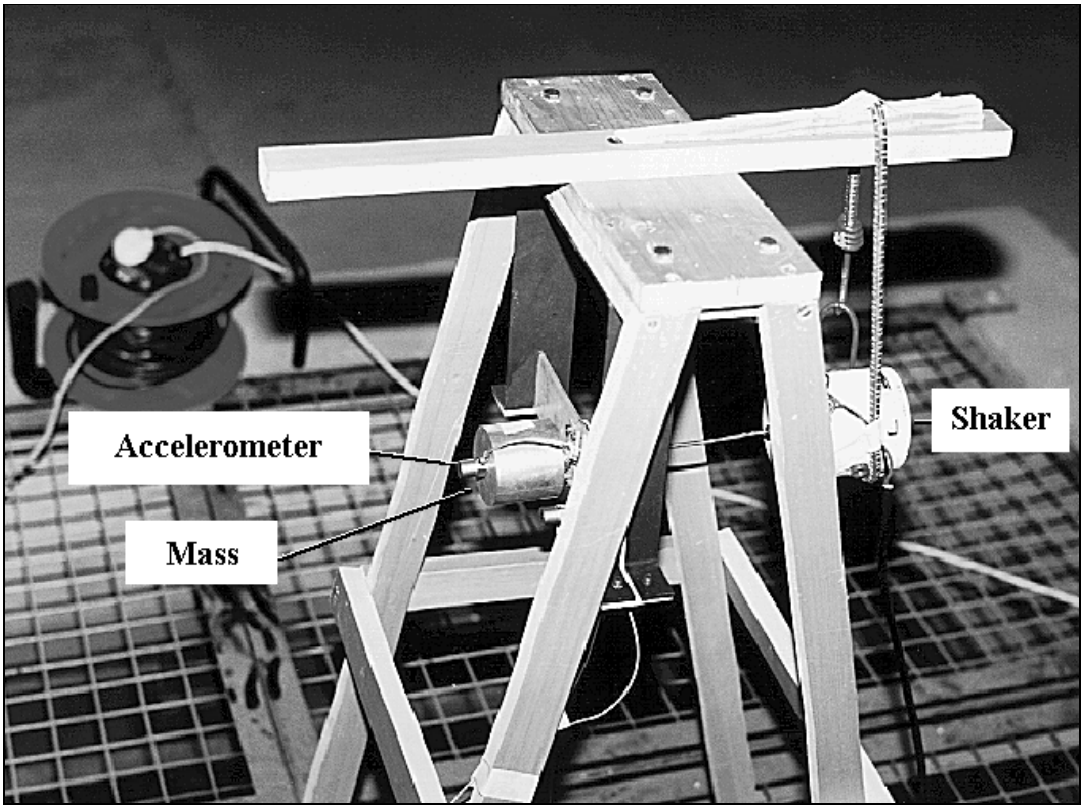

Fig. 4.3 - Upper support

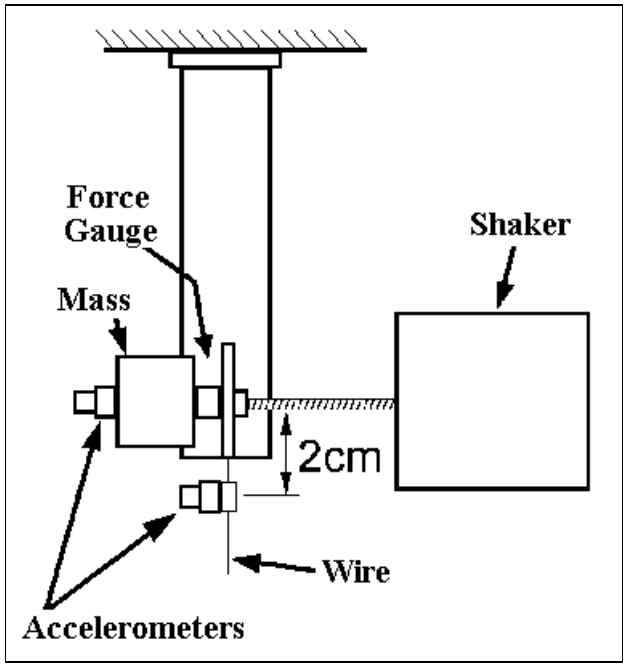

Fig. 4.4 - Configuration of the upper support (lateral view)

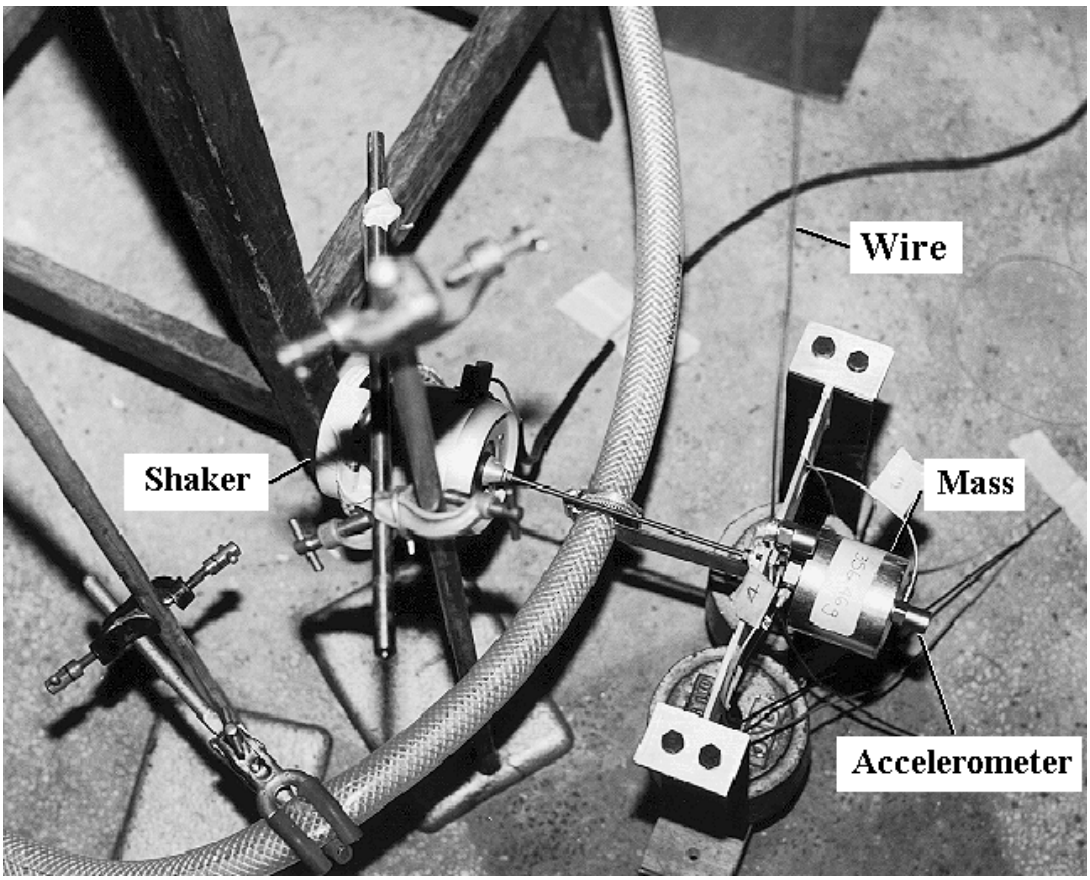

Fig. 4.5 - Lower support

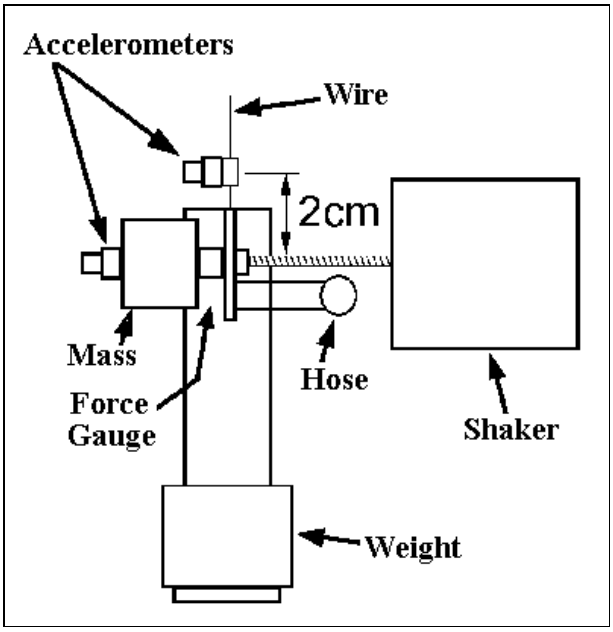

Fig. 4.6 - Configuration of the lower support (lateral view)

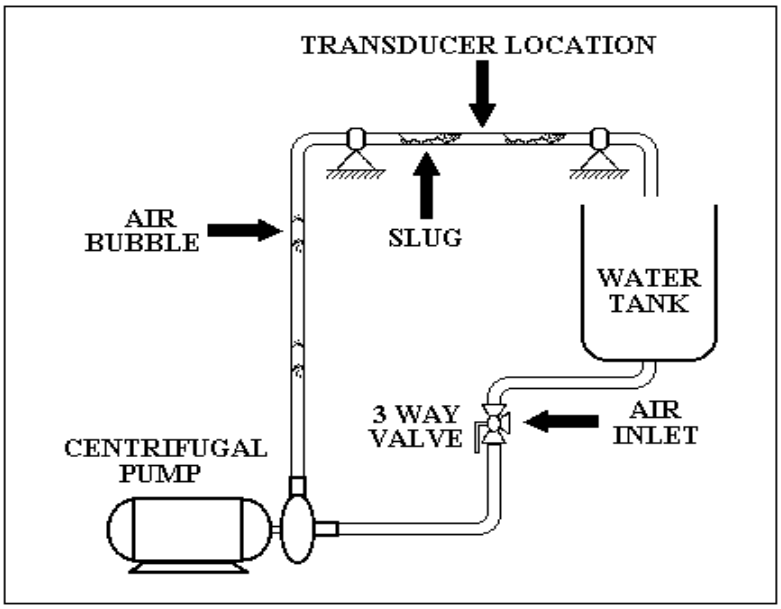

Fig. 4.7 - Experimental slug simulation rig

The Queen's Tower of Imperial College which, being an historical building, restricted the design of the rig as the authorities were concerned about the preservation of the Tower. This meant that the fluid slug rig had to be mounted on the ground floor rather than at the top of the apparatus due to the risk of water spillage on the upper floors.

The intention of the Queen's Tower experiment was not only to determine if a weak component (58 Hz) buried in a noisy signal could be detected at the upper support, but also to identify if any variation in its amplitude could be measured accurately. To this end, five accelerometers were fixed at ≈10 m intervals, to the 39.15 m wire to determine the 58 Hz vibration component propagation along the wire. Figure 4.9 shows an accelerometer on the wire installed at a height of 10.11 m from the lower support. The positions of the accelerometers were carefully selected in order to avoid 58/60 Hz vibration nodes that could reduce the chance of detecting the vibration transmission along the wire.

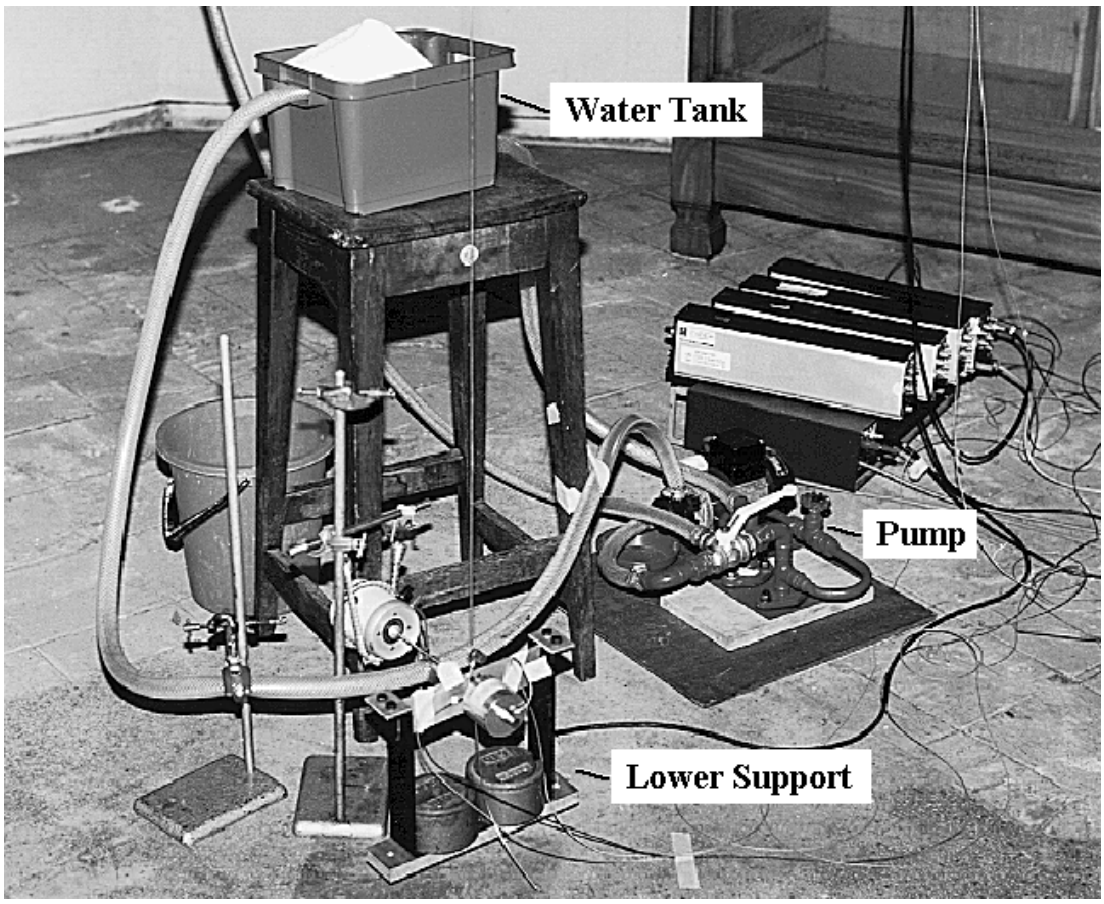

Fig. 4.8 - Rig to simulate slugs

In the case of a real wellhead installation, a mechanical moment component due to the high stiffness of the tubing transmits the amplitude of the waves through a rigid joint support. As may be seen in the diagram of Figure 4.10, no transverse vibration crosses the junction between the wellhead and the petroleum pipe, and this end effect cannot be simulated in a small-scale model. The sketches of Figure 4.10 illustrate the problem of recreating the wellhead vibration boundary conditions in the scale rig. In the case of a real installation an equivalent downhole vibration amplitude value, which corresponds to amplitude values collected above the wellhead deck plate, can be obtained below the deck plate (see Figure 4.10). In the scale-model, the vibration that represents the ESP obtained below the deck plate is collected from the accelerometer placed 2 cm below the upper shaker central axis (see Figure 4.10).

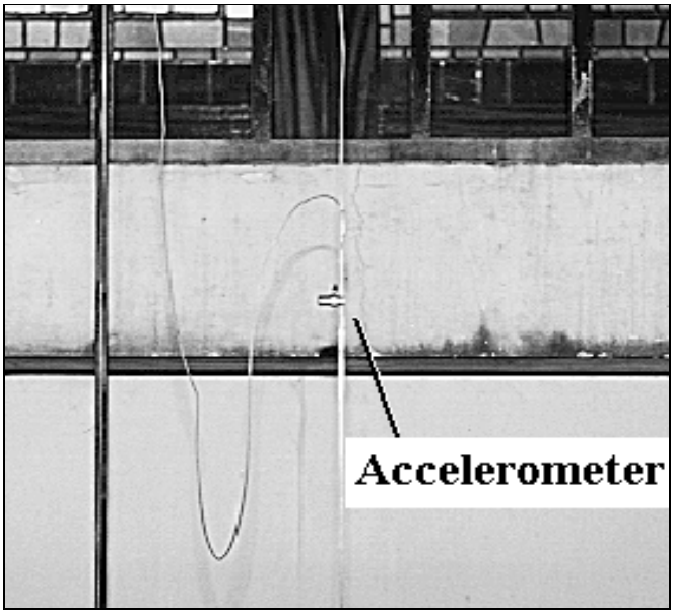

Fig. 4.9 - Accelerometer installed at 10.11 m on the cable

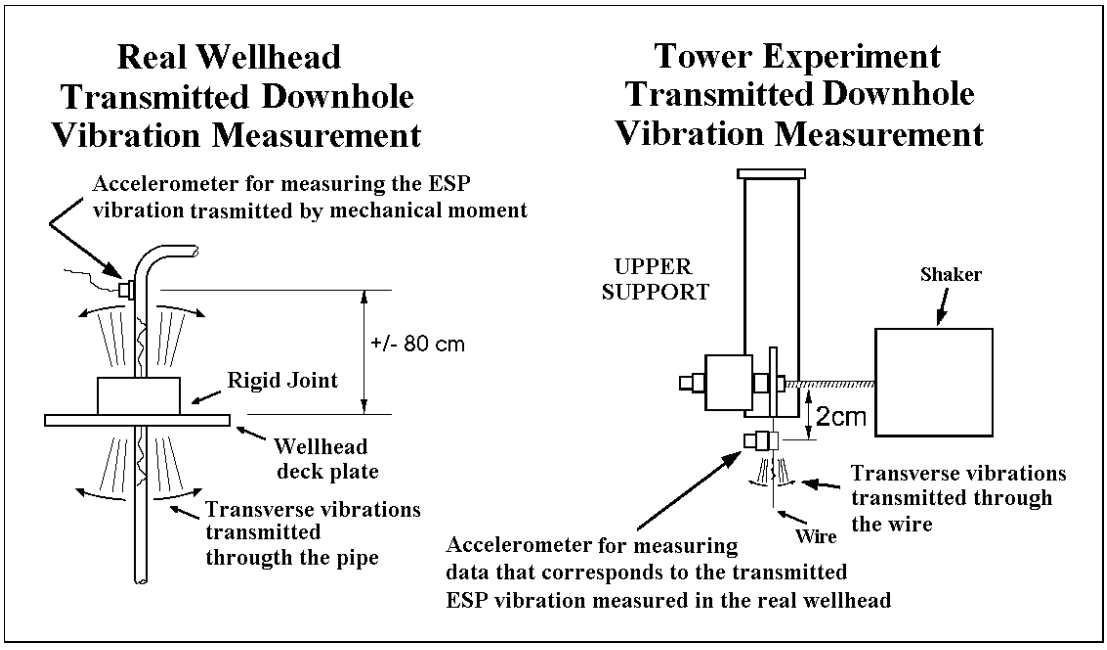

Fig. 4.10 - Wellhead junction transmission problem

The instrumentation used for collecting data in the Queen's Tower experiment included a Kiowa RTP-701 tape recorder with 14 channels, an HP-35665 dynamic analyser and a Kistler 16-channel transducer amplifier. These instruments were connected and a phase and mass calibration was performed using the force gauge prior to the tests [Ewins, 1995]. Figures 4.11 and 4.12 show the calibration graph of

the experimental facility and its respective phase. The measurements shown in the graphs are taken from the HP-35665A dynamic analyser.

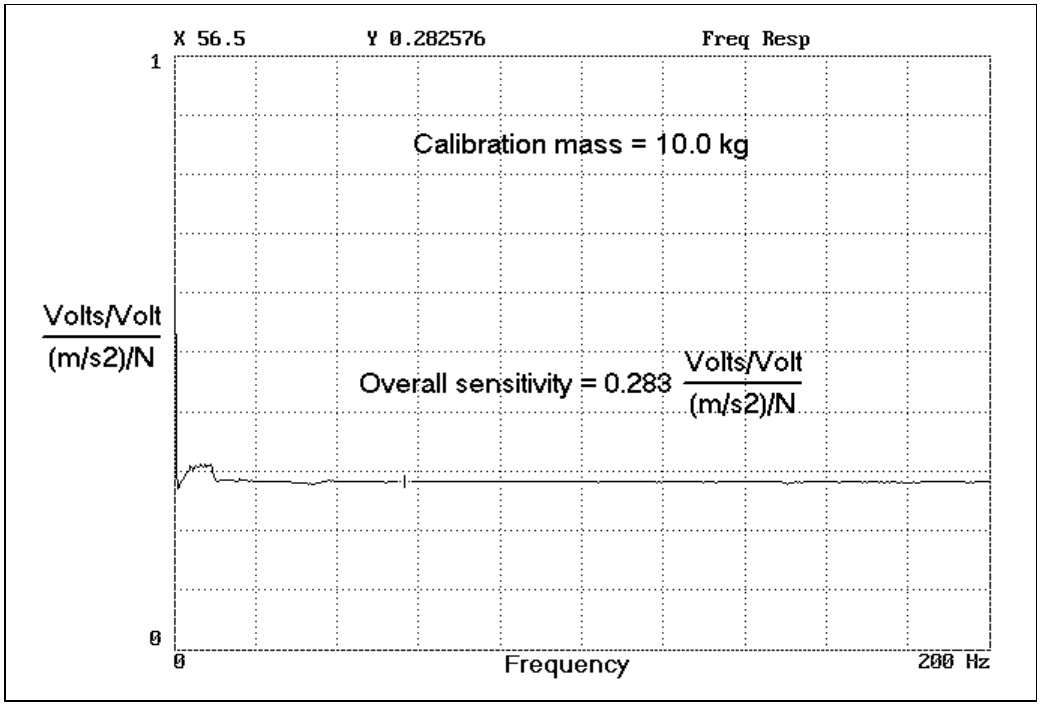

Fig. 4.11 - Equipment mass calibration graph

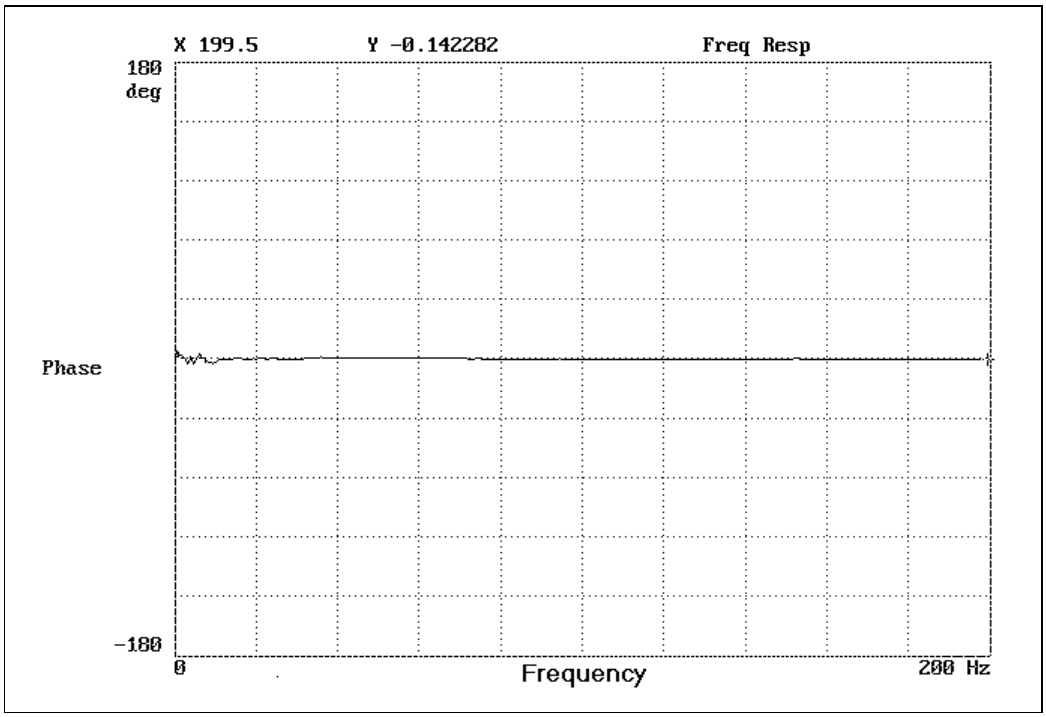

Fig. 4.12 - Equipment phase calibration graph

Figure 4.13 shows the final configuration of the experimental test-piece mounted vertically in the Queen's Tower of the College with its 39.15 m long wire and 7 accelerometers, 5 on the cable and 2 on the supports.

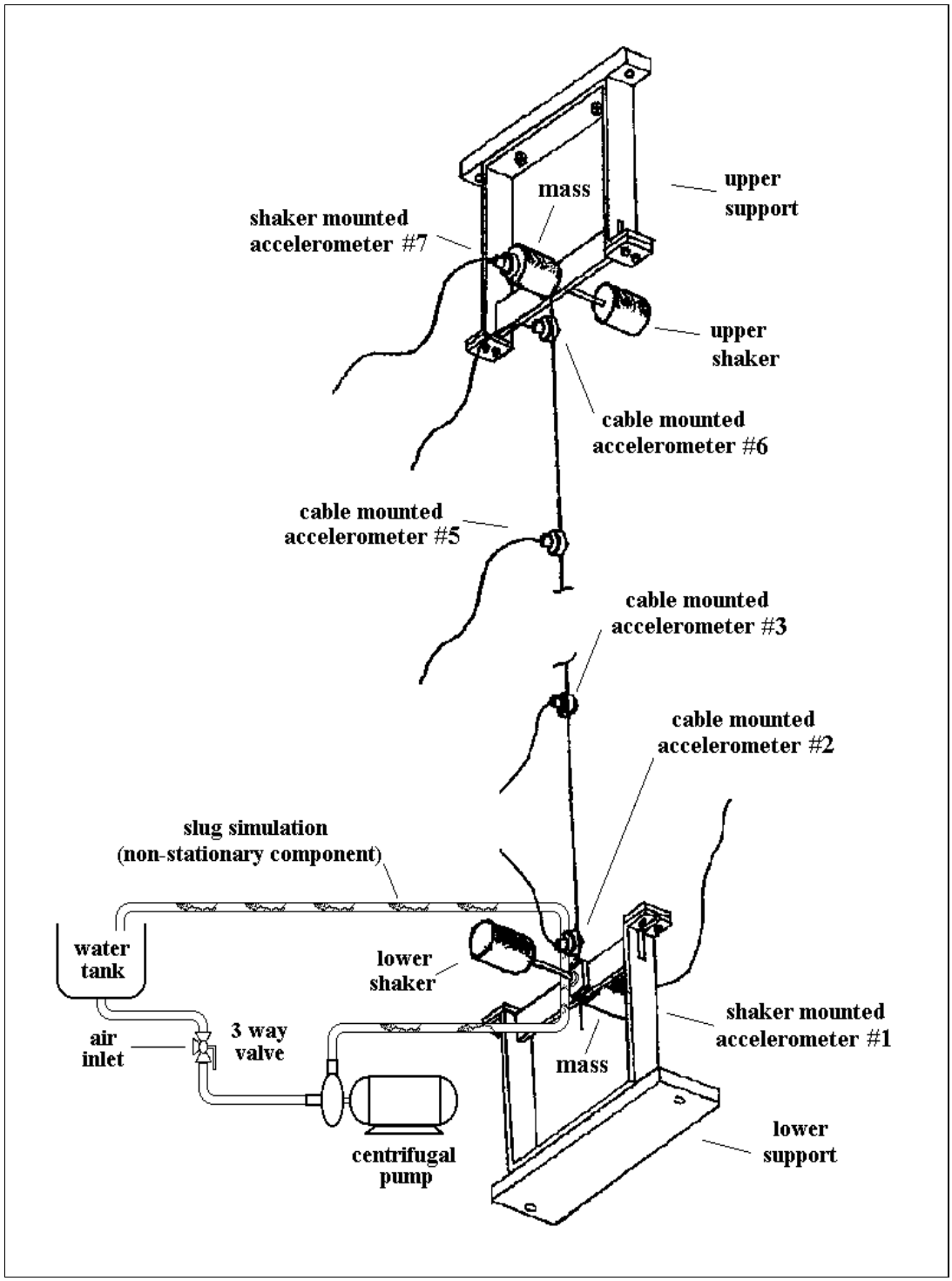

Fig. 4.13 - Experimental test-piece vertically mounted in the Queen's Tower

4.3. Experimental Data Collection

The experimental data collection set out below are based on a series of seven experiments undertaken in the Queen's Tower of the Imperial College. The experimental data collected included three hours of signals recorded on two VHS tapes. The seven experiments and the signals recorded are listed in Table 4.1 below:

Test no.	Description
1	58 Hz component generated by the lower shaker with acceleration of ±1.5 m/s^2, measured by the accelerometer #1 installed aligned with the lower shaker
2	60 Hz component generated in the lower shaker with acceleration of ±1.5 m/s^2, measured by the accelerometer #7 installed aligned with the upper shaker
3	58 and 60 Hz components, with approximately the same amplitudes, generated in the lower and the upper shakers respectively with accelerations of ±1.5 m/s^2, measured by the accelerometers #1 and #7 installed aligned with the lower and the upper shakers, respectively
4	58 and 60 Hz components, generated in the lower and upper shakers, as in test no. 3, the 58 Hz wave amplitude reduced to 1/2 of the original value
5	58 and 60 Hz components, generated in the lower and the upper shakers as in test no. 3, the 58 Hz wave amplitude reduced to 1/4 of the original value
6	58 and 60 Hz components, with approximately the same amplitudes, generated in the lower and upper shakers, as in test no. 3, and with the fluid slug vibration added
7	Pure fluid slug vibration collected from accelerometer #1 aligned with the shaker of the lower support

Table 4.1 - Test signals generated in the Tower experiments

Only the signals generated in the tests 3, 4 and 7 were considered relevant for the purpose of the experimental analysis. The signals generated in the tests 1 and 2 served the purpose of checking the operation of the experimental equipment. The signal generated in test 5 was discarded as it did not conform to the amplitude relationship of the 58 Hz and 60 Hz components used in the simulation. It can be seen in Table 4.1 that the 58 Hz wave amplitude was reduced by 1/4, whereas in the simulation it was reduced by 1/2 (see section 3.7 of Chapter 3). The signal generated in the test 6 was discarded because it was not possible to generate a fluid-slug vibration with an amplitude level at least 50 times greater than the amplitude level of the 58 Hz component. As a consequence, in test 7 a pure fluid-slug vibration had to be generated and recorded in isolation, in order to multiply its amplitude by the factor described in table 4.2 (see section 4.4 below). Figure 4.14 shows graphical plots of the signal recorded in test no. 3 and its respective Fourier transforms (58 Hz vibration generated by the upper shaker and the 60 Hz vibration generated by the lower shaker). The 58 Hz component vibration was detected by all accelerometers together with its respective amplitude variation values and its decrease over the distance.

It may be noted in the spectral graphs of Figure 4.14 that the vibration levels of the 58 Hz component are related to the distance from the generation point. This means that the longer the distance the greater the attenuation (see Figure 4.14).

Figure 4.15 shows the Fourier transform of the signal with pure 58 and 60 Hz components collected in test 4 at a height of 39.13 m.

Figure 4.16 shows the Fourier transform of the signal with pure 58 and 60 Hz components collected in test 3 at a height of 39.13 m. It should be noted that in Figure 4.16, the amplitude of the 58 Hz component is twice that in Figure 4.15. Also, Figures 4.15 and 4.16 depict the presence of some harmonics of the 58 and 60 Hz components.

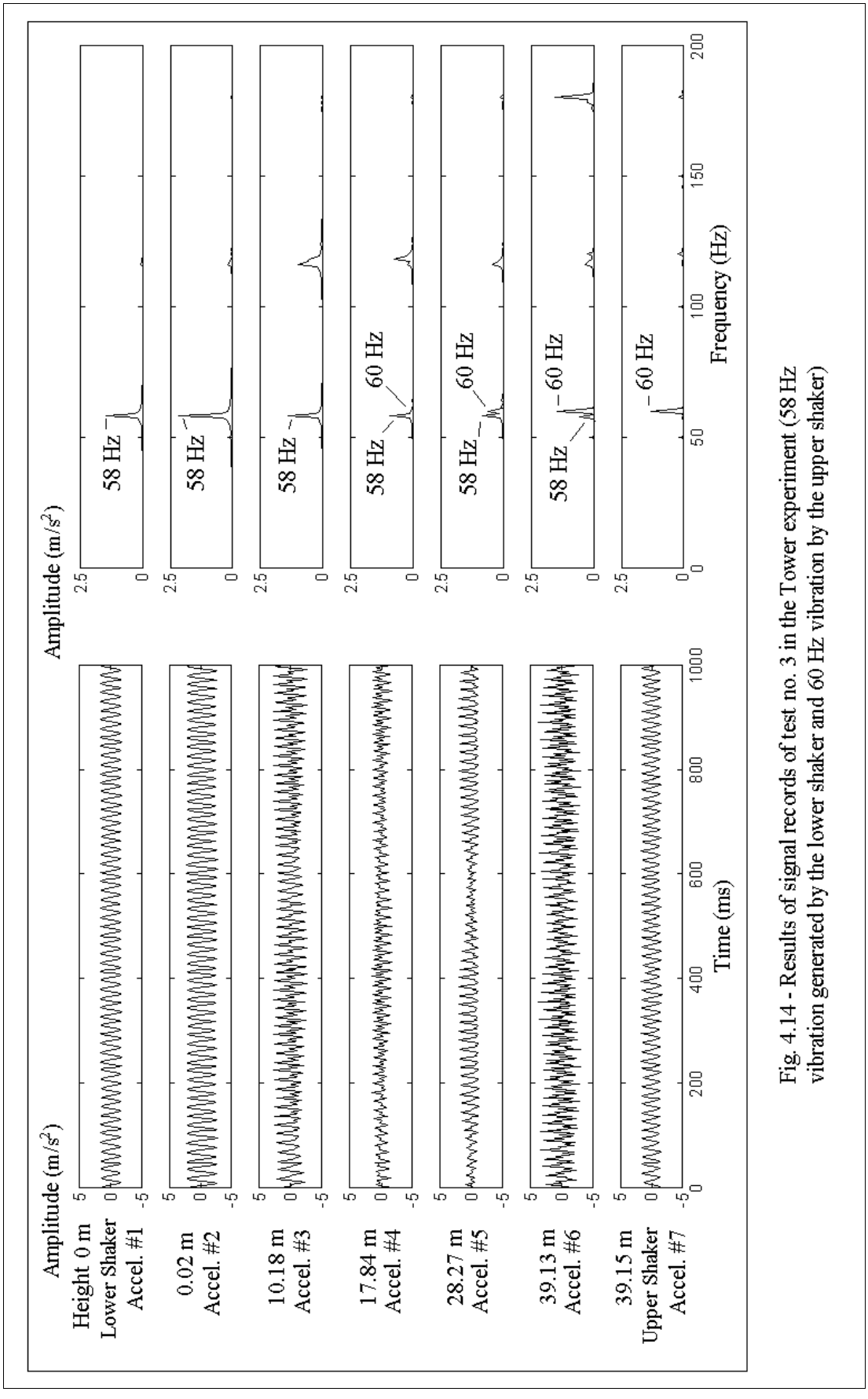

Fig. 4.14 - Results of signal records of test no. 3 in the Tower experiment (58 Hz vibration generated by the lower shaker and 60 Hz vibration by the upper shaker)

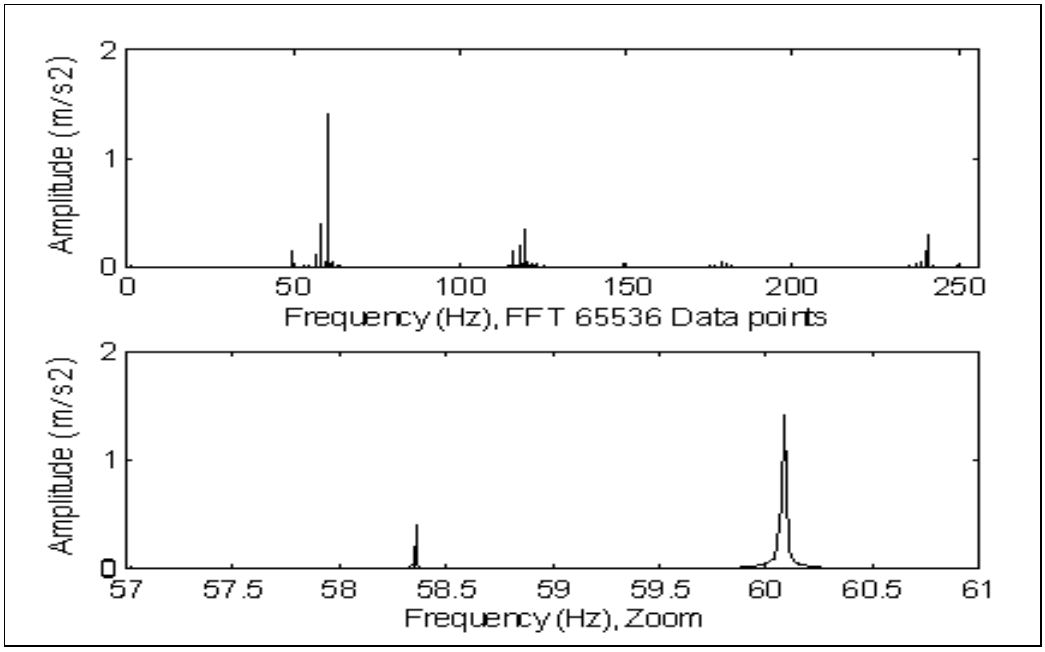

Fig. 4.15 - Long Fourier transform of the signal with 58 and 60 Hz pure components collected in the test no. 4 at a height of 39.13 m (accelerometer #6) in the Tower experiment (frequency resolution = 0.01 Hz, no window).

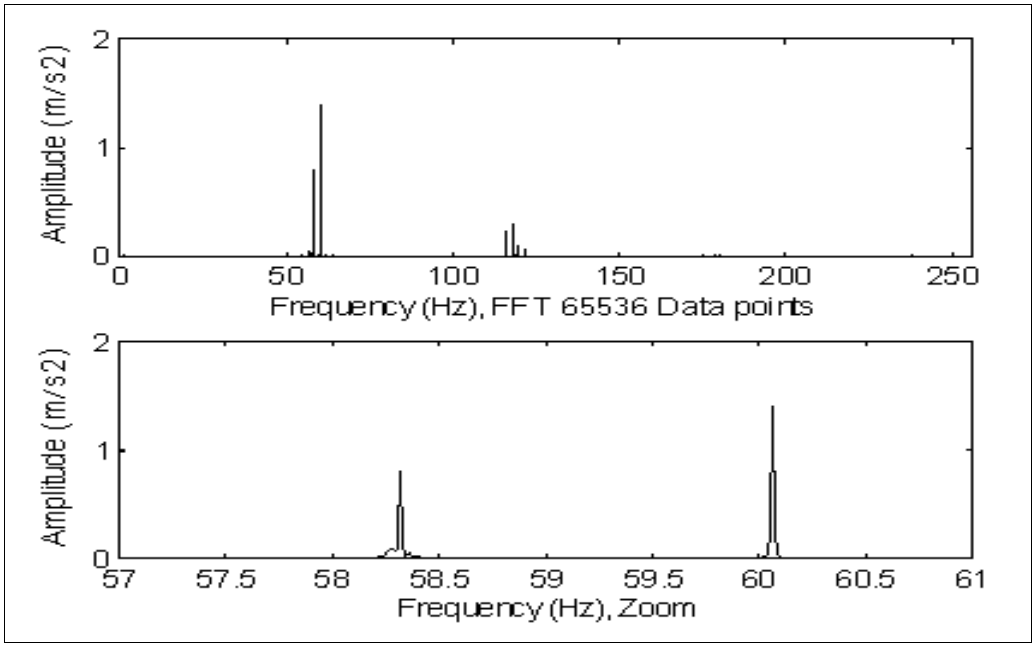

Fig. 4.16 - Long Fourier transform of the signal with 58 and 60 Hz pure components collected in the test no. 3 at a height of 39.13 m (accelerometer #6) in the Tower experiment (frequency resolution = 0.01 Hz, no window - amplitude of the original 58 Hz is doubled)

Three additional experimental signals, each containing a specific type of noise, were generated by the HP-35565A analyser and mixed with the vibration signals generated in tests 3, 4 and 7. The first signal contained random noise (Figure 4.17 (a)), the second a chirp (Figure 4.17 (c), chirp-noise frequency range 10-130 Hz and time interval 0.84 s) and the third pink noise (Figure 4.17 (e)). Figure 4.17 shows the noise signals generated by the analyser, with their respective Fourier transforms. Figure 4.18 shows plots of the autocorrelation functions of these signals containing noise. It may be noted that the noise is highly uncorrelated in each case.

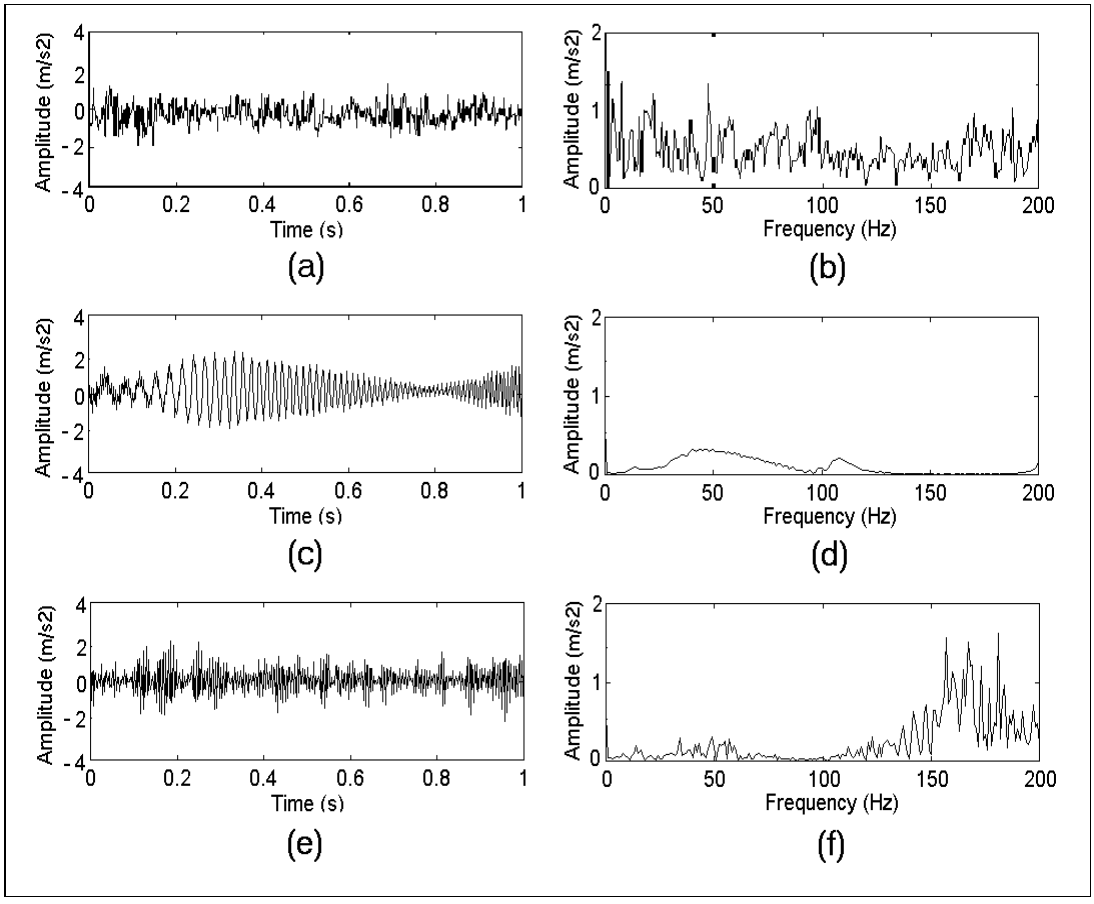

Fig. 4.17 - Additional signals containing noise utilised in the experimental analysis (random (a and b) chirp (c and d) and pink noise (e and f))

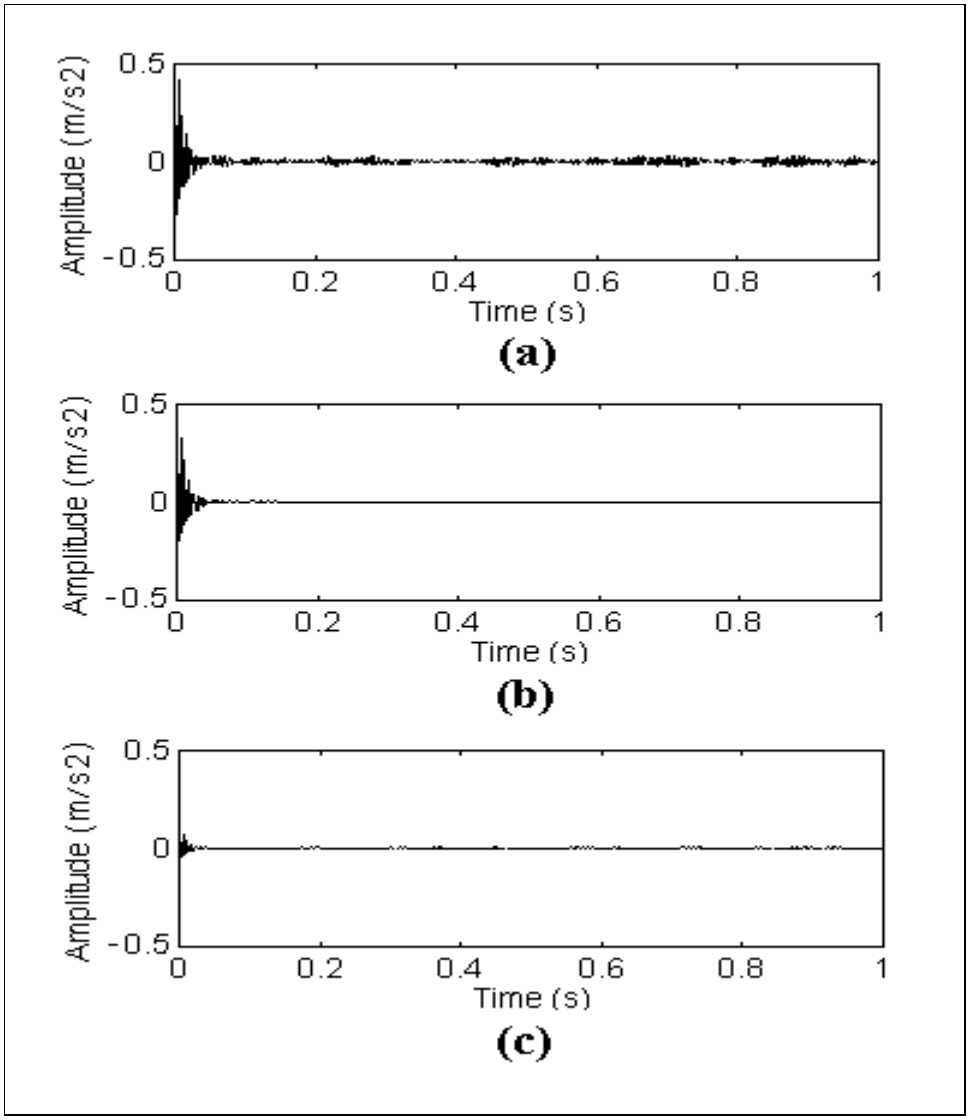

Fig. 4.18 - Autocorrelation of the noise signals (random noise (a), chirp noise (b), pink noise (c))

A statistical evaluation of the required quantity of data to be digitised and analysed from the collected signals of the experimental facility had to be made to restrict the number of points used in the signal processing analysis. It was decided to assume an uncertainty of 10% with a 95% probability to obtain correct experimental results, and to fulfil this assumption, 100 sets of data samples were prepared for each signal analysis [Harrington, Spiegel, 1961].

4.4. Results of the Application of the Extended Prony Time-Frequency Representation to the Experimental Data

As mentioned above, for the purpose of this research, the 58 and 60 Hz signals which represent the pump rotation and the electrical supply current of Brazilian ESPs, are generated in the test rig by the two shakers, and measured separately by selected accelerometers (tests 3 and 4). To these signals were added high-level noise generated by the HP-35565A analyser, and fluid-slug vibration generated by the fluid-slug experimental rig (test 7), to generate new multi-component experimental signals. Before adding noise and the signal containing fluid-slug vibration, the experimental signals were multiplied by several factors in order to: (a) generate new multi-component signals resembling a signal collected at a petroleum wellhead (see section 1.5.8 of Chapter 1 and Appendix C); and, (b) to maintain the same 58 Hz component amplitude variation between two signals, as in the simulation, in one signal of each pair the weak component amplitude is doubled (see section 3.7 of Chapter 3).

As may be noted in Table of Appendix C, the 57.15 Hz and 61.95 Hz component amplitude values, identified when the original Prony method is applied to the signal collected on the wellhead of the platform of Vermelho (see Table of Appendix C), are respectively 0.20 and 0.73 m/s^2. The maximum amplitude level of this signal is above 10 m/s^2. The 57.15 Hz component and signal amplitude relationship is -34 dB (the signal peak is approximately 50 times greater than the amplitude of the 57.15 Hz component, related to the rotation of the ESP). As the amplitude level of 58 Hz component of the signal generated in test 3 is 0.80 m/s^2, it was necessary to multiply the signal by a factor in order to set that component amplitude level to a maximum of 0.20 m/s^2. In order to maintain the appropriate component amplitude relationship, this factor multiplying-operation was performed in all experimental signals (see Table 4.2 for component amplitude values with their respective multiplying factor).

All selected signals, recorded in the Tower experiment and multiplied by their respective factor (see Table 4.2), were added to prepare multi-component signals labelled from E1 to E6. These multi-component signals are described by Table 4.3.

Component	Test no.	Accel.	Max. Ampl. (m/s^2)	Multiplying Factor	New Max. Ampl. (m/s^2)
58 Hz	4	#6	0.39	0.51	0.20
60 Hz			1.46		0.74
58 Hz	3	#6	0.80	0.50	0.40
60 Hz			1.45		0.73
Tower Fluid Slug	7	#1	0.13	153.85	20.00
Random Noise	---	#1	0.83	24.10	20.00
Chirp Noise	---	#1	1.19	16.81	20.00
Pink Noise	---	#1	1.08	18.52	20.00

Table 4.2 - Signals registered in the Tower experiment and noises with its respective multiplying factor

Component	Experimental Signals (amplitudes (m/s^2)) E1	E2	E3	E4	E5	E6
58 Hz	0.20	0.40	0.20	0.40	0.20	0.40
60 Hz	0.74	0.73	0.74	0.73	0.74	0.73
Tower fluid slug	20	20	20	20	20	20
Random noise	20	20				
Chirp noise			20	20		
Pink noise					20	20

Table 4.3 - Signal composition for the experimental analysis with the slug vibration component generated in the Tower experiment

The signals described in Table 4.3, E1 to E6, were processed through the extended Prony time-frequency representation and filtered using the same procedures as were applied in section 3.7. Each waterfall graph of Figure 4.19 shows the results of 100

Fourier transforms (frequency resolution = 1 Hz) of 100 filtered and recovered data arrays using the extended Prony time-frequency plane representations. The results shown in Figure 4.19 correspond to the application of the extended Prony time-frequency representation applied to 100 data arrays of signal E1 and 100 data arrays of E2 (signals with random noise - 512 data points per time shift - total data points per sample = 1023, order 64, maximum exponential damping 0.02 s^{-1}). The average of the Fourier transforms over these one hundred sets of one second, as seen in Figure 4.20, shows that 58 Hz component amplitude was increased 4.5 times from signal E1 to E2. The frequency band-pass filtering range for applying the extended Prony time-frequency representation plane "band-selection" is 56-59 Hz.

The waterfall graph of Figure 4.19 clearly depicts the difference that exists between 58 Hz component amplitude levels in the filtered and recovered samples using the extended Prony time-frequency representation. The correct variation has been detected in virtually all sets evaluated from the filtered samples. The larger peaks in graph (b) of Figure 4.19, related to the signal E2, indicate an increase in the 58 Hz component amplitude values over the signal E1 (graph (a) of Figure 4.19). The graph of Figure 4.20 was obtained from an averaging process, which was applied to 100 Fourier transforms of data arrays with 512 samples of signals E1 and E2 previously filtered by using the extended Prony time-frequency representation. This graph clearly depicts the 58 Hz component amplitude value variation. The amplitude value of the 58 Hz component of signal E2 noted in the graph of Figure 4.20 (0.45 - dashed line) is greater than twice the true amplitude value of this component. This oversized amplitude of the 58 Hz component may be due to residual noise that was not eliminated in the filtering process.

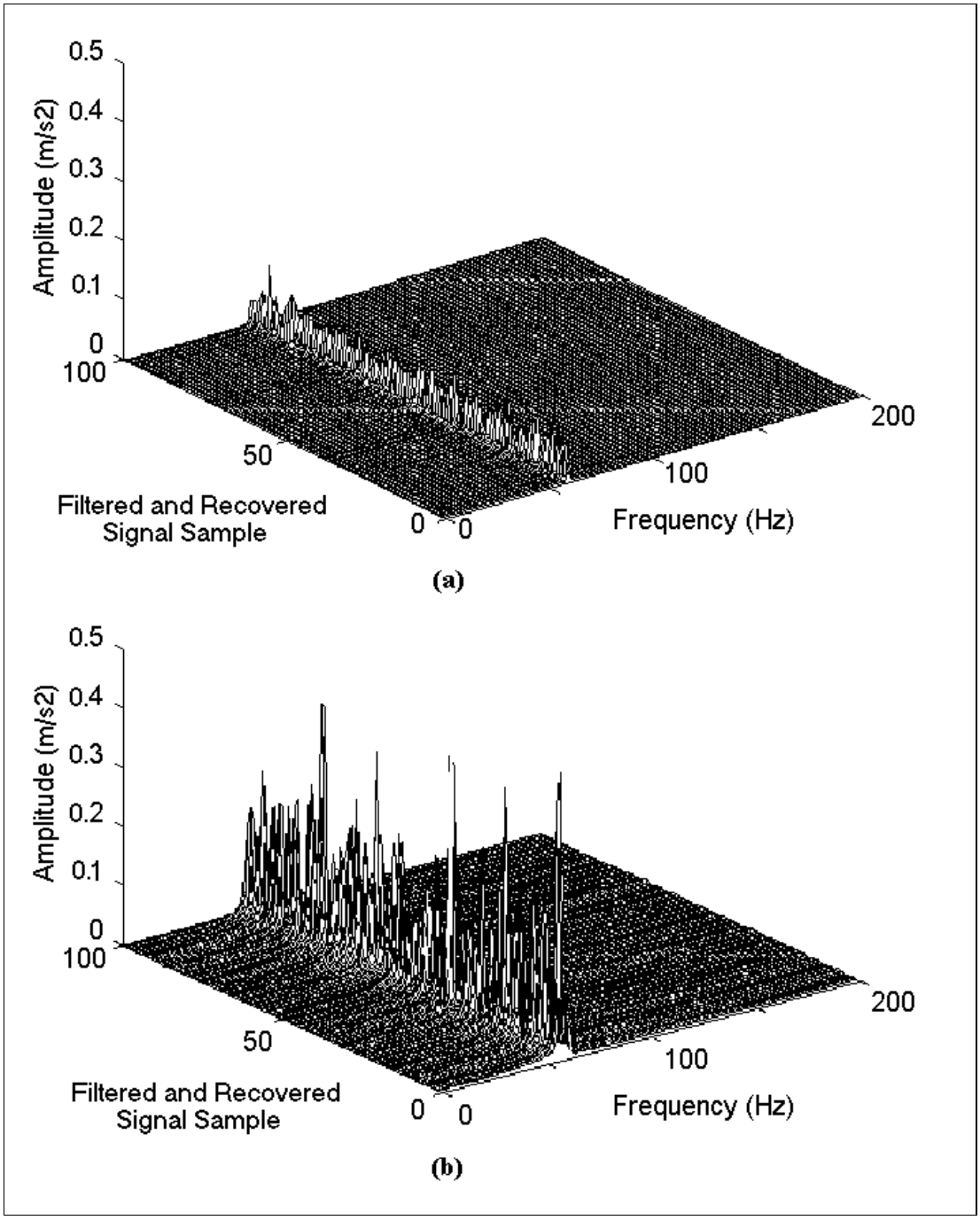

Fig. 4.19 - Waterfall graph of Fourier transforms of signal data arrays filtered and recovered by using the extended Prony time-frequency representation ((a) 100 samples of signal E1 and (b) 100 samples of signal E2, sampling frequency 512 Hz, frequency resolution =1 Hz)

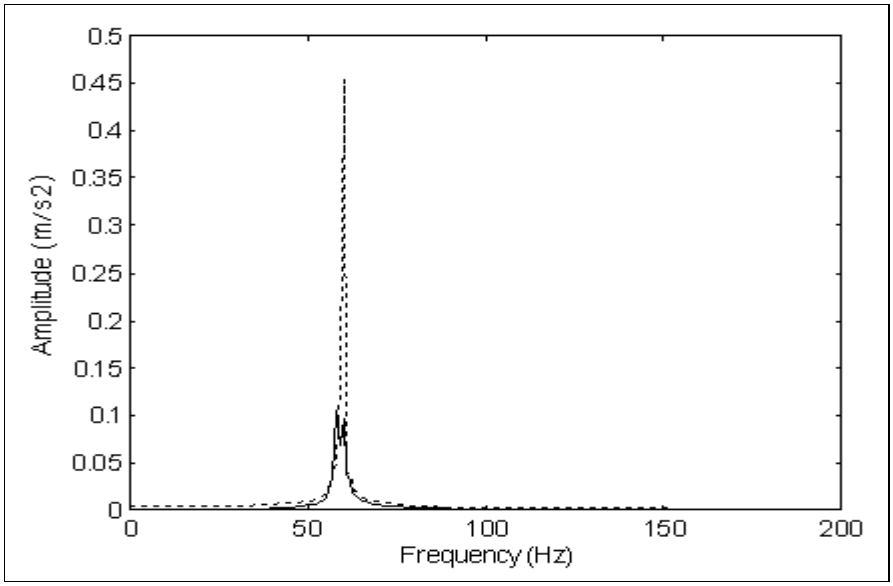

Fig. 4.20 - Average of the 100 Fourier transforms of the filtered and recovered signal data arrays shown in the waterfall graph of Figure 4.19 (signal E1 - solid line, signal E2 - dashed line)

Figures 4.21 to 4.24 show graphs of the results obtained from the analysis of the signals E3 to E6, when the same methodology used in the analysis of signals E1 and E2 above was applied.

The results shown in the graphs of Figures 4.21 to 4.24 indicate that the variations in the 58 Hz component amplitude have been clearly detected in the samples of signals E3 to E6, filtered and recovered using the Prony time-frequency representation. The fact that signals E2, E4 and E6, in which the weak component amplitude was increased, have greater amplitude values than the signals E1, E3, and E5, confirms that in all signal test cases from E1 to E6 the amplitude variation of the weak component was detected.

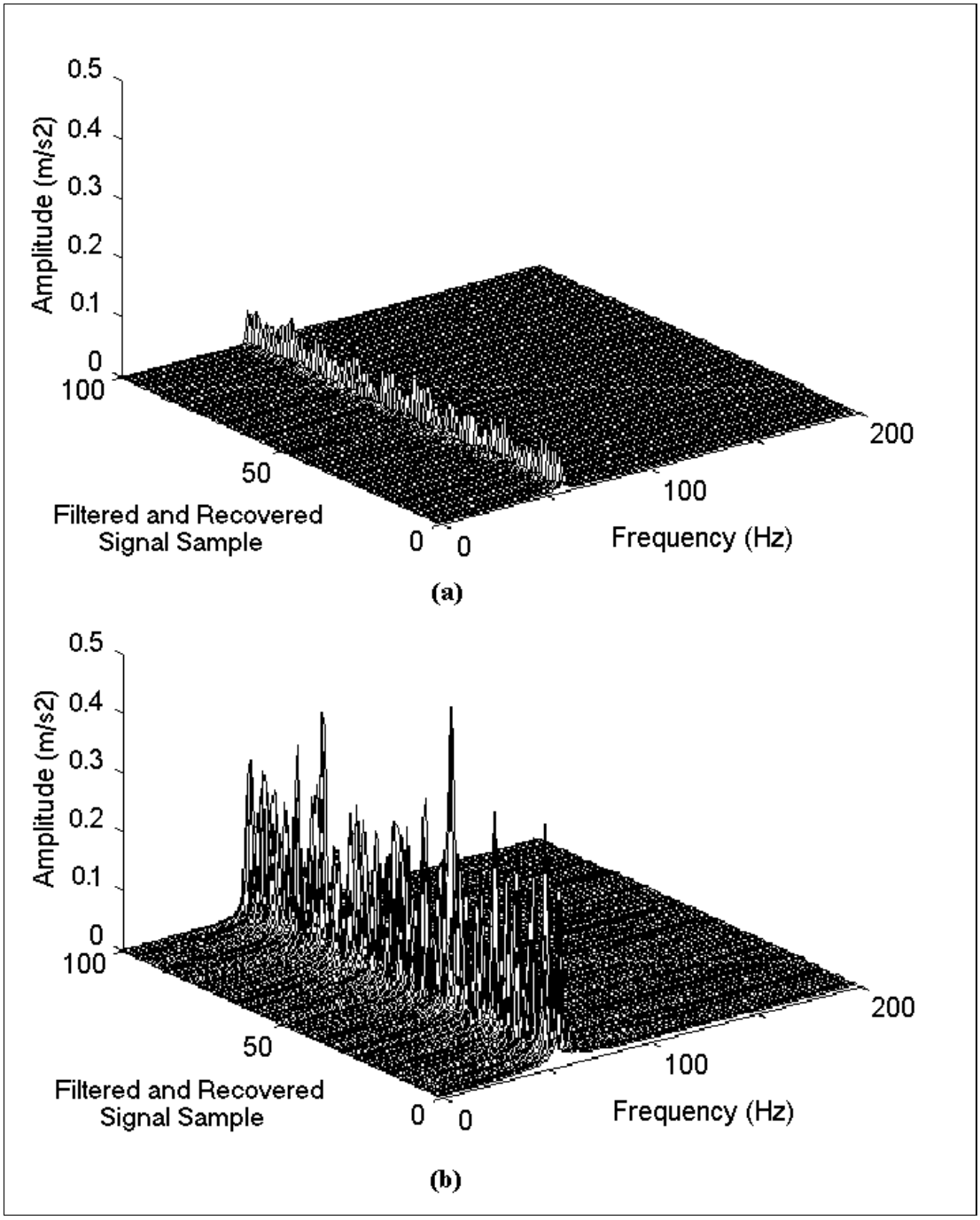

Fig. 4.21 - Waterfall graph of Fourier transforms of signal data arrays filtered and recovered by using the extended Prony time-frequency representation ((a) 100 samples of signal E3 and (b) 100 samples of signal E4, sampling frequency 512 Hz, frequency resolution =1 Hz)

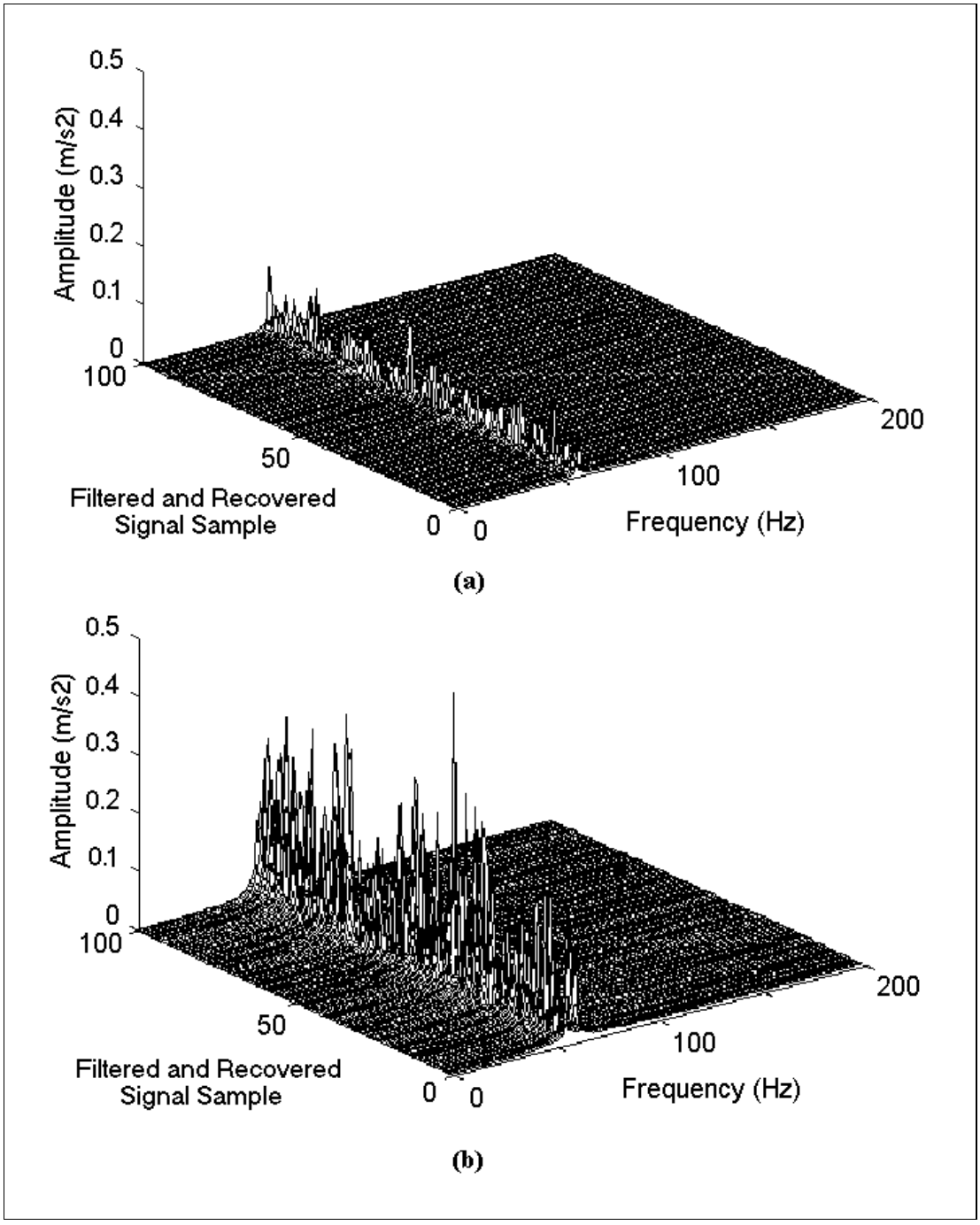

Fig. 4.22 - Waterfall graph of Fourier transforms of signal data arrays filtered and recovered by using the extended Prony time-frequency representation ((a) 100 samples of signal E5 and (b) 100 samples of signal E6, sampling frequency 512 Hz, frequency resolution =1 Hz)

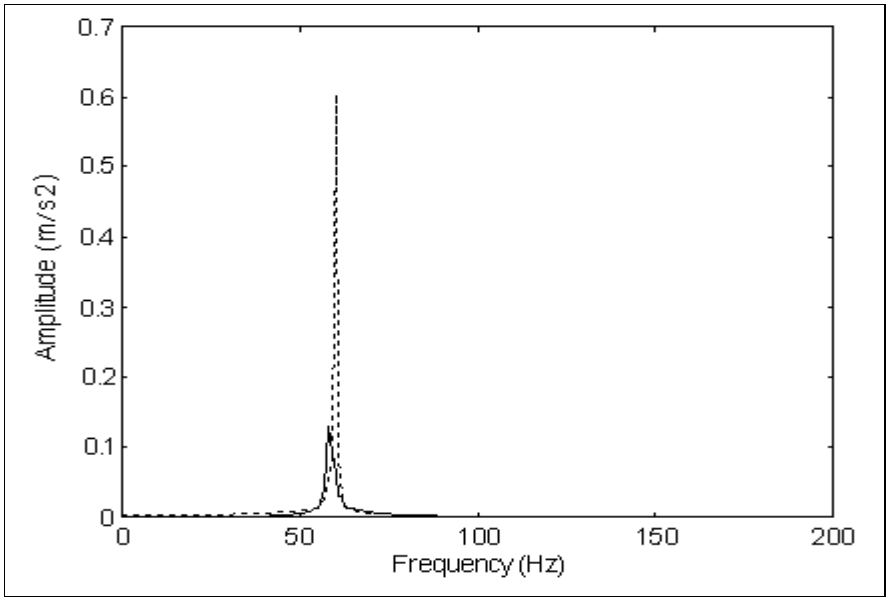

Fig. 4.23 - Average of the 100 Fourier transforms of the filtered and recovered signal data arrays shown in the waterfall graph of Figure 4.21 (signal E3 - solid line, signal E4 - dashed line)

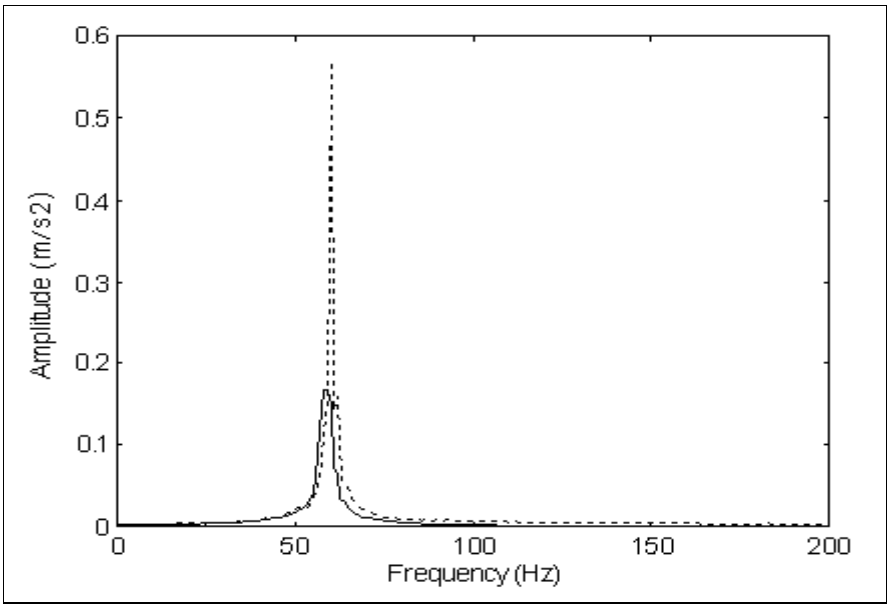

Fig. 4.24 - Average of the 100 Fourier transforms of the filtered and recovered signal data arrays shown in the waterfall graph of Figure 4.22 (signal E5 - solid line, signal E6 - dashed line)

Comparing the graphs of Figures 4.19, 4.21, and 4.22, with the graph of Figure 3.99 of Chapter 3, it is easier to detect the 58 Hz component amplitude variation in the experimental signals E1 to E6 than in the simulated signals S13 and S14. The discrimination difficulty in detecting amplitude variation that occurred in the analysis of the signal with slug component generated in the simulations (see section 3.9 of Chapter 3) was not observed in the experimental signal analysis. To confirm this, a comparison can be made between the graphs (a) and (b) of Figure 3.99 of the simulation analysis (see Chapter 3). In the waterfall graph (b) of Figure 3.99, several sets of the signal containing the 58 Hz component with greater amplitude were represented by lower peaks. In the case of simulated signals S13 and S14, it is unclear which amplitude component increased without performing a spectrum average. Also, the small difference in the average of Fourier transforms in terms of amplitude that was found in the simulation signals S13 to S14 (see Figure 3.100) suggests that it is difficult for the methodology to discriminate weak component variations in some samples of those signals.

The discrimination problem did not arise in the analysis of the signals containing slug components generated in the Tower experiment as it is less problematic than the simulated signals S13 and S14 of Chapter 3 for filtering the deterministic components using the extended Prony time-frequency representation. A possible explanation for this may be obtained by observing the graph of Figure 4.25. The Prony time-frequency representation of the signal generated in the Tower experiment contains mostly components around 90 Hz, which may be eliminated by a high-pass band filter (see Figure 4.25).

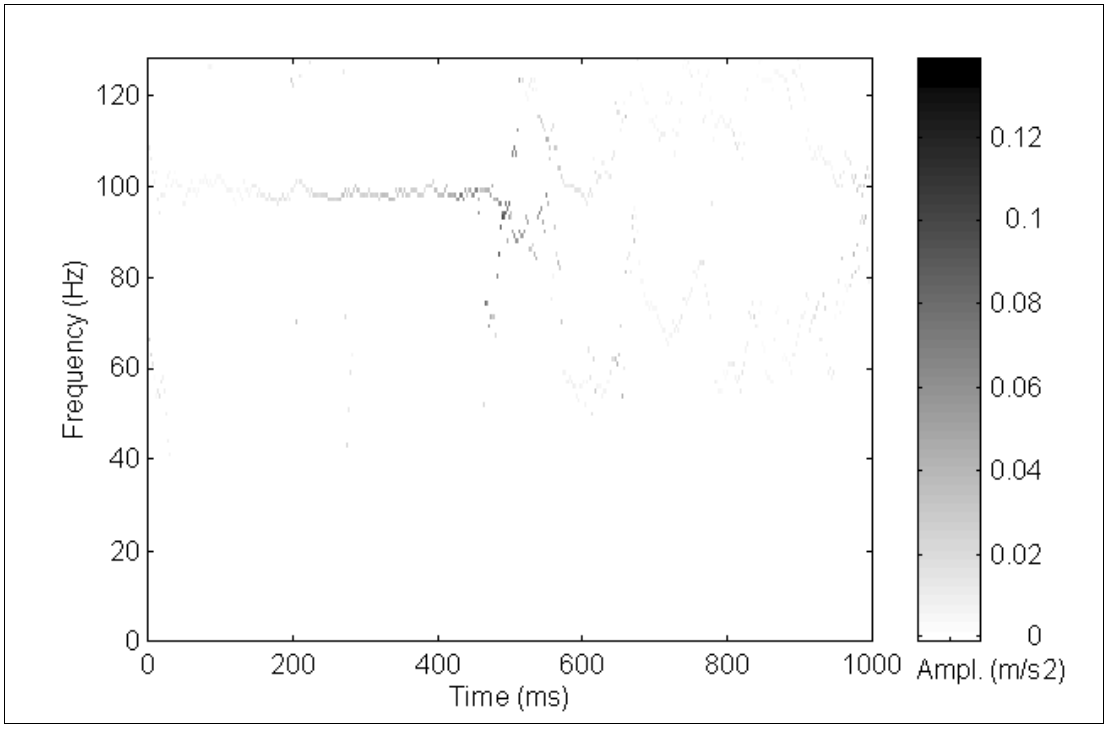

Fig. 4.25 - Extended Prony time-frequency representation of the signal with fluid slug vibration generated in the Tower experiment(32 data points per sample - total data points used = 527, order 8, no exponential damping limiting)

The detection of the correct variation in the amplitude level in virtually all signals samples to which the extended Prony time-frequency representation has been applied, indicates that the extended technique is suitable for detecting variations in ESP vibration amplitudes, transmitted through the petroleum pipe and collected in the wellhead on the surface.

The results show that the extended Prony time-frequency representation can successfully “extract” deterministic components from noisy signals, and is therefore a useful tool in the elimination of transients. A further positive feature of the results is the discovery that the application of the plane “band-selection” filtering to the extended Prony time-frequency representation (see section 3.6), can generate acceptable results.

4.5. Conclusion of the Experimental Study

The main findings of the results of the experimental study can be summarised as follows:

(a)The experimental data collection confirms that the vibration levels of the 58 Hz component are related to the distance from the generation point. That is, the longer the distance the greater the attenuation (see Figure 4.14);

(b)A successful 58 Hz weak component detection was obtained in 100 % of the Fourier transforms of signal data arrays, filtered and recovered by the plane "band-selection" and exponential damping filtering through the extended Prony time-frequency representation (minimum SNR = -34 dB and maximum SNR = - 40 dB for experimental signals E1 to E6); and,

(c)A successful non-stationary and noise process elimination was made through the extended Prony time-frequency representation, in this research study, by setting a maximum level for component exponential damping of 0.02 s^{-1}. However, the maximum level for component exponential damping of 0.02 s^{-1} may not be adequate for filtering spurious components different from that considered in this study (fluid-slug vibration). This maximum level component exponential damping has been used considering an exponential decay of the kind $\boldsymbol{e^{-ct}}$, where $\boldsymbol{c}$ is the exponential damping of the component evaluated through several preliminary tests using simulated and experimental signals. If a signal contains transients which present an amplitude decay that cannot be modelled as an approximation of an exponential decay, an error may occur in the filtering process.

It should be noted that, although a number of elements that represent a real petroleum well are reproduced in the experimental facility, a number of other intervening variables that will influence the vibration signal have to be expected in the real system. These include the variation in the fluid density along the pipe of a petroleum well,

which is not feasible to reproduce in laboratory conditions. This is due to the fact that the fluid density varies continuously in the presence of gas fractions, and in relation to the location and height of the pipe.

Chapter 5
Discussion

As stated in Chapter 1, the aim of this research is to develop tools for studying the condition of petroleum electrical submersible pumps installed downhole, by analysing the vibration signals transmitted through the petroleum tubing and collected at the surface in the wellhead. In particular, the primary objective has been to develop a signal processing technique for detecting weak components in signals with high levels of noise and containing strong non-stationary features.

At the outset, we expected to obtain weak component detection using the recently-developed Malat wavelet transform technique, given its excellent ability to recover signals. It was intended to detect the weak signal components through the Malat wavelet levels, and to recover them by separating the components through a filtering operation applied using the wavelet levels. However, a preliminary analysis showed that it was not easy to differentiate what is non-stationary from what is stationary in the Malat wavelet transform levels (see section 3.2.4 of Chapter 3). We then moved on to test the Morlet wavelet transform and the pseudo-Wigner-Ville distribution, but here difficulties were encountered with handling high-level noise using these techniques (see 3.3.3 of Chapter 3). Until this stage it was believed that it would be appropriate to use these techniques to separate stationary from non-stationary components in a signal in which the noise was eliminated using a filtering procedure.

However, tests showed that the weak component of interest was also being eliminated during the filtering procedures (see sections 3.2.1 and 3.2.2 of Chapter 3).

Existing filtering techniques, such as those using the autocorrelation and the Kalman filter, are based on statistical criteria, and weak components have a "weak" statistical weight in the signal. Therefore, we were now faced with the task of finding a technique with a different filtering criterion. One option was to test the component selection in terms of its amplitude reduction along the time axis. This reduction is associated with transient components (uncorrelated noise and non-stationary processes) that can be eliminated by this criterion, in favour of the deterministic components.

As we needed to evaluate the component amplitude reduction, the original Prony method appeared to be well-suited because it is a specific method for analysing transient components. However, for our purposes this technique had to be extended for noise and non-stationary analysis. This was achieved by positioning the amplitude, phase and exponential damping values, evaluated for a specific frequency component by the original Prony procedure (equation (2.22) of Chapter 2) in a time-frequency representation matrix (equation (2.42)). To generate the extended Prony time-frequency representation, the original Prony method is performed in a loop to evaluate amplitude, frequency, phase and exponential damping values of each time-set of the signal data points. This operation resembles the generation of a common Fourier transform waterfall graph. What differentiates the extended Prony time-frequency representation from the common Fourier transform waterfall graph is the composition of the spectral lines and the period (***dT=1/N***) in the time-shifting operation applied. As a common feature of a non-parametric method, in each signal set of data points of the waterfall graph the Fourier transform generates a spectrum containing all frequency component amplitudes in an ***N/2*** Hz frequency bandwidth, where ***N*** is the number of signal data points. As in any other parametric method, the number of frequency components evaluated by the original Prony method is limited by a polynomial order ***p<<N/2***. For this reason, it is necessary to generate a "spectrum" vector with ***N/2***

zeros that "represents" the frequency scale (see section 2.7). The component amplitude values evaluated by the original Prony method are then added to the vector zero elements associated with the frequency calculated by the method. The same procedure is performed to generate the "phase" and "exponential damping" vectors. To generate the waterfall type graph of the extended Prony time-frequency representation, the "spectrum" vectors are aligned to form a "spectrum" time-frequency matrix. To complement the extended Prony time-frequency representation for signal filtering and recovering purposes, the same procedure is performed to generate the "phase", and "exponential damping" time-frequency matrices. The final result of the procedures described above is the construction of three matrices of $N \times N/2$ points containing the time-frequency signal component spectra with their associated phase and exponential damping matrices.

5.1. Analysis of the Simulated Signals

In order to test the effectiveness of the extended Prony time-frequency representation it was subjected to a rigorous comparative analysis, using simulated signals, together with the Fourier transform, Morlet wavelet transform, and Wigner-Ville and pseudo-Wigner-Ville distribution signal processing techniques (see Chapter 3). This was followed by the application of the new representation to the analysis of experimental data generated from the small-scale model of a petroleum well installation (see Chapter 4).

Our first task for the simulation and experimental analysis was to define or classify the petroleum wellhead signal. We generated, in the simulation and in the experimental apparatus (see Chapters 3 and 4), some common features that are believed to be present in a real signal collected at the wellhead. One of these features, fluid turbulence (slugs), has been studied previously in terms of frequency content [Leducq and Hervieu, 1991], but in regard to the other, related to environment noise, it was difficult to obtain an experimental description of its composition. The sea platform

environmental noise presents such a number of different variables governing its frequency behaviour that we opted to generate four types of noise to test the signal processing methods. Although these four types of noise may not represent a real wellhead noise exactly, they were thought to contribute the major features of interest.

5.1.1. Results of the Analysis of the Simulated Signals: Detecting Deterministic and Non-stationary Components

The results of the simulation show that the extended Prony time-frequency representation with least-squares initialisation has more potential to detect deterministic components in noisy signals with non-stationary components than do the other methods we have considered for this study (see Figures 3.29, 3.79, 3.86, and 3.92). As can be seen in Figures 3.26 to 3.28, 3.75 to 3.77, 3.83 to 3.85, and 3.89 to 3.91, the deterministic components were difficult to detect on the time-frequency plane by the Fourier-based methods. This is not the case for the extended Prony time-frequency representation where a maximum set containing 1023 data points were used in the simulation of Chapter 3 (512 data points from the 1^{st} to the 512^{th} time-shift). As a consequence, the first conclusion that can be drawn is that the extended Prony time-frequency representation is more effective at detecting weak components in short length data signals containing strong spurious components such as high-levels of noise and non-stationary fluid slug vibration components. This statement is supported by the fact that in 66 % of the simulated signal analysis (S1 to S12) it was considered to be the best method to represent the signal components and by the 70 % average success obtained in detecting weak component amplitude variations, measured directly in the data signal sets (e.g. numerical results plotted in the graph of Figure 3.99 for signals S13 and S14). As an additional feature, the extended Prony time-frequency representation computes component exponential damping values, which are useful to distinguish non-stationary components that are more heavily damped than the deterministic ones (see the graphs of Figures 3.71 and 3.72).

An unexpected finding of the study is that the extended Prony time-frequency representation could also depict the non-stationary components reasonably well. This may be seen in Figures 3.36, 3.43, 3.50, and 3.57, where the non-stationary processes are represented in the graph with the correct frequency compositions. However, in some specific cases of non-stationary component analysis, the pseudo-Wigner-Ville distribution and the Morlet wavelet transform can still be better than the extended Prony time-frequency representation for this task. This is clearly seen in the representation of the Gaussian waves (see Figures 3.54 for Morlet wavelet transform, 3.56 for pseudo-Wigner-Ville distribution, and 3.57 for extended Prony time-frequency representation). Their time-frequency planes display more information about these non-stationary components than does the extended Prony time-frequency representation. In the time-frequency plane of the Morlet wavelet transform all points of the Gaussian waves are represented, and the observed distortion of their shapes in the graph of Figure 3.54 are due to the logarithm vertical scale. In the time-frequency plane of the pseudo-Wigner-Ville distribution (see Figure 3.56) the Gaussian waves are fully represented with the correct shapes. In contrast with these techniques, the Gaussian waves are represented as a few detected points by the extended Prony time-frequency representation (see Figure 3.57).

The difficulty in representing the Gaussian waves suggests that the extended Prony time-frequency representation is not adequate for representing high-density components. Such is the case, for example, of components containing a large quantity of non-stationary sub-components concentrated in a small area of the time-frequency plane. These high-density components need a large amount of data points concentrated in a small area to be properly represented in the time-frequency plane. The Prony time-frequency representation is not suited for this type of analysis as it needs to use short data sequences for representing a more localised non-stationary phenomena. The use of short data sequence generates small matrices in the equations 2.22 and 2.33 and this, in turn, reduces the solution order and hence the number of components that may be sought in a frequency line of the time-frequency plane. This

is because the Gaussian waves are represented with a lower number of wave points than used for the Wigner-Ville and the pseudo-Wigner-Ville distributions (see the graphs in Figures 3.55 to 3.57). In the case of depicting a non-stationary feature by a large number of points, concentrated in a small area of the time-frequency plane, the pseudo-Wigner-Ville distribution and the Morlet wavelet transform are still better choices than the extended Prony time-frequency representation. This can be seen by comparing the true time-frequency plane representation given in the graph of Figure 3.52 with the graphs of Figures 3.54, 3.56, and 3.57. However, in the component analysis of signals S1, S3, S4 to S6, and S8 to S12, the Wigner-Ville and the pseudo-Wigner-Ville distributions did not performed as well as the Prony time-frequency representation.

5.1.2. Malat Wavelet and the Extended Prony Time-Frequency Representation with RSL Routine in the Initialisation Step

With regard to the Malat wavelet method, it can be seen from the graphs of Figure 3.5 that it is difficult to associate deterministic components to wavelet levels, and the wavelet transform developed by Malat does not seem to be appropriate for this type of analysis. The Malat wavelet analysis has its particular component representation and, as a consequence, is somewhat difficult to interpret. The Malat wavelet of one level is not associated with physical phenomena in a clear way. The physical meaning of one wavelet level is not straightforward, as is the case for the Fourier harmonic representation, and a new way to interpret it is required. As we can see in Figure 3.5(h), this technique recovers the original signal faithfully. However, the difference between what is stationary and what is non-stationary in the levels is not explicit. This makes it difficult to apply any complementary technique to separate the deterministic components.

We sought to overcome the difficulty of handling non-stationary components in the original Prony procedure by substituting the covariance method of linear prediction

(represented by the equations (2.34) to (2.37)), which determines the initial set of AR parameters in the first Prony step, for an adaptive algorithm such as the Kalman filtering technique (represented by the equations (2.38) to (2.40)). However, this did not improve the deterministic component detection (see Figure 3.7). The recursive based technique seems to present difficulties when operating with noise. Its respective time-frequency plane representation of a signal containing high levels of noise presents points which are randomly scattered (see Figure 3.7). The degree of freedom given to the time parameter in the recursive based technique (see equations (2.38) to 2.40)) permits the method to detect non-stationary processes, and thus several spurious components that are represented by a small quantity of data, such as noise components, are detected. In the recursive based technique, the number of data points is less than the order used to perform the calculations of the method (note the indices of the equation (2.38)). As the larger the number of data points per sample the greater the probability to detect deterministic components, the limitation in the number of data points per sample of the recursive based technique makes it inefficient for stationary analysis.

5.1.3. Application of Averaging and other Statistical Methods after Signal Filtering Using the Extended Prony Time-Frequency Representation

The average of Fourier transforms of the signals recovered and filtered using the extended Prony time-frequency representation (see Figures 3.100 to 3.104), reflects the capacity of the extended technique to detect amplitude variations of a specific component. However, it must be pointed out that the variation is not clear all the time. In the Fourier transform waterfall graph of Figure 3.99 (b), some sets of filtered and recovered data points suggest that an inverse condition occurred (32 % of the cases). Instead of pointing, correctly, to an increase in the 58 Hz component amplitude value, a decrease is shown. There are some peaks of the waterfall graph (a) that are greater than some peaks in waterfall graph (b). This points to the necessity of averaging the results in order to depict the correct peak variation. The filtering

process of the extended Prony time-frequency representation removes the limitations of applying signal averaging processing or any other similar statistical method, because a great part of the noise and the non-stationary components are eliminated.

5.2. Comparison of the Extended Prony Time-Frequency Representation Applied to Simulated and Experimental Data

As we mentioned above, due to limitations of time, site location and resources, a rig was constructed to represent the conditions of a petroleum well for the experimental analysis. The Queen's Tower experiment sought to demonstrate what to expect in terms of measurable results when the vibration signal is collected at some considerable distance from the equipment. Although we would have preferred a more authentic model on which to carry out experiments, the data generated by the Tower model has served the purpose of this study.

The experimental results of Chapter 4 show that in all cases the amplitude variation of the 58 Hz weak component was detected by the extended Prony time-frequency representation. This is demonstrated in the graphs of Figures 4.19, 4.21, and 4.22, where the weak component amplitude peaks of signals E2, E4, and E6 are greater than those of the signals E1, E3, and E5. However, it is difficult to detect the 58 Hz component amplitude variations in the signal S13 with the simulated fluid slug vibration component added (see Figure 3.99). Comparing the graphs of Figures 4.19, 4.21, and 4.22 of Chapter 4 with the graphs of Figure 3.99 of Chapter 3, it may be noted that greater differences in the 58 Hz component amplitude values are encountered when the 58 Hz component amplitude is doubled in the signals with slug component generated at the Tower rig (signals E1 to E6 described by the Table 4.3 of Chapter 4) than when the 58 Hz component is doubled in the simulated signals (signals S13 to S20 described by the Tables 3.18 and 3.19 of Chapter 3). This can be seen in the graph of Figure 3.99 (see Chapter 3) of the analysis using signals containing fluid slug vibration generated in the simulation. The waterfall graphs of

Figure 3.99 reveal that several sets of data points of the signal containing the 58 Hz component with greater amplitude were represented with lower peaks (32 % of the waterfall lines). In this case, it is easier to note which amplitude component increased if a spectrum average is performed. The discrimination difficulty of the 58 Hz component amplitude variation did not occur in the analysis of the signals containing slug components generated in the Tower experiment (100 % correct peak discrimination) because it is less problematic to filter the deterministic components using the extended Prony time-frequency representation in this case. An explanation for the less problematic deterministic component filtering may be given by observing the graph of Figure 4.25 of Chapter 4 that shows the extended Prony time-frequency representation of the signal with the pure fluid slug vibration generated in the Tower experiment. The signal generated in the Tower experiment contains components mostly around 90 Hz, which may be eliminated by a high-pass band filter (see Figure 4.25).

5.3. Possible Outcome of Applying the Extended Prony Time-Frequency Representation to Live Signals

We have seen in the Chapter 4 that the experimental signals E1 to E6 have been generated to represent some relevant components that exist in the real vibration signals collected from the wellhead. These relevant components include: the 58 and 60 Hz deterministic components, the non-stationary fluid slug vibration component and the background noise introduced by the environment of a petroleum sea platform in the pipe network. Because of the limitations of our simulation and experiment to reproduce a completely realistic representation, it is necessary at this point to speculate as to what is expected to occur when the extended Prony time-frequency representation is applied to the signals collected in a petroleum wellhead.

The three types of experimental noise generated by the HP-35565A analyser added to the experimental signals of Chapter 4 (signals E1 to E6), cover a wide range of noise

situations that may be expected in the live signal and provide a fair number of signal test conditions for the extended Prony time-frequency representation, although, of course, the actual number of possible components found in the sea platform environmental noise is much larger. This is not the case of the fluid slug vibration, which has been studied widely due the fact that these vibrations cause strong shocks that may destroy well-reinforced pipe manifolds.

As some difficulty occurred when processing simulated signals containing a fluid slug vibration similar to those described in the work of Leducq [1991], which resemble real petroleum well fluid slug vibration components, one should expect to experience difficulties when filtering out real petroleum well fluid slug vibration components. This may be due to the fact that the real petroleum well fluid-slug vibration present more random behaviour than those simulated in controlled conditions.

The results of the analysis using the experimental signals, E1 to E6, shown in the graphs of Figures 4.19 to 4.24 indicate that the variations in the 58 Hz component amplitude have been clearly detected in the experimental signals, which contain a fluid slug vibration component generated in the Tower experiment with three types of noise (100 % of the cases). This did not happen in the analysis of simulated signals S13 and S14. The waterfall graph of Figure 3.99 presents 58 Hz weak component amplitude peaks that are incorrectly reduced in 32 % of their waterfall lines. This different degree of difficulty in the analysis of signals containing two types of slug vibration (simulated and experimentally generated) and practically no influence associated with different noises (see for example the analysis of the simulated signal S3 in the section 3.3.3 of Chapter 3), indicates that it might be more difficult to filter out the real petroleum well fluid slug vibration than the uncorrelated environmental high-level noise of the platform. Taking into consideration the existence of a variety of conditions that generate different fluid-slugs in the real petroleum well, there clearly still persists a degree of difficulty with live signal analysis. However, overall results suggest that significant advances have been made with the development of the

extended Prony time-frequency representation, to be speculate that the technique will be satisfactory for ESP failure detection.

5.4. An Experimental Comparison

Arguably, a valid comparison can be made between the results of Moore's study [1990], where the Fourier technique were applied to the vibration signals of an ESP (see section 1.4 of Chapter 1), and this study, where the extended Prony time-frequency representation has been applied. Moore installed an ESP at a depth of 38 metres to simulate several types of wear, and accelerometers were placed on the pump and at the wellhead. Although the Tower experiment of this study is limited in terms of simulating the various problems to be found in an ESP, the fact that vibration data was collected from an accelerometer located 39.13 metres from the source, means that some tentative conclusions can be drawn from the experimental data.

It has been demonstrated with the above results that the Fourier technique used in this study is limited for handling signals containing noise and non-stationary processes, but what is more to the point in regard to this comparison, is that in Moore's findings four weeks before the pump failed, data gathered from the accelerometer attached to the pump revealed an increase of between 30 to 60 times in the amplitude of the rotational vibration. When these findings are compared with those in this study, where variations of two times in the 58 Hz component amplitude were identified in experimental signals containing strong spurious components (SNR varying from -40 dB to -34 dB), it becomes apparent that it would be arguably less problematic for the new extended Prony time-frequency representation to deal with such a large variation as that found in Moore's study in a real ESP.

5.5. Some Limitations of the Extended Prony Time-Frequency Representation

One problem found with the extended Prony time-frequency representation is that it is difficult to determine exactly the differences in amplitude between different frequencies, as may be noted in the graphical values evaluated for 58 and 60 Hz frequencies, using signals S13 and S14 in section 3.9 of Chapter 3. In some instances, the amplitude values evaluated for the 60 Hz frequency component are lower than those evaluated for 58 Hz, which is not correct. This problem may be caused by the incorrect elimination of some time-frequency plane points which are associated with stationary components, but as they have an exponential damping level slightly above the cut-off level (0.02 s^{-1}) in the exponential damping filtering procedures, they have been deleted.

A second criticism of the method concerns the time involved for the numerical calculations. For example, to evaluate an entire extended Prony time-frequency representation, which uses the original Prony method to compute its frequency lines, may take up to 10 times longer than when using the Wigner-Ville distribution. Much of the time needed for the calculation for the original Prony procedure is taken in the second step, where the roots of large complex polynomials are evaluated. However, with the developments of new computers significance of this drawback will be diminished.

5.6. Summary and Conclusion of the Discussion

An essential feature of the extended Prony time-frequency representation has been shown to be the capacity to differentiate what is stationary from what is non-stationary in a signal. The incorporated feature of evaluating the level of signal component exponential damping to analyse transients of the extended Prony time-frequency representation is an effective tool for filtering purposes, and the decision to

treat non-stationary processes as transients has also proved to be effective. We have also seen that the extended Prony time-frequency representation has proved to be a successful method for detecting weak components in signals containing high levels of noise (maximum SNR = -34 dB and minimum SNR = -40 dB for the experimental signals E1 to E6), as well as being suitable for filtering and recovering signals for further analysis using less complex techniques such as the Fourier transform. A further feature of the extended Prony technique is the convenience of the frequency bandwidth filtering through a time-frequency plane "band-selection", as described in section 3.6 of Chapter 3. A frequency bandwidth to filter a signal may be chosen directly by observing the results in the time-frequency plane. This is particularly advantageous when attempting to identify the correct frequency of a deterministic component in a signal.

Until the present time, most research on signal processing has considered a non-stationary process as being composed of several short stationary ones [Bendat and Piersol, 1986]. Apart from Mars et al [1992], who applied an autoregressive method, very few research programmes have developed more suitable methods to analyse short-duration phenomena, and it is unclear why the majority of non-stationary analysis research is based on the Fourier transform method, when it is manifestly an inappropriate technique for this task. In the comparative analysis of section 3.4 of Chapter 3, apart from the Gaussian wave signal analysis, the results of the extended Prony time-frequency representation demonstrate that this method is clearly superior to the Morlet wavelet transform, Wigner-Ville and pseudo-Wigner-Ville distributions in analysis of non-stationary signal components. This is not to say, however, that with these results, the extended Prony time-frequency representation is suited to analyse all types of non-stationary processes. Nevertheless, given that this technique is designed specifically for analysing transients, and the practicability of considering non-stationary processes as transients, it is considered to be a good option for the analysis of these processes.

Chapter 6
Summary and Conclusion of the Study

6.1. Summary of the Results and Observations of this Research

The results of this study demonstrate that the extended Prony time-frequency representation is more effective for detecting weak components in signals containing strong spurious components, such as high-levels of noise and non-stationary fluid slug vibration components, than the Fourier transform, the Morlet wavelet transform and, the Wigner-Ville and the pseudo-Wigner-Ville distributions. In 66 % of the simulated signals (S1 to S12) it proved to be the best method to represent the signal components. A 70 % success rate was also obtained in detecting weak component amplitude variations, measured directly in the data signal sets (e.g. numerical results plotted in the graph of Figure 3.99 for signals S13 and S14). A maximum set with 1023 data points containing strong spurious components such as high-levels of noise and non-stationary fluid slug vibration components (SNR = - 34 dB) were used in the simulation of Chapter 3.

The results also show that the component exponential damping values, computed by the extended Prony time-frequency representation, are useful to distinguish non-

stationary components, those which are more heavily damped than the deterministic ones. Furthermore, the extended Prony time-frequency representation is able to depict the non-stationary components reasonably well. However, in some specific cases of non-stationary component analysis, such as in the signal containing the Gaussian waves (see section 3.5.4), the pseudo-Wigner-Ville distribution and the wavelet transform may still be marginally better than the extended Prony time-frequency representation.

With regard to the wavelet transform developed by Malat, this does not seem to be appropriate for analysing vibration signals containing harmonic components. The difference between what is stationary and what is non-stationary in the levels is not explicit. This makes it difficult to apply any complementary technique to separate the deterministic components.

It was shown above that the use of an adaptive algorithm such as the Kalman filtering technique in the first step of the extended Prony time-frequency representation did not improve the deterministic component detection. The recursive based Kalman filtering technique seems to present difficulties when operating with high-level noise (SNR - 34 dB).

The original Prony procedure normally requires a considerable amount of calculation time, and a great bulk of the procedure is consumed in the second step in which the roots of large complex polynomials are evaluated. It was shown that a defined short bandwidth is still necessary for component level comparison after the filtering of high-level spurious components through the extended Prony time-frequency representation (successful results were obtained considering a 10 Hz frequency bandwidth). However, the method is able to depict a signal containing a component that represents the rotation of an ESP under variable load (frequency component varying in the 56/59 Hz bandwidth - see the graphs of Figures 3.86 and 3.92), but the results still show some distortion.

The difficulty of detecting amplitude variations of the 58 Hz weak component in some simulated and experimental signals points to the necessity of averaging the results in order to depict the correct peak variation. This process of averaging, or any other similar statistical method, is not restricted by such factors as noise and non-stationary components as they are mostly eliminated in the extended Prony time-frequency representation signal filtering process.

With regard to filtering strong spurious components, such as those in signals containing two types of slug vibration (simulated and experimental) and the three different experimental types of noise, it was shown that greater difficulty can be expected when filtering out the real petroleum well fluid slug vibration compared with the uncorrelated environmental high-level noise of the platform.

Finally, this study revealed that the optimum value for exponential damping level filtering, for selecting what is stationary and what is non-stationary, is 0.02 s^{-1}. However, due to the noise disturbance, the component exponential damping levels will not correspond exactly on all subsequent occasions. The value of 0.02 s^{-1} seems to be adequate for differentiating deterministic components from fluid-slug vibration, as well as the three types of noise that composed the experimental signals. As a consequence, this exponential damping value may be used as a starting point for filtering out fluid-slug vibration using the extended Prony time-frequency representation. It should be noted that the exponential damping value of 0.02 s^{-1} is only relevant for the signals in this study, other signals my require their own specific exponential damping levels.

6.2. Conclusions and Contributions of this Research Study

In this study, a series of signal processing methods have been tested by means of several simulated and actual experimental signals collected by remote transducers. The main objective of the research was to provide a methodology with which to

detect variations in weak deterministic components in vibration signals in which high-level noise and non-stationary components are present, with the ultimate aim of diagnosing the condition of inaccessible machinery.

In the course of this research study to analyse equipment though remote transducers, three major research tasks were accomplished in the area of signal processing. These are:

(1) the development of an extended time-frequency processing technique based on the original Prony method to detect weak component amplitude variations in signals containing strong noise and non-stationary components (maximum SNR of -34 dB and a minimum of -40 dB for experimental signals E1 to E6).

(2) a systematic comparison of the extended Prony time-frequency representation with four other signal processing techniques: the Fourier transform, the Morlet wavelet transform, the Wigner-Ville distribution, and the pseudo-Wigner-Ville distribution (see Chapters 2 and 3) based on 12 carefully-designed simulated signals; and finally,

(3) the construction of a scale-model of an ESP installation with which to generate experimental data for the extended Prony time-frequency representation to be applied (see Chapter 4).

In relation to the first research task, the original Prony method has successfully been extended to create a time-frequency representation that can handle both stationary and non-stationary components in the presence of high-level noise. It was also demonstrated that the extended Prony time-frequency representation can be used in non-stationary analysis with satisfactory results, as well as for analysing non-stationary processes as transients. The adaptation of a technique based on an autoregressive class of method, which is also specialised in the analysis of transients, is the main contribution of this research work. The positive overall results of this

study suggest that the method is an efficient tool for detecting weak components in signals in which both these processes are present.

Based on the results of this study, it appears that the extended Prony time-frequency representation is capable of analysing signals collected in a petroleum wellhead, and is therefore arguably a major contribution to existing ESP performance analysis.

Finally, it is argued that the theoretical and methodological work carried out in this study will prove relevant for other areas of enquiry into noise reduction, non-stationary signals analysis and fault detection of different types of equipment.

6.3. Suggestions for Further Research

Further research in the analysis of fluid effects on wave transmission would be beneficial to infer how a specific equipment vibration signature will be distorted by these effects. The distortion in the wave transmission by the fluid effects may lead to complimentary techniques. Also, since the wave propagation in a fluid-filled pipe, as in the case of a petroleum well, involves coupled motions of the solid and fluid components, an investigation needs to be made in order to determine to what extent the fluid will absorb the wave energy.

Although positive results were obtained using simulated vibratory signatures, the methodology developed in this study still requires testing in the detection of amplitude variations of weak components present in noisy live signals, different from ESP signals collected in the petroleum wellhead. For example, in this research, a successful filtering elimination could be made considering components whose exponential damping value exceeded the level of 0.02 s^{-1} as non-stationary and noise processes. This value may not be adequate for signals containing non-stationary processes different from that considered in this research (fluid-slug vibration). An incorrect choice of the exponential damping level in a signal filtering operation may eliminate a relevant weak component which one wishes to

monitor. The component exponential damping level is evaluated by the original Prony method considering an exponential decay of the kind e^{-ct} , where c is the exponential damping of the component (see equation (2.22) of Chapter 2). This exponential decay assumption is not valid for all transients. If a signal contains transients which present an amplitude decay that cannot be modelled as an approximation of an exponential decay, an error may occur in the exponential damping filtering selection. Thus, to compliment research in this work a tool needs to be developed to determine the level of component exponential damping that may be associated with different kinds of non-stationary processes, and to determine how far the exponential decay model for exponential damping can be considered adequate to processes, different from the fluid-slug vibration and noise components analysed in this study.

Another related area concerns the definition of the optimum quantity of data points for non-stationary and deterministic component detection. As a starting point, this research study used 128 to 512 data points per sample if deterministic components detection was desired, and from 4 to 32 data points per sample if non-stationary processes was desired. A better signal analysis may be achieved if a new automatic statistical tool, incorporated in the extended Prony time-frequency representation, could determine the optimum quantity of data points to analyse both stationary and non-stationary processes that are present in a signal. This statistical tool may substitute, with advantage, the use of the order loop reduction in the computer program to set the order of the original Prony method, which is central to the extended Prony time-frequency representation. That is, when the quantity of data points is reduced, the order is automatically reduced due to the reduction in the rank of the matrices of the original Prony method which is the basis for the extended Prony time-frequency representation. The choice of quantity of data points to analyse is related to a "degree of non-stationarity" that a set of data points presents, and it will not restrict the "search" for any component, even for the deterministic ones.

Finally, further considerations could also be given to the spurious components added to the simulated and experimental test signals, which are not interdependent processes. The fluid-slug vibration generated in the simulation and in the experiments do not have a

relationship with the noise, or with the 58 Hz weak component, neither does the real petroleum fluid-slug vibration have a relationship with the platform noise. Sometimes a live signal contains dependent processes, an example being the noise generated by a mill which is related to its rotation. As there exists a large number of possible process dependency conditions, which are not relevant for this study, several tests are required to observe the behaviour of the extended Prony time-frequency representation in processing signals containing such dependent components.

Appendices

Appendix A - Prony Results from Platform of Vermelho

Sample number = 512	Order = 96	Pos. peak = 10.20 m/s2
Time window = 1.0 s	Covariance error = 0.19E-03	Neg. peak = - 11.18 m/s2

FREQUENCY (Hz)	DAMPING (1/s)	AMPLITUDE (m/s2)	PHASE (degrees)
7.45E-14	-1.06E-02	5.32E-01	269.9906
7.16E-13	-5.24E-02	3.75E-01	89.96252
5.308484	-3.78E-02	1.15E-01	194.9925
15.16509	-2.94E-02	5.39E-01	123.7895
17.39938	-1.16E-02	2.24E-01	225.5116
25.62237	-1.13E-02	1.30E-01	142.1156
32.88338	-2.59E-02	3.10E-02	41.50234
37.01711	-1.25E-02	3.76E-01	-87.19909
40.86618	-2.99E-02	6.24E-02	56.36644
47.77416	-1.01E-01	2.06E-01	118.14
49.45403	-5.98E-02	2.00E-02	-43.2008
57.15440	-4.38E-03	2.13E-01	103.8865
61.94883	-1.14E-02	7.22E-01	150.7605
67.58185	-1.48E-02	3.69E-01	-34.04441
70.38882	-1.51E-02	9.84E-01	92.33857
75.57373	-4.87E-02	1.47E-01	183.9954
83.74615	-1.97E-02	2.95E-01	183.0363
87.61118	-1.38E-02	2.26E-02	168.1376
93.68661	-1.06E-02	2.65E-02	214.5848
96.93795	-4.73E-02	3.71E-01	-66.76524
105.2552	-9.21E-05	7.48E-03	2.294213
111.0353	-9.58E-03	3.19E-03	114.424
116.1445	-7.80E-03	1.36E-01	3.637527
121.7553	-5.37E-03	1.42E-01	-5.672506
126.3900	-2.48E-02	5.87E-01	65.57542
130.9755	-3.92E-02	6.27E-01	159.9624
139.5112	-2.37E-02	2.79E-02	151.6044
144.2285	-2.63E-02	9.29E-03	-72.16124
150.8704	-1.95E-02	1.82E-01	80.43964
153.7809	-9.35E-03	2.58E-02	188.5381
159.9329	+1.44E-04	1.09E-01	140.419
166.7486	-2.86E-02	7.72E-02	168.331
167.8112	-1.89E-02	4.43E-01	-27.9339
174.7984	-1.54E-02	1.19E-02	154.53
181.3717	-2.87E-02	1.99E-02	197.9804
186.6613	-7.80E-03	1.28E-01	249.0752
192.3689	-1.65E-02	1.61E-01	186.7659
197.4547	-1.37E-01	1.17E-01	247.1871
199.1472	-2.05E-02	1.84E-02	262.0139

Appendix B - Technical Drawings of the Tower Supports

Upper Support Technical Drawing

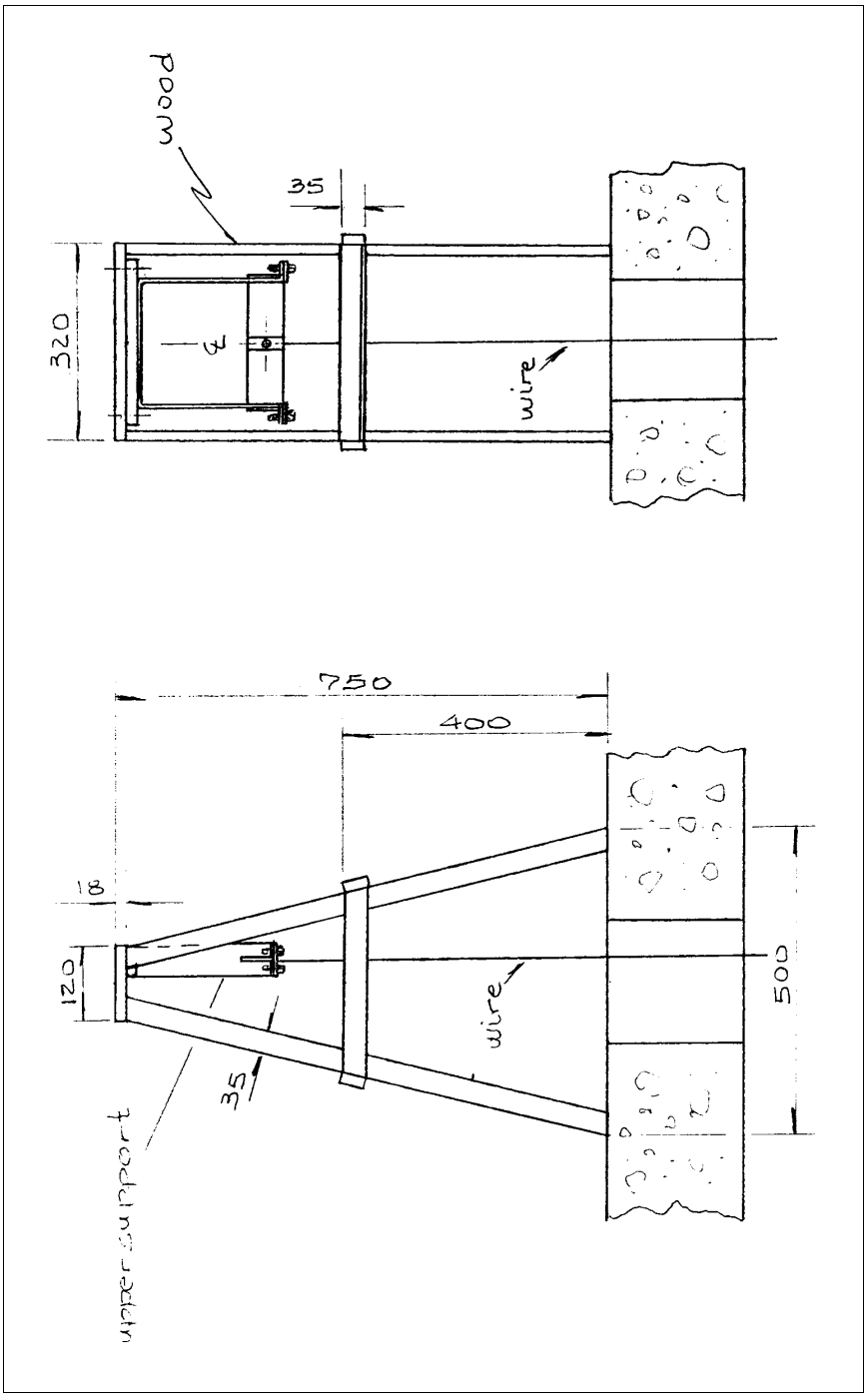

Lower Support Technical Drawing

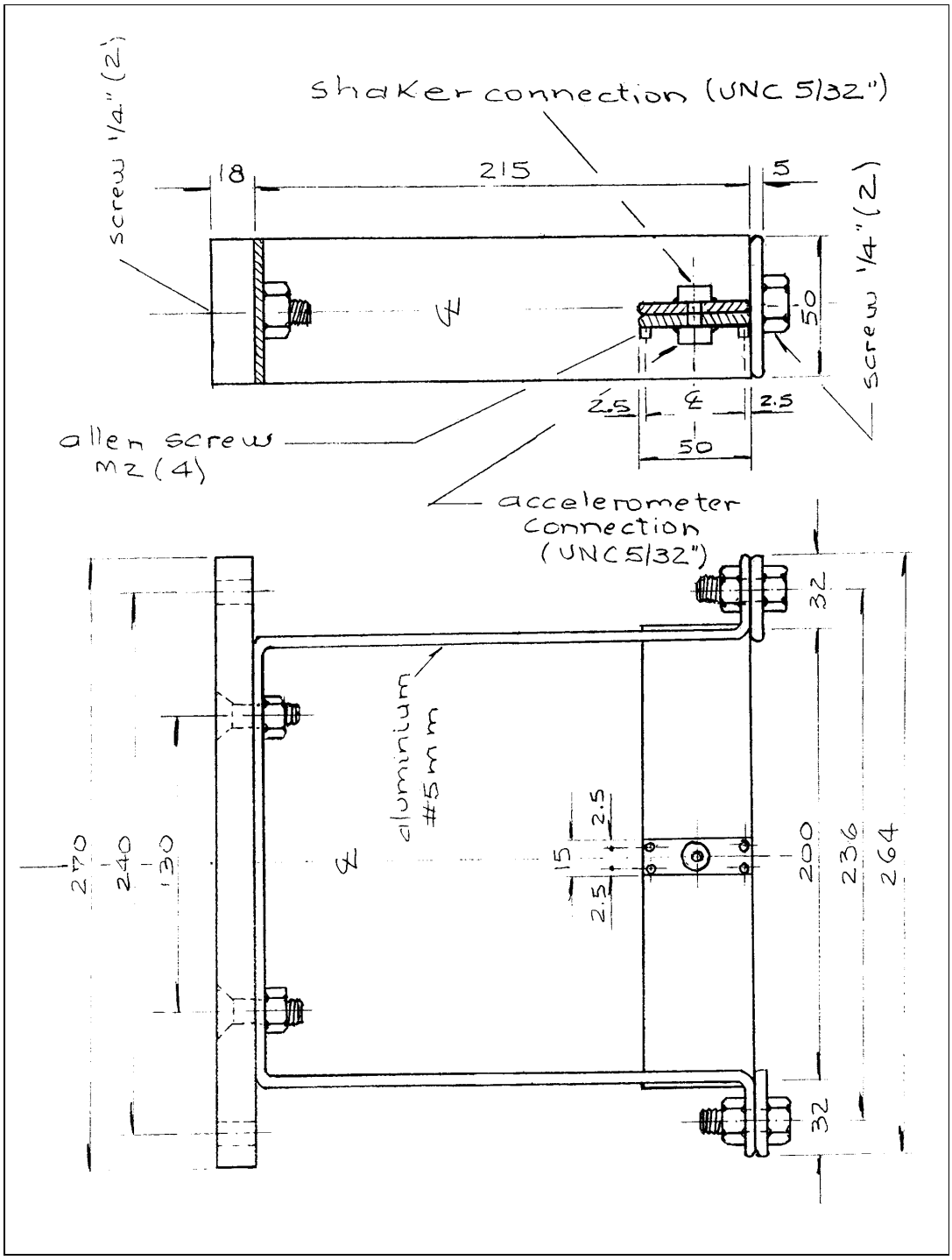

Appendix C - Theoretical Assumption for the Signal-to-Noise Ratio (SNR)

In this study, signals containing high-level noise and strong non-stationary processes together with deterministic components were prepared to represent, as near as possible, a live signal collected at the petroleum wellhead. For this purpose it was necessary to estimate a SNR for applying to the simulated signals in Chapter 3.

Preliminary data collection carried out on Brazilian sea platforms in a previous study by Ribeiro [1991] showed that the typical signal to be analysed contains strong spurious components that can reach 100 times the weak ESP vibrations. However, due to the lack of information about the ESP vibration amplitude value, an initial assumption, based on a theoretical model, will be made to estimate the amplitude values of the ESP rotation vibration (58 Hz) where the signal is transmitted through the petroleum pipe and collected at the wellhead. Another weak component present in the signal collected at the petroleum wellhead is related to the electric power supply frequency (60 Hz in Brazil), which is normally associated with the presence of some electrical equipment near the petroleum wellhead. As mentioned above, the strong spurious components present in the signal refer to high-level noise and fluid slugs. The high-level noise encountered in the platform signals is generally associated with equipment used there, such as turbines, pumps, electrical panels, gear boxes etc. In addition to the excitations generated by these equipment, a large number of vibrations come from natural frequencies of several structures (pipes, manifolds, beams etc.) that exist on the platform. Due to the large frequency span of a sea petroleum platform noise, a white noise will be used to represent this in the simulation.

To estimate the attenuation in the amplitude level due to damping in the ESP vibration pipe transmission, a theoretical model of the real petroleum well installation has to be made. For the purpose of the simulation of Chapter 3, it will be assumed that waves are generated on the lower extremity of the pipe, where a weight ***W*** is fixed, and propagated through the vertically-positioned flexible pipe. As may be noted in the diagram of Figures 1.3 (see section 1.2 of Chapter 1) and 4.10 (see section 4.2 of Chapter 4), in the case of a real petroleum wellhead, virtually no compression waves are being transmitted through the wellhead rigid joint support. Only the amplitude of transverse waves are transmitted through a mechanical moment component due to the high stiffness of the tubing. As a consequence, only transverse waves will be considered in this SNR theoretical assumption. In Figure C.1 a schematic diagram is shown of the theoretical model.

In the model shown in Figure C.1, no sharp distinction is made between what is meant by a bar and what is meant by a string. In general, tension is more important as a restoring force than stiffness for a string, and stiffness is more important for a bar [Morse and Ingard, 1968]. As very long bars are being used, the ideal system will consist of a string under tension with stiffness.

Therefore, an evaluation of the vibration transmission will be made by constructing a mathematical model which represents a vertical pipe in terms of a system composed of several strings with stiffness ***k***, and length ***l***. Figure C.2 shows a schematic diagram of this model.

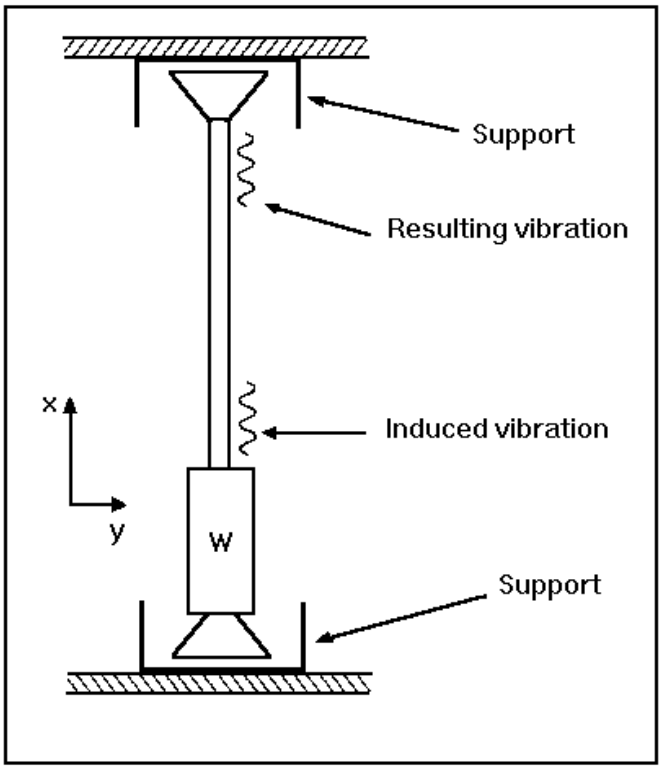

Fig. C.1 - Idealised system in analysis

The lateral stiffness of each element can be obtained from the beam deflections formulas taken from Roark [1954] and Griffel [1970].

The stiffness which represents the element that is fixed in the upper support, is [Roark, 1954, Griffel, 1970]:

$$k_{y1} = \frac{T}{l - 2\sqrt{EI/T} \cdot \tanh\left(l\sqrt{T/EI}\right)} \qquad \text{(C.1)}$$

The stiffnesses of the rest of the string elements are [Roark, 1954, Griffel, 1970]:

$$k_{y2} = \frac{T}{l/2 - \sqrt{EI/T} \cdot \tanh\left(l/2\sqrt{T/EI}\right)} \qquad \text{(C.2)}$$

where

k_{y1} = Stiffness of the fixed wire element (upper support, N/m)

k_{y2} = Stiffness of the rest of the string elements

E = Modulus of elasticity (N/m^2)

I = Second moment of inertia (m^4)

l = length of a wire element (m)

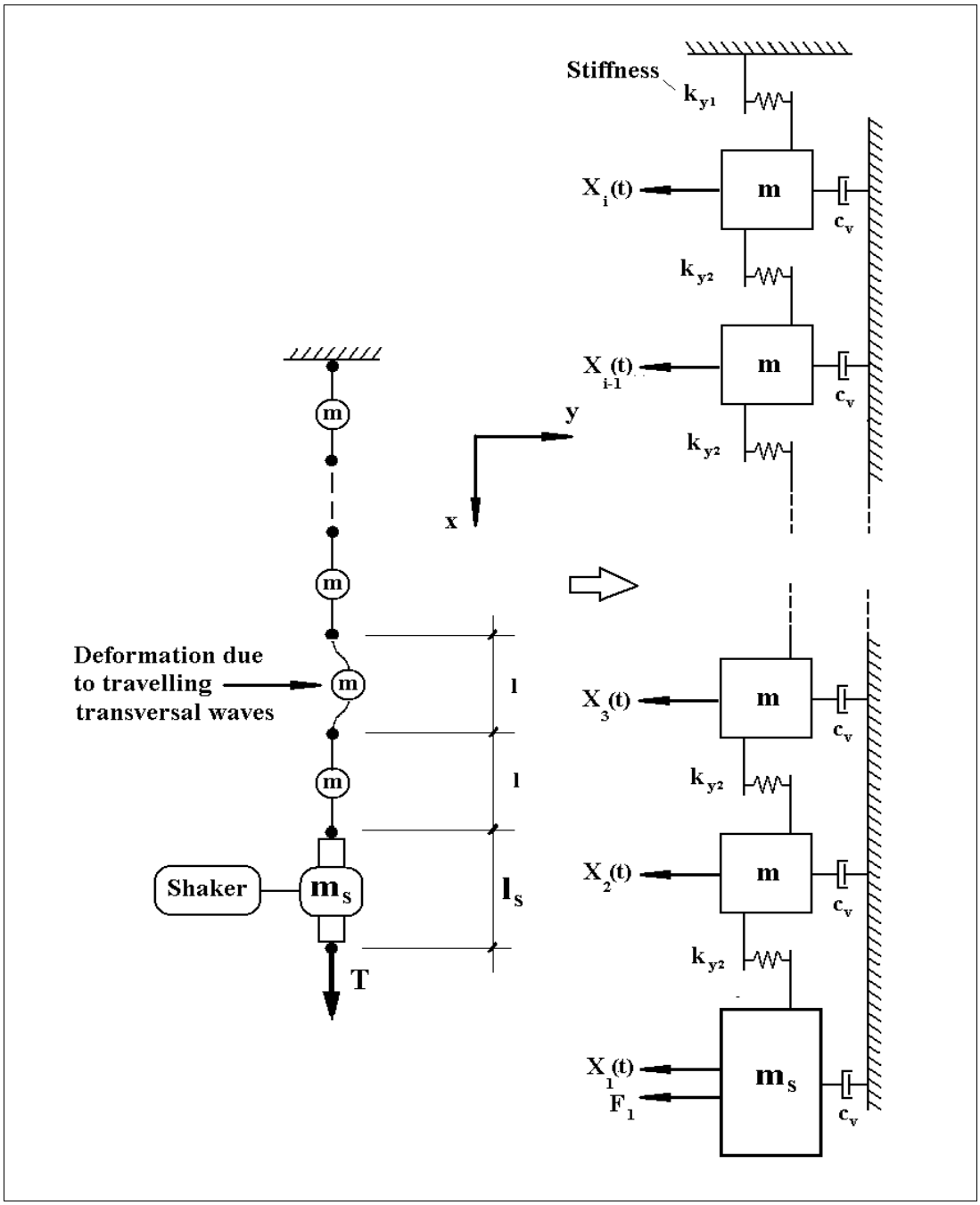

Fig. C.2 - Schematic diagram of the stiff string model analysis

The equations (C.1) and (C.2) may be used to define the elements of a matrix that represents the transverse stiffness of the entire string. The bending stiffness matrix, considering two degrees-of-freedom for each element is [Broughton and Ndumbaro, 1994, Crawley et al, 1993, and Lardner et al, 1994]:

$$[K] = \begin{bmatrix} k_{y1} & -k_{y2}/2 & 0 & \cdots & \cdots & 0 \\ -k_{y2}/2 & k_{y2} & -k_{y2}/2 & 0 & \cdots & \vdots \\ 0 & -k_{y2}/2 & k_{y2} & -k_{y2}/2 & \cdots & \vdots \\ \vdots & 0 & -k_{y2}/2 & \ddots & \ddots & 0 \\ \vdots & \vdots & 0 & \ddots & k_{y2} & -k_{y2}/2 \\ 0 & \cdots & \cdots & 0 & -k_{y2}/2 & k_{y2} \end{bmatrix} \qquad \text{(C.3)}$$

The mass matrix ***[M]*** is:

$$[M] = \begin{bmatrix} m & 0 & 0 & \cdots & 0 \\ 0 & m & 0 & \cdots & \vdots \\ \vdots & 0 & \ddots & \ddots & \vdots \\ \vdots & \vdots & \ddots & m & 0 \\ 0 & \cdots & \cdots & 0 & m_s \end{bmatrix} \qquad \text{(C.4)}$$

where m is the mass of each element (kg) and m_s is the mass of the lower support element (kg). Assuming proportional viscous damping for a simplified model, a suitable damping matrix may be represented by:

$$[C_v] = \begin{bmatrix} c_v & 0 & 0 & \cdots & 0 \\ 0 & c_v & 0 & \cdots & \vdots \\ \vdots & 0 & \ddots & \ddots & \vdots \\ \vdots & \vdots & \ddots & c_v & 0 \\ 0 & \cdots & \cdots & 0 & c_v \end{bmatrix} \qquad \text{(C.5)}$$

where c_v is the proportional viscous damping of each string element (kg/s), and $[C_v]$ is damping matrix of the system.

The receptance $[H(w)]$ of the system is defined as [Ewins, 1995]:

$$[H(w)] = ([K] + iw [C_v] - w^2 [M])^{-1} \quad \text{(C.6)}$$

The equation (C.6) may be used to generate theoretical data to obtain an estimate of what to expect in terms of amplitude values for the ESP rotation component.

A 2 7/8 inch diameter petroleum pipe of 1000 metres length composed of 100000 elements each of 0.01 metres was set to evaluate numerically the amplitude attenuation of waves due to the proportional viscous damping in the 0 to 100 Hz of frequency bandwidth. An approximate damping ratio value of 0.01 for steel [Lazan, B. J., 1968] was used to evaluate the proportional viscous damping value c_v. The results of the numerical computation using the equation (C.6) are shown in the graph of Figure C.3. The graphs (a) and (b) of Figure C.3 show the calculated values for receptance versus frequency measured at the distances of 0 and 1000 metres from the point at which a transverse dynamic force of 1 N was applied on the lower extremity of the 1000 m long pipe. The graph (c) of Figure C.3 shows the results of the calculated values for amplitude ratio X_i/X_1.

The average of the amplitude ratio due to the proportional viscous damping for 57/61 Hz waves transmitted through this model in a 1000 metre length of pipe, taken from the calculated values (see graph (c) of Figure C.3), is 52.12 times. Based on these results of the numerical computation, a 58 Hz component amplitude value 50

times lower than the strong spurious components was utilised in the simulation of the live signal (SNR -34 dB).

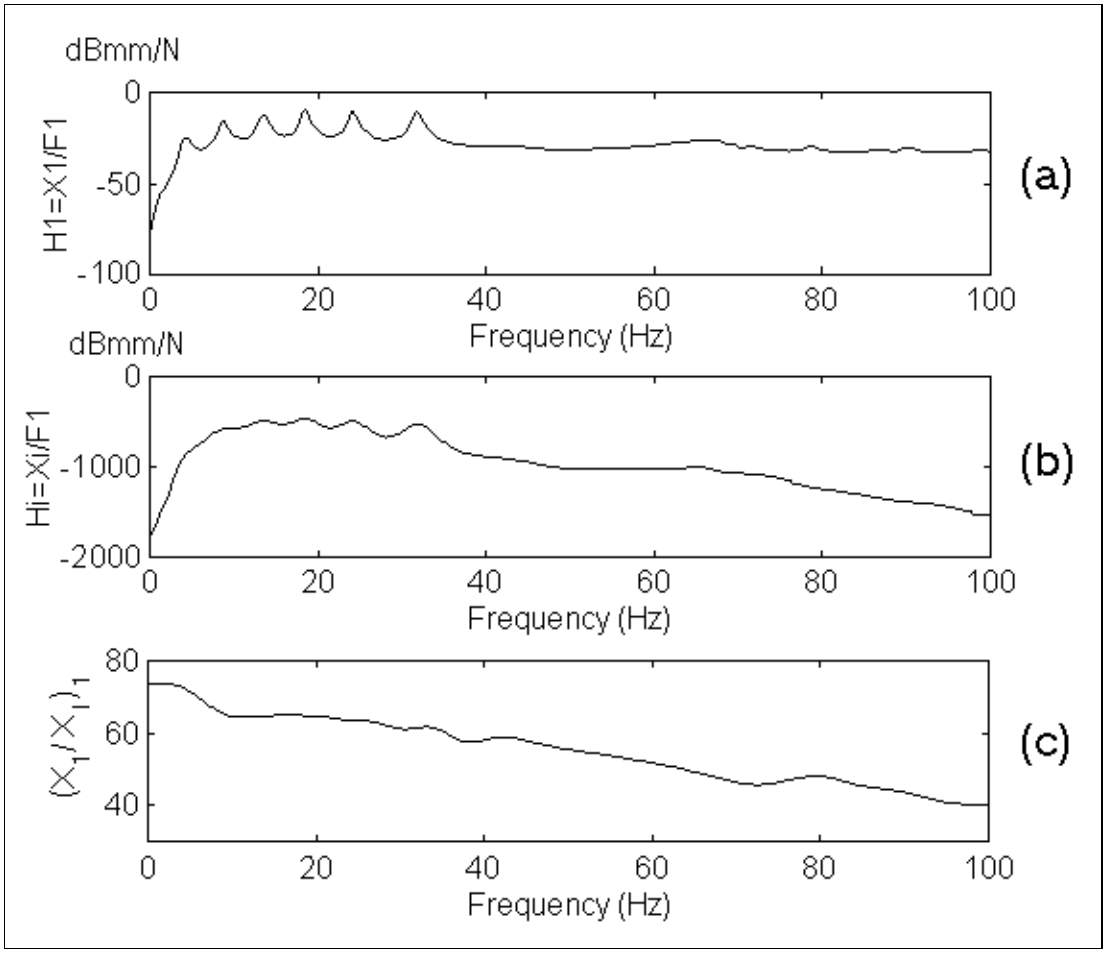

Fig. C.3 - Receptance at 0 (a) and 1000 m (b) of height or pipe length, and amplitude ratio ($\boldsymbol{X_i/X_1}$ - (c)) between 0 and 1000 m

Appendix D - Kaiser-Bessel Window

The Kaiser-Bessel window applied to generate the pseudo-Wigner-Ville distributions in this study is defined as:

$$B_{(n,b)} = i^{-n} J_n(i x) e^{-b} \tag{E.1}$$

where $J_n(i\ x)$ is a Bessel function of first kind, and b is referred as the exponential argument of the Kaiser-Bessel window. The greater the exponential argument the narrower the Kaiser-Bessel window [Chiollaz and Frave, 1993]. The Kaiser-Bessel window has been applied in this study through a MATLAB computer routine. The graph of Figure E.1 shows two Kaiser-Bessel windows of 512 data points, and exponential arguments 70 and 2, used in this study.

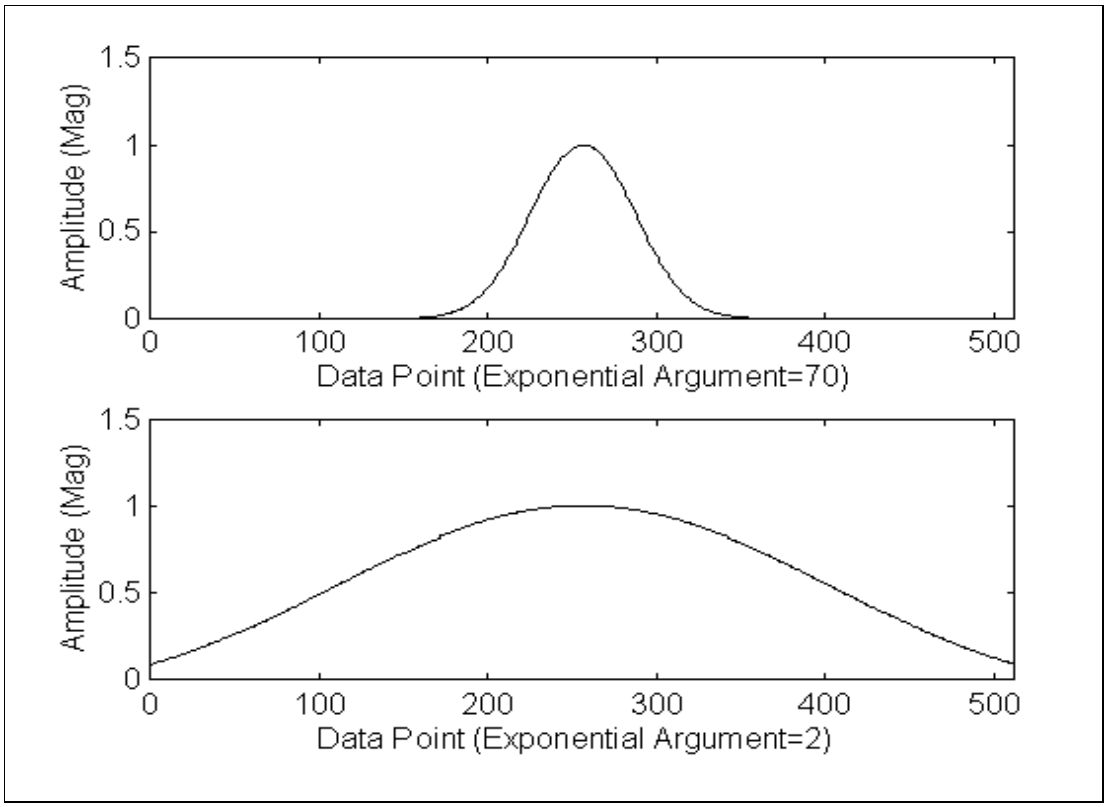

Fig. E1 - Kaiser-Bessel windows

References

ALIEV, I. M., "Investigating Method of Acoustic Oscillations of Electrical Submersible Pumps", Materiaili Resp. Nauchnoe Konferentsii Aspirantov, Baku, ed. AzNIPIneft, p. 46-49, Portuguese Translation, 1982.

BARSCHDORF, D., FEMMER, U., "Signal Processing and Pattern Recognition Methods for Biomedical Sound Analysis", Acoustical and Vibratory Surveillance Methods and Diagnostic Techniques, 2nd International Symposium, CETIM, France, p. 279-290, 10-12 October 1995.

BAYLAC, G., BAI, D., GREGOIRE, J. P., "Study of Flow and Acoustic Phenomena in a Tube Bank", Vibration Problems in Industry, Symposium Proceedings, Session 2, Keswick, 1973.

BENDAT, J. S., PIERSOL, A. G., "Random Data, Analysis and Measurement Procedures", 2nd. edition, John Wiley & Sons, Inc., 1986.

BENEDEK, S., "Fluid Vibration Induced by A Pump", Journal of Sound and Vibration, vol. 177, no. 3, p. 337-348, 1995.

BIGRET, R., DE SLOVERE, P., HAYS, G., LASSOUED, M., "Applications Industrielles de La Transformee de Wigner-Ville", Acoustical and Vibratory Surveillance Methods and Diagnostic Techniques, 2nd International Symposium, CETIM, France, p. 315-326, 10-12 October 1995.

BISHOP, R. E. D., JOHNSON, D. C., "The Mechanics of Vibration", Cambridge University Press, 1979.

BONALDO, A. V., "Wavelet Transform: Algorithm Based in Fast Fourier Transform", MSc. Thesis, Mechanical Engineering Department, Federal University of Rio de Janeiro, 1993.

BRAUN, S., "Mechanical Signature Analysis Theory and Applications", Academic Press, 1986.

BROOKBANK, E. B., "Condition Monitoring of Electrical Submersible Pumps", Electric Submersible Pump Workshop, SPE Gulf Coast Section, 1992.

BRUEL & KJÆR , “Practical Use of the Hilbert Transform”, Application Notes BO 0173-11.

BUCKER, H. P., "Comparison of FFT and Prony Algorithms for Bearing Estimation of Narrow-Band Signals in a Realist Ocean Environment", J. Acoust. Soc. Am., vol. 61, no. 3, pp. 756-762, 1977.

CAPPELLINI, V., CONSTANTINIDES, A. G., EMILIANI, P., "Digital Filters and Their Applications", Academic Press, 1978.

CERRATO, L. R., EISENSTEIN, B. A., "Deconvolution of Cyclostationary Signals", IEEE Transactions on Acoustic, Speech, and Signal Processing, vol. 25, no. 6, pp. 466-476, 1977.

CHAMPENEY, D. C., “Fourier Transform and Their Physical Applications”, Academic Press, 1973.

CHIOLLAZ, M., FRAVE, B., "Engine Noise Characterization with Wigner-Ville Time-Frequency Analysis", Mechanical Systems and Signal Processing, vol. 7, no. 5, p. 375-400, Academic Press, 1993.

CIOFFI, J. M., KAILATH, T., "Fast Recursive-Least-Squares Transversal Filters for Adaptive Filtering", IEEE Transactions on Acoustic, Speech, and Signal Processing, vol. 32, no. 2, p. 304-337, 1984.

COHEN, L., "Time-Frequency Distributions - A Review", Proceedings of the IEEE, vol.77, no. 7, pp. 941-981, 1989.

COLLINS, M. D., MAKRIS, N. C., FIALKOWSKI, L. T., "Noise Cancellation and Source Localization", Journal of Acoustic Society of America, vol. 96, pp. 1773-1776, 1994.

COVER, T. M., THOMAS, J. A., "Elements of Information Theory", John Wiley & Sons, Inc., 1991.

CRAGGS, A., STREDULINSKY, D. C., "Analysis of a Acoustic Wave Transmission in a Piping Network", J. Acoust. Soc. Am., vol. 88, no. 1, p. 542-547, 1990.

DELZINGARO, M., MATTHEWS, C., "Using Power Signature Analysis to Detect the Behaviour of Electric Motors and Motor-Driven Machines", P/PM Technology, p. 32-35, August/95.

DOKUMACI, E., "Sound Transmission in Narrow Pipes with Superimposed Uniform Mean Flow and Acoustic Modelling of Automobile Catalytic Converters", Journal of Sound and Vibration, vol. 182, no. 5, p. 799-808, 1995.

DRAKE, L. A., RUTLEDGE, J. C., COHEN, J., "Wavelet Analysis in Recruitment of Loudness Compensation", IEEE Transactions on Acoustic, Speech, and Signal Processing, vol. 41, no. 12, pp. 3306-3312, 1993.

DTA HANDBOOK, "Least Squares Complex Exponential", Item 34.8 (M, E, T), Version 1, Dynamics Section, Mechanical Engineering Dept., Imperial College, 1993.

DYNE, S. J. C., "Vibration Signature Identification", Acoustical and Vibratory Surveillance Methods and Diagnostic Techniques, 2nd International Symposium, CETIM, France, p. 199-208, 10-12 October 1995.

EWINS, D. J., "Modal Testing: Theory and Practice", John Wiley & Sons, LTD, 1995.

FAHY, F. J., FULLER, C. R., "Wave Propagation in Fluid-Filled Pipes", Proceedings of The Institute of Acoustics, Spring Conference, University of Newcastle Upon Tyne, 1981.

FENG, L., "Noise and Vibration of a Fluid Filled Elastic Pipe Coated with an Absorptive Layer on the Inner Side of the Wall", Journal of Sound and Vibration, vol. 183, no. 1, p. 169-178, 1995.

FINETTE, S., MIGNEREY, P. C., SMITH, J. F., "Broadband Source Signature Extraction Using a Vertical Array", Journal of Acoustic Society of America, vol. 94, pp. 309-318, 1993.

FLANDRIN, P., "Representation Temps-Fréquence de Sinaux Non-Stationnaires", Traitement du Sinal, vol. 6, no. 2, p. 89-101, 1989.

FLANDRIN, P., ESCUDIÉ, B., "An Interpretation of The Wigner-Ville Distribution", Signal Processing, Elsevier, vol. 6, pp. 27-36, 1984.

FLANDRIN, P., ESCUDIÉ B., "Principe et Mise en Oeuvre de L'Analyse Temps-Fréquence par Transformation de Wigner-Ville", Traitement du Sinal, vol. 2, no. 2, 1985.

FLASPOHLER, W. H., "Using Statistical Techniques to Improve Rotating Machine Monitoring and Diagnostics", Vibration in Fluid Machinery Seminar, The Institution of Mechanical Engineer, 15/11/1994.

FRID, A., "Fluid Vibration in Piping Systems - A Structural Mechanics Approach, I: Theory", Journal of Sound and Vibration, vol. 133, no. 3, p. 423-438, 1989a.

GABOR, D., “Theory of Communication”, Journal of IEE, vol. 93, pp. 429-457, 1946.

GIBSON, J. D., MELSA, J. L., JONES, S. K., "Digital Speech Analysis Using Sequential Estimation Techniques", IEEE Transactions on Acoustic, Speech, and Signal Processing, vol. 23, no. 4, pp. 369-369, 1975.

GUPTA, V. H., "A Note on Three-Dimensional Effects in Segmentation Approach for Analysis of One-Dimensional Waves in Ducts of Varying Cross-Sectional Area", Journal of Sound and Vibration, vol. 182, no. 2, p. 323-327, Letters to Editor, 1995a.

GUPTA, V. H., EASWARAN, V., MUNJAL, M., "A Modified Segmentation Approach for Analyzing Plane Wave Propagation in Non-Uniform Ducts with Mean Flow", Journal of Sound and Vibration, vol. 182, no. 5, p. 697-707, 1995b.

HARDING-PAYNE, R. A., "Acoustic Transmission and Radiation for Two-Dimensional Ducts with Flow", Ph.D. Thesis, Imperial College, 1982.

HARRINGTON Jr.., E. C., "A Procedure For Sequential Experimentation", Chemical Engineering Progress Symposium Series, no. 42, Vol. 59.

HAYNES, H. D., KRYTER, R. C., STEWART, B. K., "Use of Motor Current Signature Analysis at The EPRI M&D Center, Advanced Diagnostic Engineering R&D Center, Oak Ridge National Laboratory, Oak Ridge, Tennessee 37831-6010 (year not informed but the paper describes several experiments carried on during the years 1989 and 1990).

HSU, F. M., GIORDANO, A. A., "Line Tracking Using Autoregressive Spectral Estimates", IEEE Transactions on Acoustic, Speech, and Signal Processing, vol. 25, no. 6, pp. 510-519, 1977.

IFEACHOR, E. C., JERVIS, B. W., "Digital Signal Processing, A Practical Approach", Addison-Wesley, 1993.

JENKINS, M. A., TRAUB, J. F., "Algorithm 419: Zeros of a Complex Polynomial", Commun. ACM, vol. 15, p. 97-99, 1972.

JEON, Y. C., JAMES LI, C., "Non-Linear ARX Model-Based Kullback Index for Fault Detection of A Screw Compressor", Mechanical Systems and Signal Processing, vol. 9, no. 4, p. 341-358, Academic Press, 1995.

KASHYAP, R. L., "Inconsistency of the AIC Rule for Estimating the Order of Autoregressive Models", IEEE Transactions on Automation Control, vol. 25, p. 996-998, 1980.

KAY, S. M., "The Effects of Noise on the Autoregressive Spectral Estimator", IEEE Transactions on Acoustic, Speech, and Signal Processing, vol. 27, no. 5, p. 478-485, 1979.

KAY, S. M., "Noise Compensation for Autoregressive Spectral Estimates", IEEE Transactions on Acoustic, Speech, and Signal Processing, vol. 28, no. 3, p. 292-303, 1980.

KAY, S. M., "Fundamentals of Statistical Signal Processing", Prentice-Hall, 1993.

KOMPELA, M. S., DAVIES, P., BERNHARD, R. J., UFFORD, D. A., "A Technique to Determine the Number of Incoherent Sources Contributing to the Response of a System", Journal of Mechanical Systems and Signal Processing, vol. 8, no. 4, Academic Press, 1994.

KRYTER, R. C., HAYNES, H. D., "Condition Monitoring of Machinery Using Motor Current Signature Analysis", Sound and Vibration, September/1989.

KRYTER, R. C., HAYNES, H. D., "How to Monitor Motor-Driven Machinery by Analyzing Motor Current", Power Engineering, p. 39, (year not clear in the copy).

LANG, S. W., McCLELLAN, J. H., "Frequency Estimation with Maximum Entropy Spectral Estimators", IEEE Transactions on Acoustic, Speech, and Signal Processing, vol. 28, no. 6, p. 716-724, 1980.

LAZAN, B. J., "Damping of Materials and Members in Structural Mechanics", Pergamon Press, 1968.

LEDUCQ, D., HERVIEU, E., "Characterization of Multiphase Flow from Wall Measurements Application of the Wavelet Transform Method", Elsevier Science Publisher, 1991.

LEDUCQ, D., SCHLEGEL, R., ALLIOUD, J. P., "Methode Temps-Echelle Appliquee au Suivi du Demarrage d'Un Broyeur de Cimenterie", Acoustical and Vibratory Surveillance Methods and Diagnostic Techniques, 2nd International Symposium, CETIM, France, p. 863-872, 10-12 October 1995.

LEE, C., JOH, C., "Development of The Use of Directional Frequency Response Functions for The Diagnosis of Anisotropy and Asymmetry in Rotating Machinery: Theory", Mechanical Systems and Signal Processing, vol. 8, no. 6, p. 665-678, Academic Press, 1994.

LINEHAN, D. J., BUNCH, S. L., HANZELKA, B. B., "Cost-Effective On-Line Monitoring of Rotating Equipment Using Motor Current Analysis", Oak Ridge, TN 37831-8161 (year not informed).

LONGMORE, D. K., STAMMERS, C. W., TUC, B., "Measurement of The Longitudinal Wave Propagation Properties of Reinforced Flexible Hose", Proceedings of The Institute of Acoustics, Spring Conference, University of Newcastle Upon Tyne, 1981.

MAIA, N. M. M., EWINS, D. J., "A New Approach for The Modal Identification of Lightly Damped Structures", Mechanical Systems and Signal Processing, p. 173-193, Academic Press, 1989.

MAKIOLA, B., "Noise Characteristics of Single-Stage Pumps Under Different Speed and Conditions", Acoustical and Vibratory Surveillance Methods and Diagnostic Techniques, 2nd International Symposium, CETIM, France, p. 721-723, 10-12 October 1995.

MAKSUTOV, R. A., ALIEV, I. M., "Diagnostic of Condition of Electrical Submersible Pumps Assemblies (ESP)", Neftyanoe Khoziaystvo, no. 10, p. 38-40, October/1984.

MARPLE, S. L., "Efficient Least Squares FIR System Identification", IEEE Transactions on Acoustic, Speech, and Signal Processing, vol. 29, no. 1, p. 62-73, 1981.

MARPLE, S. L., "Spectral Line Analysis via Fast Prony Algorithm", Proceedings of the IEEE International Conference on Acoustics, Speech and Signal Processing, Paris, France, pp. 1375-1378, 1982.

MARPLE, S. L., "Digital Spectral Analysis With Applications", Prentice-Hall Inc., 1987.

MARS, J., MARTIN, N., LACOUME, J. L., DUBESSET, M., "Analysis of Signals Over Short Time-Windows", Signal Processing, Elsevier, vol. 26, pp. 147-159, 1992.

MARTIN, N., "An AR Spectral Analysis of Non-Stationary Signals", Signal Processing, Elsevier, vol. 10, pp. 61-74, 1986.

MARTIN, W., FLANDRIN, P., "Detection of Changes of Signal Structure by Using The Wigner-Ville Spectrum", Signal Processing, Elsevier, vol. 8, pp. 215-233, 1985.

MECHEFSKE, C. K., MATHEW, J., "Fault Detection and Diagnosis in Low Speed Rolling Element Bearings Part I: The Use of Parametric Spectra", Mechanical Systems and Signal Processing, vol. 6, no. 4, p. 297-307, Academic Press, 1992a.

MECHEFSKE, C. K., MATHEW, J., "Fault Detection and Diagnosis in Low Speed Rolling Element Bearings Part II: The Use of Nearest Neighbour Classification", Mechanical Systems and Signal Processing, vol. 6, no. 4, p. 309-316, Academic Press, 1992b.

MECHEFSKE, C. K., MATHEW, J., "Parametric Spectral Estimation to Detect and Diagnose Faults in Low Speed Rolling Elements Bearings: Preliminary Investigations", Mechanical Systems and Signal Processing, vol. 7, no. 1, p. 1-12, Academic Press, 1993.

MEIROVITCH, L., " Analytical Methods in Vibrations", The Macmillan Co., 1967.

MOLINARO, F., CASTANIÉ, F., "Signal Processing Pattern Classification Techniques to Improve Knock Detection in Spark Ignition Engines", Mechanical Systems and Signal Processing, vol. 9, no. 1, p. 51-62, Academic Press, 1995.

MOORE, T., "Condition Monitoring of Borehole Submersible Pumps", BHRA Fluid Engineering Center, 1990.

MORF, M., DICKINSON, B., KAILATH, T., VIEIRA, A., "Efficient Solution of Covariance Equations for Linear Prediction", IEEE Transactions on Acoustic, Speech, and Signal Processing, vol. 25, no. 5, p. 429-433, 1977.

MORSE, P. M., INGARD, K. U., "Theoretical Acoustics", McGraw-Hill, Inc., 1968.

MOSS, J. C., HAMMOND, J. K., "A Comparison Between the Modified Spectrogram and the Pseudo-Wigner-Ville Distribution with and without Modification", Mechanical Systems and Signal Processing, Academic Press, vol. 8, no. 3, p. 243-258, 1994.

NEWLAND, D. E., "An Introduction to Random Vibrations, Spectral & Wavelet Analysis", Longman Scientific & Technical, 3rd Edition, 1993.

NORIEGA, G., PASUPATHY, S., "Application of Kalman Filtering to Real-Time Preprocessing of Geophysical Data", IEEE Transactions on Geoscience and Remote Sensing, pp. 897-910, vol. 30, no. 5, 1992.

O'BRIEN, J., MacINTYRE, J., "Wavelets: an Alternative to Fourier Analysis", Vibration in Fluid Machinery Seminar, The Institution of Mechanical Engineer, 15/11/1994.

OPPENHEIM, A. V., SCHAFER, R. W., "Discrete-Time Signal Processing", Prentice-Hall, 1989.

PAGE, C. H., “Instantaneous Power Spectra”, Journal of Applied Physics, vol. 23, pp. 103-106, 1952.

PINDER, J. N., "Behaviour of Fluidborne Sound Waves in Piping Systems and its Relationship to Noise Radiated from Pipe Surfaces; A Literature Review", paper submitted to CONCAWE Noise Group STF 11, BP International Ltd., Project 2619/C8, 1983.

PITARQUE, T., ALENGRIN, G., FERRARI, A., MENEZ, J., "A New State Space Algorithm for Computing the Frequencies of Sinusoids in White Noise", Signal Processing, vol. 22, pp. 231-238, 1991.

POGGIO, A. J., VAN BLARICUM, M. L., "Evaluation of a Processing Technique for Transient Data", IEEE Transactions on Antennas Propagation, vol. 26, no. 1, pp. 165-173, 1978.

POWELL, C. D., "Machinery Troubleshooting Using Vibration Analysis Techniques", Sound and Vibration, January/1992.

PRESS, W. H., et al., "Numerical Recipes, The art of Scientific Computing", FORTRAN version, Cambridge University Press, 2nd. edition, 1992.

PRICE, A. E., "Experimental Use of Consultative Expert Systems for Machine Fault Diagnosis", 2nd International Conference on Condition Monitoring, 1988.

PROAKIS, J. G., MANOLAKIS, D. G., "Introduction to Digital Signal Processing", Macmillan Publishing Co., 1988.

QUINQUIS, A., ROSSIGNOL, S, "Noise Reduction, with a Noise Reference, of Underwater Magnetic Signals", Digital Signal Processing, vol. 6, pp. 240-248, 1996.

RANDALL, R. B., "Cepstrum Analysis and Gearbox Fault Diagnosis", Application Notes 233-80, Edition 2, Bruel & Kjaer, 1980.

RIBEIRO, M. P., "Processamento de Sinais Vibratórios de Equipamentos Situados a Longas Distâncias Via Método de Prony", COPPE/UFRJ, Engenharia Mecânica, M.Sc. Thesis, 1991.

RIBEIRO, M. P., SLAMA, J., ZINDELUK, M., "Performance Evaluation of Long Distance Placed Equipment by Vibration and Signal Processing Analysis Via Prony's Method", XI Congresso Brasileiro de Engenharia Mecanica - Sao Paulo, SP, Brazil, December 1991.

ROUSSEAX, P., TROQUET, J., "Deconvolution of Time-Varying Systems by Kalman Filtering: Its Application to The Computation of the Active State in The Muscle", Signal Processing, vol. 10, pp. 291-301, 1986.

SERVIÈRE, C., BAUDOIS, D., "Source Separation with Noisy Observations: A Noise Cancelling Application, Signal Processing, vol. 42, pp. 45-57, 1995.

SHIN, Y. S., JEON, J., "Pseudo Wigner-Ville Time-Frequency Distribution and its Applications to Machinery Condition Monitoring", Shock and Vibration, vol. 1, no. 1, pp. 65-76, 1993.

SPARKS, C., WACHEL, J. C., "Pulsation in Centrifugal Pump and Piping Systems", Hydrocarbon Processing, p. 183-189, March/1977.

SPIEGEL, M. R., "Schaum's Outline of Theory and Problems of Statistics", McGraw-Hill, 1961.

TIMOSHENKO, S., YOUNG, D. H., WEAVER, W., "Vibration Problems in Engineering", John Wiley & Sons, 1974.

TO, W. M., EWINS, D. J., "A Closed-Loop Model for Single/Multi-Shaker Modal Testing", Mechanical Systems and Signal Processing, p. 305-316, Academic Press, 1991.

TO, W. M., EWINS, D. J., "The Characteristic of Frequency Response Function Estimators Using Random Excitation", Proceedings of the 8th International Modal Analysis Conference, USA, p. 1101-1107, 1990.

TONG, H., "Autoregressive Model Fitting with Noisy Data by Akaike Information Criterion", IEEE Transactions on Information Theory, vol. 21, p. 476-480, 1975.

TONG, H., "Autoregressive Model Fitting with Noisy Data by Akaike Information Criterion", IEEE Transactions on Information Theory, vol. 23, p. 409-410, 1977.

VILLE, J., "Théorie et Applications de la Notion de Signal Analytique", Cables et Transmission, vol. 2A, pp. 61-74, 1948.

WANG, Z., NUR, A. M., BATZIE, M. L., "Acoustic Velocities in Petroleum Oils", Journal of Petroleum Technology, February/1990.

WOMACK, J. E., CRUZ, J. R., "Seismic Data Filtering Using Gabor Representation", IEEE Transactions on Geoscience and Remote Sensing, pp. 467-472, vol. 32, no. 2, 1994.